ANTTI
OLLIKAINEN

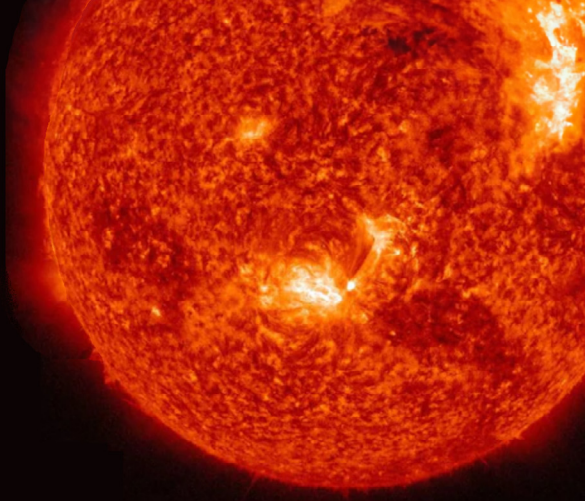

Multi-Millennial Solar Cycles

Decoding Climate Patterns and Enigmas

Multi-Millennial Solar Cycles

Multi-Millennial Solar Cycles

Decoding Climate Patterns and Enigmas

ANTTI OLLIKAINEN

In Memory of Yrjö Ollikainen (1946-2018)

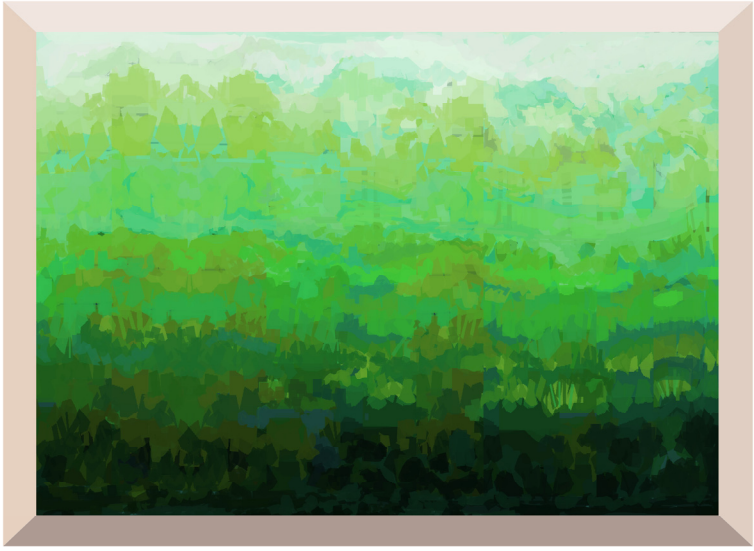

First published on December 2023.

ISBN 9798871130940 paperback

The author has no responsibility for the persistence or accuracy of URLs for external or third-party internet websites referred to in this book, and does not guarantee that any content on such websites is, or will remain, accurate or appropriate.

Author: Antti Ollikainen
Editors: Aila Schenk
Illustration: Antti Ollikainen

This book was carefully produced. Nevertheless, author, editors and publisher do not warrant the information therein to be completely error-free. Readers should be aware that data, statements, illustrations or other items may be inaccurate.

Contents

Preface iv

1 REVELATION AND PARADOX 1

1.1 Glacial–Interglacial Cycles 1
1.1.1 The Earth's Orbital Cycles and the Middle Pleistocene Transition 4
1.2 The 3650-Year Climate Cycle 7
1.2.1 The Holocene in Greenland 8
1.2.2 The Blue Column Series Coincide with the Abrupt Holocene Start 12
1.3 The Blue Trendline Is Not a Coincidence 13
1.3.1 The Hoxnian (MIS 11) 13
1.3.1.1 The Ascending Blue Trendline 16
1.3.2 The Aveley (MIS 7) 17
1.3.3 The Eemian (MIS 5e) – The Last Interglacial 20
1.4 Is There a Solar Coupling? 22
1.4.1 A Diversified 3650-Year Climate–Solar Cycle 22
1.5 A Brief Introduction to the Solar Interior 24

2 MULTI-MILLENNIAL SOLAR CYCLES 29

2.1 Main Cycles 31
2.2 Intermittent Cycles 34
2.2.1 2.5-ka Periods Show Module and Cycle Characteristics 35
2.2.2 The 2.5-ka Periodicity Partly Originates from the Quasi-Cycle 36
2.3 Cluster Formation of Intermittent Cycles 37
2.3.1 Evolutionary Pace of the Double Peak Module 40
2.4 Module Inceptions and Precise Cycle Durations 43
2.4.1 A Moment of Breakthrough 43
2.4.2 Closure of the 52.5-ka Loop 44
2.4.3 Durations and Couplings of the Theoretical Cycles 47
2.5 A Hypothetical Evolution of Module Overlappings 51
2.6 The Dual Character of the 2.5-ka Periodicity and Its Interactions with the Quasi-Cycle 53
2.6.1 Partial Overlapping of the '10-ka-BP' Modules 54

3 A MISSING LINK BETWEEN THE SUN AND CLIMATE RESPONSES 61

3.1 Past Solar Activity and Greenland Climate Variations 61
3.1.1 Climate Proxy Evidence of the 7-kyr Total Solar Irradiance Cycle 63
3.2 A Prediction for Solar Activity and Greenland Climate Variations 69
3.2.1 Emergence of a New Maunder-like Minimum 71
3.2.1.1 Exploring the 2.5-kyr Periodicity 71
3.2.1.2 How Long It Will Last? 74
3.2.1.3 Climate Couplings 79
3.3 The Quasi-Cycle Evolution of the Holocene 82
3.3.1 Positioning in Contrast to the Last Cycle 82
3.3.2 Inactivity Similarities Linking the Little Ice Age and the 8th Millennium BP 90
3.3.3 The Preboreal and Medieval Intervals 93

4 OCEAN CIRCULATION AND CLIMATE CHANGE 96

4.1 The Atlantic Meridional Overturning and Thermohaline Circulations 96
4.1.1 Alterations in the AMOC 100
4.1.2 The ITCZ in the Atlantic and Indian Ocean Sectors 101
4.1.3 The ITCZ and Variability of the Indian Monsoon 103
4.2 The Double Peak Module and Abrupt Climate Changes 105
4.2.1 The Coldest Phases of the Stadials: Heinrich Events 105
4.2.1.1 Anomaly of Western North Atlantic 108
4.2.2 End of the African Humid Period 110
4.3 Solar-Induced Variations in AMOC and Abrupt Climate Changes 115
4.3.1 Carbon Dioxide in Regional and Global Climate Changes 115
4.3.2 Future of the AMOC and Sea Level Rise 116
4.4 The Bipolar Seesaw Mechanism and the 7-kyr Climate Cycle 120
4.4.1 Marine Isotope Stage 3 120
4.4.1.1 A Conceivable Method to Confirm the 3.75-kyr Cycle Length 124
4.4.2 Glacial Terminations I–V 127
4.4.2.1 The Last Interglacial (MIS 5e) 131

5 MULTI-MILLENNIAL SOLAR CYCLES IN EXPLAINING THE CHAOTIC GLACIAL CLIMATE 139

5.1 Solar-Induced Climate Loops in Central Greenland 139
5.1.1 Was the Third Heinrich Event a Younger Dryas Equivalent? 141
5.1.2 The Holocene and The Last Glacial Maximum Correlate Via 21 kyr 144
5.2 Semi- and Full-Scale Loops 146
5.2.1 Comparing the NGRIP Record to the Holocene via the 52.5-kyr Loop 148

5.3 The Tajo Interglacial (MIS 19) 150
5.3.1 Background Conditions of the Best Orbital Analogue 150
5.3.2 Similarities between the Tajo and the Holocene 154
5.3.3 Younger Dryas and Cold Event Equivalents of the Tajo 156
5.3.4 Climate Models and the Future 159
5.4 A 1.3-million-Year Bond to the Early Pleistocene 161

References 166
Bibliography 181
Index 182
List of Abbreviations 186

PREFACE

Chapter 1 introduces a newly discovered climate paradox embedded in ice-core records spanning both hemispheres. This multi-millennial climate cycle traces a discernible trendline that has guided the course of climate evolution across nearly the entire interglacial periods of the Aveley and the Hoxnian, approximately 230 and 430 thousand years (kyr) ago. Remarkably, this same trendline manifests in the ongoing postglacial warm period, known as the Holocene, exerting a steady decline on central Greenland temperatures, while the opposite may hold true for Antarctica.

In Chapter 2, we delve into the captivating realm of Multi-millennial solar cycles (MMSCs), unraveling their intricate couplings and unprecedented evolution. The predictability of MMSCs is striking, operating with surprising accuracy and regularity over extensive time spans. Furthermore, their interactions prove comprehensible, allowing for rough estimates of how they will modulate magnetic activity in the future.

Solar dynamo simulations have produced a transient long-term cycle at the bottom of the convection zone [Käpylä, 2016], even within the relatively short time span of 2000 years. However, given the absence of an absolutely truthful reconstruction of solar activity covering at least ten thousand years, fully accurate solar dynamo models remain elusive. The signal captured is a reflection of the dynamo in action, albeit distorted before deposition into Earth's natural archives. Predictions, therefore, rely on partially imperfect proxies. Despite this, two methods have been developed – the 'analog' [Lockwood, 2010] and spectral technique [Steinhilber and Beer, 2013] – to forecast based on empirical data.

Chapters 3, 4, and 5 employ a predictive approach by amalgamating elements of regional climates and solar-activity proxies. Rooted in logical causes and consequences, these chapters illuminate unusual climate events from the North to the South Atlantic, aiming to uncover simple patterns and cyclic behavior behind these phenomena without resorting to complex formulas.

This book does not stand alone as a self-explanatory text. It assumes a foundational knowledge of climatology, solar physics, astronomical cycles, and the ocean-atmosphere system. Readers are encouraged to acquaint themselves with these subjects through the references listed at the end of the book or the bibliography, most of which are available online. Familiarity with these topics beforehand will enhance the reader's understanding of the influences and meanings underpinning the book.

I believe this book can be a valuable resource not only for scientists engaged in research across astrophysics, solar physics, earth and environmental sciences, oceanography, meteorology, and climatology but also as supplementary reading for those seeking knowledge to make informed decisions for the future.

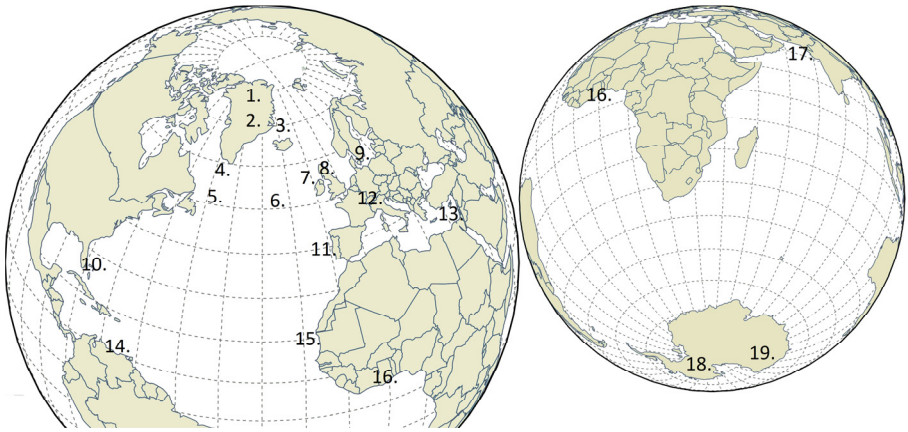

Figure 0.1. Locations of lake and ocean-floor sediments, as well as ice-core and tree-ring sites referenced in the book.

1. NGRIP
2. GISP2 and GRIP
3. M23351 - Zhuravleva et al., 2017]
4. MD03-2664 - Irvali et al., [2016]
5. U1302 - Channell et al., [2012]
6. U1308 - Obrochta et al., [2014]
   DSDP 609 - Obrochta et al., [2014]
7. MD01-2461 - Peck et al., [2006]
8. TRW - Turney et al., [2015]
9. TRW - Edvardsson et al., [2013]
10. MD99-2022 - Zhuravleva et al., [2018]
11. MD95-2040 - de Abreu et al., [2003]
11. MD01-2444 - Martrat et al., [2007]
    U1385 - Sánchez Goñi et al., [2018]
    U1385 – Birner et al., [2015]
12. Speleothem - Tzedakis et al. [2018]
13. ODP967 – Grant et al., [2017]
14. SO90-KL111 Schulz et al., [1998]
    MD03-2621 Deplazes et al., [2013]
15. 658C - deMenocal et al., [2000]
16. Lake Bosumtwi – Shanahan et al., [2015]
17. SO130-289 - Deplazes et al., [2013]
18. Byrd
19. EPICA Dome C

CHAPTER I

1 REVELATION AND PARADOX

Periodicity emerges as a captivating and foundational theme across scientific disciplines, offering a framework for insightful predictions. The realm of climate science is no exception, exemplified by the Earth's orbital cycles, commonly known as Milankovitch cycles [1941], instigating warm interglacial epochs approximately every 100,000 years. Another enduring natural chronometer, albeit of much shorter frequency, emanates from the solar interior. The 11-year sunspot cycle, discovered by Schwabe in 1844, roughly resembles a 'sawtooth'-shaped sine wave, though its amplitude and duration vary considerably.

Shifting our gaze to the opposite end of the temporal spectrum, we encounter the Sun's galactic rotation period and the Earth's continental drift. The Sun, in its journey around the center of the Milky Way galaxy, covers a staggering 240 million years. En route, Earth's surroundings transform ceaselessly, traversing galactic spirals, traversing vast emptiness, and encountering remnants of supernovae.

On the terrestrial surface, the distribution of land and sea has undergone profound transformations. The breakup of the Pangaea supercontinent led to a cooling of the greenhouse Earth by c. 10 °C. Over the past 750 million years, three major cooling events have unfolded, each accompanied by astonishing sea-level fluctuations [Brink, 2015]. These events provide glimpses into the dynamic and ever-evolving nature of our planet's geological and climatic history.

1.1 Glacial–Interglacial Cycles

Antarctica's icy landscape is a marvel of natural history, with its beginnings dating back approximately 38 million years ago. This was around the same time that Central America emerged, separating the

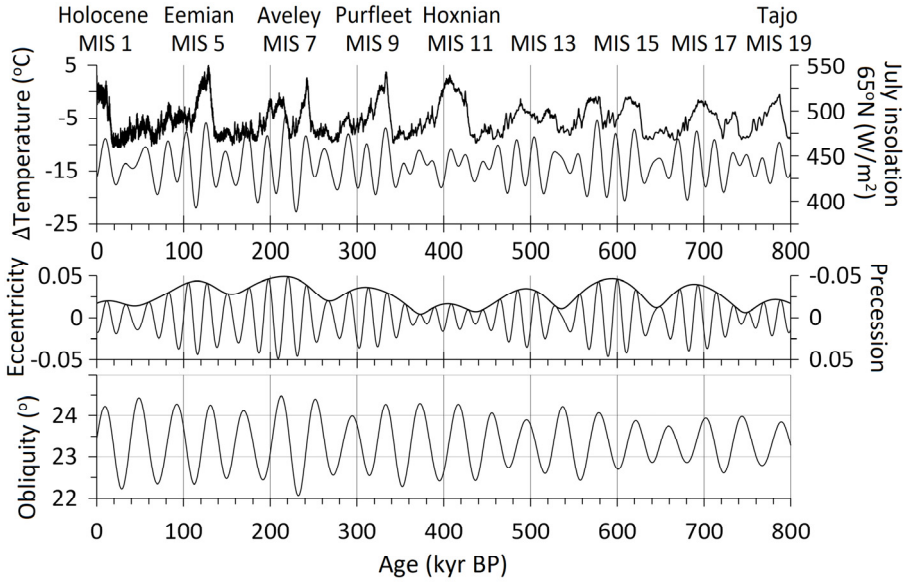

Figure 1.1. A temperature record of eastern Antarctica covers the past 800,000 years (core site EPICA Dome C). The Earth's three orbital cycles, namely eccentricity (c. 95–128 kyr), obliquity (c. 41 kyr), and precession (c. 19–26 kyr), have a modulating effect on global climate. These orbital cycles determine the temporal variations in the intensity of incoming solar irradiation (insolation) across different latitudes. The data sources are Jouzel et al. [2007] and Berger [1992].

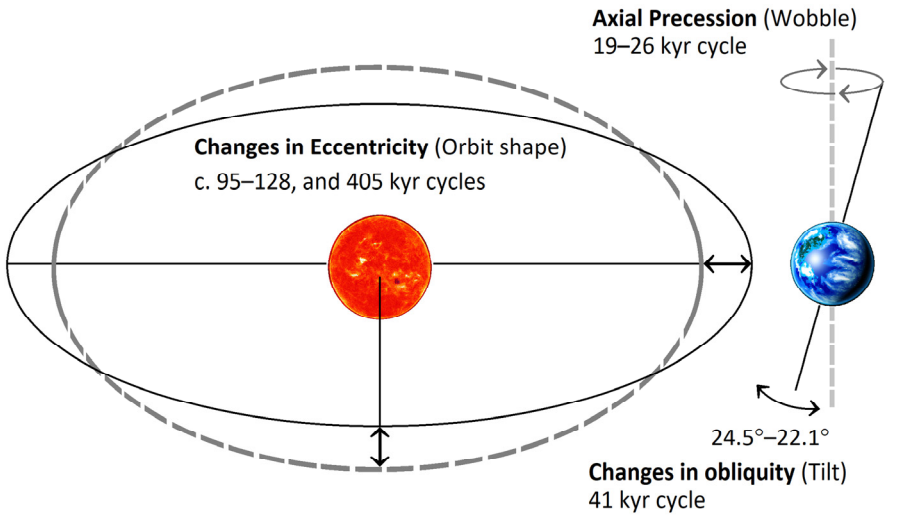

Figure 1.2. The Earth's changing orbital parameters: eccentricity, obliquity, and precession.

equatorial Pacific and Atlantic Oceans. Over the course of tens of millions of years, the South American continent drifted westward, distancing itself from Africa. This gradual movement facilitated the opening of the Drake Passage between the southernmost continents, enabling extensive water circulation around Antarctica. The combination of increased oceanic flow and prevailing westerly winds thermally isolated its climate system from the mainland.

The completion of the permanent ice cover over Antarctica was a slow process that involved the waxing and waning of its glaciers. It was not until 34 million years ago that the coldest continent became entirely glaciated. Intriguingly, the Northern Hemisphere ice sheets may not be any older than a few million years.

A large continent at the pole or at high latitudes is a prime requirement for an ice age. It is estimated that there is currently c. 33 million cubic kilometers of land ice, with the vast majority, approximately 90%, located in Antarctica. This rather incomprehensible ice volume is roughly one-third of the land ice that existed over 18,000 years ago when the last glacial period climaxed, and the ice sheets covered much of North America, northern Europe, and Asia.

An ice age denotes a geological epoch marked by a significant decrease in global temperatures, leading to the formation of widespread ice sheets in polar regions that extend toward the equator. The term 'ice age' commonly alludes to the ongoing geological period of glaciation, which commenced approximately 2.6 million years ago and continues today. However, it also encompasses a more narrowly defined cold interval c. 11.7–100 thousand years Before Present (kyr BP) situated between the current and last interglacial periods. These interglacial periods, occurring within ice ages, typically endure for 10 to 20 thousand years before transitioning back to a glacial phase.

The termination of an interglacial or glacial period is a multifaceted process influenced by diverse factors, including alterations in solar radiation distribution and quantities, Earth's albedo, greenhouse gas concentrations, and ocean currents. Nevertheless, these terminations are primarily driven by variations in the Earth's orbit around the sun, axial tilt, and precession.

1.1.1 The Earth's Orbital Cycles and the Middle Pleistocene Transition

It is yet to be resolved why the varying distance between the Sun and the Earth, known as orbital eccentricity, currently determines the 100-kyr duration of the interglacial–glacial cycle, and why its longer 405-kyr modulation strongly affects the climate profile and duration of an interglacial. The curiosity toward orbital eccentricity arises from calculations suggesting that its variations should exert the weakest influence on the climate system compared to the tilt angle of the Earth's rotation axis (orbital obliquity) and axial wobbling (precession) [Imbrie et al., 1993]. These three astronomical parameters collectively determine how the Sun's electromagnetic radiation is distributed to the Earth's surface, playing a pivotal role in the alternation of glacial and interglacial periods (see Figs. 1.1 & 1.2).

The polar regions receive more sunlight when the tilt angle is larger, intensifying seasonality at the maximum angle of 24.5 degrees (°) compared to the minimum angle of 22.1°. For a long time, this variation dominated the glacial–interglacial cycles until something disturbed the balance. Paleoclimatic records show that about 0.8–1.2 million years ago, the climate system went through a major change in oscillation frequency, from the 41-kyr obliquity cycle to the 100-kyr eccentricity cycle, as shown in Fig. 1.3. This change led to substantially colder glacial phases, while interglacial temperatures remained relatively unchanged. The trigger for this shift, known as the Middle Pleistocene Transition (MPT), is still not certain, but it is part of a sustained cooling process that has continued for about 50 million years. During this time, Antarctica has become frozen, with a 3-km-thick ice sheet on top of it.

In the distant past, these major coolings have occasionally led to a state where the entire or most of Earth's surface got covered by ice, possibly for millions of years. How the recovery succeeded in the end is still debated [Kataoka et al., 2013]. The concept of Snowball Earth was first proposed by geologists Paul F. Hoffman and Daniel P. Schrag in the early 1990s. They suggested that such an extreme glaciation event might have occurred during the Neoproterozoic Era,

approximately 700–600 million years ago. Their hypothesis was based on geological evidence, including the presence of glacial deposits in areas near the equator [Hoffman et al., 1998, 2002]. We do not need to time-travel that far to notice how complex and unpredictable the climate can be, and its future may even surprise us despite modern modeling capabilities.

The influence of variable incoming solar irradiation (insolation) on interglacial–glacial cycles is more pronounced at higher latitudes than at the Equator. This phenomenon can be attributed to the declining northern summer temperatures, which are a consequence of weaker insolation. The landmass surrounding the Arctic Ocean at about 65 degrees of northern latitude (65° N) is believed to be a significant factor in the onset of glaciation. The Arctic Circle plays a vital role in the accumulation of snow, contributing to the formation of continental ice sheets that reflect an increasing amount of solar energy back into space.

In contrast, the Southern Hemisphere lacks the presence of extensive land formations at the same latitudes, with the Southern Ocean being the predominant feature. Additionally, the permanent sea ice in this hemisphere does not extend far from the shore. Hence, it would require a tremendous leap for the Earth to once again develop large southern continental ice sheets, potentially leading to a snowball Earth scenario. However, the current distribution of continents and the orbital configuration, among other factors, may not be conducive to such an arrangement for an extended period of time.

When comparing the insolation patterns of the past million years, it becomes evident that the Earth's three orbital cycles (95–128, 41, and 19–24 kyr) synchronize approximately every 200 kyr. These periodic synchronies last for 100–130 kyr at a time and lead to a consistently progressing climate. However, the emergence of these similar insolation patterns requires a moderate suppression of the precessional effect on the climate system by eccentricity. For instance, the amplitude of the precession cycle oscillates at intermediate levels during nearly identical interglacials of Marine Isotope Stages (MIS) 5/9 and 13/17, as shown in Figure 1.3.

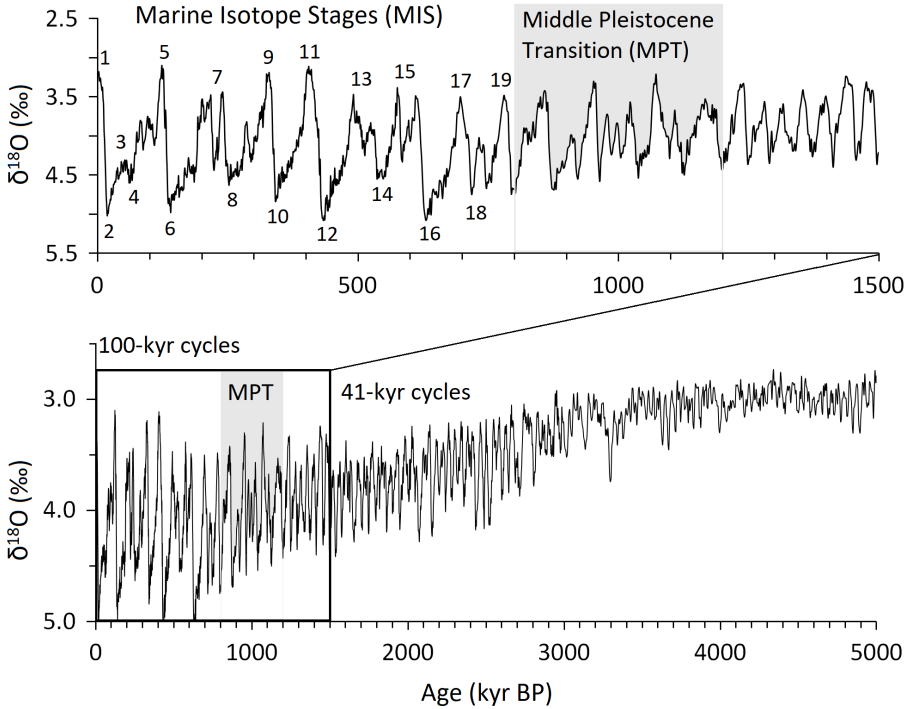

Figure 1.3. A Pliocene–Pleistocene stack comprising 57 globally distributed benthic $\delta^{18}O$ records provides insight into the cyclical climate variations of the past 5 million years [Lisiecki and Raymo, 2005]. The stack includes numbered glacial and interglacial phases, extending up to the Tajo interglacial (MIS 19) around 790 kyr BP.

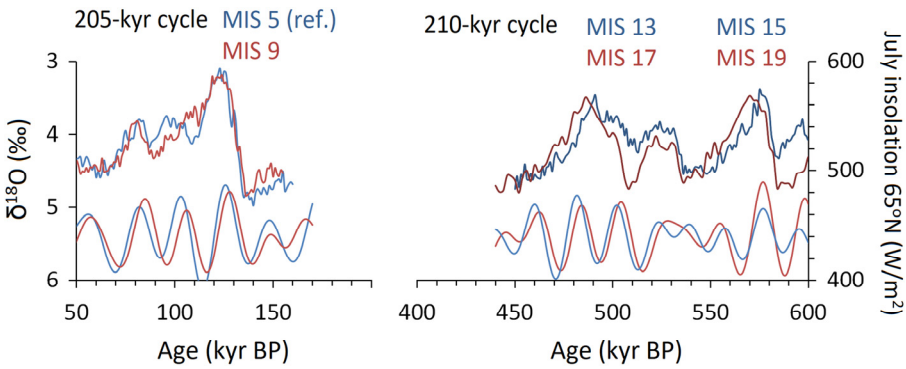

Figure 1.4. Climatic variability shows similarities among specific Marine Isotope Stages (MIS) when their July 65° N insolation (W/m²) fluctuations are coherent and the time gap between them is c. 200 kyr. The data sources are Berger [1992] and Lisiecki and Raymo [2005].

The precessional effect is primarily modulated by orbital eccentricity in cycles of about 100 and 405 kyr, although even longer million-year cycles are also involved. In the 100-kyr 'world' of glacial–interglacial cycles, extreme variations in eccentricity, ranging from perfectly circular to highly elliptical, generate climatic extremes that do not exhibit sufficient correlation to provide predictability.

To find an analogy or symmetry with the current interglacial period, scientists are more inclined to investigate the 405-kyr periodicity instead of the 200-kyr one. However, the method could prove problematic as the nearest option may not show coherency. Even the second-closest may be too distant and different from its background conditions, rendering a direct comparison irrelevant. This is the case for the Holocene, as the insolation patterns between the present and 420 kyr BP do not reflect equivalent interglacials. The correlation of important July 65° N insolation patterns ended approximately 15 thousand years ago with the early Hoxnian (MIS 11), making it inadequate to predict the duration, amplitude, and stability for the next 50 kyr. However, from 15 kyr BP onward, the MIS-19 insolation fluctuation starts to correlate with that of the Holocene through roughly 780 kyr, as illustrated in Figure 5.6. Unfortunately, the Middle Pleistocene Transition, the most prominent climate change shift in prehistory, was only about to end around 800 kyr BP, potentially still in progress when MIS 19 ended. As a result, among the most recent interglacials (<500 kyr), there is not a good insolation analog for the Holocene with similar background conditions. Nonetheless, the second option (MIS 19) might be best for drawing conclusions about possible upcoming trends.

1.2 The 3650-Year Climate Cycle

The Greenland Ice Sheet Project 2 (GISP2) proxy record provides a relatively accurate, long-term view of the past climate, extending over the last hundred thousand years. Although temporally shorter than its Antarctic counterpart, the GISP2 ice-core record is a valuable resource in the field of paleoclimatology. As surprising as it may sound, it has uncovered a notable asynchrony between polar cli-

mates [Blunier and Brook, 2001; Buizert et al., 2015], which forms a central theme of Chapter 4.

In the past, large climatic fluctuations, also known as millennial variability, occurred in the Arctic and Antarctica, but they were not correlated. This inconsistency troubled researchers for some time until they realized that the Atlantic poles consistently exhibited anti-correlative behavior. Additionally, there has been increasing interest in the extent to which a Greenland climate record reflects the climatic history of the overall Northern Hemisphere, as evidence of the Younger Dryas has been found in distant locations such as Venezuela's offshore and the Arabian Sea [Haug et al., 2001; Schulz et al., 1998], and its global impact is gradually being revealed [Zhang et al., 2019; Gebregiorgis et al., 2020].

The Younger Dryas cold interval had the most significant influence on temperature variation in the Greenland region and was likely caused by major changes in ocean circulation patterns. These changes resulted in a cooler North Atlantic, a warmer South Atlantic, and a primarily warmer Antarctica. The Younger Dryas was an integral part of the cold stadial series that also preceded the earlier glacial terminations (II–IV) and should be viewed as an inevitable phenomenon and part of glacial-to-interglacial transitions [Broecker et al., 2010]. While there are many similar examples of regional climate changes correlating with those of Greenland, the information restored to annual ice-sheet layers is less meaningful unless put into a larger context. Therefore, without periodic features, the information is less relevant, and it is necessary to consider the broader picture.

1.2.1 The Holocene in Greenland

It seems plausible that the central and northern Greenland ice-core records, comprising GISP2, GRIP, and NGRIP, provide the best representation of the overall climate changes at higher latitudes in the Northern Hemisphere. After systematically inspecting one of these Greenland climate records, its cyclical features started to appear, as illustrated in Figure 1.5. Three warm plateaus, each about a millennium long, took place in the third, seventh, and possibly tenth mille-

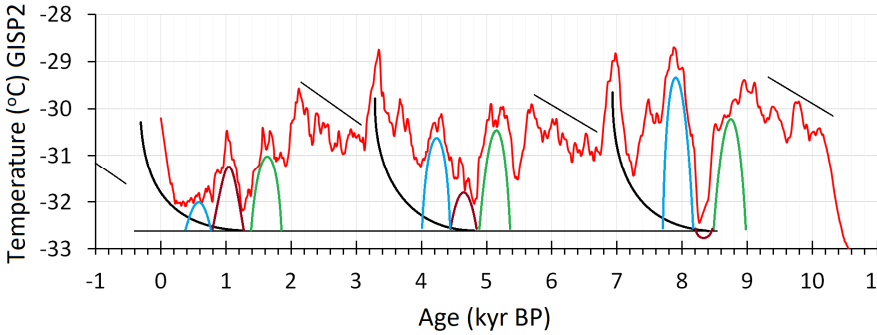

Figure 1.5. A central Greenland temperature curve (GISP2) by Alley [2004]. The steep temperature rise after the 1850s [Box, 2009] roughly corresponds to the current situation. When the climate abruptly warmed c. 11.7 kyr BP, it took some time before the temperatures reached a threshold level (black horizontal line) c. 10.5 kyr BP. The colored columns in the figure exhibit their own evolution, demonstrating a trend-like development with approximately 3.65-kyr time spans. As we will explore later, the Blue Column is particularly relevant in predicting long-term temperature trends. The black rising curve in the figure represents the 1.5-kyr-long Warming phase, followed by a Plateau phase lasting for thirteen hundred years or so. The Decline phase, which includes the Younger Dryas, begins roughly at 2.05, 5.7,...13 kyr BP, completing the entire cycle.

nia BP. The two youngest seem to have followed abrupt, short-term warmings about 3.4 and 7 kyr BP. An analogous warming spike (or anomaly) is expected to occur around AD 2300 if the current cycle continues similarly to the previous ones, although they rarely do so precisely. In every complex system, there is usually a stochastic component involved that creates sporadic features. This particular profile of a 'spike and plateau' can also be found in the interval immediately preceding the Younger Dryas cold spell (11.8–12.9 kyr BP), and it can be easily distinguished upon comparison.

One of the most prominent features of the 3.65-kyr climate cycle is the abrupt cooling event at the end of each Green Column about 1.38, 4.82, and 8.4 kyr BP. The oldest refers to the famous 8.2 kyr BP cold event (8.2k). The problem is that the declines do not quite fit into the rhythm of the 3.65-kyr climate cycle, because their pace is roughly a hundred years faster. Despite this evident discrepancy, the general 3.65-kyr climate profile was clearly visible and paved the way for the first breakthrough.

Some climatic features that are characteristic of the multi-millennial climate cycle were weakly distinguishable as early as twenty thousand years ago, during the middle of the Last Glacial Maximum (18–23 kyr BP). The 3.65-kyr climate cycle can be divided into three phases, as illustrated in Figure 1.6: the Warming phase (orange), Plateau phase (black), and Decline phase (green). The Warming phase is the longest, typically originating from the lowest point and lasting for about fifteen hundred years. These lows of the Holocene actually correspond to 3.5-kyr multiples of the 8.2k cold event. This minor temporal discrepancy will be thoroughly reviewed at the end of this chapter.

There has been a tendency for the 1.5-kyr Warming phase to occur since the Bølling warming. This significant and abrupt event marked the end of the glacial conditions around 14.5 kyr BP in the Northern Hemisphere and initiated the deglaciation or glacial termination in the Arctic. A similar process had already commenced several thousand years earlier in the Southern Hemisphere, where the transition was much more gradual. The intriguing aspect is that the 1.5-kyr-long Warming phase in Greenland also encompasses the modern era until AD 2300. However, it is important to note that this finding is based solely on visual inspection and does not provide a scientific basis for making conclusions about future climate evolution, despite the observed cyclic nature.

The 1.3-kyr-long Plateau phase begins with an abrupt cooling period lasting a few centuries, but it quickly stabilizes, as the name suggests. The term 'Plateau' is better justified for the Holocene cycles because, throughout the deglaciation period (11–18 kyr BP), the climate experienced substantial fluctuations. However, there was a relatively stable phase called the Allerød interstadial (C5) between the short-lived Older Dryas cooling (c. 13.9–14.1 kyr BP) and the Younger Dryas cold interval, which roughly fits into the plateau series. The Younger Dryas is an extreme example of the Decline phase, which began around 2.05, 5.7, (9.4), and 13 kyr BP. These cooler phases persisted for approximately 850 years and completed the 3.65-kyr climate cycle. The Younger Dryas is not the only major event in this se-

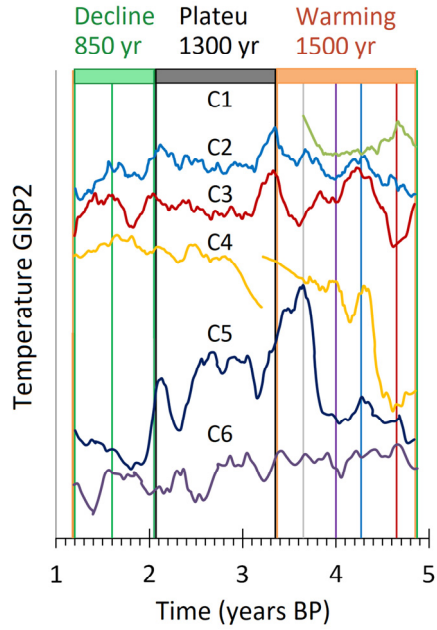

Figure 1.6. The 3.65-kyr climate cycles from 19.45 kyr BP (C6) to the present (C1) are compared to the reference period of C2 (blue). The Blue, Green and Red Columns correspond to vertical lines of the same color. Data from Alley [2004] and Box et al. [2009].

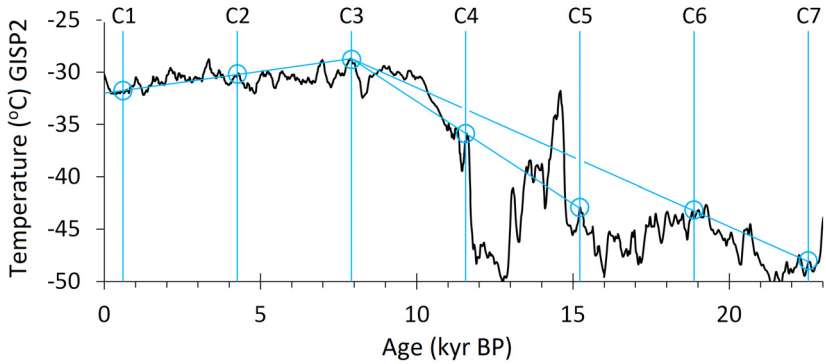

Figure 1.7. The Blue Columns at 0.60, 4.255, 7.91, etc. kyr BP have a 3655-year timespan. The 4th Blue Column marks the end of the Younger Dryas period and sets a new course for the second rising Blue line. The rising Blue trendlines intersect at the top of the 3rd Column, which also serves as the starting point for the descending Blue trendline. The data sources: Alley [2004] and Box et al. [2009].

ries; the cold Heinrich event 1 (H1) and the end of the African Humid Period (AHP) are also governed by them. While the first Heinrich event only broadly aligns with the Decline phase, it roughly corresponds to these cooler episodes. These two phenomena are extensively discussed in Chapter 4. However, an exception to this pattern arises from orbital forcing. The early Holocene warming continued for over three thousand years in central Greenland without any substantial temperature decline until the 8.2k cold event occurred. With a slight adjustment, the 8.2k cold event could be considered as completing the Decline phase of the fourth cycle (C4) and exhibiting the typical characteristics of this multi-millennial cycle. In conclusion, the climate record in central Greenland loosely reflects the three typical phases of the 3.65-kyr climate cycle since 19.45 kyr BP.

1.2.2 The Blue Column Series Coincide with the Abrupt Holocene Start

The Blue Columns reveal even more intriguing patterns prior to the onset of glacial termination. The four oldest peaks form two ascending trendlines that intersect at the warmest point of the Holocene, c. 7.9 kyr BP. Whether coincidental or not, this intersection also marks the turning point of the warming climate trend. The last three blue columns form a declining trendline with a rate of minus 0.43 °C per thousand years (see Fig. 1.7).

In comparison to Antarctica, the last deglaciation in the northern North Atlantic region occurred relatively late [Pedro et al., 2011]. When it finally transpired, the process involved turbulent climate fluctuations on a millennial scale, resembling those discovered during the stable and warm Holocene era. Eventually, the termination of the Younger Dryas and deglaciation unfolded rapidly. This abrupt warming is of similar magnitude to the Bølling warming, which commenced c. 3 kyr earlier but ultimately failed to persist [Broecker et al., 2010]. The temperature resumed its upward trajectory around 11.7 kyr BP, simultaneously marking the beginning of the second ascending blue trendline that culminated in the peak at c. 7.9 kyr BP. The Holocene climate began to stabilize, even in the northern region,

although a brief cooling episode known as the Preboreal Oscillation followed shortly after.

It was quickly discovered that the 3.65-kyr cycle is neither unique nor exclusively associated with the Northern Hemisphere.

1.3 The Blue Trendline Is Not a Coincidence

1.3.1 The Hoxnian (MIS 11)

The Milankovitch cycles offer a partial explanation for the alternating glacial and interglacial phases, which have caused sea levels to fluctuate by well over a hundred meters and sudden surges in Arctic temperatures exceeding 10 °C. However, it has not always been this way. The Middle Pleistocene Transition refers to a dramatic step-change in climate oscillations about 1.2–0.8 million years Before Present (myr BP) when relatively mild ice ages permanently transitioned into much greater ones [Feng et al., 2015]. The ice ages became colder while the interglacial periods retained their warmth. Before this transition, the climate system primarily oscillated in terms of the 41-kyr orbital obliquity cycles. Paradoxically, orbital eccentricity is calculated to be the most insignificant factor of these three astronomical cycles, yet it currently determines the interglacial frequency.

The European Project for Ice Coring in Antarctica (EPICA) was one of many of its kind, aiming to unravel the missing pieces of climate history, including, what happened during the Middle Pleistocene Transition. Antarctica can provide information on the climate even much older than 800 kyr, which is the maximum age of the EPICA Dome C (EDC) ice core [Jouzel et al., 2007]. The most recent drilling project, Beyond EPICA, is about to go even deeper than that [Dahl-Jensen, 2018]. Its ambitious goal is to reach 1.5-myr-old ice. Unfortunately, the oldest layers of the Greenland ice sheet barely encompass the last interglacial (c. 130–115 kyr BP), making the interhemispheric comparison prior to it uncertain.

The gravitational mass balance and geothermal heating modulate the internal dynamics of major ice sheets, maintaining a balance be-

tween the input of snow at the top and the output of ice at the edges. The absence of old layers in Greenland can be explained by the process in which lower layers become compressed under the increasing amount of ice above them. Layers at the bottom also slide sideways and eventually disappear into neighboring oceans. Therefore, we cannot draw precise conclusions about the profile and characteristics of the Hoxnian (MIS 11) climate as we would prefer. Specifically, it is challenging to determine whether the Greenland climate exhibited a declining trend while an increasing trend existed in Antarctica. However, North Atlantic sea-floor sediments decisively indicate a similar upward trend in temperatures despite the lack of ice-core data.

This hypothetical yet intriguing controversy between polar temperatures has been a subject of interest for the Holocene period, because the 405-kyr eccentricity cycle provides a potential link to its possible analog, the Hoxnian [Candy, 2014]. While Antarctica shows

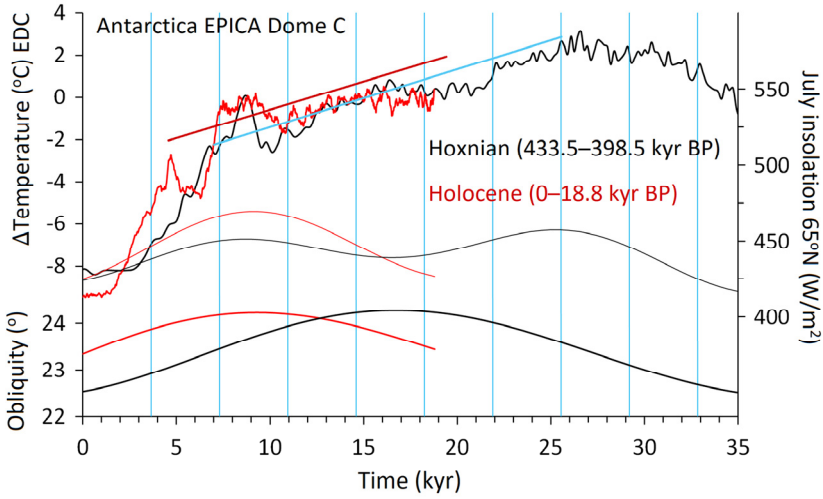

Figure 1.8. The EDC Antarctica ice-core record gives perspective on climatic variability between the Hoxnian (433.5–398.5 kyr ago) and the current interglacial through a 415-kyr cycle. The source of the data is Jouzel et al., [2007]. The orbital eccentricity cycle is close to its minimum. It will apparently produce a longer and warmer interglacial than on average, despite anything else. The astronomical parameters are from Berger [1992].

a glimpse of an ascending temperature trend over the Holocene so far, Greenland, on the other hand, shows a descending trend based on the Blue trendline (Figs. 1.7 and 1.8). Although the Blue Columns of Holocene-time Antarctica form a nonlinear zigzag pattern, they still exhibit a rising trend. When compared, it becomes apparent that the first half of the Hoxnian interglacial greatly resembles our Holocene-time Antarctica. The Hoxnian temperatures closely followed a Blue trendline during the first five cycles (Fig. 1.8), with a calculated temperature increase of 0.274 °C per thousand years.

A comparison of astronomical cycles and records from natural archives suggests that when the Earth orbits the Sun in an almost symmetrical manner, it leads to longer and warmer interglacial periods compared to the average. The available records indicate a relatively good analogy between the Holocene and the Hoxnian. Both interglacials experience a close-to-minimum 405-kyr eccentricity cycle, i.e. a round orbit, making them almost identical [Tzedakis, 2010]. Additionally, their precessional amplitudes and fluctuations resemble each other. However, a noticeable discrepancy in their climatic coherence primarily arises from differences in summer insolation (65° N) and obliquity tempos [Tzedakis et al., 2010]. During an interglacial phase, the alignment of insolation maxima and obliquity maxima is characteristic. In the Holocene, the obliquity maximum and insolation maximum almost coincide, while they are in complete antiphase during the Hoxnian. The reason the Hoxnian responded directly to the first, weaker insolation maximum also accounts for its exceptional length. A cycle of obliquity maximum spanning over two precession-driven insolation maxima is not a unique occurrence in the past two million years. Nor is it unique to have a long interglacial induced by such an occurrence after the Middle Pleistocene Transition. Similar orbital configurations have previously caused several long and mild interglacials. However, they were not as warm as the two interglacials in question, nor did they experience such significant shifts from extreme cold. Prior to the Middle Pleistocene Transition, a long interglacial did not even require the lowest eccentricity values to maintain favorable polar conditions for approximately 20,000 years.

Over the next ten thousand years, summer insolation at 65° N gradually recovers from its weak minimum but only increases moderately. The low eccentricity value limits precessional amplitude, and in combination with low obliquity, it maintains intermediate levels of high latitudinal summer insolation in the northern hemisphere. The intensity remains close to its long-term average, which could indicate a gradual termination of the interglacial period despite the upcoming obliquity minimum. The obliquity minimum typically ranges between 23 and 22 degrees, and the next incidence is close to the average [Laskar et al., 2004].

1.3.1.1 The Ascending Blue Trendline

While a Blue trendline cannot be identified in the Antarctic EDC records since the deglaciation, it does not mean that an average trendline cannot be plotted on the curve. However, the comparison in Figure 1.8 reveals that the Hoxnian climate experienced a rapid warming again due to the second insolation maximum, rather than continuing its decline. This unexpected turn of events led to another warm period lasting for 10–15 kyr. Could this indicate similar prospects for the Holocene? Unlikely, as the Hoxnian had the advantage of a 5- to 7-thousand-year gap in obliquity maxima. The 41-kyr tilt angle cycle of the Earth's spin axis still significantly influences glacial inceptions and terminations, despite the dominant 100-kyr glacial–interglacial cycle [Tzedakis et al., 2012].

One of the most intriguing phenomena of the Hoxnian Antarctica is the rapid warming around 411 kyr BP (or 22 kyr in Fig. 1.8). This is particularly fascinating because the preceding climatic progression suggests that the thermal optimum had already been reached five thousand years earlier, during the peak of obliquity. The rapid warming resembles the termination of the Younger Dryas period, characterized by a steep rise and the coincidence of the Blue Column. Was the ascending Blue trendline destined to continue for such a long period due to astronomical forcing? It appears so. The Blue trendline could have broken at any moment, but it remained on course as if a magnet had pulled the temperature curve back into line, precisely at the right moment.

After a steady progression lasting eighteen thousand years, the climate gradually entered a decline phase. The ascending Blue trendline of the Hoxnian ultimately ended around 408 (26) kyr BP. The subsequent cooling initially followed a linear pattern but became steeper towards the end. Glacial conditions were eventually reached around 393 kyr BP, after another fifteen thousand years of decline.

1.3.2 The Aveley (MIS 7)

The Aveley (c. 250–200 kyr BP) stands out as potentially the most remarkable interglacial of the past million years. It displayed contradictory characteristics in terms of amplitude and duration, almost resembling the fading echoes of the 41-kyr 'world'. A genuine glacial condition divided the Aveley into two warm phases (Fig. 1.9). Interestingly, a similar climate evolution occurred around 400 kyr earlier, suggesting a possible association with a significant orbital asymmetry around the Sun. This distortion in the Earth's orbit could be closely linked to the 405-kyr eccentricity cycle. Additionally, the deep plunge of the obliquity minimum (22.2°) during the Aveley represents one of the lowest values recorded in at least a million years and may have had a catalyzing effect.

The initial phase of the Aveley began with a rapid temperature increase, a characteristic commonly observed during the terminations of recent glacials (Fig. 1.9). In Antarctica, peak temperatures reached the thermal optimum within a single Blue Column cycle and briefly matched those of the Hoxnian. It was the Aveley's delayed response to the effect of the obliquity maximum that appears to have contributed to its steep rise and sudden end.

The Aveley indicates that once the Blue trendline is identified, it can accurately predict the end of an interglacial period, given that the temperature decline is steep enough (-0.81 °C per 1 kyr). However, this is not the case for the Greenland Holocene, as its decline rate is much smaller at only -0.43 °C per thousand years. With this rate, it would take 40 kyr for the climatic conditions of glacial times to be reached. This contradicts the evidence at the given rate, suggesting a more probable scenario for the Greenland Holocene is that changing

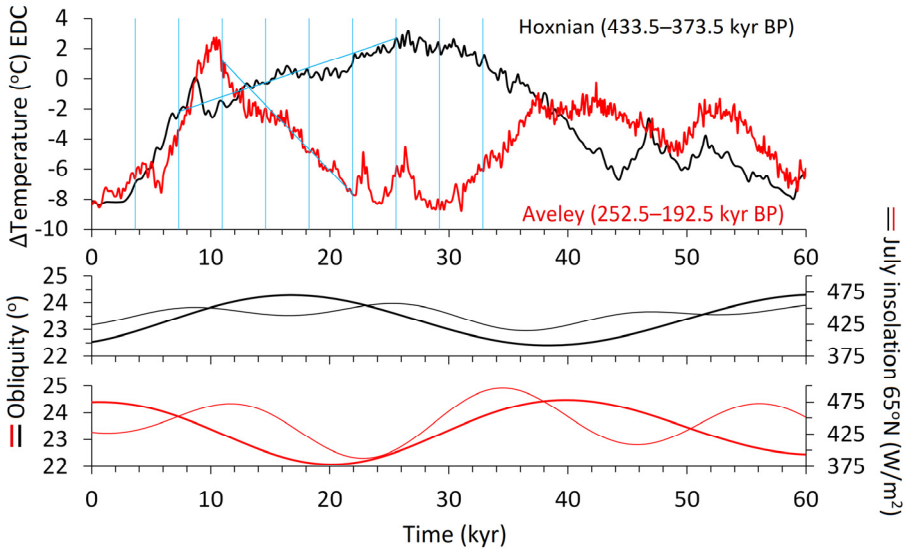

Figure 1.9. Orbital asymmetry between the Hoxnian and the Aveley reflects their climatic variability. Sources of data: Berger [1992] and Jouzel et al., [2007].

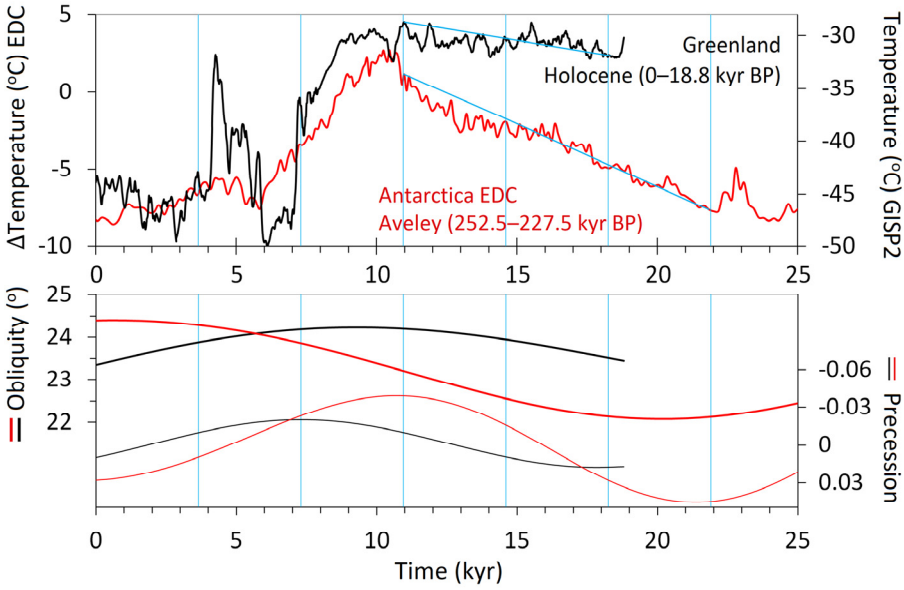

Figure 1.10. The Aveley (MIS 7) interglacial, 252.5–227.5 kyr BP (red), was forced into a steep decline trend of -0.81 °C per kyr after a conventional beginning. Sources of data: Berger [1992], Jouzel et al. [2007], and Alley [2004].

orbital forcing gradually increases the potential for abrupt mid-term fluctuations (>1 kyr) in climate. These fluctuations could be triggered by changes in external forcing (solar variability) and internal dynamics (ocean circulations) and could lead to temperatures touching glacial levels earlier than expected. Several sources have linked disruptions in ocean circulation to these prolonged cooling periods in the North Atlantic [Clark et al., 2002; Rahmstorf, 2006]. On the other hand, there could also be instances of well-above-average temperatures occasionally observed, reminiscent of the fading warmth of the polar regions.

However, it's important to note that the Blue trendline is merely a prediction. Thus, the Aveley provides insight into potential future scenarios, including a prolonged interglacial period with a gradual decline in temperature. When compared, these three interglacial periods suggest that a faster response to the obliquity maximum has resulted in a warmer and longer era.

The Earth's axial tilt is projected to reach its minimum angle in ten thousand years from now, which is estimated to worryingly increase the potential for temperature fluctuations to decrease beyond what has been thus far observed in the Holocene. Consequently, the predictability of the Blue trendline is likely to diminish after the next appearance of the Blue Column. Tzedakis et al. [2012] have suggested that glacial inceptions have been determined by obliquity minimums during the last eight interglacials.

In the Greenland record of the Holocene, the Blue Columns align with local temperature peaks, except for the last one occurring around 600 years BP, which coincided with the middle of the Little Ice Age (LIA). It could be speculated that the deteriorating climatic conditions during the Little Ice Age (c. AD 1300–1700) were influenced by the declining Blue trendline along with the overall suppressive temperature trends (Fig. 1.10). However, there is a lack of scientific explanation for this observation.

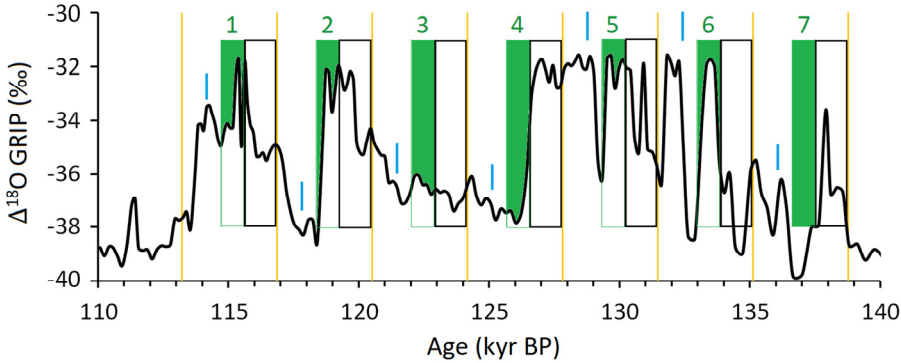

Figure 1.11. The Eemian temperature proxy (GRIP) from central Greenland, dating back to 110–140 kyr BP [Johnsen et al., 1997], implies that the climate in the Northern Hemisphere was occasionally highly unstable compared to the Holocene. There is evidence of abrupt cooling that corresponds to the Decline phases of the 3.65-kyr cycle (green field), which exhibits similarities to the Holocene. The letters 'O_{Min}/O_{Max}' refer to obliquity, and 'I_{Min}/I_{Max}' refers to July insolation at 65° N [Berger, 1992].

1.3.3 The Eemian (MIS 5e) – The Last Interglacial

Ice-core records indicate that the orbital-driven Blue trendline is generated by an eccentricity extreme, recurring every 200 kyr. However, the record may not be entirely flawless. Almost zero eccentricity conditions create an environment particularly conducive to a stable and prolonged interglacial period. The 3650-year cycle and Blue trendline provide a sense of predictability. Although it may not sound significant, a quick review of the rather chaotic last interglacial (c. 129–116 kyr BP) could make one feel fortunate today (Fig. 1.11). Predictability would have been highly appreciated during the dramatic ups and downs of the Eemian. This kind of behavior undoubtedly sparks arguments about whether the GRIP ice-core record reliably describes the last interglacial, especially when compared to the relatively stable conditions in Antarctica. However, the other ice-coring sites in Greenland (GISP2 and NGRIP) do not offer any better insights either. It is the northernmost Camp Century record that proves to be more stable and perhaps represents the most realistic climatic advancements. But even at its best, the picture of the last interglacial remains highly contradictory [Tzedakis et al., 2018; Deaney et al., 2017; Irvali et al., 2012; White et al., 1998]. The relatively good

anti-correlation that existed between polar climates during the last ice age indicates that Antarctica should have also reflected abrupt climate changes more prominently. The last interglacial, under these circumstances, does not fit into the context very well. Yet, lacking better knowledge, we are compelled to accept the data as recorded in GRIP. The main objective here is to emphasize the presence of the cycle itself rather than present an absolutely flawless temperature range for the Eemian's climatic progression.

Characteristic features of the 3.65-kyr cycle are selectively discernible in the GRIP record of the Eemian era, although the initial establishment of interglacial conditions encountered difficulties. A sudden and significant cooling event around 127 kyr BP effectively ended the Northern Hemisphere interglacial, which had barely even begun. The preceding sequence of abrupt climate swings cannot be solely explained by extraordinary solar activity events that prevailed, for instance, during the Little Ice Age. Instead, another climatic factor, related to internal dynamics, must be involved in these swings, which bear a striking resemblance to the warm Dansgaard–Oeschger (DO) events of the last ice age. Studies interpreting past climate fluctuations have shown that only modest declines and rises of around 2 °C have occurred during the Holocene, which pale in comparison to the extreme climate changes of the Eemian era. As a result, no consistent Blue trendline based on the 3.65-kyr cycle could form in this perplexing and possibly chaotic interglacial period.

Numerous abrupt coolings during the Eemian period often occurred towards the end or shortly after the so-called stable Plateau phase, which may have been rare in the case of the Eemian. These intensely cold episodes reached their lowest point at the conclusion of each Decline phase, indicating a strong association with the 3.65-kyr cycle based on current understanding. This sheds light on the division of roles between two major forces that contribute to abrupt climate changes in the northern Atlantic region. The gradual alterations in astronomical forcing tilt the balance towards the notion that the multi-millennial climate cycle is the strongest candidate for periodic abrupt changes, but grand-scale cold spells are only possible when the polar regions are insufficiently saturated with insolation to main-

tain interglacial warmth. Nevertheless, solar variability appears to exert a substantial influence, temporarily disrupting the Greenland interglacial mode during its periodic phases. These topics will be further discussed in Chapter 4.

1.4 Is There a Solar Coupling?

It is obviously impossible for orbital forcing alone to generate the frequency of climatic rhythm required for millennial variability. This leaves only a few potential alternatives, unless there are disregarded forces in the surroundings or within the system. Therefore, the search for reasons behind millennial climatic variability needs to be directed elsewhere, and what could be a more appropriate subject than the Sun? The variation in Total Solar Irradiance (TSI) is traditionally deemed too insignificant to have an impact on the global climate. However, this viewpoint has not achieved unanimous consensus [Gray et al., 2010; Haigh, 2007].

It is important to note that the solar influence may not necessarily manifest solely through global temperature changes. It can have regional effects, as highlighted by Bond et al. [2001]. The major challenge lies in the fact that the potential centennial-to-millennial solar cycles exhibit stochastic and chaotic characteristics, making their connections to climate variations highly uncertain. Here, 'stochastic' refers to the randomness in the solar dynamo system, where the amplitude and duration of the relatively regular 11-year activity cycle constantly vary [Hanslmeier et al., 2010]. These longer centennial-to-millennial cycles are thought to be the primary modulators of the 11-year cycle, but so far, they have not been clearly distinguished [Usoskin, 2008].

1.4.1 A Diversified 3650-Year Climate–Solar Cycle

Upon closer examination, it becomes apparent that the fundamental problem lies in the lack of a direct correspondence between the 3.65-kyr climate cycle and any solar activity reconstructions. However,

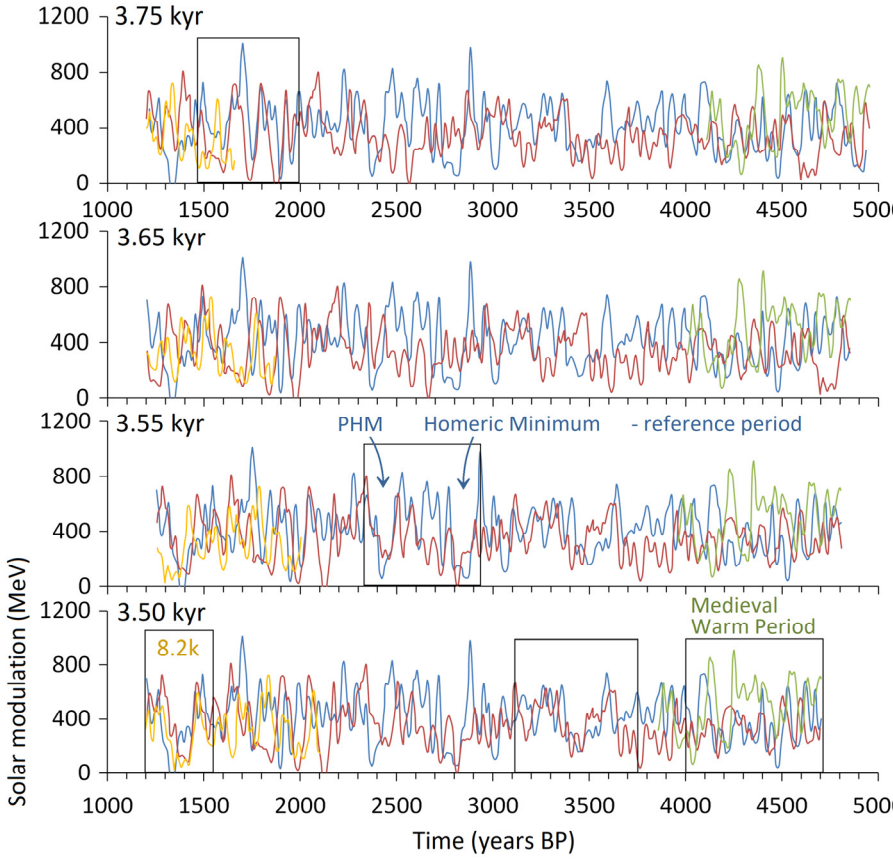

Figure 1.12. What is the actual length of the solar–climate cycle? The 3.50- and 3.55-kyr cycles exhibit multiple highly correlated phases (indicated by the boxed areas), especially due to the overlap of grand minima: the Homeric minimum (HM), the post-Homeric minimum (PHM), and the cooling event of 8.2 kyr BP (8.2k). Additionally, each 3.70- and 3.75-kyr cycle includes a well-correlating phase that persists for about a half millennium. Solar modulation data is derived from Vonmoos et al. [2006]. The reconstruction is based on the relative abundances of the Beryllium-10 (^{10}Be) isotope.

two distinct time periods stand out. Within the 3750- and 3700-year cycles, there is noticeable coherency spanning several centuries. Furthermore, even more substantial coherency is observed in slightly shorter cycles of a few hundred years (3500–3550 years), with numerous phases exhibiting a strong correlation. Together, these two cycle groups seem to encompass a substantial portion of the multi-millennial period (see Fig. 1.12). The intermittent nature of the

emerging solar cycles adds to the genuine puzzlement and calls for closer scrutiny. Nevertheless, this complex outcome is not entirely unexpected. As mentioned earlier, the occurrence of the 8.2k cold event, along with other cooling periods, already hinted at the presence of an intrinsic 3.5 kyr periodicity. Finally, there is some rationale behind the minor waxing and waning of cycles. Figure 1.12 illustrates that the Homeric minimum (HM), post-Homeric minimum (PHM), and the 8.2k cold event emerge at a regular rate of approximately 3.55–3.50 kyr per cycle. As a result, these cold events progress at a slower pace and lag behind the climatic Blue, Red, and Green Columns by approximately 100–150 years per cycle.

There is little doubt that solar variability has left a noticeable impact on the climatic history of Greenland, although its influence on Antarctica is not as clearly evident. The reasons for this controversy are discussed more extensively in Chapter 4, but the greater susceptibility of the Northern Hemisphere must have some underlying factors that differentiate it from the poles.

Based on the aforementioned findings, it appears plausible that the 3650-year climate cycle is undergoing slight changes that may bring it closer to a duration of 3500–3550 years. In light of this, the temperature record suggests that the climate could be heading towards a similar type of abrupt warming as was experienced during the Late Bronze Age (see Fig. 1.13). Interpretations of this possibility vary significantly, leading to considerable controversy. However, the behavior observed in the central Greenland climate, where it follows one periodicity for over a thousand years and then abruptly transitions to another cycle before returning, bears some resemblance to the behavior seen in solar variability. This aspect will be further explored and assessed in greater detail in Chapters 3 and 5.

1.5 A Brief Introduction to the Solar Interior

The Sun has a vast 695,700 km radius, which is roughly a hundred times greater than that of the Earth. It consists of three major zones: the core, radiative envelope, and convective envelope. Each zone occupies roughly one-third of the solar radius (Fig. 1.14). A thin yet

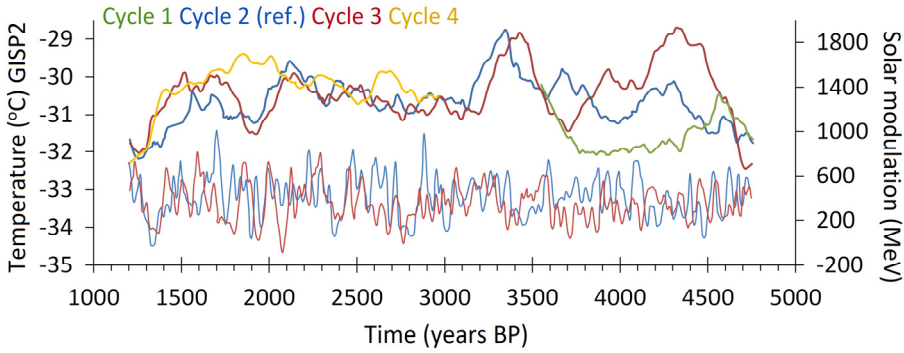

Figure 1.13. The 3.55-kyr cycle poses a challenge. Is the current climate already approaching its peak, resembling the warming seen during the Late Bronze Age around 3.4 kyr BP? Data are sourced from Vonmoos et al. [2006], Alley [2004].

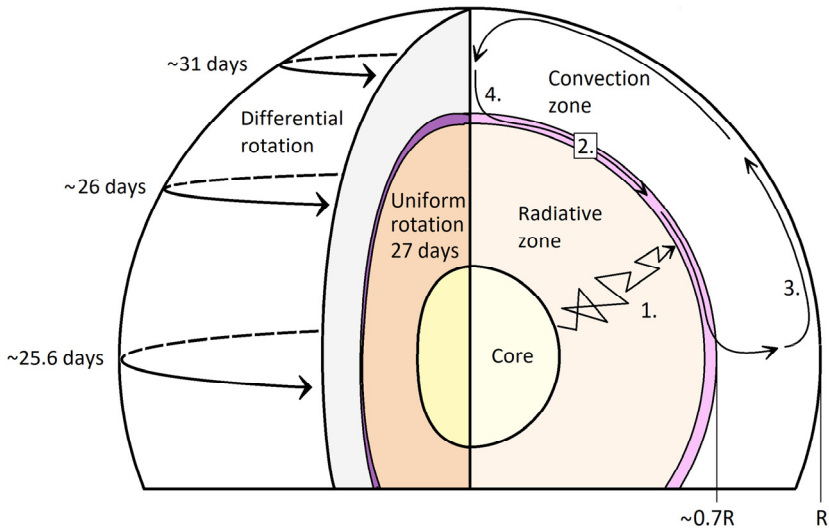

Figure 1.14. A simplified illustration of the solar interior and differential rotation. (1) The dense radiative zone prolongs a photon's journey out of the Sun from thousands of years to over a hundred thousand years. However, once at the surface, the photon reaches the Earth in 8 minutes. The rigid body of the Sun spins uniformly around its axis in 27 days. The gaseous plasma at the surface moves faster at the equator compared to higher latitudes. (2) The 11-year sunspot cycle originates c. 210 000 km below the solar surface. This is the region where the quasi-solid radiative zone and the fluid-like convection zone intersect. (3) A poleward meridional circulation near the surface moves at a rate of 20 m/s or so [Schou and Bogart, 1998]. (4) The return flow is much slower, taking about 11 years to complete the circulation at speeds ranging from 1–3 m/s [Miesch, 2012].

significant transition layer between the dense radiative and turbulent convective envelopes is known as the tachocline [Brown et al., 1989; Howe, 2009]. It occupies only 1–4% of the solar radius [Elliott & Gough, 1999; Charbonneau et al., 1999], but this global dynamo gives rise to magnetic activity and an 11-year sunspot cycle.

The location and shape of this active layer have been revealed through a relatively new field of science called helioseismology [Christensen-Dalsgaard, 2002; Chaplin, 2006]. Helioseismology studies internal conditions by harnessing and analyzing acoustic waves emanating from the solar surface—millions of different tones resonate outward, akin to 'the music of the Sun'. The interpretation of these measurements relies, to some extent, on the same physical principles employed in seismology. Helioseismic measurements indicate that the radiative zone rotates like a rigid body, possibly as a consequence of the magnetic tension exerted by the fossil poloidal magnetic field of the radiative core. This uniform rotation roughly defines the outer boundary of the radiative zone. A sharp transition from uniform rotation of plasma to differential rotation of plasma takes place between 0.65 and 0.75 R_{sun} [Kosovichev, 1996].

Differential rotation of gaseous plasma lanes is not only increasing inside spherical layers from the equator to the poles but it also occurs in radial-direction. Gaseous plasma lanes rotate at the equator around the Sun in c. 25.6 days, while the rotation period at polar latitudes is 33–36 days. It is notable that the rigid body of the radiative zone is spinning c. 1.4 days slower than the equatorial surface but, on the other hand, markedly faster than the poles.

Differential rotation of gaseous lanes at the bottom of the convection zone generates strong rotational shearing, which in turn induces toroidal magnetic fields and ultimately the sunspots. These magnetic flux tubes rise to the surface from the tachocline by buoyance and magnetic shearing. However, they must be strong enough, or else the turbulent movement of the convection zone will demolish them. Alternating toroidal (azimuthal) and poloidal (meridional) fields normally correspond to the solar cycle maximum and minimum. During the latter, the toroidal magnetic flux is stored in the overshoot region of the tachocline. Instead, the exact location of the po-

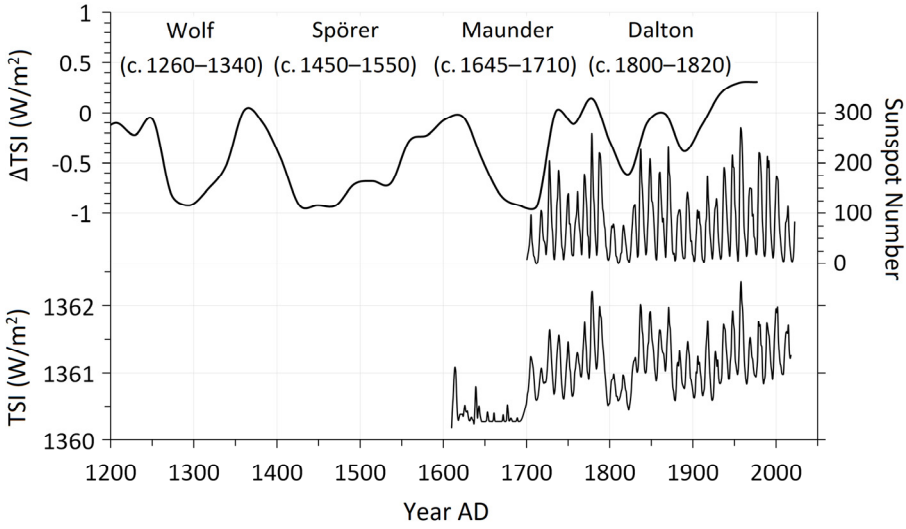

Figure 1.15. The 11-year sunspot cycle modulates the Total Solar Irradiance (TSI), which represents the total electromagnetic radiation (W/m²) measured at the Earth's upper atmosphere, at a distance of 1 AU from the Sun. The reconstructions of TSI are sourced from Steinhilber et al. [2009] and [LISIRD, Colorado USA], while the Sunspot number data is from [SILSO, Belgium].

loidal field is not known, but its existence is inevitable because both components would be unstable on their own [Braithwaite, 2009].

At the solar surface, the emerging magnetic flux bundles produce bipolar active regions. The convective heat and movement of plasma get suppressed inside, making it cooler than its surroundings. When the magnetic field strength of an active region decreases below c. 1500 gauss, the plasma is able to flow through a magnetic flux bundle. The contrast with its surroundings decreases to a level that leads to a spotless Sun (Fig. 1.15). It is estimated that a secular trend toward this boundary value exists and will be reached at the end of this decade [Penn and Livingston 2010].

A continuous stream of charged particles escapes from the gravitational field of the Sun and produces the solar wind [Parker, 1958]. The stream gets its characteristic shapes from the spinning movement and activity cycles, but is also heavily influenced by the Coronal mass ejections and flares. The solar wind plasma, being an excellent conductor, is capable of 'freezing' and expanding the open mag-

netic field throughout the solar system. This interplanetary magnetic field of the Sun is called the Heliosphere. Its varying strength, together with the Earth's geomagnetic field, modulates the intensity of the incoming flux of galactic cosmic-ray particles hitting the upper atmosphere. These collisions with atomic nuclei (predominately nitrogen and oxygen) yield a cascade of secondary particles and ultimately relatively stable isotopes like Beryllium-10, Carbon-14, and Chloride-36 (^{10}Be, ^{14}C, and ^{36}Cl) [Masarik and Beer, 1999; 2009]. These cosmogenic isotopes, or radionuclides, are transported downward by atmospheric aerosols within a few years and become stored into ice-sheet layers and tree growth-rings [Beer, 2000; Abreu et al., 2012a]. Their relatively long half-lives, ranging from several thousand years to over a million years, enable detective work on historical solar magnetic activity.

CHAPTER II

2 MULTI-MILLENNIAL SOLAR CYCLES

The multi-millennial solar cycles have, so far, received less attention because they have not been well distinguished but instead are considered chaotic and stochastic by nature. However, the c. 2.5-ka Bray–Hallstatt cycle and a phenomenon that combines several grand minima together have been recognized earlier. One of those frequent series of grand minima, including Wolf, Spörer, and Maunder, terminated the Medieval Warm Period (MWP) after AD 1250 and lasted until around AD 1700. The Dalton minimum, occurring a hundred years later (AD 1800–1820), could be considered part of this series, although it is a matter of definition. In this book, the Dalton-type brief grand minima play a minor role, but they have been addressed as a vital part of the centennial solar cycles.

Abstract

An examination was conducted to investigate the connection between the 2.4–2.6-ka Bray–Hallstatt cycle and the 3.65-ka climate cycle to confirm that the latter also originates from the intrinsic periodicities of the Sun. Solar-activity reconstructions based on cosmogenic ^{10}Be isotope data indicate that the Sun operates in 3.5-ka cycles but also intermittently in 2.50- (±0.15) and 3.75- (±0.05) ka cycles. These intermittent cycles, referred to as modules, last about 0.5 (±0.1) ka and 0.4 (±0.1) ka, respectively.

The modules act as significant disturbance factors and are the main reason why the 3.5-ka cycle loses its regular features. Because of the 250-year pace difference, the 3.75-ka module and its grand minima progress while the 3.5-ka cycle stays stationary. This perturbation module, along with the 2.5-ka module, forms a cluster every 7.5 ±0.1 ka, which is their common multiple. Surprisingly, this module, with an average periodicity of 3.75 ka, shows a pronounced

temporal coupling with the formation of ocean-floor carbonate layers near the western North Atlantic shore of Ireland. These carbonate layers, primarily resulting from massive iceberg discharges from the Laurentide ice sheet, were deposited between 16.8 and 46.7 ka BP (before the present, AD 2000) during the ice age. These layers, known as Heinrich layers, responded to the presence of every other 3.75-ka module, consistently skipping the one that formed a cluster with the 2.5-ka module. Furthermore, there is a strong suspicion that the rapid termination of the African Humid Period around 5.7 ka BP was triggered by the clustered 3.75 ka module, suggesting its significant role in influencing climate changes over the Atlantic region.

Introduction

Since the sunspot record covers roughly the past 400 years, a longer solar-activity proxy was needed to detect and confirm the intrinsic centennial-to-millennial-scale cycles of the Sun. Past solar-activity variations can be indirectly determined from the production rates of cosmogenic isotopes, such as ^{10}Be and ^{14}C. These isotopes are produced at rates comparable to the flux of galactic cosmic-ray particles hitting the upper atmosphere [Muscheler et al., 2016]. The cosmic-ray flux inversely correlates with heliospheric activity, which is generated and expanded by the open magnetic field and solar wind [Lockwood et al., 2001a, 2006]. The abundances of these isotopes, measured from ice cores, tree rings, or other natural archives, provide the basis for reconstructing past solar activity once the Earth's geomagnetic field effect has been removed [Masarik and Beer, 1999, 2009]. Several high-resolution reconstructions, covering almost the entire Holocene, are available [Vonmoos et al., 2006; Steinhilber et al., 2009; Vieira et al., 2011].

A few mid- and long-term solar activity cycles have been confirmed since Schwabe discovered the 11-year sunspot cycle in 1843 [Schwabe, 1844]. For instance, the Gleissberg 88-year cycle [Peristykh et al., 2003] and the Suess–De Vries 208-year cycle [Lüdecke et al., 2015] have been established. There have also been suggestions of longer cycles, such as the Bray–Hallstatt 2.4–2.6 ka cycle [Bray, 1968; Usoskin, 2008] and Eddy's 1-ka cycles [Abreu et al., 2010]. However,

these multi-millennial-scale cycles are commonly classified as semi- or quasi-type due to their irregular nature [Usoskin, 2008]. As the time span increases, the perturbation effect induced by other cycles also increases. This is why multi-millennial cycles tend to lose their recognizable features. This chapter aims to clarify some of the causes that transform the seemingly solid 3.5-ka solar cycle into an unrecognizable quasi-type. To understand the couplings between the multi-millennially reappearing 2.5- and 3.75-ka intermittent modules, along with the 3.5-ka main or quasi-cycle, a combined and simultaneous examination is required to reveal their stability and interactions in the long run.

2.1 Main Cycles

The shortest periods within the 3.5–3.8-ka range exhibit the best match, primarily due to the presence of three recurring grand minima that have nearly constant temporal positions. Additionally, other relevant similarities will be demonstrated (see Fig. 2.3). In this context, the three essential grand minima form two solar-activity modules: one with a single grand minimum (s3.5 ka) and the other with a double grand minimum (3.5 ka). These modules last about 150 (±50) years and 500 (±50) years, respectively. A typical 3.5-ka (Homeric) or

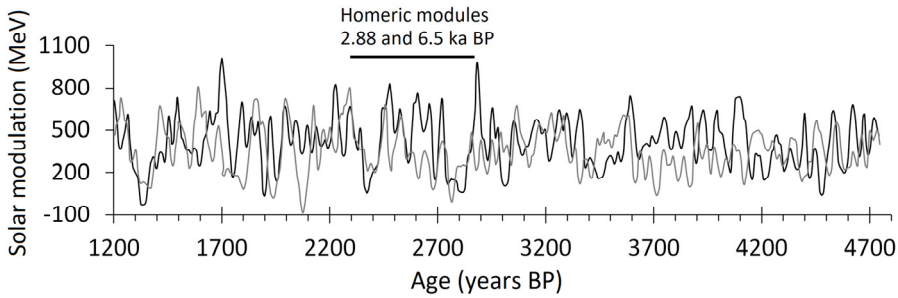

Figure 2.1. Two successive 3.55-ka periods based on ^{10}Be isotope data [Vonmoos et al., 2006]. The cycle appears to follow a 3.50-ka pace between 3.4 and 4.5 ka BP. Its three grand minima, occurring around 1.45 ka, 2.48 ka, and 2.88 ka BP, seem to align better with the 3.55-ka pace. Notably, Homeric modules are clearly superimposed between c. 2.3 and 2.9 ka BP.

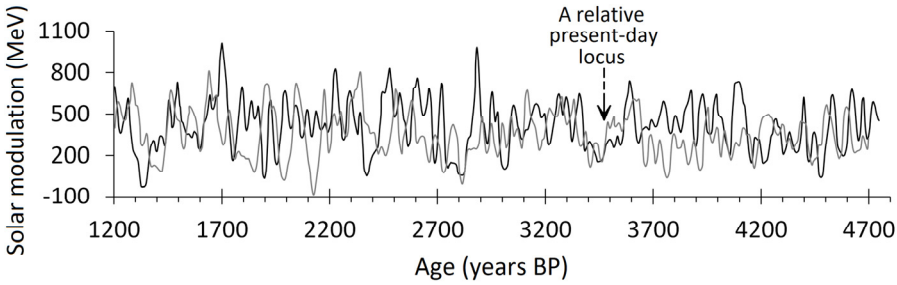

Figure 2.2. Two successive 3.50-ka periods based on ^{10}Be isotope data [Vonmoos et al., 2006]. Two partially diverging DP modules introduce prominent perturbations to the Quasi-cycle between 1.50 and 2.20 ka BP. An Oort-like grand minimum is observed around 4500 years BP, and on both sides of it, there are high-activity epochs that follow the 1.45 ka BP Cold event periodicity.

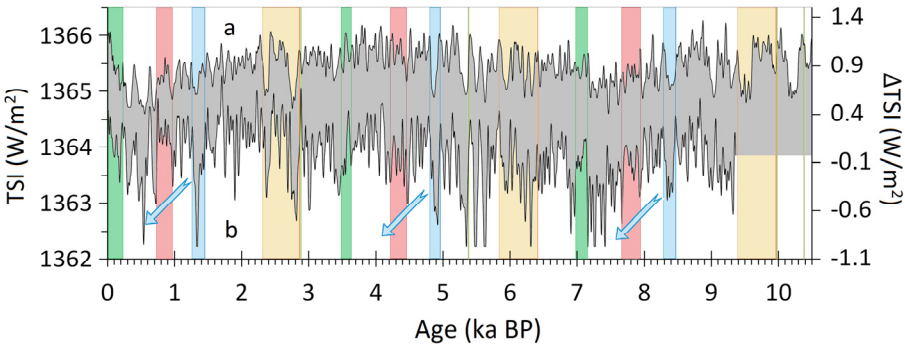

Figure 2.3. The reconstructions of Total Solar Irradiance (TSI) by Vieira et al. [2011] (a) and Steinhilber et al. [2009] (b) are shown. The regular phases of the 3.50–3.55-ka cycle are indicated by colored sections. The blue arrow represents a downward trend following the 8.2k cold event and its multiples at 3.51-ka intervals (blue field). The red field (750–1000 a BP) highlights the Medieval Warm Period. Inside the green field, starting around AD 1900, there is no decline in activity, which may be a result of the ongoing 2.5-ka module dominating since the early 1600s. The orange field corresponds to the 3.53-ka paced Homeric module. The Solar Surge events (green field) persisted for c. 150 years and coincided with abrupt warmings.

2.5-ka (Maunder) module consists of two grand minima separated by a high-to-mid-activity epoch lasting about three centuries.

The modules with a single grand minimum started around 1.45, 4.96, and 8.47 ka BP. Each module is separated by 3.51 ka (depicted by the blue field in Fig. 2.3). An interesting observation is the coincidence between the 8.2k cold event and its reappearances every 3.5-ka

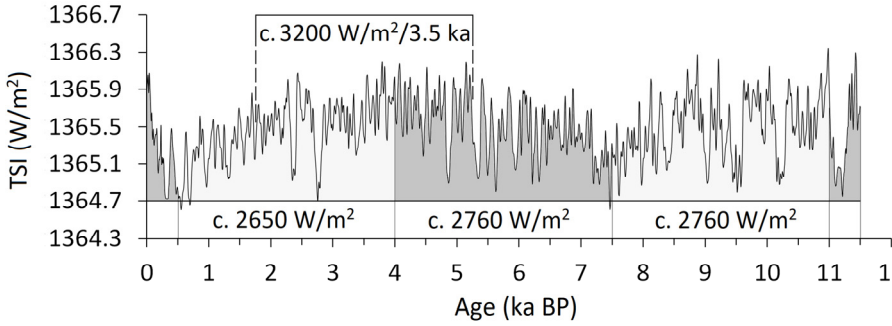

Figure 2.4. The Sun radiated a nearly equal amount of energy during the 3.5-ka intervals of 4–7.5 ka BP and 7.5–11 ka BP. In this book, the Spörer minimum and its 3.5-ka recurrences are considered the TSI minima and maxima. The TSI reconstruction is from Vieira et al. [2011].

period with these s3.5-ka modules. This regular tendency to respond to activity declines suggests a possible mechanistic pattern.

Several other periodic phases with evident similarity were found within the past 11 ka (see Fig. 2.3). For instance, the period of high activity between the Oort and Wolf minima corresponds to the Medieval Warm Period (MWP; c. 0.75–0.95 ka BP). The MWP aligns with a high-activity epoch, where the intensity varies from cycle to cycle, partly due to the 7-ka oscillations. These MWP-related high-activity equivalents are recognizable throughout the Holocene. Additionally, the high-activity epoch following the grand minimum at 1.45 ka BP (s3.5 module) represents a highly repeatable phase of the 3.5-ka Quasi-cycle, persisting for c. 200 years until it is usually terminated by an Oort-like grand minimum.

The 7,000-year periodicity in total solar irradiance (TSI) appears to be a primary driver of activity variations between the Quasi-cycles, surpassing even the combined effect of intermittent modules. In the book, brief activity segments occurring around 0.5, 4, 7, and 11 ka BP are identified as alternating TSI maxima and minima. The activity perturbations between these 3.5-ka intervals are also noticeable due to the considerable asymmetry in solar variability, particularly during the early Holocene.

Nevertheless, the calculated amounts of radiated solar energy (measured in W/m²) for each 3.5-ka interval affirm the main cycles'

stability, with short segments around these Spörer-like minima acting as pivotal moments of activity. It is worth noting that the spots of minima and maxima in the Total Solar Irradiance cycle are not fixed. For example, a Spörer-like minimum and a Wolf-like minimum did not manifest as anticipated around 4 ka BP, in sharp contrast to their substantial occurrences during the early Holocene. While such extreme events may slightly shift the dates of the 7-ka TSI minima and maxima, the impact is relatively minor (see Fig. 2.4).

In the early Holocene intervals of 4–7.5 and 7.5–11 ka BP, the radiation amounts are highly equal despite their distinct profile asymmetry. However, the last complete epoch spanning from 0.5 to 4 ka BP remained below their levels and delayed the periodic release of energy. As a logical response to the prolonged suppression of solar activity during the Little Ice Age, we witnessed an upswing in activity, higher than usual, commencing around the 1850s.

2.2 Intermittent Cycles

Two regularly emerging solar-activity phases have been identified as causing perturbations to the Quasi-cycle. These modules appear approximately every 3.75 (±0.05) ka and 2.5 (±0.15) ka and have durations of 0.4 (±0.1) ka and 0.5 (±0.1) ka, respectively. They exhibit mirror-image activity profiles, where two grand minima located at the edges of the modules are separated by a period of high activity in the middle. The modules commence with the onset of a grand minimum, followed by a 250 (±50)-year epoch of high activity.

The 3.75-ka module differs from the others in typically having three grand minima instead of two. Its peaks are usually of high amplitude and display a distinctive Double Peak (DP) profile. It also shows an authentic module character in the way it leaps forward relative to the 3.5-ka Quasi-cycle, which establishes a loose connection with the 208-year De Vries–Suess periodicity.

A precise, Double Peak comparison was carried out for the 11.5-ka TSI reconstruction [Vieira et al., 2011], resulting in a mean periodicity of 3.725 ka. After fine-tuning the two most recent modules to align on the same line, they appeared to match the approximate 3.75-

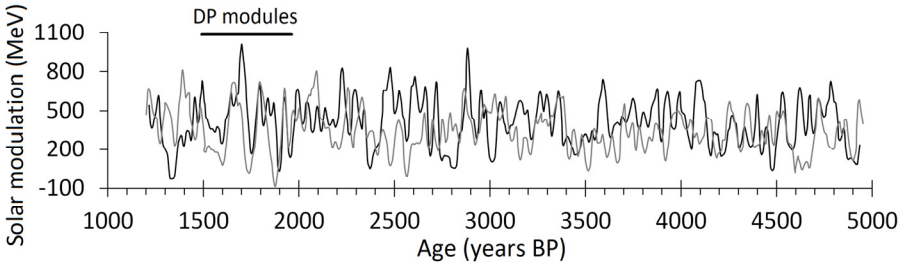

Figure 2.5. Two Double Peak (DP) modules can be observed for the 3.75-ka periods. The ^{10}Be isotope data by Vonmoos et al. [2006].

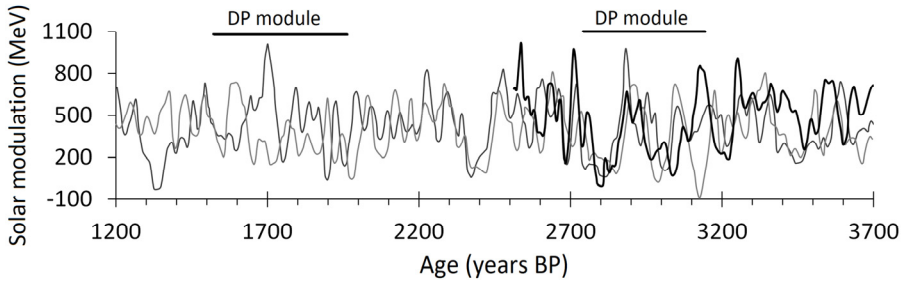

Figure 2.6. The reconstruction of the ^{10}Be isotope [Vonmoos et al., 2006; Muscheler et al., 2007] over the past 6.2 ka BP is presented here in 2.5-ka periods. The reference period from 1.20 to 3.70 ka BP is indicated in mid-grey. The end of the tail, c. 2.5 ka BP (black), corresponds to the year AD 1987. The onset of the grand minima at 2.88 ka and 2.45 ka BP separates the high-activity epoch, which lasts for about 300 years. The current 2.5-ka module, which began around AD 1610, exhibits substantial similarity in terms of amplitude, timing, and duration with the previous modules. The 3.75-ka Double Peak modules are expected to cluster around 3.2–2.7 ka BP and appear as individual modules around 2–1.5 ka BP (indicated by black lines).

ka pace. However, the two oldest modules at around 9.4 and 5.7 ka BP exhibited the best coherence with a periodicity of 3.70 ka. Consequently, based on Holocene data alone, it is not possible to determine the exact module periodicity. The 3.75-ka intermittent cycle appears to fluctuate and allows for flexible transitions to cluster with the 2.5-ka module by sharing a grand minimum.

2.2.1 2.5-ka Periods Show Module and Cycle Characteristics

The 2.5-ka Maunder module exhibits pronounced similarity to the 3.5-ka Homeric module, and interestingly, the module that begins in

the early Iron Age (c. 2.88 ka BP) is part of both series. This suggests that these modules from different series have consistently emerged together in a repeated manner every 17.5 ka, which represents their smallest common multiple. The high-activity epoch during modern times (AD 1700–2000) resembles both the Homeric module that started nearly three thousand years ago and the one preceding it. The timing of grand minima is remarkably accurate across the last three cycles, as depicted in Figure 2.6. The 2.5-ka Bray–Hallstatt cycle displays less periodicity compared to the Quasi-cycle, but it demonstrates more regularity than the proposed 0.5 (±0.1)-ka module alone. Figure 2.6 provides evidence to support this claim. However, upon increasing the number of cycles to its maximum of 4.3, only the module stands out, suggesting that the exact 2.5-ka periodicity is not sustainable. Nevertheless, a slight adjustment of ±25 years reveals that grand minima do overlap throughout the Holocene, indicating the presence of factors beyond a single periodic module.

2.2.2 The 2.5-ka Periodicity Partly Originates from the Quasi-Cycle

The two modules within the Quasi-cycle enhance the 1-ka and 2.5-ka periodicities through the regular time intervals between their grand minima. Consequently, each Quasi-cycle generates a new series of grand minima that align with the 2.5-ka periodicity (see Chapter 3 for more details). For example, notable ages such as 8.5, 6, 3.5, and 1 ka BP represent a series of both well-known and lesser-known grand minima: the 8.2k cold event, the post-Homeric multiples, the AD 2000-minimum multiples, and the Oort minimum, respectively. Numerous series extend beyond the boundaries of the Quasi-cycle, highlighting the integration of millennial cycles. These series culminate in an Oort-like minimum, as the Double Peak module following every Oort-like minimum conceals the true activity profile of the Quasi-cycle throughout the Holocene era. Therefore, in addition to the 2.5-ka module, an internally generated grand-minima series emerges every 3.5 ka.

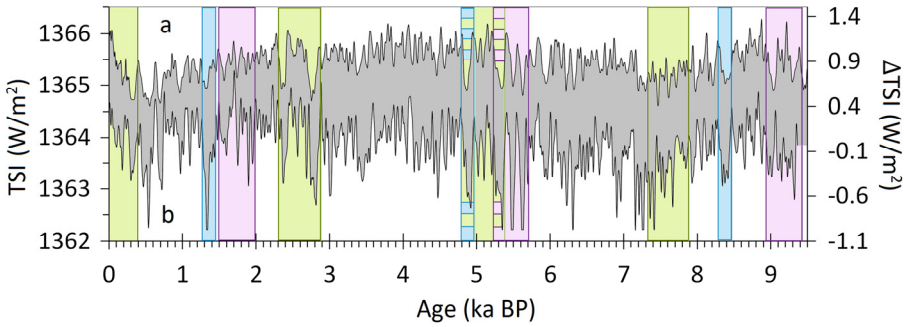

Figure 2.7. The evolution of the 2.5-ka (green), s3.5-ka (blue), and 3.7-ka (violet) modules during the Holocene is shown in TSI reconstructions from: a) Vieira et al. [2011] and b) Steinhilber et al. [2009]. The three overlapping modules created a cluster between 4.8 and 5.7 ka BP, resembling the movement of rolling cogwheels. It appears that the accurate timing, duration, and amplitude of these modules made two grand minima out of four disappear.

2.3 Cluster Formation of Intermittent Cycles

In theory, the 3.75-ka modules should accumulate within parallel 2.5-ka cycles (Fig. 2.6). However, Figure 2.6 shows the opposite effect, as the DP modules of the 3.7–3.8-ka cycles appear in their regular spot every third cycle, instead of providing support and amplifying the 2.5-ka cyclicity. Over the past 8,000 years, the Maunder module has emerged in relatively accurate 2.50-ka cycles. Nevertheless, maintaining the DP module in its constant place from cycle to cycle requires slight adjustments in the 3.7–3.8-ka periodicity, specifically small shifts every 7.5 ka. Due to the scarcity of high-resolution data, we cannot directly infer all the long-term characteristics of modules and cycles. Nonetheless, we can observe some delicate processes, such as the overlapping procedure of three modules at 5.7–4.8 ka BP. The evolution of s3.5, 2.5, and 3.7 activity modules reveals an interesting feature prior to the paleoclimatic Neo-glacial transition that began around 4–5 ka BP (Fig. 2.7). Between 5.7 and 4.8 ka BP, these modules overlapped without generating a chaotic activity signal. Instead, the outcome was expected and coherent, with each module (3.7, 2.5, and s3.5) maintaining its distinctive features and recognizable profile.

The most intriguing aspect of this process is the formation of the 2.5-ka module as a result of the 3.7-ka module approaching the s3.5-ka module. This 'evolution of approaching' narrowed the previously existing approximately 500-year gap between them to a more suitable duration of c. 300 years, autonomously generating the 2.5-ka module between 5.4 and 4.8 ka BP (green field). Apparently, in the absence of other factors, these joint grand minima would have also been generated solely by the 2.5-ka module. The integration and folding of these three modules and their grand minima into one significant cluster suggest how the mechanistic actions of the dynamo are beautifully modified by the long-term cycles.

Discussion

Based on the regular appearance of modules, it is expected that a cluster-like formation will happen again in the foreseeable future. This formation can be achieved through extrapolation. It is estimated that the latter grand minimum of the DP module (1.65 ka BP) will align with the s3.5 module (1.45 ka BP) around -2.06 ka BP, resulting in a joint grand minimum. In order to achieve this, the 200-year gap between the onsets of the grand minima would need to close. Such time-shifts are consistent with the 200–300-year movements of the DP module compared to the s3.5-ka pace.

If the regularity of the Quasi-cycle persists in the future, there will be an Oort-like minimum during which the second minimum of the Maunder component emerges. In this scenario, the 208-year cycle appears to be important as it provides flexibility for large modules to roughly emerge in their expected places. However, the past 1,500 years may be more conveniently phased for the interactions of large modules with the 208-year cycle compared to the rest of the Quasi-cycle.

The last major decline in activity began around AD 1610, leading to the nearly spotless Maunder Minimum. Consequently, it is expected that the first grand minimum of a Maunder-like module will commence around -2.10 ka BP and join the group of the other two grand minima, resulting in partial superimposition of the three modules once again. Today, there appears to be a 40-year gap between

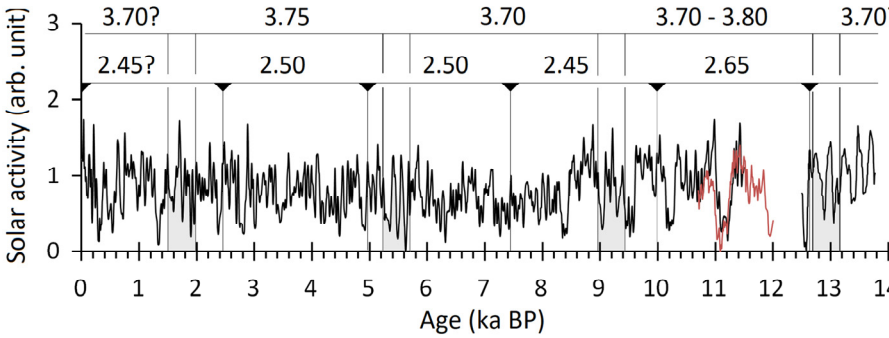

Figure 2.8. An extended solar-activity reconstruction based on 5 data sets. In the upper row, only two cycle durations of the 3.7-ka modules can be accurately determined, while the remaining ones involve speculative elements. The measurement of the last cycle is derived from ocean-floor sediments and will be discussed in the next section. It appears that the DP module's cycle length alternates between 3.70 and 3.80 ka. In the lower row, the onset of the latter grand minimum was chosen as the reference point for the 2.5-ka modules due to its clear visibility in each module over the last 13 ka BP. The three 2.5-ka cycles between 2.45 and 7.45 ka BP are associated with a 3.75-ka pace, while the shorter 2.45-ka cycle could be linked to a 3.70-ka pace. Some uncertainty exists regarding the exact onsets, timings, and durations of the modules during 12–13.8 ka BP. The red curve represents activity fluctuations during the Preboreal interval and at the end of the Younger Dryas. The reconstruction is a synthesis of data from [Muscheler et al., 2007 and 2008; Vonmoos et al., 2006; Vieira et al., 2011; van der Plicht et al., 2004].

the onsets of the upcoming grand minima. However, indications of a possible transition in periodicity, leading to perfect synchronization, may have already emerged. The previous high-activity epoch (around AD 1700–2000) started and ended approximately 40 years earlier than the two preceding Maunder modules, suggesting that the cycle length will be shortened by forty years, thereby resolving this gap dilemma.

Based on the forward extrapolation, the results further consolidate the view of a recurring cluster formation every 7.5 (±0.1) ka, comprising alternating cycles of the 3.7-/3.8-ka module (Fig. 2.8). The stage is set for the next DP module to close the 200-year gap and form a shared grand minimum. However, a question arises as to whether a suitable difference in the gap may predefine the actual shift length of the module or if it is merely a potential. How inevitable is the trajectory that the Sun has set for itself, and is it already ir-

reversible? This question is relevant because crossing over the double peak formation at the end of the next cycle necessitates a closer 300-year shift instead of the norm value. The norm shift could potentially disrupt the delicate DP profile. Some evidence supporting a larger leap can be found in the pre-Holocene era, as illustrated in Figure 2.8.

An analysis of the Younger Dryas–Allerød interval using ^{14}C data from Muscheler et al. [2008] reveals the existence of the c. 7.45-ka cluster during that time. However, the Double Peaks of this cluster were not well-formed. Additionally, it took an unusually long time for the joint grand minimum to reach a minimum level of activity, and it did not last very long. On the contrary, it seems likely that around 13.2 ka BP, the commencing DP module abruptly terminated the high-activity epoch of the 3.5-ka module after a 160-year run. This is another instance of the Sun's unsuccessful attempt to form a joint grand minimum between different cycle groups. These events are too infrequent to draw further conclusions based on the currently available cosmogenic isotope data. Eventually, as more data with higher resolution becomes available, more clusters will be unveiled, and it must be acknowledged that new examples may invalidate some of the existing concepts.

The s3.5 module also plays a part in these dynamics, despite its consistent appearance during the Holocene. The question arises as to whether it exhibits flexibility when required by other cycle processes or if, as might be the case, the modules of the Quasi-cycle do not easily compromise with the intermittent cycle group, as the tentatively shared Homeric module suggests. At present, there is no clear understanding of what defines a successful configuration in the Sun that guarantees a perfect overlapping.

2.3.1 Evolutionary Pace of the Double Peak Module

Significant instabilities in the North Atlantic ice sheets have periodically led to massive ice-rafting events, most recently during the last ice age [Heinrich, 1988]. Discharged icebergs carrying lithic grains have added ice-rafted debris (IRD) layers to the ocean-floor sedi-

ments. These so-called Heinrich layers contain varying amounts of ash shards, volcanic material, quartz, and dolomite carbonate, among other components, depending on their place of origin. However, the presence of carbonate layers is primarily associated with the North American Laurentide ice sheet.

The carbonate layers recovered from the core MD01-2461 [Peck et al., 2006], located in the eastern North Atlantic (51º 45´N, 12º 55´W), were found to consistently coincide with the DP modules (Table 2.1). Matching the carbonate layers with the 3.72 ka pace showed that their temporal difference varied from -100 to +260 years, which had somewhat better coherency than the 3.75 ka pace for the 2–54 ka BP interval. As such, this startling discovery could help to determine the mean pace of the DP module in the long run. Therefore, this remarkable discovery has the potential to contribute to determining the average pace of the DP module in the long term. These findings are consistent with those of Bond et al. [2001], who demonstrated a significant correlation between cosmogenic isotope abundances and drift-ice records throughout the Holocene period.

When discussing the Sun, the concept of the 'long run' is highly relative, but it is now possible to challenge the perception that a module exclusively existed during the Holocene. Furthermore, there appears to be a notable temporal connection between the discharge of icebergs from the Laurentide ice sheet, the DP module, and the accumulation of ice-rafted debris layers on the coast of Ireland. The carbonate-rich layers dating back approximately 16.9, 24.3, 39.3, and 46.7 ka BP can be considered as part of the true Heinrich events (H1, H2, H4, and H5) respectively. Although the H3 (31.8 ka) and H5a (54.0 ka) events are also regarded as Heinrich events, they lack carbonate content, suggesting either their debris layers originate from elsewhere or their carbonate layers do not extend as far into the eastern North Atlantic [Hemming, 2004]. The classification of the Younger Dryas (c. 12.9–11.8 ka BP) as a Heinrich event (H0) remains controversial [Alley, 2000; Andrews et al., 1995]. Although relatively abundant ash shards clearly link the Younger Dryas to events such as H3 and H5a, it is not widely accepted as a one. The Heinrich events (H1–H5a) appear to have consistently responded in relation

to every other DP module, excluding the Younger Dryas. However, the definition is not overly strict, as the distribution of lithic grains is not uniform across the North Atlantic.

Another intriguing temporal correlation was discovered in the sedimentary records off the coast of West Africa, specifically at the ocean-drilling site 658C (refer to Fig. 4.9). This finding may give rise to speculative thoughts regarding the function of the DP module as a trigger for global-scale climate change. For instance, around 5.7 ka BP, there was a shift in northern African weather patterns, leading to the sudden end of its humid period [deMenocal et al., 2000]. Interestingly, this aridification process coincided with the onset of the DP module, suggesting its potential influence as a trigger. However, it is important to note that the reverse phenomenon occurred within a few thousand years and involved two abrupt steps around 12.3 and 14.5 ka BP at site 658C (20.8° N). Additionally, there is evidence of increased ice drift in the northern North Atlantic during this period (6–5 ka BP) [Moros et al., 2006], indicating that despite warmer conditions and receding sea ice, the module still induced climate anomalies.

Table 2.1. The onset dates of the accumulated ocean-floor carbonate and non-carbonate Heinrich layers (site MD01-2461) and the 3.72/3.75-ka solar-activity cycles are compared. The results indicate that massive discharges of ice-rafted debris during the last glaciation were synchronized with every other DP module. However, the Younger Dryas, which is a debatable Heinrich event, deviates from the 7.45-ka periodicity as it followed H1. A starting point of 2 ka BP was utilized for both module series.

Heinrich Event	MD01-2461 site carb. and non-carb.*		Module of 3.72 ka	Difference	Module of 3.75 ka	Difference
	Age (ka)	Age (ka)	Age (ka)	Δ Age (ka)	Age (ka)	Δ Age (ka)
H0		13.00	13.16	0.16	13.25	0.25
H1	16.90		16.88	-0.02	17.00	0.10
H2	24.30		24.32	0.02	24.50	0.20
H3		31.50	31.76	0.26	32.00	0.50
H4	39.30		39.20	-0.10	39.50	0.20
H5	46.70		46.64	-0.06	47.00	0.30
H5a		54.00	54.08	0.08	54.50	0.50

*non-carbonate means vulcanic debris or ash shards or both

Whether something profoundly different happens in the Sun while it shifts from one multi-millennial cycle to another is beyond the author's knowledge. Nonetheless, it is reasonable to question whether proxy records of solar activity provide any clues about unusual processes. According to Muscheler et al. [2015], intense solar storms do leave detectable traces in ice cores. Two notable solar storms have been identified in the years AD 774 and AD 993. However, no evidence of unusual behavior has been found around 2 ka BP, which roughly corresponds to the initiation of the last DP module. Exceptional solar events have also been witnessed in more recent history, such as the 'white' light solar flare of AD 1859 observed by Carrington. The magnitude and scale were so immense that the resulting geomagnetic storm was observed at mid- and low-latitudes several hours later as the aurora borealis [Green et al., 2006; Shea et al., 2006].

2.4 Module Inceptions and Precise Cycle Durations

2.4.1 A Moment of Breakthrough

An examination of the recently published ^{10}Be reconstruction by Adolphi et al. [2018] led to a significant breakthrough in determining the precise pace of the module. The discovery of a 7.5-ka cluster between 43.3 and 42.5 ka BP confirms the long-term sustainability of this pattern (refer to Fig. 2.9). The Maunder-module component within this cluster demonstrates the remarkable accuracy of the MMSCs, as it precisely follows a 2.5-ka periodicity. In total, 17 cycles fit within the range of 0.39 to 42.95 ka BP, resulting in an average cycle length of 2.503 ka for consecutive Maunder-like minima. It is important to note that the variability over the last 14 ka has been relatively large (±150 years). Furthermore, it appears that the most plausible explanation for the timing is that a Spörer-like minimum was seamlessly incorporated into the end of the cluster, forming its Maunder component. On the other hand, the DP module apparently caused disarray in the periodic, grand-minima order during the me-

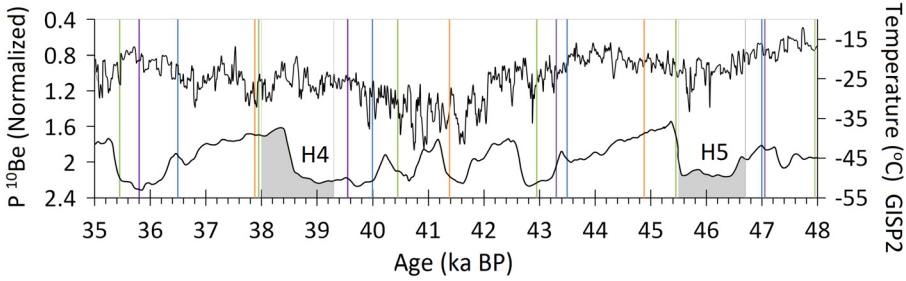

Figure 2.9. Solar activity is represented by the production rate of the Beryllium-10 isotope [Adolphi et al., 2018], while the central Greenland temperature is based on data from Alley [2004] spanning from 36 to 48 ka BP. The clustered DP–Maunder module at 43.3/42.95 ka BP is used as an anchor point for extrapolation. The exact periodicities of the s3.5-ka and 3.55-ka modules were not entirely clear during the Holocene. However, longer-term measurements from anchor points at 1.45 ka and 2.88 ka BP to module onsets at 29.55 ka and 41.41 ka BP, respectively, suggest that both modules adopt the same periodicity as the 3.5-ka Quasi-cycle. The deposition of Heinrich 4 and 5 layers on the Irish coast [Peck et al., 2006] appears to have commenced during the second half of the DP module. It seems that a strong Solar Surge equivalent terminated the cold H4 stadial around 38.6 ka BP or so, as there is evidence of notable activity during that time.

dieval-like, high-activity epoch. Either one may not come as a surprise.

This magnificent finding demonstrates the genuine coupling of the modules, and the 7.5-ka cluster is a consistent component of the Multi-millennial solar cycles, despite the fluctuations, variations, and continuous profile changes of the DP module. It also confirms that short-term variations over the past 14,000 years are compensated for in the long run. In light of this new evidence, it is advisable to utilize the 7.50/3.75/2.50 ka cycles when examining time spans exceeding 10,000 years.

2.4.2 Closure of the 52.5-ka Loop

The existence of the Maunder module as an independent entity, similar to the Homeric module, remains somewhat uncertain. Its occurrences appear to depend on the interplay between the grand minima of the Quasi-cycle and the 208-year cycle. However, its existence also relies on the coordinated interaction of the DP module with the

grand minima of the Quasi-cycle, as observed at 5.7 ka BP. While the rotation of its minima remains within a limited range, the extent of occasional significant deviations is more speculative than known.

Fitting together the 250- and 500-year shifts of the intermittent cycles with the general 208-year periodicity involves a systemic problem, although large modules on each side of cyclicity are inherently built on the latter. The Quasi-cycle over the past 1,500 years has mostly provided the desired flexibility (Fig. 2.10), but the remaining period (excluding the Homeric module) may be less suitable for accommodating the 250- and 500-year shifts and the emergence of the DP cluster on top of the predictable grand minima. This perception stems from the understanding that the intermittent cycles are likely to substantially reduce activity and thereby alter the released energy, which is normally influenced by the smoothly shaped 7-ka Total Solar Irradiance cycle described in Fig. 2.4.

The existence of the Maunder module is based on several hypotheses. The first hypothesis relies heavily on the observation that the spotless phase of the late 17th century should not have appeared as a regular part of the Quasi-cycle. However, some grand minima exhibit greater variability in amplitude over cycles than others. Particularly near the extremes of total solar irradiance, the Maunder and Spörer minima may not stand out or regenerate as effectively as others due to the markedly lower or higher base-level activity surrounding them. Another hypothesis is based on the discovery of three accurately dated cluster formations and the logic behind their rotation mechanism. Moreover, it seems that a partial overlapping of the Maunder and Homeric modules took place in the early Holocene (10 ka BP), but it likely partially failed, as will be discussed later.

When a joint or normal grand minimum of the intermittent cycles coincides with a consistently higher activity period, such as the Medieval Warm Period (MWP; c. AD 1250–1000), the outcome is largely unknown. The example discovered around 43 ka BP provides insight into a possible scenario (see Fig. 2.10). The habit of the intermittent cycles modifying their surroundings resembles the case already familiar from the mid-Holocene, around 5.7 ka BP. However, it could

Table 2.2. Pattern recognition for module dependencies and extrapolated module inceptions over the time span of -2–25 ka BP. The letter 'c' refers to cluster formation, and 's' denotes a singularly emerging DP module. The gap between modules is indicated by smaller font sizes. The dates with grey backgrounds were inferred and extrapolated.

Module															
2.5 ka	-2.10	0.39		2.88	5.40	7.90		10.32	12.97	15.40		17.90	20.40	22.90	
		2.49	2.49	2.52		2.50	2.42	2.65		2.43	2.50	2.50		2.50	
		c	s		c		s		c		s		c		s
3.75 ka	-1.75	3.73	1.98	3.74	5.72	3.67	9.39	3.81	13.20	3.75	16.95	3.75	20.70	3.80	24.50
3.5 ka	-0.60	3.48	2.88	3.52	6.40	3.59	9.99	3.52	13.51	3.39	16.90	3.50	20.40	3.50	23.90
s3.5 ka	-2.05	3.50	1.45	3.51	4.96	3.51	8.47	3.58	12.05	3.45	15.50	3.50	19.00	3.50	22.50

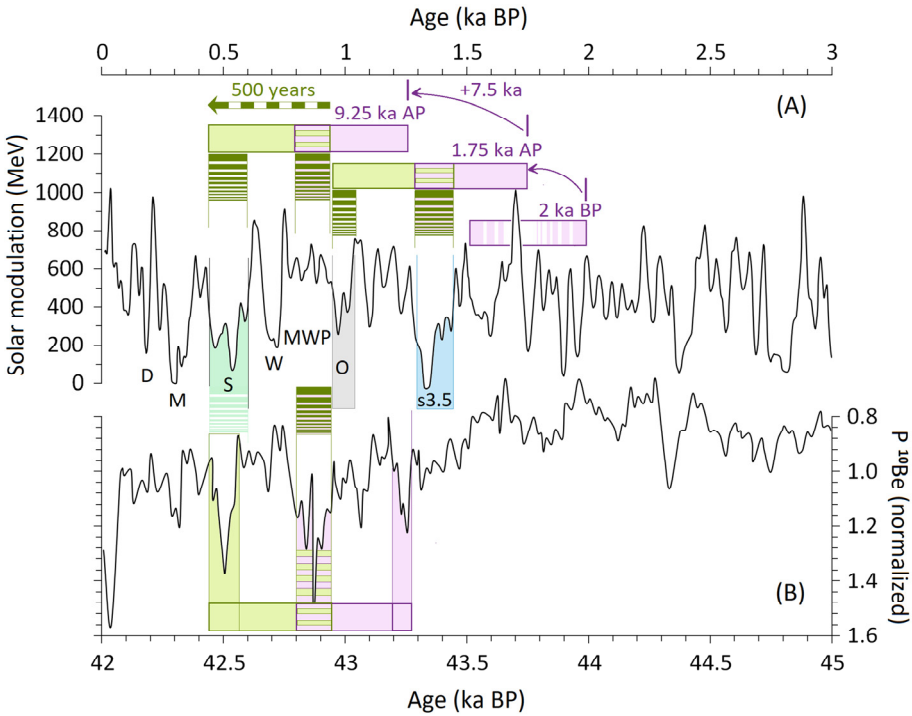

Figure 2.10. (A) An illustration of the anticipated evolution of the DP-clustered Maunder modules and their potential interaction with the Medieval Warm Period (MWP) and Little Ice Age (LIA) interval around 1.75 and 9.25 ka after present (AP). (B) The confirmed DP cluster around 43.3 ka BP may complete its 52.5-ka journey within the Quasi-cycle, as theorized, around 9.25 ka AP. Sources of reconstructions: (A) a synthesis of Muscheler et al. [2007] and Vonmoos et al. [2006]; and (B) Adolphi et al. [2018].

be argued that this well-known activity segment, mainly characterized by mean variability, was more susceptible or adaptable to modification by the DP cluster than the MWP–LIA interval, which features stark, distinct, and repeatable events. The activity interval from 1.5 to 2.3 ka BP appears remarkably stable without the presence of the DP module, which may potentially hide at least one mean grand minimum around 2 ka BP.

It is unlikely that the shifts taken by the Maunder module over time relative to the Quasi-cycle are utterly fixed beforehand. However, understanding the degree of true variability is crucial to achieving success with probabilities and comprehending the fundamental behavioral mechanism behind the rotation. If the Homeric–Maunder modules completely overlap every time, it is possible that partial overlaps do not exist, as the 500-year leap is equally long as the Maunder module itself. However, the example at 10 ka BP does not unambiguously support this notion. We will further examine this later.

2.4.3 Durations and Couplings of the Theoretical Cycles

Solar activity shows remarkable multi-millennial periodicity, which contributes to the presence of patterns. By utilizing precisely dated ocean-floor sediments, it becomes possible to deduce and calculate the probable starting dates for past and future modules, as depicted in Table 2.2. Notably, there appear to be relatively stable time spans of 1.6/0.9-ka and 0.3/2.2-ka between the DP and Maunder modules when scaling backward. It is worth mentioning an intriguing trend regarding the widening time span of the DP modules' grand-minima inceptions over the past four DP modules. This gap expands from 0.23 ka to 0.33 ka between the Younger Dryas and AD 20. This widening, in conjunction with the relatively constant 250-year leap per cycle, seems to offer flexibility for the DP module to overlap its grand minima with other modules and form clusters with the s3.5 during the Holocene. Consequently, an adaptive process ensures that the subsequent cluster takes shape, despite the minor asynchrony among modules.

How long does it take for the DP module to complete a Quasi-cycle? A simple calculation yields 52.5 ka [3.75 ka x (3.500/0.250)], which is theoretically accurate, but what about in practice? As discussed earlier in the Discussion Section and illustrated in Figures 2.7 and 2.10, the overlap between the s3.5-ka module and the later grand minimum of the DP module is bound to happen around c. -2.1 (-1.75) ka BP. Additionally, it appears highly likely (Fig. 2.9) that the s3.5-ka module and the former grand minimum of the DP module overlapped at c. 47.05 ka BP. However, the profiles are too vague to be entirely certain, although the confirmed neighboring modules and their temporal placements strongly suggest this. In conclusion, similar positioning of solar modules (including the 7.5-ka cluster formations) began around c. 50.8 and -1.75 ka BP, resulting in a 52.55 ka interval between them. Since the extent of their overlap cannot be determined, it remains uncertain whether the circle is complete or not. Nonetheless, dividing the number by 15 cycles gives an average of 3.503 ka per cycle, which is likely very close to reality.

Theoretically, the 2.5 and 3.5-ka modules overlap every 17.5 ka, while it takes 52.5 ka for the 3.75-ka module to complete a full Quasi-cycle. Therefore, in theory, the 17.5 ka loop should close itself three times before the full circle (17.5 x 3 = 52.5) is completed, and the solar module setup becomes identical once again. However, in this case, the 7-ka TSI cycle is uneven, resulting in a total period of 105 ka to regain a similar activity setup in theory. It is a phenomenally long time, comparable even to the duration of the orbital eccentricity cycle. A table encompassing all the multiples is placed at the end of this chapter (Table 2.3). Below are the multiples for the modules forming the activity loops.

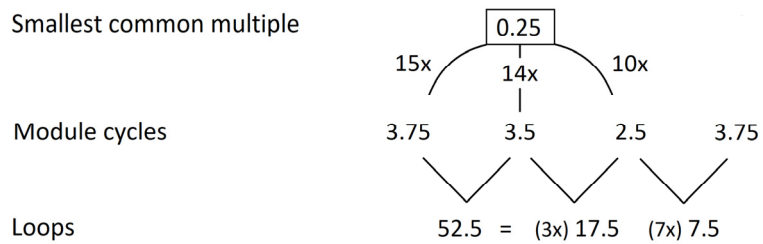

The common multiple among the multi-millennial cycles is 250 years, which does not correspond to any previously known centennial cycle. This discrepancy prompts us to study the characteristics of the Sun, such as solar mass, rotation rate, or the proportions and properties of the convection zone, to understand the possible reasons behind this peculiar multiple. These factors are known to be significant in determining the strength of the global magnetic field [Donati and Landstreet 2009; Reiners 2012; Brun et al., 2017]. Are the ratios of the millennial-scale magnetic cycle durations unique or common parameters for an active star, and can these ratios be scaled based on specific characteristics? Complex numerical patterns like this are rarely observed in nature, and the underlying explanation for their synchrony will likely remain elusive for the time being. According to Berdyugina et al. [2002], an analogous 11-year sunspot cycle was discovered in an active solar-type dwarf star. Their group reported a variation period of 15 years in mean brightness and a modulation cycle of 7.7 years. Although this does not directly answer the question, it highlights the expected diversity in cycle durations.

A vast array of different millennial cycle combinations can be generated by altering the common denominator while maintaining the same multiple patterns observed in the Sun. It would be remarkable if such an elegant number became essential among all the available options without any significance in a broader context. However, from the perspective of the Sun, one Earth year holds little relevance in any aspect. Therefore, the value of 250 years may seem as arbitrary as its conversion to 91,312 days. It is important to note that the number of days per year has changed over geological time, whereas the orbital period has evolved very little, if at all. A study has indicated that 70 million years ago, Earth days were half an hour shorter as a result of faster spinning [de Winter et al., 2020]. Thus, it is not the number of days that matters in this context.

The interaction between the Sun and planets has sparked debates regarding Jupiter's 11.9-year orbit. However, given the numerous moving bodies in the solar system, it is likely that with various combinations, there will always be approximate matches. Nevertheless, it is worth noting that the most distant planet Pluto has an orbital peri-

od of c. 248.6 years, which resonates with Neptune in a 2:3 ratio. The orbital period of Pluto yields multiples of 10.06, 14.08, and 15.08, which could potentially align with the MMSCs, albeit with some deviation. Explaining how Pluto could serve as the pacemaker of the MMSCs, or vice versa, would be an arduous task.

In a direct numerical simulation of a convection-driven dynamo, there is a suggestion that long-term cycles could reside at the bottom of the convection zone [Käpylä et al., 2016]. However, it remains uncertain whether these cycles are sustainable. The simulation only covered a duration of two millennia due to the computationally intensive nature of the work. To accurately simulate solar activity variations, a dynamo model must consider the MMSCs, despite the unknown mechanism of their propagation. The coarse modulation of the 11-year sunspot cycle is now understood as a consequence of the MMSCs' influence. Specifically, the prolonged periods of suppressed activity serve as significant indicators of the MMSCs. Their unique characteristics form the basis for constructing a probability pattern, which can be utilized for long-term predictions.

The MMSCs can elucidate the formation pattern of the grand-minima phenomenon. However, what explains the origin of the MMSCs themselves? Two distinct cycle-group systems operate concurrently and intermittently, tightly linked through actions recorded in the imprint (Fig. 2.11). The occurrence of prolonged states of suppressed activity, as witnessed in the past millennium, is not as frequent as one might assume. There have been instances, such as during the early Holocene, where a 700-year span transpired without substantial hibernation in solar activity. Perturbation modules restrict the progression of the cycles, while the main cycles establish maximum durations. Interestingly, the presence of a prolonged, high-activity epoch can be inferred from the MMSCs.

The auto-correcting nature of the MMSCs ensures their accurate pacing in the longer term (>40 ka), indicating that the cycles are primarily independent of each other's influence, although not necessarily entirely so. Consecutive cycles may experience perturbation waves that propagate through them, manifesting as waxing and waning phases. The origin of these perturbation waves, whether

from the cycles' source itself or interactions with the surroundings, remains unknown. However, the long-term stability suggests that the source or breeding mechanism is self-sustaining, despite the harsh circumstances within the solar tachocline.

2.5 A Hypothetical Evolution of Module Overlappings

The interaction between the 3.75-ka and 3.5-ka modules presumably occurred during three cycles in the 14th, 17th, and 21st millennia BP. Figure 2.12 provides a schematic illustration of their evolutionary bypass. On the left side of the figure, we observe the final phase of the series, where a leap of 200–300 years marked the end of the high-activity epoch around 13.2 ka BP. However, what precedes it is even

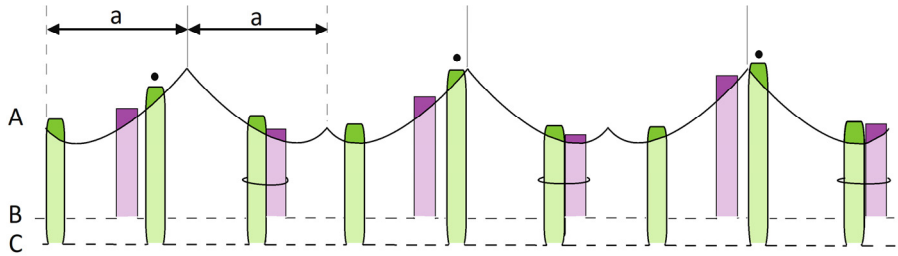

Figure 2.11. Two cycle–group systems are operating side-by-side in a continuous and intermittent manner: (A) the combined quasi- and TSI cycle, (B) the 3.75-ka module, and (C) the 2.5-ka module.

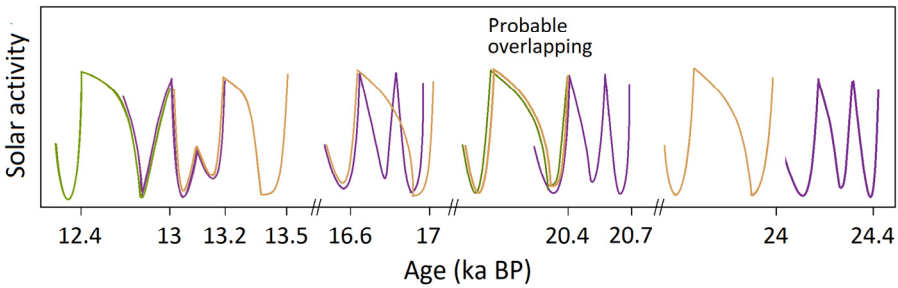

Figure 2.12. A schematic illustrating the potential evolution of the 3.75-ka module bypassing the 3.5-ka module during three cycles in the 14th, 17th, and 21st millennia BP. If the 2.5-ka module (green) and the 3.5-ka module (orange) overlapped by sharing both of their minima in the 21st millennium BP, then a genuine 17.5-ka loop between them would indeed exist.

more intriguing. Considering the periodicity over the Holocene, it is expected that the 3.75-ka module could not have made a leap of c. 400 years, which would have maintained both module profiles intact.

The most intriguing question pertains to the interaction among the three major modules during the 21st millennium BP. Did the 2.5-ka and 3.75-ka modules form the anticipated cluster, and did the 2.5-ka and 3.5-ka modules completely overlap, sharing their respective grand minima as observed during the Homeric minimum around 2.88 ka BP? This triple cluster represents the culmination of a substantial amount of information, providing insights into coincidental overlapping versus functional overlapping and the underlying purpose served by the latter through a successful rotation event.

A significant amount of interest also arises from the evolutionary expansion of the gap between grand minima within each DP module since the onset of the Younger Dryas. This gap seems to offer flexibility for module–module interactions, even though the widening trend persists independently of attachments to other modules. The extrapolated beginnings suggest that the distorted DP module around 13.2 ka BP is linked to a perturbation wave of c. 100 years and could serve as the starting point for a sequence of modules with an increasingly wider gap between the starts of grand minima. It is important to be cautious about overanalyzing past changes without considering error margins. What can be said with any certainty still largely depends on the accuracy of dating methods.

Despite the remarkable discoveries mentioned earlier, uncertainties persist, particularly regarding the randomness of module interactions or, more specifically, module overlaps. As deduced earlier, the joint Homeric–Maunder module should have occurred around 37.9 and 20.4 ka BP, based on the 17.5-ka loop (refer to Fig. 2.9). Annoyingly, the extrapolated pace of the c. 2.5-ka module from the identified 7.5-ka cluster (c. 43.3 ka BP) appears to be slightly ahead of the onset of the 3.5-ka module (c. 100 years). However, upon closer examination, a typical, intact 3.5-ka module profile emerges, which would be unusual if the 2.5-ka module had truly preceded it and exposed it to perturbation. These findings suggest that the modules are

one and the same at around 37.9 ka BP. The same solar activity proxy employed by Adolphi et al. [2018] also suggests the possibility of a perfect overlap occurring around 20.4 ka BP, based on the same argument regarding the typical activity profile. The probability of anticipated module overlaps taking place is relatively high, given the proven accuracy of millennial cycles. However, there are a few compelling examples that counter the notion of predetermination, as outlined below.

2.6 The Dual Character of the 2.5-ka Periodicity and Its Interactions with the Quasi-Cycle

The 2.5 and 3.75-ka modules have the potential to form a permanent pair every 7.5 (±0.1) ka. Unfortunately, the pacing of the MMSCs during the Holocene is such that we can observe only one pair. The ability of their cluster to tolerate module shifts and perturbation waves is another question, but within the error margin, it can be concluded that the Maunder and DP modules are likely to form another integrated pair around -1.7 ka BP. Moreover, they likely emerged together during the early Younger Dryas period, specifically between 13.2 and 12.4 ka BP. The claim is supported by the changing profiles in the DP module. In subsequent cycles, the grand-minima inceptions at the edges of the module get progressively spaced, approximately 30 years apart per cycle (see Table 2.2).

In some DP modules, pinpointing the exact starting point proves challenging. However, a noticeable long-term trend has emerged over the past 14,000 years. The gap between grand minima inceptions continues to increase, regardless of whether a singular or clustered DP module is examined. This counters the notion of an adjusting tendency within the DP modules and, instead, highlights the unifying characteristics of these millennial cycles. The recalibrated carbon-14 reconstruction presented by Muscheler et al. [2008] covers a period from the Older Dryas (around 13.9–14.1 ka BP) to the mid-Younger Dryas. It suggests the presence of a typical 2.5-ka module profile, where the first grand minimum is shared with the 3.75-ka

module, indicating cluster formation. However, the double-peak profile shows strong polarization. Unfortunately, resolution issues make it difficult to determine definitively whether this polarization is a result of perturbation induced by the preceding Homeric-like module. Factors such as the carbon-cycle effect and the ^{14}C deposition effect may have influenced activity levels [Muscheler et al., 2016]. Regrettably, the recalibrated ^{14}C data has an error margin of ±50 years when compared with other reconstructions, which is too large to draw strict conclusions about the precise pacing of modules and grand minima. An additional difficulty in determining module pacing arises from an inexplicable delay of 50–150 years within the MMSCs between 13.2 and 6 ka BP. All modules exhibit stretching in their periodicity. The DP and Maunder modules, in particular, demonstrate a prolongation of c. 50 years and 100–150 years, respectively, between the Younger Dryas and 9 ka BP. A similar perturbation wave can be observed later in the Quasi-cycle and its modules between 10 and 6 ka BP.

2.6.1 Partial Overlapping of the '10-ka-BP' Modules

When observing from the past to the present, it appears that a Maunder-like module should have commenced around 10.38 ka BP, but it underwent a delay of c. 60 years. This delay seems to have shortened the subsequent cycle to last only about 2.45 ka (see Fig. 2.13). The postponement of the first grand minimum implies that cluster formation occurred on the brink of the Younger Dryas, but the gap between grand-minima inceptions within the DP module was only around 230 years. It is roughly a hundred years less than the measurement for the most recent DP module, which began approximately two thousand years ago.

The high-activity epoch of a Maunder-like module had progressed by two hundred years when a Homeric-like minimum abruptly terminated it around 10.0 ka BP. This example offers valuable insight into the phenomenon of the failure-to-launch. The failure is the reason why the term 'grand' poorly describes this particular minimum. Mean activity levels remained sustained throughout this

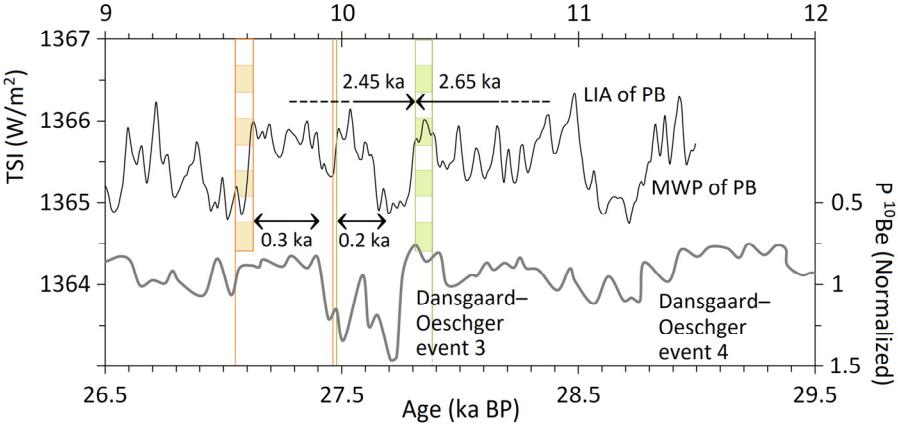

Figure 2.13. It would be convenient to consider that the distinct 300-year-long, high-activity epoch of a Maunder-like module, occurring c. 10.2 ka BP, was compressed by about 100 years due to the delayed occurrence of its first minimum. Conversely, the temporally accurate onset of a Homeric-like minimum around 10 ka BP further contributed to this compression. The Pre-boreal (PB) interval consisted of alternating high- and low-activity epochs, comparable to the equivalents of the Little Ice Age (LIA) and Medieval Warm Period (MWP). The TSI data and Beryllium-10 isotope data are sourced from Vieira et al. [2011] and [Adolphi et al., 2018].

period, although the exact impact of the nearly maximal TSI levels cannot be determined. Nevertheless, it is clear that there were deviations from the ideal pacing of grand minima. The Homeric-like minimum was unable to fully interrupt the advancing high-activity epoch of the 2.5-ka module, and conversely, the latter grand minimum of the 2.5-ka module failed to decrease activity levels of the Homeric-like module in subsequent years. The reasons behind the sudden and substantial extension of the cycle length in the Maunder-like module remain unknown, but it appears to have caused mixing in the overlapping process.

Whether this mixing is merely a result of normal variation or an intended auto-correction arising from the principles governing cycle groups can only be determined with a greater amount of high-resolution data. The relationships and dependencies between cycles should be carefully examined to identify possible connections. Passive phases with minimal activity variance are particularly valuable in the search for anomalies. Understanding the peculiarity of this

'failure' could be better contextualized empirically if there were sufficient data covering numerous similar overlapping events from the past. The importance of data quality would be emphasized in such predictions.

Another example of a failure-to-launch scenario focuses on module/Quasi-cycle interactions. One particularly interesting clash between a Maunder-like module and the Quasi-cycle occurred around 7.9 ka BP (refer to Figs. 2.3 and 2.7). It was anticipated that a medieval-like, high-activity epoch would be interrupted by the first grand minimum of the Maunder-like module. However, an examination of the reconstructions [Steinhilber et al., 2009; Vonmoos et al., 2006] suggests that this attempt to form a grand minimum was only partially successful. While a clear indication of this attempt is visible, the Maunder-like minimum could not suppress the activity levels below the local average.

One cannot help but consider how the earlier disarray of Maunder-like modules influenced the overlapping procedure, given that this medieval-like, high-activity epoch is situated between two progenitors of the well-known grand minima (Wolf and Oort), both of which were suitable for a seamless coupling. However, it managed to evade them both. This example significantly weakens the consistency of the Maunder-module sequence, despite the predominately low TSI levels during that period. The latter grand minimum, on the other hand, fared better in terms of both amplitude and duration, shedding light on the unusual relationship between the intermittent cycles and the Quasi-cycle. It appears plausible that certain distinct phases of the Quasi-cycle are so robust that the formation of a grand-type minimum becomes less likely to succeed.

A similarly contentious relationship continues to govern our modern times. Although a Maunder-like module currently controls the longer-term activity modulation, there are indications of the presence of the Quasi-cycle since AD 1850 in the form of unusually high activity, as discussed in more detail in Chapter 3. These observations suggest that the interplay between cycles is not always as evident as depicted by module pacing and profiles. Can climate proxy data help distinguish these intertwined solar phenomena? The find-

ings, at the very least, support this conclusion and provide a compelling impetus to advance in this multidisciplinary scientific field.

Conclusions

Two separate groupings of multi-millennial solar cycles with notable coupling properties have been identified: the continuous 3.5-ka Quasi-cycle, which is influenced by the apparent 7-ka TSI cycle, and the group of intermittent cycles that occur at intervals of approx. 2.5 and 3.75 ka. These intermittent cycles, also known as modules, are characterized by their distinct features and regular duration of 0.4–0.6 ka. The dual nature of the 2.5-ka periodicity, acting as both a module and a cycle, is subject to controversy. While it appears to be generated by the consecutive Quasi-cycles (as discussed in Chapter 3), it exhibits less periodicity compared to its progenitor. However, due to its intermittent nature, it forms a partially overlapping cluster with the 3.75-ka module every 7.5 (±0.1) ka.

It has been confirmed through the examination of solar activity and paleoclimatic records that the 7.5-ka cluster plays a part in the processes by which the Sun adjusts its rhythm to sustain the formation. This realization is important because, over the long term (> 50 ka), even a small change in per-cycle accuracy can lead to significant time shifts due to cumulative effects without self-correction. The 3.75-ka module is particularly intriguing due to its temporal connection with various abrupt climate changes spanning at least the past 54 ka. The future may provide further clarity regarding the degree of synchronism and the smooth transition of the 3.75-ka module across the 3.5-ka module during the 14th, 17th, and 21st millennia BP. Additionally, the interplay between the modules remains inadequately understood during the transitional periods.

The 2.5, 3.5, and 3.75-ka modules are unmistakable evidence of the Sun's systematic behavior, forming a distinct class of their own. The s3.5-ka module, accompanied by a subsequent period of high activity, is a unique phase that appears prominently in each cycle. The Solar Surge event and other features, however, are not always easily distinguishable due to their occurrence within the 7-ka TSI cycle. Together, the s3.5, 3.5, 3.75, and 2.5-ka modules, along with the repeat-

able phases of the Quasi-cycle, account for at least 75% of solar activity during the last 10 ka BP. These minima often seem to mimic the characteristics of a real grand minimum, aligned with the 208-year DeVries–Suess cycle. However, they do not consistently form an unbroken series of grand minima, partly due to the unique phases of the Quasi-cycle. Although a reconstruction spanning the last 14 ka provides valuable insights, it is not sufficient to fully resolve all issues concerning the interactions between modules, as well as module–Quasi-cycle dynamics, including movement, dominance, bypassing, and overlapping.

The 2.5-ka module functions like a satellite, orbiting the 3.75-ka module and forming a partially integrated module cluster with it within 7.5-ka cycles. Determining which one acts as the pacemaker may not be a relevant question. However, the DP module shows greater variability in duration compared to the 2.5-ka module, which sometimes leaves only faint traces. The time spans of approximately 1.6/0.9 ka and 0.3/2.2 ka intermittently and systematically perturb the Quasi-cycle, serving as intervals that separate the 2.5-ka and 3.75-ka modules. The precise structure of the sun's millennial clockwork and the degree of randomness within its manifestations are not yet fully understood. Theoretical inferences, combined with observations, suggest the existence of several activity loops, among which the 52.5-ka semi-loop and the 105-ka full-scale loop are perhaps the most significant.

The precise starting point of the 2.5 and 3.5-ka modules is not definitively established. It is plausible that their beginnings occurred possibly 100 to 200 years earlier than indicated by the first grand minimum (as defined). The Spörer minimum, an exceptionally long period from AD 1450 to 1550, might have extended for additional decades after AD 1500 due to the inclusion of a pre-grand minimum phase in the Maunder module. Similar declining phases of strong pre-fluctuations are also observed in the Homeric module and several other grand minima modules. These high-amplitude fluctuations that commonly precede the modules may indeed be an integral part of them. In the case of clustered modules, the pre-fluctuation is naturally created by the Double Peak itself, but in other instances, it ap-

pears to result from external 'forcing.' The Spörer minimum serves as a flawed example since it has a remarkably similar counterpart around 11.2 ka BP (as shown in Figs. 2.8 and 3.12), indicating that its extended duration is not unique within the context of the Quasi-cycle.

Methods

The 3.65-ka climate cycle or trend was discovered from the central Greenland climate record (GISP2) and later from Antarctica's Epica Dome C site (Chapter 1). The possible solar coupling was confirmed through the power spectrum data of the carbon-14 (^{14}C) isotope. The Fast Fourier Transformation (FFT) of the ^{14}C power spectrum data suggests that solar activity could exhibit regularity in the 3.5–3.8 ka period. To conduct more comprehensive research, the analysis also included previously well-studied periods from 2.40 to 2.55 ka.

A solar-activity reconstruction that incorporates the effect of the geomagnetic dipole field [Masarik and Beer, 1999, 2009] is referred to as a solar-modulation reconstruction [Vonmoos et al., 2006]. The research primarily utilized the results of Vonmoos et al. [2006]. For the cycle comparison and fine-tuning, the reconstruction based on the ^{10}Be isotope abundances from the past 0.35–9.4 ka BP was employed. The solar-modulation reconstruction offered the best framework for visual comparison across various time periods. Muscheler et al. [2007] extended their reconstruction to include the modern-day solar maximum and the Maunder minimum between AD 1650 and 1987. Additionally, two other reconstructions of Total Solar Irradiance [Steinhilber et al., 2009; Vieira et al., 2011] were examined to provide support for the findings.

The date 1.2 ka BP was utilized as the initial anchor point, and a reference time interval was scaled to the desired length. The selected endpoint served as the starting year for the subsequent phase. Visual inspection proves to be an effective method for identifying periodicity, as the intermittent and coherent nature of millennial-scale solar activity can be easily observed..

In this chapter, and more generally in this book, the modules are defined to begin from the onset of the first grand minimum, which

also includes the 40 (±10)-year declining phase. For instance, the Maunder minimum is defined to commence around AD 1610 and conclude around 1700, rather than adhering to the commonly accepted dating range of AD 1645–1710 [Eddy, 1976].

Table 2.3. Multiples for each multi-millennial solar module, cycle, and loop.

2.5	3.5	3.75	7 TSI	7.5	17.5	35	52.5
5	7	7.5	14	15	35	70	105
7.5	10.5	11.25	21	22.5	52.5	105	157.5
10	14	15	28	30	70	140	210
12.5	17.5	18.75	35	37.5	87.5	175	262.5
15	21	22.5	42	45	105	210	315
17.5	24.5	26.25	49	52.5	122.5	245	367.5
20	28	30	56	60	140	280	420
22.5	31.5	33.75	63	67.5	157.5	315	472.5
25	35	37.5	70	75	175	350	525
27.5	38.5	41.25	77	82.5	192.5	385	577.5
30	42	45	84	90	210	420	630
32.5	45.5	48.75	91	97.5	227.5	455	682.5
35	49	52.5	98	105	245	490	735
37.5	52.5	56.25	105	112.5	262.5	525	787.5
40	56	60	112	120	280	560	840
42.5	59.5	63.75	119	127.5	297.5	595	892.5
45	63	67.5	126	135	315	630	945
47.5	66.5	71.25	133	142.5	332.5	665	997.5
50	70	75	140	150	350	700	1050
52.5	73.5	78.75	147	157.5	367.5	735	1102.5
55	77	82.5	154	165	385	770	1155
57.5	80.5	86.25	161	172.5	402.5	805	1207.5
60	84	90	168	180	420	840	1260

CHAPTER III

3 A MISSING LINK BETWEEN THE SUN AND CLIMATE RESPONSES

3.1 Past Solar Activity and Greenland Climate Variations

The current 3.65-kyr climate cycle in Greenland appears to be experiencing minor variations compared to the two previous cycles. These variations are likely a result of the multi-millennial solar variability discussed in detail in Chapter 2. The 3.5-kyr Quasi-cycle is formed by intermittent cycles and the apparent 7-kyr Total Solar Irradiance (TSI) cycle. Consequently, the intriguing interplay between the periodic modules (s3.5 and 3.75) and fluctuations in Greenland's temperature is clearly observable in the Holocene proxy, as depicted in Figure 3.1. In Chapter 1, it was estimated that a sudden warming event similar to the Late Bronze Age would occur around AD 2300 if the regular pace and pattern of the 3.65-kyr cycle persisted. However, considering that the current warming trend began in the 1850s, there is a reasonable basis to believe that the recent abrupt warming in the northern Atlantic region can be attributed to the Solar Surge event, which occurred within the past 150 years, along with the influence of TSI and orbital forcings. This explanation would fit into the wider picture, where its Late Bronze Age predecessor was anomalously late. Thus, what was originally identified as a 3.65-kyr climate cycle is now understood to be influenced by multi-millennial solar cycles. In this chapter, we will delve deeper into the causal relationship between solar activity and climate anomalies, examining potential factors that may cause or trigger these unusual climate events.

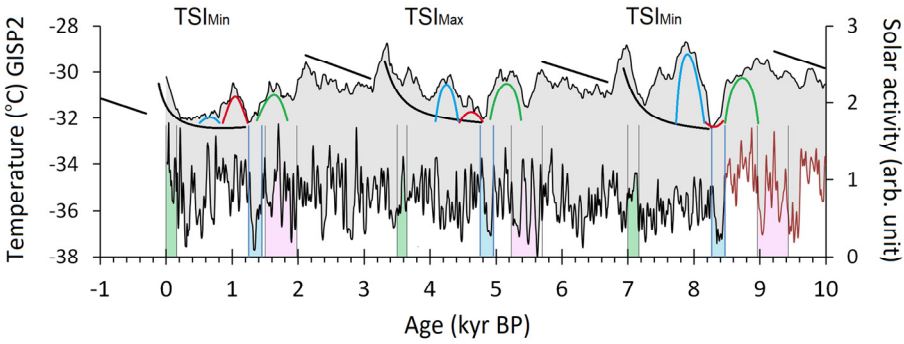

Figure 3.1. The impact of the 3.75-kyr module (violet) on the central Greenland climate is not fully understood. The module's ability to reduce temperatures in the northern North Atlantic appears to have been dramatic in prehistory (the Heinrich events). However, the mechanism by which it operates does not always consistently result in hazardous climate episodes (e.g., at 9.4 kyr BP). When the 3.75-kyr module (violet field) approaches the s3.5-kyr module (blue field), the Green Climatic Column in the upper panel appears to diminish. The GISP2 data used in this analysis are from Alley [2004], see also Box [2009]. The solar-activity reconstruction is a synthesis of [Muscheler et al., 2007; Vonmoos et al., 2006; Vieira et al., 2011].

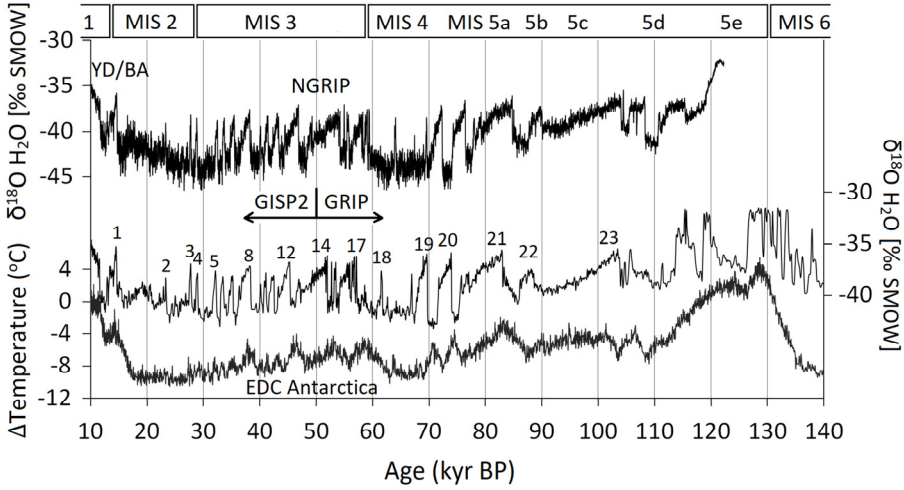

Figure 3.2. The combination of the GISP2 and GRIP records compared to the NGRIP record reveals a relatively strong correlation between 48 and 63 kyr BP. Transitions between Marine Isotope Stages (MIS) vary depending on the hemisphere and region. Warm interstadials, also known as Dansgaard–Oeschger (DO) events, are numbered from 1 to 23. The sources of data: Johnsen [1999], Grootes et al. [1999], and North Greenland Ice Core Project members [2004].

The diagram in Fig. 3.1 provides valuable insights into the relationship between the Blue Column and solar activity. During the early to mid-Holocene, the Blue Column consistently coincided with local temperature peaks until the onset of the Little Ice Age, which brought about significant changes in this pattern. The high-activity period that coincided with the warm medieval era gradually moved away from the local climatic maximum and was replaced by a series of grand minima associated with a cooling similar to the Little Ice Age. As a result, the rate of warming has noticeably decreased.

This finding provides a clear answer to whether all Blue Column series are synchronized based on the Quasi-cycle or if a medieval-like high-activity period always generates the Blue Columns in each interglacial. In the Antarctic EDC record, the Blue Column series of Aveley and Hoxnian do not begin at the same Quasi-cycle position as those in the Holocene. The Quasi-cyclic locus differs in each of the three interglacials, indicating interhemispheric contrast. On the other hand, in Greenland, a potential Blue Column series during the Tajo interglacial (792 kyr BP) shows a relatively close resemblance to the climatic disturbance of H3/DO 5 when visually examined using the 105-kyr solar loop. This suggests that the Blue Column series of Tajo could potentially result from a solar activity phase similar to that of the Holocene. The analogies and relationships between these observations will be further discussed in Chapter 5.

3.1.1 Climate Proxy Evidence of the 7-kyr Total Solar Irradiance Cycle

Attempts to directly align the GISP2 ice-core record with the GRIP and NGRIP records reveal discrepancies, primarily due to dating inaccuracies. These uncertainties, thoroughly discussed by Svensson et al. [2008], result in each Greenland record depicting a slightly different and temporally distinct picture of the evolving ice-age climate. While their average profiles and key events are generally similar, synchronizing them comes at the expense of losing absolute dates. Fortunately, a high-resolution methane (CH_4) record from Antarctica effectively captures abrupt climate swings in the Arctic, aiding in the

cross-matching of their inherently incoherent interpolar climate changes [Blunier and Brook, 2001; Buizert et al., 2015].

Over the past 40,000 years BP, NGRIP and GISP2 have exhibited close correlation, but their discrepancy rapidly widens in the preceding 10,000 years, from a few hundred years to nearly 3,000 years. Conversely, GRIP and GISP2 reach near synchrony during this interval, with the interstadials from the 12th to the 14th drawing particular attention due to waxing and waning. Prior to the Bølling event, the climatic progression of GRIP and GISP2 diverges substantially. This disparity can be attributed to the flow-modeling technique employed in determining GRIP dates, as opposed to the layer-by-layer counting method [Meese et al., 1997]. Despite the core sites being in close proximity (28 km), they yield slightly different climate data. Overall, the GISP2 record exhibits the most logical connection with the unique phases of the MMSCs extending beyond the Holocene era. However, its dating error becomes more pronounced prior to 51 kyr BP as the layer-by-layer dating method reaches its limit [Rahmstorf, 2003].

The Quasi-cycle appears to operate in synchronization with the 7-kyr climate cycle, most notably observed during Marine Isotope Stage 3 (MIS 3) in the middle of the ice age. Of particular note is the TSI variation discovered in the Holocene, which logically aligns with the three well-known interstadials (numbered 8, 12, and 14). The abrupt starts of these interstadials correspond to the GISP2 dates of 38.4, 45.3, and 52.3 kyr BP (see Fig. 3.3). They provide key evidence of similarities between the Holocene and ice age climates, illustrating how periodic variations in Earth's obliquity promote or suppress the solar effect on the North Atlantic climate. These interstadials exhibit nearly identical amplitudes, durations, and timings, supporting their classification as more than spontaneous events.

The warm interstadials and cold stadials observed in the GISP2 record further support the existence of a permanent 7-kyr TSI cycle. They display a clear connection with the climate variations of the Holocene, as depicted in Figure 3.2. Notably, the 1850s Solar Surge event and the s3.5-kyr module have left distinct imprints on the climate record. The Solar Surge event can be seen as a reverse phe-

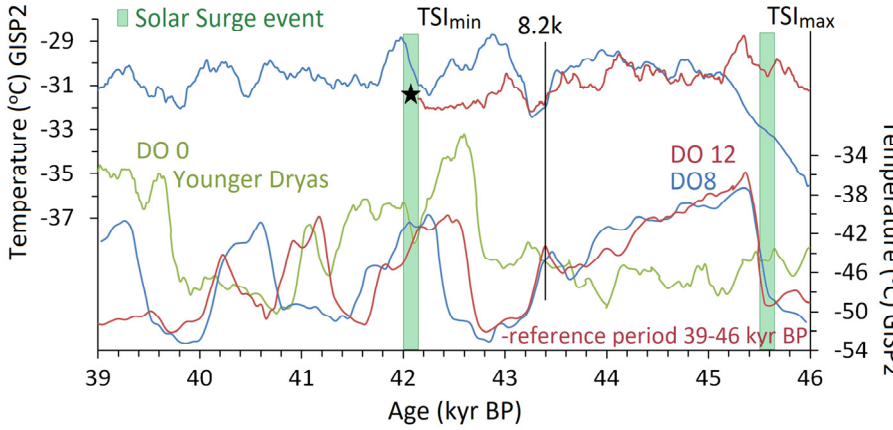

Figure 3.3. The selected 7-kyr periods from the GISP2 temperature record [Alley, 2004] are presented, with the reference period of 39–46 kyr BP (red, at the bottom). In the top panel, the red and blue curves cover the interval of 0.15–11 kyr BP, where the current warming (a black star) aligns with the Solar Surge event (green field) during the TSI minimum phase. One notable difference is that cold stadial conditions occurred after the Solar Surge events during the last glaciation. In the lower panel, the green curve starts at 18 kyr BP, the blue curve at 39 kyr BP, and the red curve at 46 kyr BP. The Solar Surge event during the TSI maximum phase led to abrupt warmings that were independent of the glacial–interglacial cycle. The onsets of the 8th and 12th interstadials (c. 38.5 and 45.5 kyr BP, respectively) perfectly coincide with the Solar Surge event during the TSI maximum. Interestingly, the onset of the 'Mystery Interval' at 17.5 kyr BP [Denton 2006; Broecker et al., 2010] seems to align with the beginning of the same interstadials.

nomenon of the s3.5-kyr module, adding to the intrigue. Interestingly, these intense surges and anti-surges observed in both the Greenland climate and solar-activity records are pieces of the 3.5-kyr cycle.

The three sudden warmings at around 0.15, 3.4, and 7.15 kyr BP provide credence to the theory of a significant and abrupt warming event being initiated, and possibly even caused, by solar activity (see Fig. 3.2). However, the sequence of Solar Surges does not align precisely with the sudden onset of the Holocene, despite a noticeable resemblance. The exact mechanism behind this relationship remains incompletely understood, which makes it challenging to differentiate between causation and triggering. Furthermore, the response times vary from decades to centuries, suggesting the presence of a highly regular amplification process that occasionally evolves gradually.

Figure 3.3 illustrates the controversial nature of the Solar Surge event (green field) during the middle of the last glaciation (43–57 kyr BP). It demonstrates that the Solar Surge had the potential to induce significant and rapid warming during the peak of the TSI cycle, while potentially leading to severe declines during the TSI minimum. This suggests that the same solar event, under different intensity levels, circumstances, and timings, could have triggered an inverse climate response. However, this explanation appears contradictory and requires further investigation and time to ascertain. In a broader context, one could argue that these relatively short bursts of heat eventually lost momentum, and not even an equivalent Solar Surge could reverse their decline.

It is noteworthy that the 8th and 12th interstadials, along with their subsequent climatic fluctuations, remained remarkably similar for nearly four millennia. Their sudden terminations at approx. 43.3 and 36.3 kyr BP align closely with the 8.2k cold event when examined in the context of the TSI cycle. Following these events, Heinrich events 4 and 5 were accompanied by severe and rapid temperature declines of up to minus 6 °C. What followed these Heinrich events, in this peculiar episode of 7-kyr periodicities, is worth mentioning. A sudden and unexpected warming event, known as Bølling (DO 1), began to unfold around 14.8 kyr BP. It profoundly disrupted the Arctic's tranquility only after a few centuries of progress. By 14.5 kyr BP, there had been a 12 °C rise in Greenland's climate, nearly reaching the temperatures observed during the Little Ice Age. The Bølling event was exceptional but pertained to the period after the Last Glacial Maximum (18–23 kyr BP). Prior to this period, warm interstadials, also referred to as Dansgaard–Oeschger events [Dansgaard et al., 1993], frequently interrupted typical glacial conditions and were numbered from 1 to 24.

A similar type of precursor that likely triggered the Bølling–Allerød (BA) warming and several other Dansgaard–Oeschger events likely played a vital part in restoring interglacial conditions. Interestingly, the BA–YD interval bears a strong resemblance to interstadials that began around 43 and 36 kyr BP, although they do not perfectly align in rhythm (refer to Fig. 3.3). These slight discrepancies

regarding the onset of interstadials suggest that factors related to accumulation may sometimes have a greater influence than specific activity events or modules. However, this remains an unresolved dilemma encompassing various aspects such as external forcings, interhemispheric energy balance, and the ocean–atmosphere system.

The interaction of the TSI cycle, orbital obliquity, and the Solar Surge event complicates the coherent understanding of the 3.65-kyr climate cycle as the governing pacemaker. The analysis presented above supports the notion that the climate in the northern North Atlantic region currently operates on a 3.5-/7-kyr tempo, as speculated in Chapter 1 (see Fig. 1.12). While the temporal deviation is small, the short-term outcomes show pronounced differences. For instance, a warming spike resembling the Late Bronze Age (around 3.4 kyr BP) is markedly distinct from a century-long cooling period or a grand minimum.

The paradox of the inactive Sun and its impact on the warming climate in Greenland suggests that we are facing a critical juncture due to a potential slowdown in the formation of North Atlantic Deep-Water (NADW). The sinking of denser surface waters in the Labrador and Nordic Seas (Greenland, Iceland, and Norway Seas) maintains the thermohaline circulation, which, in turn, supplies heat to the higher latitudes in the north [Rahmstorf, 2006]. Disturbances that took place over eight thousand years ago had substantial climatic consequences [Ágústsdottir et al., 2005]. The triggering effect of the 3.5-kyr solar-activity module is evidently responsible for initiating the 8.2k cold event, as it has consistently demonstrated the ability to induce a cooler climate episode in Greenland. The primary cause appears to be a reduction in North Atlantic Deep-Water formation, which affects oceanic convection throughout the northern Atlantic. Conversely, the Solar Surge event seems to have the opposite effect by warming the northern Atlantic through the bipolar seesaw mechanism, possibly originating near the Equator.

The underlying cause for the frequent generation of climate changes by the two solar events, compared to others, remains uncertain. It is possible that their temporal alignment with the 7-kyr TSI cycle, as well as the amplitude and duration of changing activity,

play a vital part. The Solar Surge event typically develops shortly after the peak of the TSI cycle, potentially providing the final push to surpass the necessary threshold for initiating abrupt climate changes. However, the rationale behind its impact is less clear during the TSI minimum. In the Holocene, the northern North Atlantic climate has responded to both solar events each time, unlike the 53–35 kyr BP period when it occurred only every 7 kyr (Figs. 3.1 and 3.3). An exception to this pattern is the Solar Surge event, which may have triggered cold stadial conditions twice, around 35 and 42 kyr BP, within the famous 7-kyr climate oscillation. The timing suggests such a possibility. However, these shorter Dansgaard–Oeschger events exhibit considerable randomness and do not always correlate, leaving uncertainties regarding how their conclusions are linked to the Multi-Millennial Solar Cycles.

The notion that the Sun was exceptionally active during the last century, contrasting with the Holocene, has been questioned by Vonmoos et al. [2006], who considered the effect of the Earth's geomagnetic dipole field, leading to a more nuanced range of oscillations. The Greenland climate proxy provides unambiguous evidence. While the recent response can be attributed to higher-than-usual solar activity, the 3.5-kyr climate cycle indirectly suggests that nothing out of ordinary has happened. Each of the three warmth spikes reached almost the same temperature level during the Holocene, although the current one is ongoing. The Dansgaard–Oeschger warmings show a similar pattern, as if their increases were constrained by a metaphorical glass ceiling.

Solar variability has been the topic of active research over the past centuries. Therefore, it would be a pity to miss the magnificent opportunity to discern and characterize unusual behavior associated with the warming of the northern Atlantic. A powerful solar flare, the Carrington event in AD 1859, may have signaled the return of the Quasi-cycle's active presence, despite the prevailing dominance of the 2.5-kyr module. What made the subsequent aurora borealis particularly legendary was their reported appearance at such a low latitude as Puerto Rico [Cliver et al., 2004]. It is worth noting that the extensive list of ^{10}Be and ^{14}C cosmogenic isotope records spanning the

past eleven thousand years only includes nineteen solar particle events (SPE), as reported by Usoskin et al. [2012]. Interestingly, the Carrington flare was not among them. The occurrence of two of these rare events at 3485 and 7165 years BP, corresponding to the time of Solar Surge equivalents, further supports the notion that solar activity can be markedly different at this stage of the Quasi-cycle. Flares can erupt in any direction and bypass the Earth entirely. Unless the overall rate of flares was significantly elevated during these short intervals, it is difficult to understand how they could regularly impact the Earth in 3.5-kyr cycles. However, the role of solar flares as a warming agent remains unclear [Gray et al., 2010]. While the other seventeen solar particle events should have initiated warming, this cannot be confirmed in the central Greenland records. The absence of the Carrington event undermines the credibility of their collective recognition.

3.2 A Prediction for Solar Activity and Greenland Climate Variations

The accuracy of solar activity predictions relies on both the quantity and quality of proxy data, but only up to a certain point. The credibility of predictive power increases considerably when results can be compared against millions of years of data rather than just thousands of years. This has been demonstrated for the Bray–Hallstatt cycle, with evidence found in mineral layers suggesting that the 2.5-kyr cycle existed 240 million years ago during the Upper Permian [Anderson, 1982]. This perspective provides a different outlook on what to expect from the future compared to models based solely on historical observations of sunspots since AD 1610.

Predicting the evolving climate in Greenland based on millennial cycles can only provide a rough estimate of the future (Fig. 3.4). However, some characteristic details of these cycles over the past fourteen thousand years seem to have been restored. This may tempt us to identify regularity and trends where none exist and overlook the influence of randomness and change. Nevertheless, the solar cy-

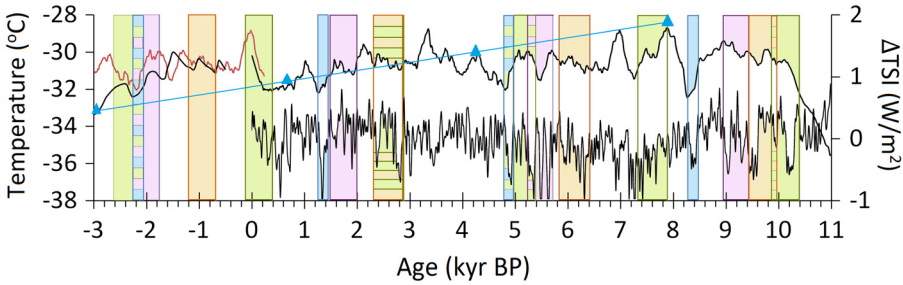

Figure 3.4. The four solar activity modules are shown in relation to the GISP2 temperature record [Alley, 2004] and the ΔTSI records [Steinhilber et al., 2009; Vieira et al., 2011]. Predictions for both proxies extend for the next 3000 years. A rough temperature forecast is derived from the previous 3650-year cycles (black), while considering the Blue trendline, which is expected to lead to temperatures below minus 33 °C in central Greenland in about 3,000 years. The red GISP2 curve has been time-shifted 7,000 years forward to approximate the influence of the TSI and Quasi-cycles. The first two blank intervals (c. -0.15 and -1.2 kyr BP) represent activity phases during which only Dalton-like grand minima are anticipated, as part of the Gleissberg 88-year and De Vries–Suess 208-year cycles.

cles, like cogwheels, offer a relatively straightforward method for predicting activity variations.

Of particular interest is the mechanism involved when a long-lasting and severe grand minimum emerges, especially when its recurrences may sometimes barely meet the criteria. Does the grand minimum carry a historical burden from previous cycles other than solar irradiance accumulation, and how do module–module interactions come into play? How are the different cycles interdependent? Surprisingly, estimating the broad features of upcoming climatic fluctuations in Greenland may prove more difficult than predicting orderly progressing solar activity variations.

If we examine the five Maunder-like modules of the Holocene, we observe that the two oldest modules partially failed to initiate one of their grand minima. From this, we can infer that the probability of an average grand minimum (30+50 years) occurring in this century is 7 out of 9 (77.7%), based on the 11-kyr reconstruction data. Alternatively, if we consider only the latter grand minima of the 2.5-kyr modules, the probability becomes 3 out of 4 (75%). Having high-resolution data covering the past 100 kyr would significantly en-

hance the credibility of the forecast, even if the probability remains the same. However, the success of intermittent modules in maintaining their typical profiles is inevitably tied to the surrounding Quasi-cycle and cannot be solely calculated based on their earlier records.

To investigate the movement of the 2.5-kyr modules relative to the Quasi-cycle, it is most convenient to separate the clustered and singular 2.5-kyr modules. By comparing every third 2.5-kyr module, they should theoretically advance five hundred years forward relative to the Quasi-cycle. For example, ages 7.90 and 0.93 kyr BP are identical from the Quasi-cycle's perspective, with the latter representing the onset of a high-activity epoch in the Medieval Warm Period. The Maunder Minimum began around 0.39 kyr BP as a result of a five-hundred-year leap taken by the 2.5-kyr module from cycle 3 to cycle 1, relative to the Quasi-cycle. It is worth noting that these modules' grand minima often overlap with each other.

Therefore, gaining an improved knowledge of this phenomenon is essential for making better real-world predictions. The details matter, including those related to solar activity. The duration of the module itself is about five hundred years, and this leap of five hundred years is strongly associated with the time gap between the two cycle groups.

3.2.1 Emergence of a New Maunder-like Minimum

3.2.1.1 Exploring the 2.5-kyr Periodicity

A comprehensive investigation of inactivity phases reveals a concealed 2.5-kyr periodicity characterized by strong dual module–cycle features. This periodicity stems from the Quasi-cycle and its two modules. A continuous series of Quasi-cycles gives rise to a sequence of inactivity phases separated by 2.5-kyr intervals. The term ‘grand minimum’ is not employed here exclusively because the inactivity phases may not always meet the criteria of $\Phi<175$ MeV [Lockwood et al., 2010]. For example, the inactivity phase that took place c. 3.5 kyr BP, immediately following a Solar Surge equivalent, poses uncertainty regarding its categorization. This uncertainty arises due to the presence of adjacent TSI maximum and elevated activity levels.

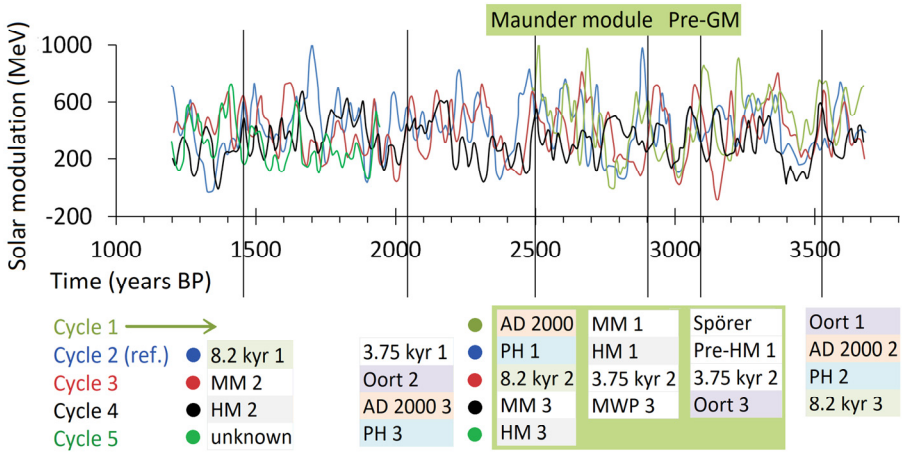

Figure 3.5. A synthesis of cosmogenic ^{10}Be reconstructions covering the past 9.4 kyr is presented here in 2475-year periods. Inactivity phases are stacked and arranged in a specific order. Note that the black line represents the starting points of a group of grand minima, rather than a single grand minimum. The second stack from the left (c. 2050 years BP) resembles the current stack we are in (c. 2500 years BP). The data used in this representation are sourced from Vonmoos et al. [2006] and Muscheler et al. [2007].

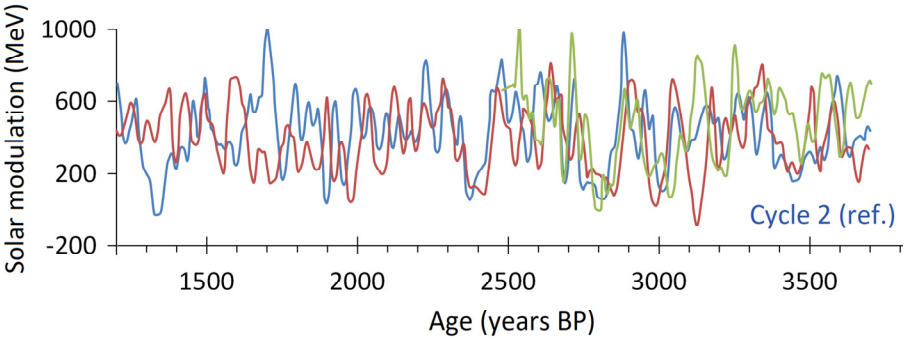

Figure 3.6. The 2.5-kyr solar activity cycles indicate that we are currently in the middle of a millennium-long period that has shown remarkable consistency and precise repetition during the last three cycles: the 3rd (red), 2nd (blue), and 1st (green). This repetitive pattern is highly convincing and difficult to argue against. For clarity, Cycle 4 has been omitted. In each of these cycles, a decline in solar activity began around the same time and lasted for a century. Given the consistency of this pattern, it is reasonable to question if there is any reason to expect an exception to it. The data used in this analysis are sourced from Vonmoos et al. [2006] and Muscheler et al. [2007].

Table 3.1. The characteristics of the 2.5-kyr cycle originate from several series of superimposed grand minima generated by the continuous chain of the 3.5-kyr Quasi-cycles. Moreover, the 2.5-kyr module itself, along with the thousand-year interval between the identical 3.5-kyr and 2.5-kyr modules, contributes to the production of these grand-minima series. Some of them are listed below.

Grand Minimum	Age (kyr BP)	Grand Minimum	Age (kyr BP)	Grand Minimum	Age (kyr BP)
AD 2000 1	0	Oort 1	1	8.2 kyr 1	1.45
PH1	2.5	AD 2000 2	3.5	Spörer 2	3.95
8.2 kyr 2	5	PH 2	6	HM 2	6.45
MM 3	7.5	8.2 kyr 3	8.5	None	8.95
HM 3	10	None	11	None	11.45

Abbreviations	
Homeric	HM
Post-Homeric	PH
Maunder Minimum	MM
Post-Maunder	PM

Each Quasi-cycle generates multiple new inactivity series while continuing the existing ones (Fig. 3.5). In total, this combines three consecutive Quasi-cycles, with each inactivity series typically spanning 7.5 kyr (Table 3.1). For instance, the time span from the Oort Minimum to 8.5 kyr BP amounts to 7.5 kyr. Practically, this implies that during a Quasi-cycle, there are constantly six ongoing minima-series, enhancing the 2.5-kyr periodicity (Fig. 3.5). For instance, the initiation of grand minima at approximately 1, 3.5, 6, and 8.5 kyr BP corresponds to the Oort minimum, a Quasi-cycle equivalent of AD 2000, a post-Homeric equivalent, and the 8.2k cold event.

As depicted in Figure 3.5, these inactivity phases appear to overlap and form stacks. A closer inspection reveals a specific order in these inactivity phases, which is essentially a mathematical pattern. However, observing the regularity or the fact that multiple concurrent 2.5-kyr inactivity series coincide with consecutive Quasi-cycles is not easy. The grand minima of the 3.75- and 2.5-kyr modules sometimes extend these inactivity series originating from the Quasi-cycles. Whether this is coincidental or indicative of a trend is a much more intriguing question, as it relates to the steps taken by these modules relative to the Quasi-cycle. The last Maunder-like module perfectly aligned with that of the Homeric period and, prior to that, overlapped with the s3.5 module. It can be concluded that the 2.5-kyr module ensures the continuity of these inactivity series through a rolling mechanism.

3.2.1.2 How Long It Will Last?

The 2.5-kyr Bray–Hallstatt cycle, or more precisely, its module in this case, explicitly demonstrates that the question is not whether we will witness a grand minimum during this century, but rather how severe and long it will be. There are several approaches to tackle this problem. One method is to study different cycle combinations; another is to rely on statistical averages; and alternatively, one can analyze the actions of previous corresponding modules. However, none of these methods are entirely reliable due to natural variations in the amplitude and duration of grand minima. Nonetheless, the latter approach appears to be more sophisticated.

A previous corresponding module occurred around 35 kyr BP, resulting from a combination of the TSI cycle and 17.5-kyr loops. However, this approach neglects the movement of the DP module. Moreover, the relative position on the Quasi-cycle seems to have a potentially influential role in the development of a module profile, surpassing the importance of correspondence through long-term loops. Nonetheless, such long time spans can pose challenges in terms of resolution due to the presence of noise. To make precise observations, a more convenient approach is to study the most recent cycles and the details within them without compromising reliability. However, it is essential to ensure a broad range of coherency issues align consistently over multiple Quasi-cycles. This 'shortcut' principle is particularly applicable to the last two Maunder modules, which show strong similarities, and the current module has followed a similar pattern to its predecessors (Fig. 3.6). The faster pace of the Maunder module compared to the grand minima of the Quasi-cycle has significantly contributed to its precise repetition.

Since the early Holocene, the average length of a grand minimum has been estimated to be 70 years when a sunspot number of 15 was used as the boundary value [Usoskin et al., 2007]. It is worth considering whether the twenty-year Dalton minimum should also be classified as a grand minimum. If it is indeed included, then the range of grand minima shows notable variation, as the other extreme is ten times longer. Although the boundary value of the solar modulation function, $\Phi<175$ MeV, for a grand minimum does not perfectly corre-

late with the sunspot number, the results are in good agreement. Calculating an average may provide an approximation for the future, but it does not offer profound arguments.

If the Quasi-cycle had been the dominant factor since the early seventeenth century, the Sun would have maintained its average activity levels, and the low-activity phase would have likely been avoided. However, the current situation is different. Even without the presence of the Maunder module, there is a high probability that the Sun will enter a century-long phase of low activity starting around AD 2000. This can be inferred from the typical inactivity period that follows each Solar Surge event, which is a regular part of the Quasi-cycle.

Nevertheless, the Maunder module is active, and we currently witness with very high confidence the onset of a grand minimum that relatively well compares to the post-Homeric minimum (BC 360–450). The interaction between different cycles has made the past few centuries intriguing, offering insights into what the dominance of the Maunder module over the Quasi-cycle could imply. An intriguing controversy surrounding the relationship between solar activity and climate exists. The outcome of the recent DO-type warming suggests that the Solar Surge event would have occurred simultaneously, despite the presence of the Maunder module, which obscures the comparison. This represents a significant turning point, separating the effect of the Solar Surge event from the accumulation of total solar irradiance in abrupt warming. While the involvement of the Maunder module complicates the analysis, this case is not unique and will be addressed later. For instance, the impact of a DP module on the abrupt Solar Surge warming around 28 kyr BP is extensively discussed in the context of Quasi-cycle Evolution and the African Humid Period.

Decoupling different solar events may prove to be an impossible task. Thus, finding alternative explanations for their peculiar behavior becomes crucial. One potential avenue is the study of planetary interactions [Charvatova, 2000; Scafletta, 2014]. However, thus far, no convincing evidence of coupling between solar events and plane-

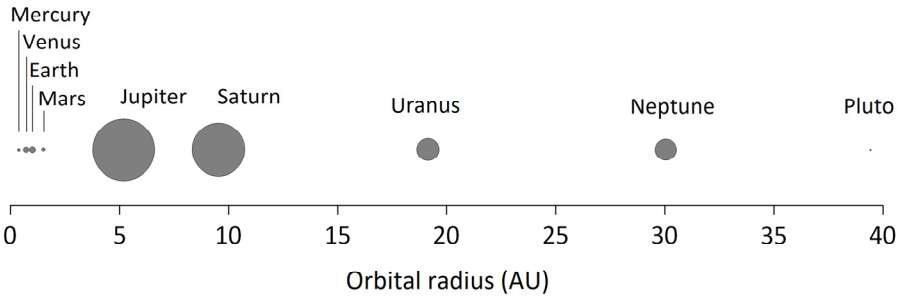

Figure 3.7. The nine planets of the solar system are in order of distance from the Sun. One astronomical unit (AU) equals Earth's distance from the Sun.

tary interactions has been presented. Nonetheless, abstract comparisons suggest some similarities may exist, although further investigation is warranted.

From outer space, the solar system appears as a thin disk, with Pluto and other minor bodies being exceptions due to their highly eccentric orbits tilted against the disk. Pluto completes one orbit every 248.6 years at the farthest reaches of the solar system, while the innermost planet, Mercury, completes about 1031 orbits. The differences between these celestial bodies are immense, both in terms of their distances and numerical values. Longer distances correspond to smaller gravitational forces, and within our solar system, the influence exerted on the Sun by Pluto and Neptune, for example, is relatively minimal compared to the effect of gigantic gas giants like Jupiter and Saturn (Fig. 3.7). It would be problematic to justify the significance of Pluto and Neptune while simultaneously ignoring the potential impact of these massive inner planets.

The orbital resonance between Pluto and Neptune is as an example of a self-correcting system. These celestial bodies resonate with each other in a ratio of 2:3, which immediately draws attention as it corresponds to the cycle ratio of the 2.5 and 3.75-kyr modules in the following manner:

Pluto : Neptune : Uranus = 248 yr : 165 yr : 84 yr
248 yr : 165 yr : 84 yr = 3 : 2 : 1
3750 : 2500 : (1250) = 3 : 2 : (1).

However, the issue is that these correlations do not directly match with the highly accurate MMSCs and instead require arbitrary multiples to achieve evenness. The challenge lies not only in identifying planetary combinations that could propagate their intended effects to the depths of the Sun but also in providing valid arguments for excluding the gigantic inner planets with shorter orbital periods from the equation.

In the broader context, the Earth's climate is influenced by its gravitational interaction with other planets. For instance, Jupiter and Saturn primarily contribute to the 100- and 405-kyr eccentricity cycles. However, it remains uncertain whether this interaction extends to the deep solar interior in a way that could modify solar activity. According to Callebaut et al. [2012], the distances between the planets and the Sun are too vast to exert anything more than insignificant gravitational forcing on the magnetic shearing layer located at the bottom of the convection zone. It is increasingly likely that if any significant coupling existed, it would have already been noticed.

A 500-year sequence, encompassing the phases of solar grand minimum, maximum, and minimum, has an amazing tendency to repeat itself in 2.5-kyr cycles, presenting a real challenge to scientific understanding. The question arises: How can such consistent behavior be explained? The time intervals for essential processes within the convective envelope range from days to decades, rather than millennia. This raises a clear yet difficult question: What could possibly account for such long-term regularity in the Sun? One potential answer lies in the existence of a relic poloidal magnetic field within the radiative core [Ossendrijver, 2003], which can only be inferred indirectly from a few conceptual theorems. The nearly solid-body rotation of the radiative interior suggests efficient angular momentum transport, possibly facilitated by the presence of such a field.

The grand maxima that preceded the Homeric and Maunder minimums peaked around 2.88 and 0.39 kyr BP, respectively, with 2490 years separating them. Considering that the post-Homeric minimum began evolving at 2.45 kyr BP, a little over four hundred years after the start of the Homeric minimum, we can conclude that the same four hundred years have now passed since the Italian astronomer

Galileo Galilei (1564–1642) witnessed the elusive sunspot minimum and the onset of the last intense activity cycle around 1610.

The remarkable precision in duration, timing, and amplitude of periodic Maunder-like modules is emphasized in Figure 3.8. Three successive post-Maunder-like minima, including the current one, conveniently coincide with a grand minimum that is also part of the Quasi-cycle. The period from the edge of the cliff (0, 2.45, and 4.96 kyr BP) to the end of the grand minimum lasted about 90 years, encompassing a 30-year decline in activity followed by a 60-year period of low activity characterized by scarce sunspots. If we draw a starting line between AD 1990 and 2000, the last decade of the post-Maunder minimum would be marked as the 2080s. Consequently, the succeeding five 11-year sunspot cycles are likely to be prolonged because historically, lower sunspot numbers have correlated with longer cycles [Charbonneau, 2014], fulfilling the 60-year low-activity period. However, apart from cycle statistics, there are no strong arguments for the upcoming post-Maunder minimum to persist for 30+60 years.

Furthermore, these modules sometimes exhibit small features that can provide information regarding the incidence of unusually lengthy or short grand minima, as discussed in Chapter 2. One such

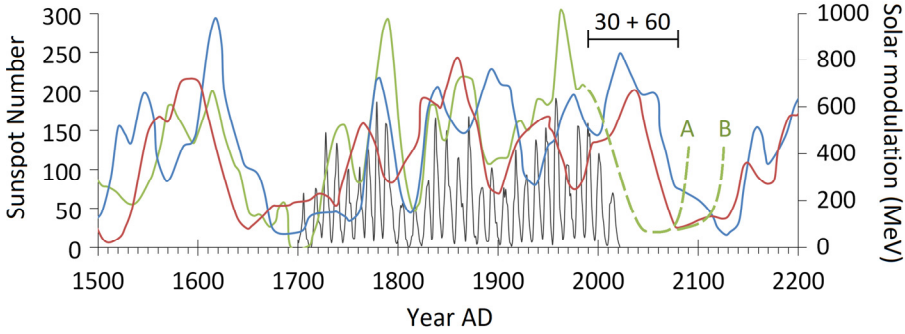

Figure 3.8. An enlarged version of Figure 3.6 provides a more detailed view of the current state of solar activity and offers a rough prediction of solar behavior for the upcoming centuries. Line (A) represents the average projection for a 30+60-year grand minimum, while line (B) illustrates an extended 30-plus-90-year variation resembling a Homeric-like grand minimum. The Sunspot Number record [SILSO] is used as a reference for this analysis.

detail was the unusually short-lived first grand minimum, which was prematurely ended by a high-activity period around 9.93 thousand years BP, ultimately leading to the extended second grand minimum of a Homeric-like module. A similar interpretation could be applied to the evolving Maunder module since its grand maximum ended approximately fifty years earlier compared to the previous two instances (see Fig. 3.8). However, the length of the Maunder minimum is close to the average, and the subsequent high-activity epoch aligns well with the expected duration of c. 300 years. This contradicts the argument for a significant prolongation of inactivity. If the modern activity maximum had continued for another fifty years like the previous ones, it would have overlapped with the inactivity phase of the Quasi-cycles, scheduled to begin around AD 2000. The synchronization with the Quasi-cycle indicates improved coherence, making the next overlapping procedure with the 3.5-thousand-year module more likely to be successful.

3.2.1.3 Climate Couplings

The abrupt climate responses observed in the northern Atlantic have revealed that nearly identical Maunder modules do not result in similar periodic climate patterns. This suggests that solar variability has a negligible impact on climate change or that the laws of physics may not apply as expected. When one grand minimum significantly affects the climatic conditions in the northern Atlantic differently from another, it implies that they must fundamentally differ in some way or their effects must be substantially modulated. The worst-case scenario would be if these impacts were inherently random, making them spatially and temporally unpredictable. These nearly identical half-millennium-long modules appear to decouple solar activity variations from climate variations in Greenland, almost as if they operate at the wrong frequency. There must be additional components or amplifying mechanisms involved, considering the puzzling variability in response times. The question arises whether this deduction also applies on a global scale, and if so, how it can be reliably measured when ocean currents efficiently redistribute heat, creating regional anomalies at the expense of symmetrical global distribution.

The Greenland climate's responsiveness to prolonged activity suppressions in the distant past has varied widely, which raises doubts about the causal relationship based on both physics and observations. Consequently, there is an ongoing lively debate regarding the existence of coupling and the extent to which the GISP2 record reflects climatic fluctuations over the North Atlantic region, the Northern Hemisphere, or even globally.

Considering the ocean–atmosphere system as a discrete component decoupled from solar variation seems radical and bold in the context of this book. Climate models predicting global temperature increases for the twenty-first century have, until recently, not accounted for the effects of grand minima. This is partly due to the uncertainty surrounding their occurrence and the current understanding that their influence is negligible. Recent studies support this view [Meehl et al., 2013; Maycock et al., 2015], indicating a relatively broad consensus that their impact on global temperatures is minimal (> -0.1 °C) [Anet et al., 2013; Feulner et al., 2010]. However, a delayed regional impact on the northern North Atlantic climate could be much larger than expected. The peculiar irony of abrupt climate changes lies in their varying response times, a perplexing subject that introduces uncertainty as to why they fluctuate so greatly. Undoubtedly, this variability is associated with ocean circulation, making interpretation demanding. While relying on the perceived certainty of a warming climate scenario, it is important to be prepared for the possibility of the other extreme surprising us when least expected.

When Galileo Galilei began observing the Sun in 1610 using his telescope, he immediately noticed strange reflections of dark spots projected onto a white screen. Since then, the appearances of sunspots have been consistently recorded, albeit with some variations in frequency [Hoyt et al., 1997; Eddy, 1976]. The initial discovery of sunspots generated both frustration and enthusiasm among researchers, but interest in them diminished over the years as their rate of appearance declined. The task of filling in the historical data gaps from the first hundred years of sunspot research has proven to be a laborious undertaking. Even today, many centuries later, we still do not have a definitive understanding of how the sunspot maxima

gradually diminished until they virtually disappeared for a half-century, although rough estimates can be obtained.

Recent studies have revealed an intriguing and uncertain abnormality during the late Maunder minimum, where a strong hemispheric asymmetry in sunspot distribution was observed [Ribes and Nesme-Ribes, 1993]. This phenomenon, which awaits further observation in the mid-century, deviated from the typical symmetrical latitude–time shape resembling butterfly wings that emerges with the appearance of sunspots.

The end of the Maunder minimum marked a significant turning point in the European climate. While the debate continues on whether higher solar activity was the cause, the timing coincides with a decrease in hazardous events and a rise in temperatures. Notably, the medieval and modern warm periods brought social stability, reducing instances of crop failures, famine, and plague epidemics that had frequently troubled nations since the start of the Little Ice Age [Crawford, 2007]. Furthermore, the 1690s witnessed the coldest decade on record in England [CET series since 1659; Manley, 1974], coinciding with the end of the Sun's hibernation phase. The 1670s and 1680s were also exceptionally cold. Northern Europe, in particular, experienced severe hardships during the latter half of the 1690s, including crop failures and famine, with temperatures at least 2 °C below present-day averages.

Over the past three hundred years, climatic conditions in central Scandinavia have undergone dramatic changes. Sporadic years without a proper summer have been replaced by sporadic years without a permanent snow cover in the winter season. If these intermittent occurrences were to become long-term trends, it would be easier to understand the retreat or advancement of the Arctic sea-ice margin in alignment with these trends.

During the Maunder minimum, the weakened open solar magnetic field and solar wind had a reduced interplanetary shielding effect against low-energy galactic cosmic-ray particles. These physical particles can acquire their kinetic energy from blast waves and travel over vast distances, even at the speed of light, before colliding with Earth's atmospheric molecules. The increased production rates of

cosmogenic isotopes (^{10}Be and ^{14}C) by the mid-17th century signify the contraction of the extensive 100 AU Heliosphere. Some studies suggest that an elevated cosmic-ray flux could directly lead to increased precipitation [Svensmark, 2016 and references therein]. Supporting this notion, a subfossil bog-tree study spanning a 3,000-year-old segment in southern Sweden reveals similar behavior, as discussed in the following section. Periods of excessive wetness appear to be more frequent during declining solar activity compared to phases of increasing activity. This implies a higher risk of consecutive years with excessive rainfall in northern and northwestern Europe toward the end of the twenty-first century, as observed during the Homeric minimum [Kilian et al., 1995; Mauquoy et al., 2004; Martin-Puertas, 2012].

Empirical evidence suggests that the climate over the European continent is substantially influenced by solar inactivity, despite its relatively smaller impact on global temperatures [Mauquoy et al., 2004; Wanner et al., 2011]. Evidence also indicates that during the Younger Dryas period, the Gulf Stream shifted southward. This connection is evident in the Greenland ice-core record (GISP2), where temperatures experienced abrupt declines during major inactive phases such as the 8.2k cold event, followed by systematic 3.5-kyr cycles. Although the 3.5- and 2.5-kyr solar cycles are closely linked, there is no clear indication of the 2.5-kyr cycle in the GISP2 temperature record. Recently, the desynchronized progression between solar activity and temperatures has become more pronounced in the northern Atlantic region, similar to the conditions 7 kyr ago during the 8th millennium BP. The subsequent sections will focus on individual Quasi-cycles.

3.3 The Quasi-Cycle Evolution of the Holocene

3.3.1 Positioning in Contrast to the Last Cycle

There is a growing interest in understanding the climatic conditions that governed 3500–3300 years ago, as they hold the potential to offer insights into contemporary weather patterns. If we were to travel

back in time and scrutinize the evolution of solar–climate conditions, we would discern a notable warming of over 1 °C and an occurrence of a Solar Surge event that was roughly 150 years out of sync. Determining whether this Solar Surge event alone was the catalyst for the warming during the Late Bronze Age (LBA) poses a complex question, given the evident lag response (see Fig. 3.9). This delay persists even beyond the subsequent grand solar minimum, underscoring the implication of the subsequent surge in activity that

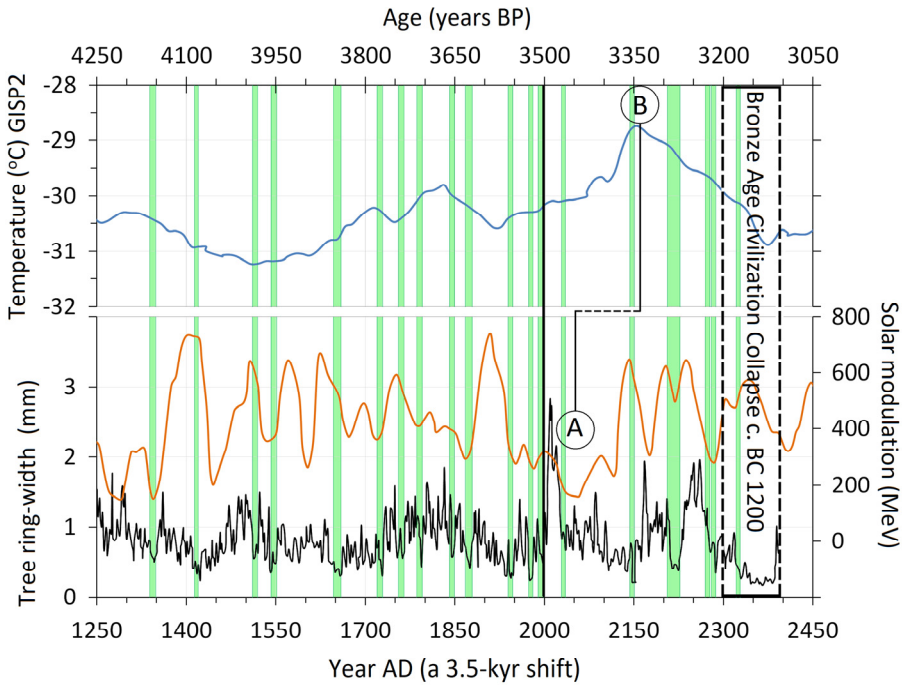

Figure 3.9. Three proxy records: GISP2 [Alley, 2004], solar activity [Vonmoos et al., 2006], and tree ring-width from southern Sweden [Edvardsson, 2013], are converted and compared to the present day using a 3.5-kyr shift. In this figure, AD 2000 corresponds to 3500 years BP. (A) depicts the expected Solar Surge-related abrupt warming event, while (B) shows the observed abrupt warming during the Late Bronze Age (LBA). These two were roughly aligned during the last two TSI minima, but the TSI maximum caused an unexplained transition lasting c. 150 years. The subsequent LBA cooling changed the climatic conditions in Europe, extending from Scandinavia to the eastern Mediterranean. This change is illustrated by the decline of the bog-pine population around 1200–1500 BC [Edvardsson, 2013]. The contrast between the abrupt warming and cooling during the LBA is notable in terms of successive wet years (the green bar represents at least three successive wet years).

aligns convincingly with the abrupt warming of the Late Bronze Age. Although certainty is elusive, the lagged response may suggest centennial variability in the timing of tipping points in the Northern Hemisphere. This variability is notably linked to the sudden arrivals of interstadial periods near the TSI maxima.

Subfossil tree-ring and peat samples excavated from southern Sweden [Edvardsson, 2013] reveal a significant contrast between the warming and cooling phases of the Late Bronze Age in terms of consecutive wet years. The LBA warming phase did not result in a prolonged period of excessive rainfall in southern Sweden or conspicuous snowfall in central Greenland. While warmer air can hold more moisture, leading to increased humidity of about 7% per one degree Celsius [Trenberth, 2005], this behavior was not observed during the LBA warming. In contrast to the abrupt LBA warming, the subsequent multi-century cooling period from c. 1350 BC to 1150 BC included two extended and two shorter phases of excessive rainfall. The first severe phase occurred around 1300 BC, just half a century after the peak of the LBA. It drastically suppressed tree-ring growth for approximately two decades, serving as an early indication of forthcoming difficulties. The two-hundred-year decline in temperatures observed in Greenland culminated in the LBA crisis in the eastern Mediterranean around 1200 BC to 1150 BC. The delayed Solar Surge warming necessitates a fresh perspective on the solar–climate coupling compared to its closest occurrences during periods of minimum total solar irradiance.

The apparent decoupling during the LBA challenges the notion of a strict association with the Solar Surge-like event. The LBA warming emphasizes the cumulative effect rather than an accurate, solar-event-specific climate response at the TSI maximum. So far in the book, I have focused on the temporal coupling between specific solar events and abrupt climate changes, rather than gradual accumulation processes, which appear to be a recurring feature of the mid-ice age (MIS 3). This stands in contrast to the TSI minima at about 0, 7, 14, and 28 kyr BP, as their climatic interactions have generated precisely timed and abrupt warmings in Greenland.

The Late Bronze Age crisis (c. 3200–3150 yr BP) marked the downfall of many advanced societies in the eastern Mediterranean. Trade and diplomatic relations ceased, written records became scarce, and cities were abandoned. Pollen samples, preserved writings, and excavations provide clues to possible causes, often described as a destructive cycle of environmental hazards and manmade devastation [Knapp et al., 2016; Cline, 2014]. While it is increasingly clear that severe drought anomalies had a persistent grip on the eastern Mediterranean and played a central role in the crisis [Kaniewski et al., 2010, 2013; Finne et al., 2017], the burning of cities throughout the region was a deliberate act of warfare. It was a chain of events that spread like a wave of destruction from Greece (the Myceneas) to Hittite, Assyria, and Cyprus within decades rather than years. Famine and political instability are educated guesses regarding the driving forces, in addition to the invasions by the enigmatic Sea Peoples, whose origins remain uncertain but whose existence is well-documented in Cyprus and Egypt. Only Egypt under Ramses III partially succeeded in adapting to this complex new environmental threat. They fought against the Sea Peoples on several occasions, underscoring the role of invasions in the crisis. The persistent drought was likely the root cause and part of a larger climate change pattern. It initially escalated in Greenland with falling temperatures since approximately 3350 years BP, and eventually, people on the northern and southern borders of Europe experienced climate shifts in opposite phases before Greenland's cooling ceased around 3150 years BP.

Bog-tree and peat-stratigraphic studies in northern and northwestern Europe have revealed an abrupt turning point in climate around 1200 BC, characterized by rising lake levels [Edvardsson, 2013; Turney et al., 2016]. Substantially moister and about 1 °C colder climatic conditions led to a phase of tree population decline from approximately 3200 to 3150 years BP. This apparent ‘phase-locked’ climate mode aligns with large-scale shifts in atmospheric circulation, drawing energy from ocean circulations across the entire Atlantic. Polarized precipitation patterns across Europe, from north to south, coincided with a rapid weakening of the Atlantic overturning

circulation, which transports heat from the South Atlantic to the Northern Hemisphere and displaces the Intertropical Convergence Zone from the Equator. In these large-scale ocean circulation changes, the thermal equator can deviate from its geographical counterpart (see Chapter 4).

The drought, which can be attributed to the migration of polar waters, bears resemblance to another particularly severe event that took place between 28 and 29 thousand years BP in northern Africa and the eastern Mediterranean. Interestingly, this early phase of Marine Isotope Stage 2 (MIS 2) is connected to the same region through its megadroughts. It is uncertain whether the sharpest decline in humidity around 28 kyr BP preceded, coincided with, or followed the abrupt warm event known as Dansgaard–Oeschger event 3 (DO 3). It may not be possible to precisely date the most significant reduction in humidity. However, it is plausible that the most severe drought is closely linked to the occurrence of the Double Peak module, similar to the mid-Holocene event 5.7 kyr BP. The Double Peak module at 28.3 kyr BP likely overlapped with an equivalent Solar Surge event and occurred during a period of minimum total solar irradiance. Considering that aridity began to evolve gradually about a thousand years earlier, it places a Little Ice Age-like sequence of inactivity at the center of hyperaridity. This period was characterized by plummeting temperatures and occupied the second half of the millennium between the short-term DO 3 and DO 4 events (Fig. 3.10). In this new context, it becomes more apparent that the climate change in the eastern Mediterranean during the equivalent of the Little Ice Age (c. 28.3–28.8 kyr BP) took a dramatic turn when the Double Peak module emerged (c. 28.3 kyr BP), influenced by the southward movement of the Intertropical Convergence Zone (ITCZ), also known as the thermal equator. What makes this example particularly intriguing is the nearly simultaneous occurrence of the Solar Surge warming around 28.15 kyr BP (DO 3), which seemingly led to a rapid latitudinal reversal of the Intertropical Convergence Zone, as suggested by the theory.

The Indian and East Asian summer monsoons have their own stadial–interstadial phases but exhibit a strong tendency to correlate

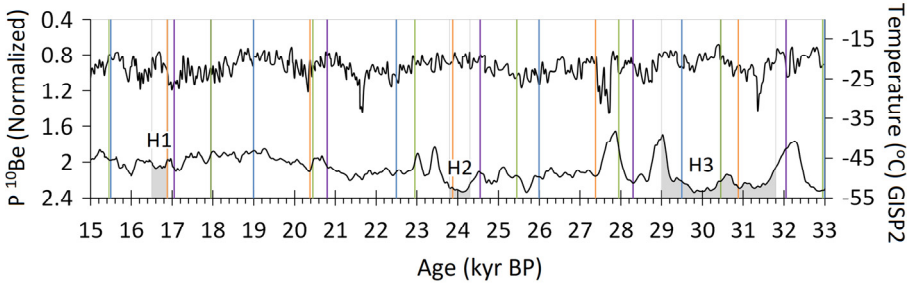

Figure 3.10. Solar activity [Adolphi et al., 2018] is presented as a production rate of ^{10}Be in relation to the central Greenland temperature from 15 to 33 kyr BP [Alley, 2004]. The deposition of Heinrich layers 1, 2, and 3 at the Irish coast site MD01-2461 [Peck et al., 2006] consistently followed the 3.75-kyr module (violet) and the TSI maximum.

with those observed in Greenland [Schulz, 1998; Fleitmann et al., 2007; Kathayat et al., 2016]. The early Marine Isotope Stage 2 is discussed in two sections: the African Humid Period and Solar-Induced Climate Loops.

During the crisis in the Late Bronze Age, the North Atlantic region experienced significant climatic shifts that appeared to be unrelated to the typical solar–climate interactions associated with multi-millennial cycles. The orbital and multi-millennial variability create slightly different conditions for each cycle, making it less meaningful to directly apply historical knowledge to the present. However, similar climate disruptions or anomalies may likely occur again, although the severity, location, spatial scale, and timing of these events are speculative and uncertain.

What will written history remember about the years of crisis in modern-day Syria? Was it a result of escalating climate change [Kaniewski et al., 2012] or a lack of political leadership? In either case, these events will likely be relegated to historical archives, much like the fall of the Akkadian Empire during the Early Bronze Age (EBA) in the present-day Syria–Iraq region. The difficulties faced by Akkadian culture coincided with a prolonged period of aridification (c. BC 2200–1900) and a cooling of the northern Atlantic. This well-documented megadrought marked the end of a prosperous phase not only in the Mesopotamia–Northern Africa axis but also in vari-

ous regions worldwide. These climate changes during the Early Bronze Age are now recognized as part of a broader pattern [Weiss et al., 2001, 2016; Booth et al., 2005; MacDonald, 2011; Yang et al., 2015]. The dry-farming areas in the northern Fertile Crescent were abandoned for two to three centuries before new opportunities allowed for resettlement. There is also some evidence suggesting moister conditions in Scandinavia, which could potentially resemble another episode where a polarized precipitation mode became phase-locked over Europe. Interestingly, the Early Bronze Age megadrought happened roughly one Quasi-cycle before the onset of the Little Ice Age. By subtracting 3.5 kyr from these dates, we arrive at the temporal proximity of the beginning of the Wolf Minimum (c. AD 1260–1340) and the subsequent Spörer Minimum (c. AD 1450–1550).

A large portion of Europe experienced two years of unusually heavy and sustained rainfall during the Wolf Minimum in the early 14th century. This miserable episode, which took on almost biblical proportions, began in the spring of AD 1315 and mercifully subsided before the third summer of AD 1317. It triggered the Great Famine of AD 1315–22 in northern and central Europe [Lucas, 1930; Baek et al., 2020]. While crop failures were common in medieval Europe, this particular episode created a vicious cycle for the food supply. The prosperous Medieval Warm Period had increased the population that needed to be fed, but the ratio of planted seeds to harvested seeds decreased. The phrase 'boom and bust' found its time and place to flourish [Lima et al., 2014]. Furthermore, difficulties in producing fodder led to malnutrition and made livestock more vulnerable to diseases, prolonging the miserable circumstances for many years.

Although the transition from the Medieval Warm Period to the Little Ice Age cannot be considered as devastating as the climate-induced crises during the Late and Early Bronze Ages, it did include an unprecedented element: a horrifying pandemic that showed no signs of disappearing soon. The beginning of the Hundred Years' War and the arrival of the bubonic plague from the Mongolian-invaded Black Sea port sealed the fate of countless Europeans by the

mid-14th century. Fortunately, the climate played a minor role in this terrifying drama. However, it still had a profound impact on densely populated societies by significantly altering rainfall patterns, which led to these few years being categorized as a 'once-in-a-millennium' occurrence. While the future implications of the imminent weakening of the Atlantic meridional overturning circulation (AMOC) may not be fully understood, it is essential to be prepared based on various examples of similar changes. It is reasonable to suggest that the orbital configuration has not changed substantially in the past thousand years, which justifies a stronger connection with the recent LIA rather than the Late Bronze Age, not to mention the warming and cooling that occurred c. 7,000 years ago.

The decline of the Akkadian Empire and associated megadroughts appear to have coincided with elevated lake levels and the dying-off of bog pines in Scandinavia between 2200 and 2100 BC [Gunnarson, 2008; Edvardsson, 2013]. In comparison, the transition from the Medieval Warm Period (MWP) to the Little Ice Age (LIA) was much milder in this regard. There does not appear to have been any severe and sustained drought in the vast Middle East and West Asia region when the northern North Atlantic cooled after c. AD 1000. The precipitation pattern across Europe during the cooling period may have been weak and erratic, as there is very little evidence of prolonged anomalies [Bauch et al., 2020]. Referring to the Great Famine years, which were recorded as an exceedingly wet and brief episode, the concurrent high-activity period in the Middle Ages and the warm European climate (while Greenland was cooling) could explain the difference observed during the megadrought, 4.2 thousand years before the present. It coincided with a cooling phase in the northern North Atlantic and a Wolf-like minimum, highlighting a clear causal link.

The interaction between declining solar activity, cooling in the northern Atlantic, and the southward shift of the Intertropical Convergence Zone does not always follow simple guidelines. Therefore, it is unlikely that solar variability solely affects climatic conditions in the equatorial Atlantic, but rather through the involvement of larger interhemispheric and global Conveyor Belt anomalies.

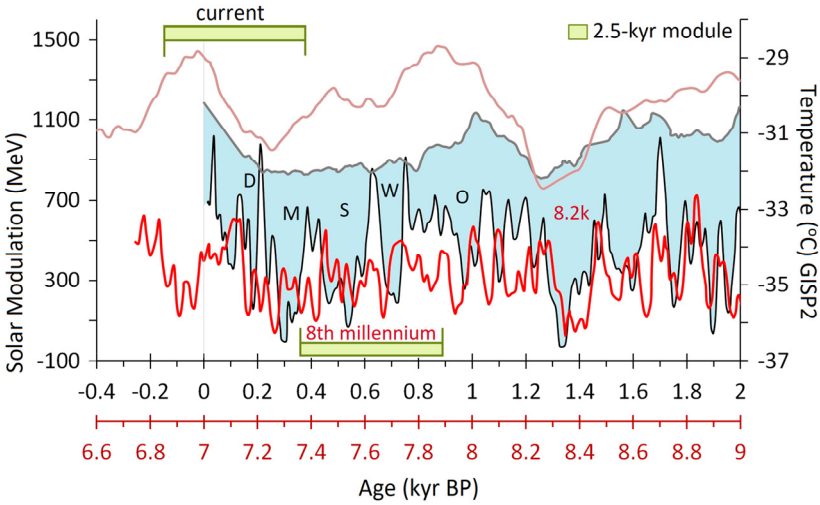

Figure 3.11. The climate and solar activity profiles during the first and eighth millennia BP exhibit striking similarities by centering the local TSI minima around 500 and 7500 years BP. The recent grand minima events, namely Dalton (M), Maunder (M), Spörer (S), Wolf (W), Oort (O), and the 8.2 kyr BP cold event, correspond reasonably well with their respective minima. This figure demonstrates how every third 2.5-kyr module (represented in green) advances by c. 500 years relative to the Quasi-cycle. The data used in this analysis are sourced from [Muscheler et al., 2007; Vonmoos et al., 2006].

3.3.2 Inactivity Similarities Linking the Little Ice Age and the 8th Millennium BP

The DeVries–Suess cycle, which spans 208 years, has been markedly present since the early fifteenth century. The emergence of the Maunder module, characterized by three distinct starting points for grand minima, plays a part in generating a series of dormant periods: the 1400s, 1600s, early 1800s, and 2000s. However, the medieval high-activity epoch from around AD 700 to 1250 disrupted this periodicity, despite the relatively appropriate positioning of the Oort minimum (centered around AD 1000) in the middle. The Maunder module acts as a wild card among the modules, constantly reshaping the 3.5-kyr Quasi-cycle by appearing more frequently than the slowly progressing DP module. A four-hundred-year gap between the arrivals of its grand minima amplifies the overall two-hundred-year

cyclicity, with a notable Dalton-like minimum typically occurring in the middle.

When considering that every third 2.5-kyr module advances approximately 500 years relative to two Quasi-cycles, it becomes evident that strong similarities can be drawn between the 1st and 8th millennia BP. The influence of the 7-kyr TSI cycle on activity correspondence is expected to be significant. A Maunder-like module began around 7.9 kyr BP, coinciding with a medieval-like high-activity period. Since then, it has shifted forward relative to the Quasi-cycle and commenced around AD 1600 instead of AD 1100 (see Figure 3.11). The recent observation of the subsequent inactivity phase of the Solar Surge event overlapping with the post-Maunder minimum supports the idea of a strong solar tendency to impose grand minima on a regular basis. It is naturally intriguing to speculate about the potential impact of this on regional climates.

Around 7.5 kyr BP, there is a noticeable suppression of solar activity levels compared to the past millennium. Understanding the accuracy of these suppressed activity variations is of special interest, as this segment of reduced activity generated more pronounced climate oscillations, contrary to what one might expect. However, it should be noted that the climate in the North Atlantic region is heavily influenced by the Atlantic meridional overturning circulation (AMOC), also known as the Atlantic portion of the thermohaline circulation (THC) (see Figure 4.1). Despite its name, not all the mechanisms and dynamics affecting the complex AMOC are fully understood, which makes the climate susceptible to surprising anomalies.

Regarding climate change, one of the most significant differences between a regular inactivity phase and a Maunder-like minimum is a question that is gaining importance with each passing year. However, one thing is certain: climate proxies from central Greenland do not accurately reflect the influence of a random grand minimum on climate patterns in other regions.

While the Late Bronze Age warming serves as the closest intrinsic model for the recent warming, its solar variability is not as comparable as that of the 8th millennium. Furthermore, the changes in orbital geometry over the past seven thousand years have substantially un-

dermined its relevance to the present-day situation. Despite these challenges, it is vital to thoroughly survey these parallel events, as their intimate connections raise serious concerns about the future.

Shortly after a Solar Surge equivalent concluded (6.99 kyr BP), similar to the present day, the centennial-long warming ceased in central Greenland. However, the temperature remained elevated for several decades afterward, despite the declining solar activity. This period of inactivity persisted for approximately 80 years (30+50), which is very close to the average. It was only when solar activity surged again that the temperature began to decline. In comparison to the current situation, the cooling process began around 70 years after the present and lasted for about 180 years. It progressed in a stepwise manner, with three notable setbacks observed approximately 50, 120, and 180 years from now (2020s). Eventually, the climate stabilized, and the temperature returned to its pre-excursion level. It is puzzling why the weakening of the Atlantic meridional overturning circulation did not respond to the increasing solar activity during the most severe cooling period (around 6.75–6.90 kyr BP).

Understanding the abrupt and enduring nature of climate change reversals is critical. Take, for instance, the initial resurgence of cooling during the Late Bronze Age, which ushered in wetter conditions in southern Sweden and stunted tree-ring growth for two decades. These parallel discoveries reveal inconveniences that may come as a surprise. Based on a rough estimate, the first wetter episode may occur around the 2070s. Additionally, should we anticipate that the momentum of the late Holocene warming will persevere longer in the Arctic compared to the previous two instances? Our limited awareness and knowledge of its resources and thresholds are uncomfortably evident. The fact that diminishing orbital forcing at the poles still generates similar heat momentum as it did seven thousand years ago is indeed surprising. Yet, even in those ancient times, it was a matter of achieving a balance between hemispheres.

3.3.3 The Preboreal and Medieval Intervals

The Preboreal interval was a climate period that lasted less than a millennium and immediately followed the termination of the Younger Dryas. It encompassed both cooling and warming episodes in central Greenland between 10.9 and 11.6 kyr BP [van der Plicht et al., 2004, Mekhaldi et al., 2020]. The past millennium provides an intriguing comparison through the Quasi-cycles. The solar activity profile of the Preboreal resembles the high and low activity epochs of the Medieval Warm Period (MWP) and the Little Ice Age (LIA), with the notable absence of a Maunder-like minimum. The solar perturbation wave, which influenced the Quasi- and intermittent cycles, temporarily extended these periodicities between 6 and 13.2 kyr BP. This was considered when the far-end Quasi-cycles were superimposed (see Figure 3.12). The abrupt onsets of the Holocene and the MWP appear to correspond relatively well based on the central Greenland temperature record, suggesting a similar oceanic circulation pattern as the source. Even their climatic tipping points seem to align. The Oort-like minima marked a joint transition point in both periods by initiating short-term coolings. However, unlike the MWP, which took considerable time to recover from the cold LIA, the Preboreal quickly experienced a ramp-warming rate. It is possible that this rapid warming was an underlying trend cleverly concealed behind the climatic upheaval of the BA/YD period. Nevertheless, gradually warming, steady deglacials have been relatively rare in northern Atlantic chronologies due to the often accompanying cold Heinrich stadials, which introduce volatility [Alley and Clark, 1999; Hodell et al., 2008].

The late Preboreal period in Europe commenced with a cool phase known as the Preboreal Oscillation, which can be compared to the early stages of the Little Ice Age (LIA) through the Quasi-cycle. However, there was a notable difference: instead of the usual two grand minima (Wolf and Spörer), an extremely long minimum occurred. A shared characteristic between the early LIA and the late Preboreal is the cool and humid climate that prevailed in northern and central Europe after the Sun entered a period of reduced activity around AD 1260 and 11.3 kyr BP. The presence of such climatic

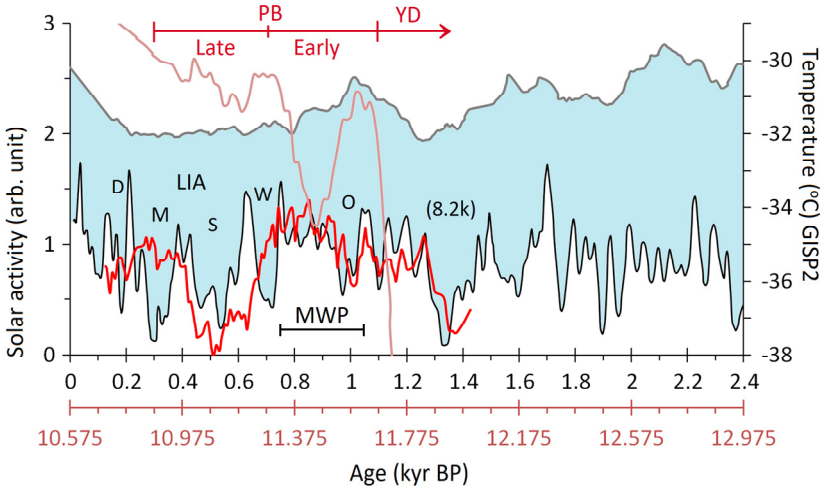

Figure 3.12. The Quasi-cycle had remarkably similar activity profiles in the 1st and 12th millennia BP. The identified inactivity periods are Dalton (D), Maunder (M), Spörer (S), Wolf (W), Oort (O), and an equivalent event to the 8.2k cooling (8.2). These phases are separated by three 3525-year cycles. Additionally, a perturbation wave extends solar periodicities between c. 6 and 13 kyr BP. The Preboreal (red) and medieval (black) solar activity periods demonstrate the continuity of the Quasi-cycle. The source of data: [van der Plicht et al., 2004; Muscheler et al., 2007; Vonmoos et al., 2006]. Please note that the Preboreal temperature curve (red) has been adjusted upwards by +5 °C.

asynchrony between Greenland and Europe, recurring in another cycle, suggests a significant similarity in solar forcings. Indeed, the Preboreal interval can be well compared to the combined Medieval Warm Period and Little Ice Age. The climatic changes that struck Europe and Greenland around AD 1250 and AD 1000, respectively, were on a much larger scale and took place precisely three Quasi-cycles earlier. The turning point in the climate of central Greenland, following an Oort-like minimum, served as a prelude to the climatic reversal in Europe, albeit a few hundred years later. Similar shifts in climatic conditions are evident in the terrestrial records of northwest Europe. Around 11.45 kyr BP, during a medieval-like high-activity epoch, warm and dry summers interrupted the expansion phase of the birch forest. Subsequently, a climate change occurred around 11.3 kyr BP, which is characteristic of transitions resembling the

MWP–LIA. Proxy records indicate that the onset of moister conditions in northwestern Europe coincided with a sharp increase in galactic cosmic-ray intensity and a temporary decline in atmospheric CO_2 concentration.

It would be challenging to attribute the Preboreal temperature oscillation solely to solar variability, especially considering the apparent insensitivity of the late Preboreal in Greenland after 11.3 kyr BP to large-scale changes in solar activity. According to the GISP2 record, there was also a phase of notable insensitivity in the climate between AD 1250 and 1800. Despite their reverse positioning on the Total Solar Irradiance cycle, these two episodes at the far ends of the Holocene share many similarities. This is an intriguing anomaly because their activity profiles still exhibit robust likenesses, even though the 10.5-kyr time span itself does not correspond to any known periodicity.

In Chapter 2, most of the grand minima of the Holocene have been associated with the Multi-millennial solar cycles. However, some uncertainty arises when distinguishing grand minima cases near the TSI minimum from the pointedly low, base-level activity variations. On the other hand, the TSI maximum introduces an entirely different scenario. For instance, in the early Holocene, there seem to have been a few exceptionally long-lasting, high-activity epochs without clear evidence of severe declines. The longest one persisted for seven hundred years, from roughly 11 to 10.3 kyr BP, showcasing remarkable stability in contrast to the past millennium. Even the effects of solar cycles, extending from decades to centuries, were not distinctly observed during this robustly active epoch.

This reasoning brings us to the fundamental aspects of the solar dynamo theory [Ossendrijver, 2003; Charbonneau, 2010, 2020] and raises the question of why grand minima exist at all, as they do not appear to be a straightforward phenomenon. Several simple dynamo models have successfully produced suppressed states resembling Maunder-like minima [Charbonneau, 2014]. The extent to which these findings can be translated into more complex models is an active area of research. An insightful exploration of the dynamics of the solar tachocline is reviewed by Miesch in Schrijver et al. [2010].

CHAPTER IV

4 OCEAN CIRCULATION AND CLIMATE CHANGE

The oceans are relatively shallow compared to their vast surface area. The average ocean floor could be reached in less than an hour simply by walking. However, separating the same 4 km distance from a space view (Fig. 4.1) would be challenging. It seems most evident that the Sun's properties play a significant role in abrupt climate changes, and these changes are based on the interactions within this quite thin but vast liquid medium, which covers about two-thirds of the Earth's surface area. The characteristics of oceans are continually exposed to solar variability and could potentially affect the climate system. It appears that ocean-circulation patterns can respond fairly quickly to variations in solar activity under the right circumstances.

The oceans' significance for climate stability lies in their relatively high heat capacity and viscosity compared to that of the air. However, these properties also compensate for each other and form a medium for the dynamic climate system in which heat, water, gases, and particles are continuously exchanged to achieve a steady state. This state is never fully reached, mainly due to the seasonal cycles at higher latitudes, which contribute to the somewhat large inclination of the Earth.

4.1 The Atlantic Meridional Overturning and Thermohaline Circulations

The Atlantic meridional overturning circulation (AMOC) is an important component of the climate system. The terms 'thermohaline circulation' (THC) and 'meridional overturning circulation' (MOC)

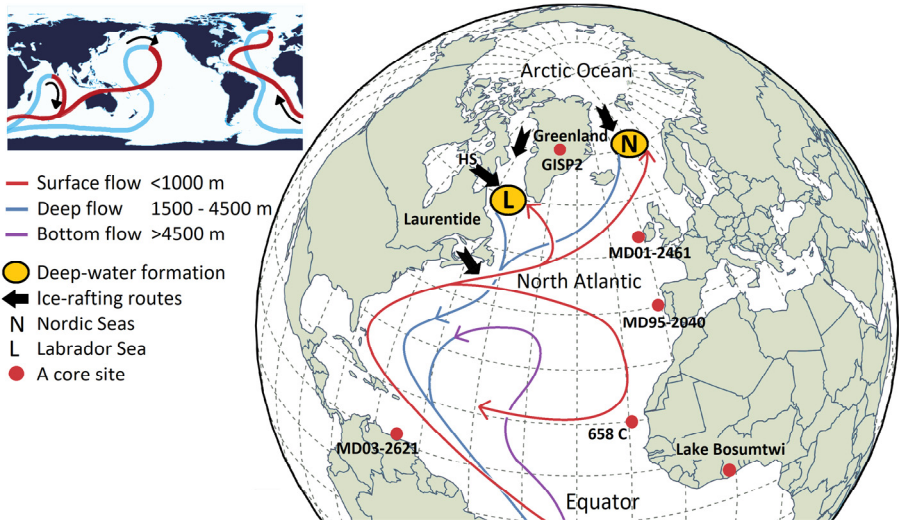

Figure 4.1. A schematic illustrates the Atlantic Meridional Overturning Circulation, also known as the Atlantic portion of the global Conveyor Belt. Its warm surface currents (red) in the upper 1,000 m sink at higher latitudes and form cold deep return currents (blue). Major sources of ice-rafted debris (IRD) are indicated by black arrows [Andrews, 1998]. In the literature, the Hudson Strait (HS) is often referred to as the primary source for Heinrich layers 1, 2, 4, and 5, while layers 3 and 6 originate from different sources [Hemming, 2004]. Some ocean-drilling and ice-core sites mentioned in this chapter are represented by red dots.

are often used inaccurately as synonyms, even though the MOC includes wind-driven parts [Wunsch, 2002; Rahmstorf, 2006, 2009], and its definition is not based on any specific driving mechanism. The Atlantic MOC purely measures a basin-wide flux of water at certain latitudes and depths. In contrast, the thermohaline circulation strictly refers to heat and salinity, i.e., the water-density-driven parts of ocean circulation and convection. The AMOC is more commonly used in research because separating 'wind-driven' and 'density-driven' components is complicated. The two factors, temperature, and salt concentration, virtually determine the water-density differences that generate the oceanic convection to the intermediate, deep, and bottom levels. The pressure is a minor factor in the water-density equation, increasing its density by only 4% from the ocean surface to 10 km depth [Bigg, 2003].

Warm tropical surface waters have a natural tendency to flow towards the Arctic region. In this context, the Atlantic overturning circulation offers a straightforward mechanism for mixing salty, warm waters with their cooler counterparts. It serves as a direct response to the Earth's topography, occasionally encountering minor disruptions in the convection process. Notably, if the Pacific Ocean were to transport an equivalent amount of water and heat to the Arctic, it is unlikely that the DO oscillations would have manifested in the same manner. Such an alternative scenario might have allowed the grand cycles of the Sun to go unnoticed.

As warm tropical surface currents move towards higher latitudes, they undergo processes of evaporation, leading to the removal of freshwater and the release of heat. In these physical processes, surface waters become saltier and cooler, collectively increasing their density. However, as temperatures approach the freezing point (c. -1.8 °C), the rise in salt concentration becomes more critical than the decrease in temperature. The formation of sea ice is another pivotal process that contributes to enhanced surface-water density by extracting freshwater from the ocean's surface.

Throughout the winter season, as surface waters cool and undergo processes of evaporative salinification, along with the salt-rejection mechanism during sea-ice formation, North Atlantic Deep Waters (NADWs) are generated in the Nordic and Labrador Seas. Likewise, the primary production zones for Antarctic Bottom Waters (AABW) are situated in the Weddell and Ross Seas, as illustrated in Figure 4.2. These submersed waters disperse into adjacent basins, with NADW typically found below approximately 1,500 meters and AABW at depths of around 4,500 meters, driven by disparities in abyssal water density.

The Gulf Stream and its extension, the North Atlantic Drift, are the warm currents that keep Northwestern Europe's climate mild and moist. At these northern latitudes, they transport up to 20% of the total heat in the ocean–atmosphere system, essential for ensuring Europe's moderate temperature. Without this equatorial warmth, Europe's high latitudinal location would make it a much harsher environment. The Trade Winds and AMOC transport the heat to the

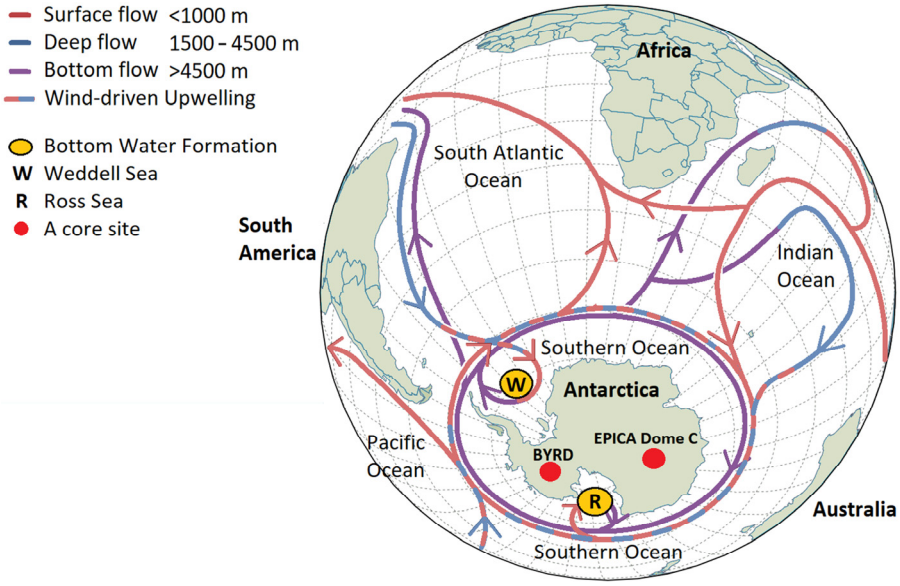

Figure 4.2. A schematic illustrates a portion of the Southern Hemisphere thermohaline circulation, showing its surface-ocean flows (red) and bottom-ocean flows (violet). These flows are generated by density differences, as indicated by the terms 'thermo' and 'saline'. The thermohaline circulation, along with surface winds and tidal forces, contribute to the formation of large oceanic circulations. The formation of Antarctic Bottom Water in the Weddell (W) and Ross (R) Seas is influenced by strong westerly winds and the Antarctic Circumpolar Current (ACC). The ACC is the only current that completely encircles the globe. A schematic map of the global thermohaline circulation is depicted in 2-D by Kuhlbrodt et al. [2007] and in 3-D by Talley [2013].

Gulf of Mexico, from where the Gulf Stream and southwesterly winds carry it to the North Atlantic mid-latitudes. While the mainly wind-driven Gulf Stream primarily drives the heat transport, the thermohaline circulation also plays a part in this process by transferring an impressive 20 million cubic meters of water per second northward, or twenty percent of the total mass transport [EASAC policy report; Msadek et al., 2013; Johnson et al., 2019]. However, the thermohaline circulation is crucial for transporting heat across the Equator and linking polar climates through the bipolar seesaw mechanism. It fundamentally differs from wind-driven ocean circulations in how it generates momentum. While these two driving forces are not entirely separable, neither are the powerful westerly

winds sweeping over the Southern Ocean, which transfer energy to the Atlantic overturning circulation by increasing the upwelling of deep and bottom return flows around Antarctica [Toggweiler et al., 1993; Rahmstorf 2009]. All things considered, the thermohaline circulation and the Gulf Stream are essential for controlling Earth's temperature and weather patterns.

4.1.1 Alterations in the AMOC

The oceanic surface current of the AMOC in the upper 1,000 m transports warm water across the Equator to the North Atlantic, and the deep return currents deliver cooled, sunken water back to the Southern Ocean in depths between 1,500 m and 4,500 m. The convection of overturning circulation has the potential to produce heat imbalances between the hemispheres. In a simplistic presentation, the deep water is brought to the surface by wind-driven upwelling, mostly around Antarctica [Kuhlbrodt et al., 2007]. Strong westerly winds blowing over the Antarctic Circumpolar Current (ACC) generate enormous stress on the Southern Ocean and transfer momentum to deeper layers. Maintaining a smoothly operating AMOC in the northern Atlantic is crucial, and the sinking of cold waters is a central process in achieving this. However, the circulation process along the southern borders also contributes to the AMOC's overall functionality.

The variability of the AMOC is best described by the three-mode model proposed by Sarnthein et al. [1995], Rahmstorf [2003], and Kuhlbrodt et al. [2007]. This model consists of three modes: acceleration, deceleration, and shutdown. During the acceleration mode, the AMOC gains momentum by harnessing heat from the South Atlantic and the Southern Hemisphere. As a result, a North Atlantic deep-water cell shifts to higher latitudes (specifically, to the Nordic Seas). In the deceleration mode, the sinking of surface waters declines and shifts southward (below Iceland). Consequently, the northward heat supply decreases. In the extreme case, deep-water formation may cease, presumably due to the large quantities of freshwater that reduce the sea-surface salinity.

Antarctica, the fifth-largest continent, is situated in the center of the global oceanic region, mainly above 66 degrees of southern latitude. The Southern Ocean and the Circumpolar Current effectively isolate it from adjacent continents. The air–sea circulation around Antarctica is one of the factors that affect the strength and stability of the AMOC, along with meltwater perturbations and the import–export salt balance of the Atlantic basin. As a result, the Antarctic climate is less affected solely by changes in the Atlantic MOC, and it smoothly follows the Total Solar Irradiance cycle, with fewer abrupt changes that are not typical of the Greenland climate.

The equatorial Pacific Ocean and the Indian Ocean absorb solar energy over a vast surface area, and they are both directly open to the outer reaches of Antarctica through the Circumpolar Current, which is the only oceanic current that circles the globe. This environment is entirely different from the mostly enclosed Arctic Ocean.

4.1.2 The ITCZ in the Atlantic and Indian Ocean Sectors

The geographical peculiarities on both sides of the equatorial Atlantic slightly favor the northwestward oceanic heat flow. The Gold Coast of Africa is situated above the Equator, while the coastal wedge formation of Brazil lies below the Equator. The northeasterly and southeasterly Trade Winds converge at the equatorial low-pressure zone, where the warm air, especially on land, vigorously rises during the daylight hours. The ascending air migrates to the subtropical zones, where it descends and closes the tropical Hadley cell. This circulation is also known as the Intertropical Convergence Zone (ITCZ), which in different parts of the world experiences anomalous seasonal or year-round displacements from its geographical location (0°).

The Intertropical Convergence Zone exhibits diverse behaviors in different parts of the globe, resulting in regional variances in climatic patterns. In the eastern and central Pacific sectors, the ITCZ remains consistently on the Northern Hemisphere side, while in the western Pacific, it can experience a substantial shift during the southern summer. Meanwhile, the Indian Ocean sector displays notable sea-

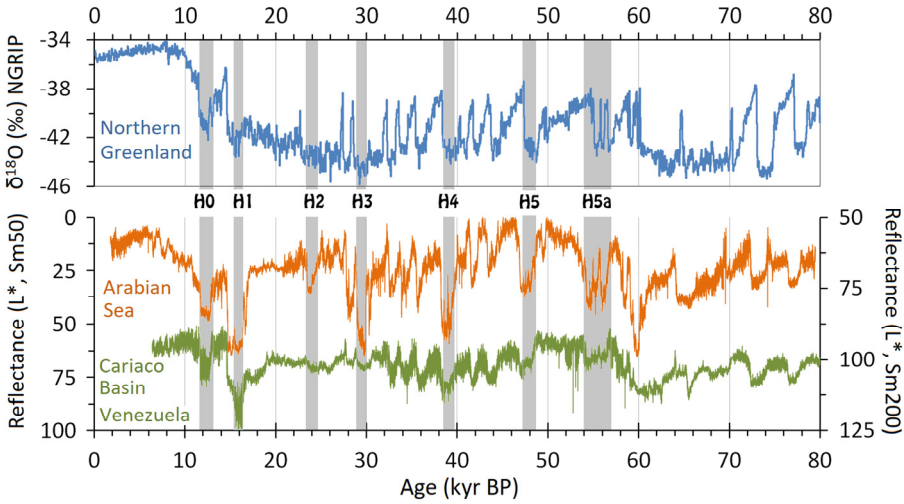

Figure 4.3. The strength of the Indian monsoon (orange) demonstrates a distinct correlation with the temperature of Greenland (blue) as the Intertropical Convergence Zone (ITCZ) fluctuates (green). The influence of variable Atlantic Ocean circulation on the ITCZ is prominent during halts in the Atlantic Meridional Overturning Circulation (AMOC) known as Heinrich events (H). The data for sediment color reflectances (L*) were obtained from core sites MD03-2621 and SO130-289, located off the Venezuela margin and Arabian Sea, respectively [Deplazes et al., 2013], as well as from NGRIP members [2004].

sonal variations due to the stark contrast between the relatively stable surface temperature of the ocean and the extreme climatic conditions of the Eurasian continent, characterized by cold northern winters and hot summers. These stark contrasts in regional ocean–atmosphere system result in pronounced seasonal fluctuations in precipitation over the Indian sub-continent, with the monsoon belt shifting dramatically northward during the northern summer and accounting for around 80% of the annual rainfall in a short time.

In the Atlantic sector, the ITCZ follows the hemispheric summer and twists slightly across the sector due to the polarization of land distribution. The interpolar heat and salt exchange flows through the Atlantic Ocean, while the El Niño–Southern Oscillation (ENSO), the largest interannual ocean–atmosphere interaction, characterizes the tropical Pacific climate. It markedly operates in the opposite direction to the Atlantic overturning circulation [McPhaden, 2006]. Un-

derstanding the dynamics of the ITCZ and its interactions with other components of the climate system is essential for predicting and managing the impacts of regional climate variability and change.

The influence of the El Niño–Southern Oscillation climate phenomena on the bipolar seesaw mechanism and the Atlantic overturning circulation remains a topic of ongoing research. Despite considerable efforts, there is limited documentation of how the ENSO affects the Atlantic overturning circulation, which typically operates on a 3- to 7-year cycle [Wang et al., 2006; Koutavas et al., 2012]. However, recent evidence suggests that a reduced AMOC can impact the eastern tropical Pacific climate through the northeasterly Trade Winds blowing over Central America's narrow land corridor [Timmerman et al., 2007; Williamson et al., 2018]. Notably, the Southern Ocean and Southern Pacific comprise a single massive body of water, extending over 140 longitudinal degrees. This interconnectedness highlights the need for a comprehensive understanding of the oceanic and atmospheric systems, including the ENSO, that influence the Atlantic and Southern Ocean circulation.

4.1.3 The ITCZ and Variability of the Indian Monsoon

Figure 4.2 highlights the central role of the warm current in the Indian Ocean in maintaining the Atlantic Meridional Overturning Circulation. This current carries warm, salty surface water that flows towards the Southern Ocean, but a portion of it also enters the South Atlantic by passing through the Agulhas leakage at the tip of South Africa. Changes in the flow ratio of these dividing currents could have considerable implications for the North Atlantic's climate. Peeters et al. [2004] suggested that the AMOC could derive some of its momentum from the thermohaline properties of the Indian Ocean. However, the worst-case scenario is that the AMOC could completely stop, leading to a larger proportion of the warm surface flow being redirected toward the Southern Ocean. The exact consequences of such a redirection remain uncertain, with some studies suggesting that it may be due to increased Antarctic Bottom Water formation in the Ross and Weddell seas, as proposed by Broecker in

[1998], Gordon et al. in [2007], and Hayes et al. in [2014]. An alternative scenario is that an increase in the AMOC rate would result in a stronger pull from the Atlantic Ocean, causing substantial warming as a result of the switching mechanism.

The sedimentation records suggest a remote connection between strong Indian summer monsoons and Greenland warm events, as indicated by Altabet et al. [2002], Zhang & Delworth [2005, 2006], and Deplazes et al. [2014]. Recent summers (2021 and 2022) have brought this phenomenon into clear focus. In contrast, during the ice age, a switch to cold, stadial conditions in Greenland coincided with less intense precipitation intervals in India, according to Kathayat et al. [2016] and Lauterbach et al. [2020]. Some studies have even suggested that the East Asian Monsoon is in sync with these events [Zhang et al., 2019]. As we move toward the mid-phases of the next century, the AMOC is expected to experience its steepest decline, resulting in a total drop of minus 1 °C in Arctic temperatures. This, in turn, is likely to weaken the Indian summer monsoon, as illustrated in Figure 4.3.

Paleoclimatic records provide a valuable perspective on present-day global climate phenomena, ranging from the Indian subcontinent to the Arctic. Throughout history, the occurrence of strong Indian summer monsoons has been concurrent with warm Arctic summers, indicating a teleconnection that spans the vast Eurasian continent. Changes in the position of the ITCZ due to intra-annual, multi-decadal, and centennial alterations of the thermal equator can result in prolonged drought conditions at latitudes not witnessed for many generations. The tropical summer monsoon season is, in part, a manifestation of the shifting ITCZ during the year.

If the variable behavior of the ITCZ mirrors ancient global climate patterns, even in modern times, as suggested by the paleoclimatic records, a pressing question arises: What is the current status of the interhemispheric heat balance, especially in light of the observable abrupt warming in the Northern Hemisphere? The growing concern centers on the potential far-reaching consequences when the intrinsic climate cycle in the Atlantic loses its momentum, possibly impacting the global climate on a significant scale.

4.2 The Double Peak Module and Abrupt Climate Changes

4.2.1 The Coldest Phases of the Stadials: Heinrich Events

Massive ice-sheet instabilities have caused meltwater runoffs that greatly perturbed the northern North Atlantic salinity in the past, resulting in lighter-than-usual surface waters with severe climatic consequences. The Laurentide ice sheet in North America was the primary source of icebergs carrying lithic grains that were deposited all over the northern North Atlantic seafloor. The flow of icebergs was especially abundant during the true Heinrich events (H) [Peck et al., 2006].

Heinrich layers can reach thicknesses of 50 cm off the Canadian margin, while on the European side they can be as little as a few centimeters [Jullien et al., 2006]. Despite the fact that the primary sources of debris are from Canada and Greenland, the ice-rafted debris (IRD) belt, as described by Ruddiman [1977] and Grousset et al. [1993], covers a vast band of the eastern North Atlantic (40°–50° N). These layers took a long time to form, with estimates suggesting an accumulation of more than a hundred, but usually less than a thousand years, depending on the event [Dowdeswell et al., 1995].

When the salinity of oceanic surface flux stops increasing, its ability to become denser and heavier than its surroundings diminishes, making the surface water unsinkable. As a result of the cessation of convection, the northern North Atlantic region receives substantially less heat, leading to the production of cold stadial events by Heinrich events. Whether a massive ice-rafting event is the cause or consequence of deep-water-cell collapse is still debated [Maslin et al., 1995, 1999; Seidov et al., 1996]. Possible explanations for ice-sheet instabilities include sea surface fluctuation [Chappell, 2002; Siddall et al., 2008] and North Atlantic subsurface warming [Marcott et al., 2011]. However, it now seems certain that the Sun is strongly involved in these events.

Maybe it is the Atlantic Ocean, virtually reaching from pole to pole, that acts like an instrument and resonates with the intrinsic cy-

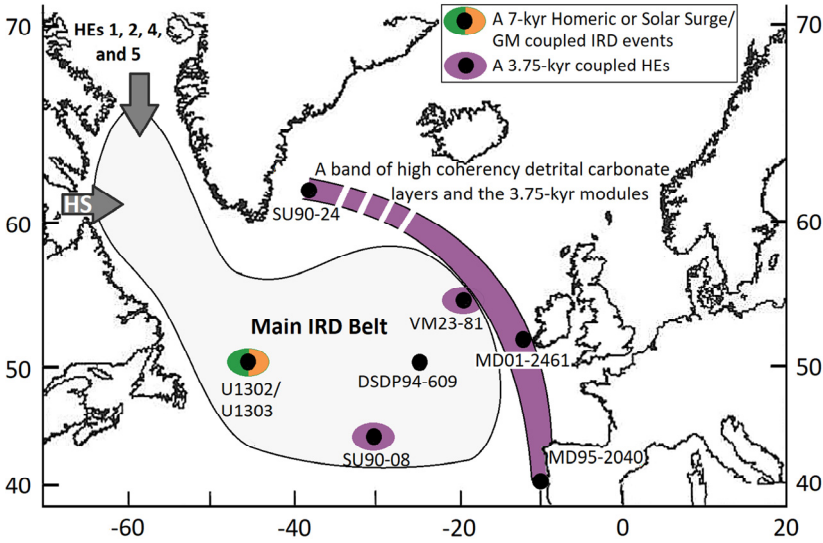

Figure 4.4. Detrital carbonate layers H1, H2, H4, and H5, located in the eastern and southern parts of the main ice-rafted debris (IRD) belt, correspond to the occurrences of the 3.75-kyr module during the last ice age. These layers are observed in SU90-24, VM23-81 [Bond et al., 1999], MD01-2461 [de Aberu et al., 2003], MD95-2040 [Peck et al., 2006], and SU90-08 [Paterne et al., 1999]. Among these, the DSDP94-609 core is positioned in the middle and consistently displays advanced detrital layers rich in carbonate compared to others. Interestingly, IRD events at the western North Atlantic site U1302/U1303 [Channell et al., 2012] are consistently linked to adjacent TSI-minimum events, including a Homeric-like module and a Solar Surge/grand minimum equivalent (refer to Fig. 4.6).

cles of the Sun. Perturbations caused by the 3.75-kyr solar cycle seem to have repeatedly launched a substantially colder period lasting several centuries, but often close to a millennium. The YD and H4 events are examples of such persistent cases (Fig. 4.5).

Physical feedback effects are considered important for maintaining Arctic cold spells such as the Younger Dryas. A sea-ice cover not only blocks heat and moisture from being released into the atmosphere but also efficiently reflects solar radiation back to space. The sea ice has an albedo (reflectivity of a surface) that is approximately five times larger than the average ocean surface. During the YD, the prevailing climate in central Greenland was cold and dry, with notably thin ice-sheet layers and barely recognizable interannual varia-

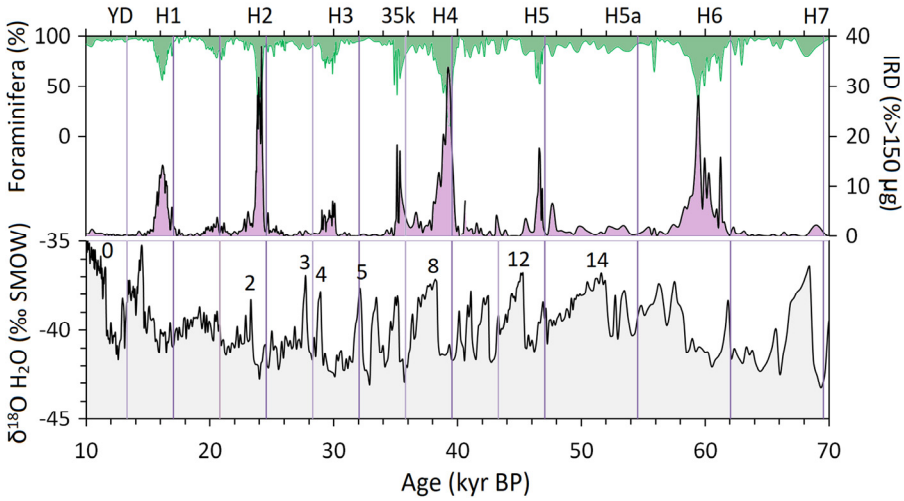

Figure 4.5. Abrupt changes in IRD (violet) and planktonic foraminifera abundances (green) repeatedly coincided with the 3.75-kyr module (violet line). Foraminifera are a group of single-cell marine organisms, and their relative abundances and chemical shell compositions are influenced by prevailing oceanic conditions. Both proxies were obtained from MD-95-2040 site off the Iberian margin [de Abreu et al., 2003]. The elevated abundance of lithic grains around 35.8 kyr BP is associated with the clustered module, which is an anomaly among IRD events as they typically follow a 7.5-kyr pace. In the lower panel, a Greenland climate proxy for $\delta^{18}O$ [Grootes et al., 1999] illustrates the coldest stadials during the glaciation.

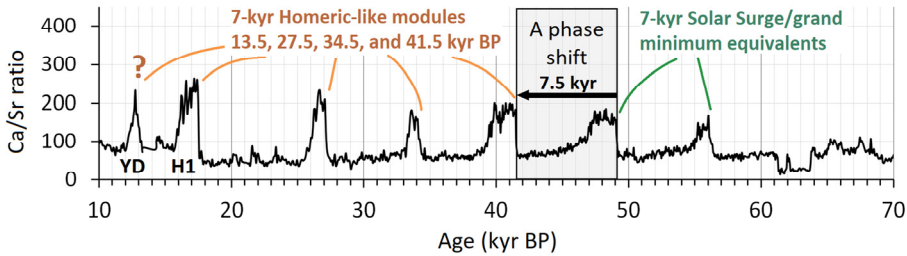

Figure 4.6. A calcium/strontium ratio measured from the western North Atlantic core site U1302/U1303 [Channell et al., 2012] documented two different IRD periodicities. Apart from the well-known H1, they are all associated with TSI minima. This regional anomaly suggests that the maximum TSI in the background may have had a greater influence on the pacing of main IRD events than previously recognized. Furthermore, a record from the Orphan Knoll site in the Labrador Sea (50° 10′N, 45° 38.3′W) presents a controversial perspective on the ice age dynamics in the North Atlantic.

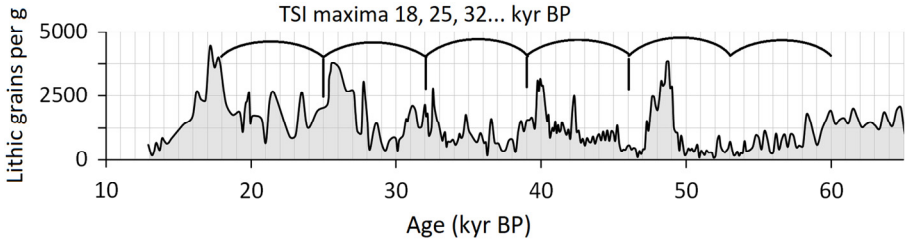

Figure 4.7. A lithic-grain record from the central IRD belt, specifically core site DODS94-609, provides evidence of cyclical ice-rafting coupled with TSI_{max}. The data is sourced from Obrochta et al. [2012].

tion in snowfall. It is estimated that the accumulation rate of snow doubled after the start of the Holocene [Alley, 2000].

Despite our relatively good understanding of the so-called Ocean Conveyor Belt and its global movements, it remains partly unclear how far-reaching the ocean-current system is that ultimately shuts down the Atlantic Meridional Overturning Circulation (AMOC). Integrating all major basins, from the central Pacific to the fringes of the Arctic, reveals the implications of this system for the global climate. While flowing air is largely unobstructed by terrain formations, oceanic heat flows are more constrained by continental configurations, which can alter the effective redistribution of solar energy and cause cyclic variations. These physical differences can further amplify periodicity. It is important to note that a 2.5-meter-thick layer of the ocean transfers an equal amount of heat as the entire air column above it. Therefore, the ocean currents' larger heat capacities compensate for their slower motion, providing stability wherever they extend yet occasionally exposing regional climates to considerable upheavals.

4.2.1.1 Anomaly of Western North Atlantic

In the light of the evidence, the ringing of the millennial solar clock triggers an unknown sequence of events that ultimately leads to massive ice rafting. If a massive discharge of icebergs eventually shuts down or substantially reduces the deep-water formation, then solar variability is to blame for these abrupt changes. A growing body of evidence from different parts of the northern Atlantic sug-

gests that ice-rafting events are even more complexly integrated into the multi-millennial solar cycles than has thus far been explained in the book.

The western North Atlantic core site U1302/U1303 [Channell et al., 2012] documented two different IRD periodicities instead of one. These carbonate-rich detrital layers, peaking near the TSI minima, underline their robust periodic nature and consistent responsiveness, first on a Solar Surge equivalent and then on a Homeric-like module (Fig. 4.6). The western North Atlantic IRD layers are primarily a signature of iceberg calvings in the North American Laurentide.

This rather bizarre finding from the Labrador Sea site urges us to reexamine the unrealized potential of the TSI cycle on Heinrich events in the eastern and central North Atlantic (Fig. 4.7). If an ice rafting is more susceptible to the TSI maximum than the DP module, it should then seemingly explain some differences in IRD events between group 1 (long-term and gradual) and group 2 (short-term and abrupt).

Some Heinrich events strangely advanced the appearance of DP module for as little as a few hundred years and sometimes even more without a proper explanation. In the mid-ice age, the DP module passed the TSI maximum of around 32 kyr BP. Their match point seems to mark a great division. By adding ±15 kyr to 32 kyr BP, we get a time range from 47 to 17 kyr BP, which quite accurately encompasses the Heinrich events from H5 to H1. During this period, the DP module shifts from a thousand-year lead (+1000 yr) to an equal lag (-1000 yr) relative to the TSI maximum. As we move even further back in time, the gap between the TSI_{max} and the DP module spreads over two millennia at the time of H6. It could partly explain the ice-rafting endurance of H6 (see Fig. 4.5). The TSI cycle may thus be one of the factors that explains why the single DP module generated most of the last ice age IRD events and the clustered one did not. This captivating perception will definitively clarify the lead–lag issues.

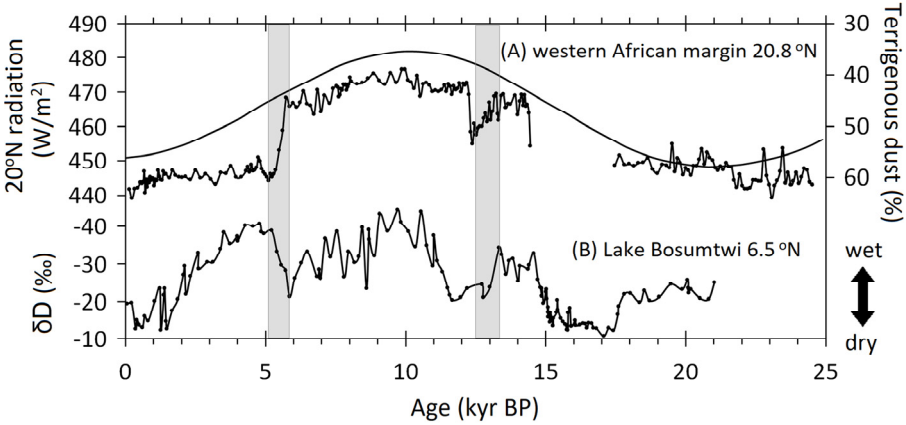

Figure 4.8. The last African Humid Period can be described by the following indicators: (A) the percentage of terrigenous dust at core site 658C off the coast of West Africa (20.8° N) and summer insolation (W/m²) during June–August at 20° N, and (B) the leaf wax hydrogen (δD) isotope record from Lake Bosumtwi (6.5° N). The data sources for these indicators are deMenocal et al. [2000] and Shanahan et al. [2015], respectively.

4.2.2 End of the African Humid Period

The colossal gas giants, Jupiter and Saturn, exert their gravitational influence on Earth, creating periodic disturbances in its otherwise circular orbit around the Sun. These gravitational interactions mainly produce orbital eccentricity cycles of c. 100, 405 kyr, and 2.4 myr, which modulate the spatial and temporal amplitudes of the incoming solar irradiation. Insolation is the most commonly used parameter for tracking paleoclimatic changes on timescales of less than half a million years. The periodic variability of planetary interactions can be observed, for instance, in the long-term records of the northern African climate, where the 405-kyr cycle has been particularly prominent in inhibiting large-scale hydrological transitions over its vast and hot surface [deMenocal, 2004; Larrasoaña et al., 2013; Grant et al., 2017].

The augmentation of summer insolation over North African land induces an air circulation pattern, replacing warm, buoyant land air with moist air from nearby oceans. During the Green Sahara Periods, the amount of rain was sufficient to keep the land habitable despite

higher insolation. However, in the current era with a nearly circular orbit, Green Sahara periods tend to be more restrained or distinctly divided into east–west African monsoon regimes, not occurring simultaneously. Over 5,000 years ago, the northernmost part (30–25° N) of today's Sahara (30–17° N) remained a mosaic desert, primarily because there was not enough contrast between land and sea surface temperatures during summer days, hindering natural convection dynamics.

The intrinsic prospects for the Green Sahara seem very limited over the coming decadal millennia due to mildly evolving insolation around c. 25° N. This kind of orbital configuration controversially favors longer-than-usual interglacials and warm conditions in the polar regions. Orbital precession-driven wet–dry periods broadly oscillate in 20-kyr cycles over the northern African continent, but they are particularly prominent around interglacials or times when insolation over North Africa is clearly above its long-term average, as can be seen in long-term records [Larrasoaña et al., 2013; Grant et al., 2017]. Thus, one starts to consider whether the warmer Arctic contributes to vegetation shifts not only at higher latitudes but also near the Equator via climatic feedback loops [Pausata, 2020].

The termination of the last African Humid Period was not a uniform process. It started around 6.5 kyr BP in the northernmost part of the Sahara (31° N), but later underwent an abrupt latitudinal shift between 27° and 19° N after 5.7 kyr BP, as illustrated in Figure 4.8 [deMenocal et al., 2000; McGee et al., 2013; Tierney et al., 2017]. It then progressed toward the Equator over the next few thousand years [Shanahan et al., 2015]. As a result of the cessation of the monsoon climate, the numerous perennial lakes and river networks in the current Sahara region dried up, causing the area to become a desert. However, closer to the Equator, the transition was not a linear process. Rather, it was a complex one that included an interesting twist. Records indicate that the Lake Bosumtwi region (6° N) began to flourish again at 5.5 kyr BP, while the site 658c (21° N) turned into a desert. It was almost as if the monsoon climate had shifted southward, reinvigorating the Lake Bosumtwi region, where the rains gradually declined after 9 kyr BP [Shanahan et al., 2015]. This date

corresponds to the previous DP module of 9.4 kyr BP. The Bosumtwi record shows much greater sensitivity to each DP module than the site 658c does since the Last Glacial Maximum.

Altogether, the abrupt transition towards aridity began around 5.7 kyr BP, according to records from site 658C. It is particularly noteworthy considering the established pattern of alternating between humid and arid climates in response to shifting summer insolation levels across the African continent. While summer insolation represents a slowly evolving factor capable of creating favorable conditions, it alone lacks the capacity to induce intense and drastic climate changes. Interestingly, another impressive climate mode gained momentum on the other side of the world around the same time, although it is unclear whether this was a coincidence.

The meteorological phenomenon, El Niño–Southern Oscillation (ENSO), in the tropical Pacific was mainly absent in the early Holocene, until about seven thousand years ago, some significance in the frequency of events occurred. The returned ENSO took on a more frequent form about the same time when the Intertropical Convergence Zone (ITCZ) shifted southward in North Africa at about 5.5 kyr BP [Burroughs, 2005]. That seems strange because the millennial, quasi-cyclic nature of the ENSO with alternating phases did not commonly respond to the same solar-activity event as the African monsoon, although their paths crossed in such a pronounced manner in the mid-Holocene. Despite this oddity, several studies have identified key dates and time intervals of ENSO evolution over the Holocene period as 1–1.7, 2.5–3.5, 4.8–5.6, and 7 kyr BP [Thompson et al., 1998; Moy et al., 2002; Rein et al., 2005]. A rough examination reveals that these dates are closely linked to the Multi-millennial solar cycles. At least the importance of the Solar Surge event, the s3.5-kyr module, and their immediate surroundings are notably present. The appearance of the s3.5-kyr modules coincided with peaks in ENSO frequencies. This is to say that we are currently living in fabulous times to observe and study many aspects of the El Niño–Southern Oscillation, also from the perspective of solar variability.

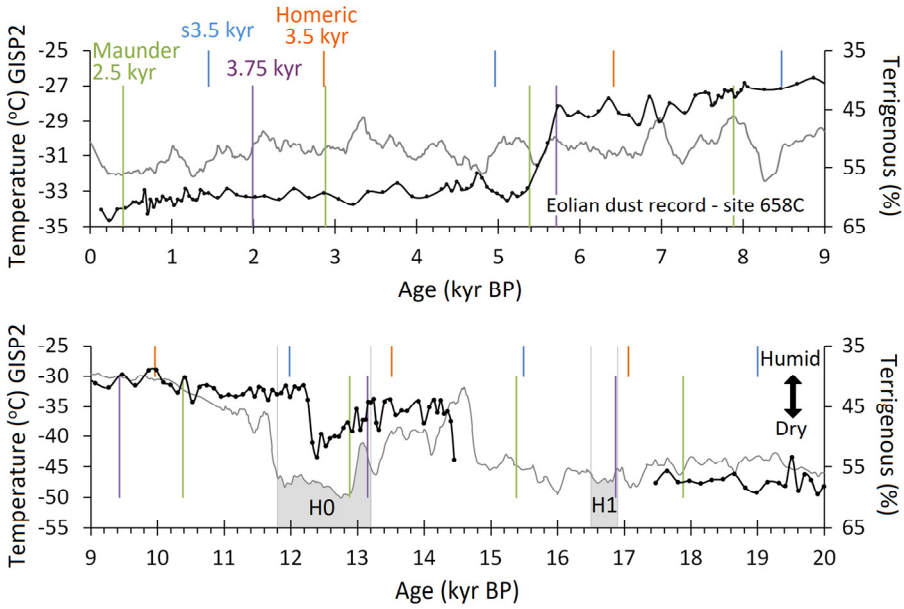

Figure 4.9. The terrigenous dust percentage (black dots) from the West African margin [site 658C; deMenocal et al., 2000] is shown along with the onsets of the 3.75-kyr solar module (violet). The grey areas represent the Heinrich layers H0 and H1. The Mystery Interval commenced c. 17.5 kyr BP, preceding the first Heinrich event, but aligned with the notable inceptions of the 8th and 12th interstadials through the 7-kyr TSI cycle. Additionally, it coincided with the abrupt drop in sea-surface temperature around 17.5 kyr BP [Broecker et al., 2010].

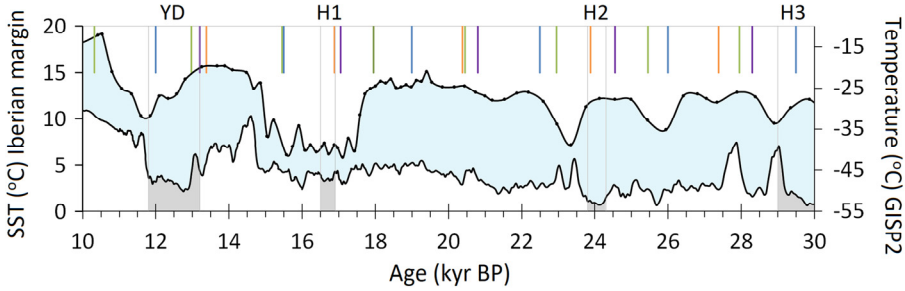

Figure 4.10. A sea-surface temperature (SST) record off the Iberian margin [Bard et al., 2000] versus central Greenland temperature [Alley, 2004]. The period known as the Mystery Interval (17.5–14.5 kyr BP) stands out in both records with substantial coldness. Notably, during this interval, there is a lack of the usual Solar Surge warming around 17.5 kyr BP, which coincides with a sharp cooling trend. This unusual arrangement, along with the terminations of the YD, Heinrich events H2 and H3, and the simultaneous decline in SST, suggests unique circumstances during that time.

In northern Africa, the first major shift to wetter conditions immediately followed the Bølling warming of 14.5 kyr BP, as if there had been a causal link between them. This humid climate arrived as quickly as it later vanished in the mid-Holocene. More importantly, they were apparently part of a sequence of events: a coincidental emergence of rising sea-surface temperatures and a medieval-like, high-activity epoch of c. 15.4 kyr BP. These events preceded the abrupt climate changes in central Greenland and North Africa during the transition phase of 12.2–14.5 kyr BP, when grassland and shrubs spread northward along with the migrating rain belt. Yet, on the way to flourishing land, there was a significant perturbation phase that coincided with the onset of the Younger Dryas. The northern African vegetation astonishingly recovered from this setback, and the wetter climate continued to thrive long before the Greenland cold spell ended. It is quite the opposite of what happened in the mid-Holocene (5.7 kyr BP), when only a minor cooling occurred in Greenland with the establishment of a permanent drought. But it is common for both that the DP module was present (see Fig. 4.9).

At about the same time when the Antarctic deglaciation process began (c. 17–18 kyr BP), the amount of windblown African dust virtually ceased, indicating a profound change in the climate system. The versatility and activity of this stage cannot be overstated with numerous climate anomalies occurring around the world [Denton et al., 2006], ranging from the gradual onset of glacial termination in the Southern Hemisphere to the Asian monsoon and massive ice rafting in the northern Atlantic. In normal circumstances, the mean accumulation rate of windblown dust and surface ocean productivity creates a 2-cm-thick sediment layer in about a century (site 658C), yet during the hiatus period (17.2–14.8 kyr BP), they were almost absent near 21° N. Only a 4-cm-thick layer on the ocean floor was left from the 2.4-kyr period, indicating unusual climatic conditions in the region. The onset broadly matches the first Heinrich event, which started about 17 kyr BP. Yet, careful assessment better justifies the match with the Mystery Interval of 14.5–17.5 kyr BP [Denton et al., 2006]. Not only because the abrupt sea-surface cooling off the Iberian margin preceded the hiatus (see Fig. 4.10) but also because both

anomalies were so persistent. At about the same time the Total Solar Irradiance cycle peaked, the gradual warming of Antarctica began, and glaciers retreated in New Zealand and South America.

The kind of complexity the multi-layered structure of solar activity shows, together with varying response times, makes causal relations less obvious. It is not perfectly clear, what caused the climatic turnaround of c. 15 kyr BP in terms of different activity factors. But there is some strong indication that the 17.5-kyr loop (induced by the intertwined 2.5- and 3.5-kyr solar cycles) is clearly showing its influence over the North Atlantic in an intermittent manner. The outcome seems to compromise the role of a singular medieval-like, high-activity epoch as an omnipotent trigger for several other DOs (see Chapter 5).

4.3 Solar-Induced Variations in AMOC and Abrupt Climate Changes

4.3.1 Carbon Dioxide in Regional and Global Climate Changes

It has become a common and widely accepted view that the current climate change is entirely manmade and caused by increasing carbon dioxide (CO_2) levels in the lower atmosphere. If there was previously any doubt that solar variability had anything to do with Arctic warming or global climate change, these claims are now in the minority. In this context, one cannot avoid noticing the possibility of a misconception where regional and global climate changes get mixed up. Most of the world's population lives in the Northern Hemisphere, and the developed countries are mainly situated around the North Atlantic. Climate change may have received additional attention because of these facts. Scientific uncertainty, fears, and technological advances are fundamental motives for starting a new chapter in energy production.

The continued consumption of fossil fuels over the last centuries has resulted in a high partial pressure of CO_2 in the air. It has considerably distorted the natural balance of CO_2 in the ocean–

atmosphere system, with a much higher concentration of gaseous CO_2 in the air than in the sea. However, this ratio can be deceptive, as greenhouse gases are relatively reactive with water. The solubility properties of CO_2 will determine where the equilibrium eventually settles if anthropogenic global warming continues in the 21st century, as projected by the IPCC [2013]. In a simplified ocean–atmosphere system, only about two out of every one hundred CO_2 molecules ultimately stays in the atmosphere, while the rest are absorbed by the world's oceans. It is due to their relatively good reactivity with water, yielding carbonic acid (H_2CO_3). Only a fraction of the absorbed CO_2 remains in gaseous form in the oceans, which is a typical behavior for greenhouse gases but not for the predominantly inert nitrogen (N_2) and oxygen (O_2) that make up the majority of the Earth's atmosphere.

Although some excess CO_2 has already absorbed and dissolved, regaining the phase equilibrium of CO_2 gas molecules between the two media could take several decades or even centuries after production ceases. The CO_2 concentration in the atmosphere is expected to follow the global mean sea temperature in the long run. Ice-core records show that once the global ocean basin began to warm after the last ice age [Niebler et al., 2003], it caused a roughly 50% increase in atmospheric CO_2 and CH_4 as a side effect [Loulergue et al., 2008; Buizert et al., 2015]. Geological records indicate that atmospheric CO_2 concentration is a global mean sea-temperature dependent [Westerhold et al., 2020; Shackleton, 2000]. If it were the other way around, nothing would prevent the oceanic decarbonization process from taking place after a deglaciation, leading to global warming. Such a loop would be catastrophic for modern life and societies. However, so far, its further progression has always ceased.

4.3.2 Future of the AMOC and Sea Level Rise

Climate models suggest that the AMOC strength or flux will decrease as a natural response to both increased atmospheric CO_2 concentration and global warming [Manabe et al., 1994; Stouffer et al., 2003; Cheng et al., 2013; Weijer et al., 2020]. In contrast, during the

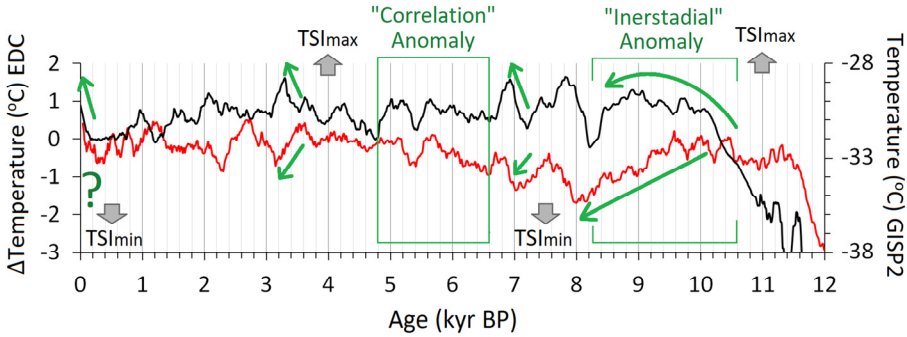

Figure 4.11. Since the early Holocene, the climate fluctuations in Antarctica (red; EDC) and Greenland (black; GISP2) have primarily been characterized by 'bipolar seesaw' intervals. Solar Surge warmings in Greenland have previously corresponded to cooling in Antarctica (EDC) around 3.5 and 7 kyr BP. The temperature data are sourced from Jouzel et al. [2007], Alley [2004], and Box [2009].

ice age, an accumulation of oceanic heat in the Southern Hemisphere was a precondition for abrupt Arctic warming. However, this bipolar coupling has not been as dominant and pronounced a feature throughout the Holocene, making it difficult to infer the present-day systemic state and near-future direction of the Antarctic climate. To approach this question, we can examine climatic conditions during the last solar irradiance minimum of around 7,500 years BP (Fig. 4.11). Controversially, local temperature minima in Antarctica around 8 and 7 kyr BP caused abrupt warmings in Greenland, demonstrating the interhemispheric coupling mechanism. The thermal seesaw between polar regions reflects the climatic changes of the 8th millennium BP. Once Greenland's centennial warmings had nearly reached their maxima, the cool Antarctic climates followed and then reversed. These substantial warmings in Greenland started and ended approximately 200 years before those in the Antarctic.

It is unlikely that today's northern Atlantic warming marks the beginning of a multi-millennial cooling event because the TSI minimum is already behind us. Instead, stable or even reversed development is a more probable prospect for Antarctica. It would bear a resemblance to the mid-7th millennium BP when a bipolar seesaw phase momentarily evaded and the peculiar correlation anomaly

started (Fig. 4.11); there was a clear shift to almost synchronized climate fluctuations soon after the Solar Surge warming ended c. 6.7 kyr BP – relatively speaking, only a few centuries from today.

There is a common assumption that the looming greenhouse gas warming in the twenty-first century will eventually mitigate the projected Northern Hemisphere cooling effect caused by declining AMOC strength. However, what if the global warming prospects do not come true? In global climate models, the effect of CO_2 replaces the Sun's role as the primary agent altering the AMOC strength, which is a somewhat contradictory finding. This interpretation is inconsistent with paleoclimate records when viewed in the context of MMSCs.

The anticipated significant weakening and shallowing of the Atlantic Meridional Overturning Circulation during the twenty-first century, coupled with the effects of greenhouse gas-induced warming, give rise to two major concerns, as highlighted by Weijer et al. [2020], Thomas et al. [2019], and the Intergovernmental Panel on Climate Change (IPCC) in 2019. The first concern pertains to the rise in sea levels in the North Atlantic, primarily attributed to the weakening of the AMOC. This phenomenon, as outlined by Levermann et al. [2005] and discussed by Little et al. [2019], can lead to a relative increase in sea level. The second concern is a global mean sea-level rise, driven by the melting of ice sheets and the thermal expansion of water, as described by Widlansky et al. [2020]. Since the Last Glacial Maximum (18–23 kyr BP), sea levels have already risen by approximately 130 meters, and it is estimated that the complete melting of global ice sheets could raise them by an additional 70 meters [Bamber et al., 2018]. Various factors influence both regional and global sea levels, with short- and long-term consequences, including tidal- and wind-driven movements, alterations in the AMOC, thermal expansion, and glacier melting, and their subsequent repercussions.

Satellite altimetry data reveals that the global mean sea level has been rising at an annual rate of 3 (±0.4) mm since the early 1990s, as reported by Nerem et al. [2018]. The combined impact of melting glaciers in Antarctica and Greenland could contribute an additional 1.2 mm per year to sea-level rise. According to Nerem et al. [2018], if

the annual acceleration rate of sea-level rise were to increase by 0.1 mm, the sea level could be 65 cm higher than today by the year 2100. Nevertheless, projections for sea-level rise by 2100 vary widely in the literature, ranging from 0.5 to 2 meters [EASAC policy report], though the 2019 IPCC report narrowed the estimate to below 1.1 meters. While the alteration of the Atlantic MOC remains a wildcard in predicting sea-level rise, it's important to note that its flow strength is continuously monitored. Aside from a brief weakening in 2009, the RAPID Array measurement system in the North Atlantic (26° N) has not detected a substantial decrease [Moat et al., 2020]. Nevertheless, predictions based on MMSCs and the GISP2 record suggest that an AMOC slowdown could occur between c. 2140 and 2240, leading to a decline of around -1 °C, with only a minor reduction expected around the 2070s (see Fig. 3.11). Overall, this suggests that the projected influence of the AMOC on sea-level rise in this century may not be as substantial as previously estimated. From this perspective, the present-day abrupt warming in the northern Atlantic due to Solar Surge activity has likely accelerated the melting of Greenland.

It is reasonable to assume that the near-future centennial cooling phase will follow a trajectory similar to that observed 7,000 years ago. The recent warming trend has mirrored its predecessor with remarkable precision, establishing a strong climatic correlation between the 1st and 8th millennia BP based on the GISP2 record (Fig. 3.11).

The dynamics of deep-water cells are intricately linked with freshwater influx from Greenland, exerting a considerable impact on the AMOC, as highlighted by Hu et al. [2011]. Rising temperatures lead to accelerated freshwater inflow around Greenland, ultimately weakening the AMOC. However, current climate models struggle to incorporate all relevant factors, making it difficult to predict the sequence of events that could result in catastrophic consequences. As we have seen throughout this book, several unknown factors remain unaccounted for in these models, which can have a more significant impact than anticipated but are difficult to quantify. In the upcoming sections, we will delve into how solar influence manifests in deglaciations.

Solar-activity proxies, combined with synchronized polar temperature data, suggest that events like the Solar Surge are capable of initiating a climate mode that can persist for centuries or even millennia. A discernible interhemispheric pattern is associated with alternating climate modes across the entire Atlantic Ocean. During ice ages, transitions in climate modes are characterized by fluctuating temperature thresholds in Antarctica. Despite the notable variability in these threshold values, the pattern has shown broad consistency over time: a gradual increase in temperature levels in Antarctica ultimately culminates in a seemingly arbitrary tipping point at higher northern latitudes, where the main body of warming occurs in less than a century. This tipping point initiates a decline in Antarctic temperatures, typically 1–3 centuries later, showcasing a dynamic, condition-dependent system with partially elusive equilibrium mechanisms and frontiers [Buizert et al., 2015; Henry et al., 2016; Pedro et al., 2018]. However, it's essential to note that this relationship can be quite complex, as observed during the Holocene.

4.4 The Bipolar Seesaw Mechanism and the 7-kyr Climate Cycle

4.4.1 Marine Isotope Stage 3

A manifestation of the 7-kyr TSI cycle strongly correlates with the three famous interstadials in the middle of the last ice age, even though not all records (NGRIP) completely support the view. Perhaps even more importantly, the Total Solar Irradiance cycle seems to be among the factors that have modulated the deglacial pace in Antarctica from the beginning to the first interglacial peak. It is in contrast to the climate over Greenland, which has been more sensitive to the Quasi-cyclic solar variations.

Greenland's 'Great Warm Plateau' intervals were stable climatic phases during the Holocene that occurred following each solar surge warming episode. In terms of resilience and stability, they are similar to the well-known interstadials. However, it is legitimate to wonder

why these sudden warmings lost momentum so quickly throughout the warm Holocene, or why they occurred at all, unless they were triggered by a capacity similar to that of interstadials. We should also consider why, over the past 9,000 years, the AMOC failed to sustain the highest temperatures, which are the Eemian's peculiarity as indicated by a 4 to 6-meter higher relative sea level. The wild climate swings of the Eemian may be explainable by the intermediate orbital eccentricity values that increased the precessional effect on seasons. This effect was even stronger during the Aveley, which was split into two halves in both hemispheres [Obrochta et al., 2014]. However, it is still uncertain how unstable and fragmented the northern Atlantic was during the Eemian period. Although the Holocene also had climatic discrepancies, none of them compare to the Aveley in this respect. The GISP2 ice-core record does not accurately describe the regional climates of the Northern Hemisphere, including Europe. Similarly, GRIP does not fully represent the Eemian climate in the Northern Hemisphere. Some primary features of this last interglacial are surveyed at the end of this chapter.

The longer-term interstadials from the 8th to the 16th were visibly influenced by the increasing summer insolation at higher latitudes, as shown in Figure 4.12. These interstadials exhibit a climate profile that seems to be reversed near the peaking orbital obliquity around 50 kyr BP, indicating the stability provided by an optimal range of tilt angles. Among these interstadials, the 14th was the most stable and was centered on the optimum tilt angle. Polar climate regions experienced a prolonged and notably cold phase between 62 and 66 kyr BP because the obliquity had passed its minimum only a few thousand years earlier. This time interval links to the Younger Dryas event via the 52.5-kyr activity loop, and indeed, their climate profiles show the most evident similarities. The transition to a full glacial state after a Younger Dryas replica around 66 kyr BP indicates the absence of abrupt Dansgaard–Oeschger (DO) events in Greenland and no apparent Antarctic climate fluctuations caused by the Total Solar Irradiance cycle. The TSI-cycle-related oscillations were only about to begin, and as a result, unusually icy conditions likely prevailed in the Southern Hemisphere. There is very little evidence of

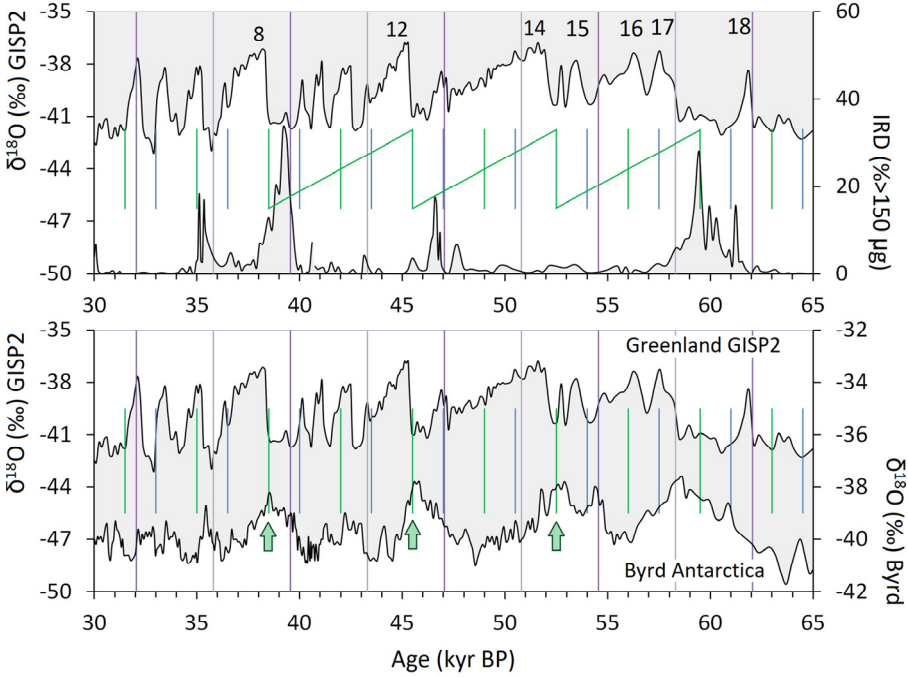

Figure 4.12. The Earth's obliquity reduced from 24.4° to 22.3° in the middle of the last ice age, and the stability of the c. 7-kyr climatic cycle deteriorated. Ice-rafted debris data were collected off the coast of Portugal at site MD-95-2040 [de Abreu et al., 2003]. A clear lack of synchronization existed between the climates of Antarctica (Byrd) and Greenland (GISP2) [Blunier and Brook, 2001]. The abrupt Dansgaard–Oeschger (DO) warmings numbered 8, 12, and 14, coinciding with Solar Surge equivalents, and occurred c. 500 years after the 7-kyr TSI maximum. The blue, violet, and green lines respectively represent the 3.5-kyr and 3.75-kyr modules, and the Solar Surge event.

accumulated heat in the Southern Ocean during this period, as it would have radiated to adjacent Antarctica and its EDC and Byrd core sites. This exceptional cold period provides an orbital-driven counterpart for the Last Glacial Maximum, which occurred around 18–23 kyr BP and appeared roughly forty-three thousand years apart.

The climactic interplay between the polar regions c. 60 kyr BP catches the observer's attention as it heralds the time of the three famous Greenland interstadials [Clark et al., 2007]. There were weak attempts to punctuate the glacial conditions in the Arctic already six

to eight thousand years before the famous interstadials, but they were nothing more than quick turnarounds resulting in even more heat accumulation in the Southern Hemisphere. It was during a high-activity epoch, similar to the medieval period, when the cold stadial conditions finally began to crackle at around 57.5 kyr BP, undermined by an exceedingly high heat gradient between the poles. Relatively frequent but modest climate fluctuations preceded the first extensive interstadial (DO 16), accompanied by rising temperatures of 5 to 10 degrees Celsius. The early phase of this precursor is particularly interesting due to its instability, characterized by frequent climatic ups and downs, each lasting merely centuries rather than millennia, as if they were miniature versions of the preceding deglaciation. The underlying mechanism was bound to the presence of both maxima, the 41-kyr obliquity, and the 7-kyr TSI cycles. This behavior was otherwise prominently absent during the last ice age, and its traces, well beyond the Eemian, are only visible in the records of Antarctica.

The GRIP record prior to c. 50 kyr BP is under inspection here, followed by an evaluation of the GISP2 record. By focusing on these two datasets, we can potentially avoid contentious disputes among various ice-core records. In contrast to the conclusions drawn from the NGRIP record, the GISP2 data convincingly indicate that interstadials 8, 12, and 14 are responding to peaks in the 7-kyr TSI cycle. These climatic oscillations got started with DO event 18. It was a single, isolated warming event and was closely associated with the onset of the H6 event. During the most intense phase of this IRD formation, c. 59.5 kyr BP, the Atlantic overturning circulation was not reinvigorated by the progressing TSI-maximum phase. Instead, the IRD flux was apparently reduced by the subsequent Solar Surge event (Fig. 4.12). This reduction was particularly sharp. Although we cannot yet be certain of the Solar Surge event's involvement, a similar analysis of the MIS-8 ice age suggests that this sudden halt was likely not an isolated incident but instead has a high probability of recurring. We will discuss this further in a later section, which aims to determine the precise cycle length through a comparison of IRD layers from different ice ages. There I show again that the

largest common multiple of the MMSCs must be very close to 250 years, a round number that is a subject of great curiosity. The reasons behind the convenient coupling of this number with Earth's orbital period of 365 days remain unclear unless the MMSCs themselves exert fundamental control over our planet. It is otherwise difficult to argue for the existence of such a function for an arbitrary body in our solar system. However, neighboring planets such as Venus (225 days), Mars (687 days), and Jupiter (4333 days) do not exhibit such a coupling with the MMSCs as the Earth does, which has sparked controversy. The Sun's surprisingly well-suited cycle lengths urge scientists to objectively investigate this puzzle, which may not be a paradox after all. However, a finding where adjacent planetary climates would potentially be bound to the Earth's orbital period is confusing. Multiple couplings to adjacent planets would make the MMSCs feel less dazzling, but such precise links do not seem to exist. The study of past solar variability is a well-established discipline [Beer, 2000; McCracken et al., 2004a, 2007]. Furthermore, the last three to four centuries of sunspot cycle data align well with the production rates of cosmogenic radionuclides (such as ^{10}Be and ^{14}C), providing direct context for observational evidence and theory.

4.4.1.1 A Conceivable Method to Confirm the 3.75-kyr Cycle Length

Marine Isotope Stages (MIS) 6 and 8 roughly cover the preceding glacial periods prior to the Eemian and the Aveley. However, MIS 6 presents a very different picture of glacial phenomena, with muted DO oscillations and scarce IRD layers. Its missing Hudson Strait minerals combined with the relatively high background abundances of IRD are indications of unusual circulation routes and a continuous stream of icebergs at the time [Hodell et al., 2008]. This apparently led to a persistent perturbation of the thermohaline circulation, making it more susceptible to forcing.

According to Obrochta et al. [2014], four distinct IRD events occurred during MIS 8 at around 276, 263, 249, and 243 kyr BP. The three youngest were of Hudson Strait origin, but the oldest is a different type, potentially representing a Younger Dryas replica. By subtracting the full-scale solar loops of these dates, it becomes obvi-

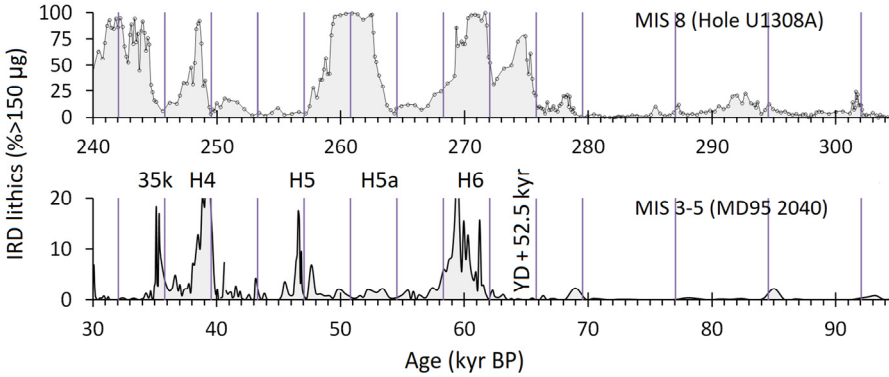

Figure 4.13. Ice-rafted debris (IRD) abundances from the MIS 8 and MIS 3–5 intervals were analyzed at sites U1308A and MD95-2040. The source of the data: Obrochta et al. [2014] and de Abreu et al. [2003].

ous that the events can be seen as reflections of the last ice age Heinrich events and correspond to the H5a, H4, and 35 kyr BP events. The corresponding IRD layers in both stages represent a systematic response to the DP module. Not only does it address the unchanged periodicity but also the importance of certain solar activity phases over others. An IRD comparison in Figure 4.13 suggests that the resemblance between stages does not continue throughout the stages. Nevertheless, the similarities that surround, for instance, the H4 and H6 events stand out particularly well. The abrupt onsets of the corresponding H6 events and their sharp terminations near a potential Solar Surge event emphasize a certain order in the sequence. Moreover, they both persisted for around 3,000 years. Even though a YD-related debris layer is absent around 66 kyr BP, a multi-millennial counterpart is noticeable in MIS 8, peaking at around 275 kyr BP.

One of the benefits of studying IRD layers is that they can provide us with precise timing information. By comparing multiple IRD layers between the two ice ages, we can resolve small inaccuracies associated with the exact cycle length. A ten- to twenty-year mistake in the 3.75-kyr cycle length could accumulate to 560 to 1120 years between the two stages. However, there is no marked shift in IRD onsets, suggesting that the variability in the inceptions of IRD is caused by the randomness in the system rather than a small deviation in the cycle length. Although there is still some skepticism towards the

round numbers of the MMSCs, the comparison of IRD layers in Figure 4.13 suggests that the link between an H4 progenitor and its 52.5-kyr predecessor seems to document the semi-loop precisely. Both were rather sharp responses and prominent enough to convincingly reveal the exact DP occurrences. However, it is the multi-layered structure rather than a single event that is needed to seal the round numbers of the MMSCs for good. In this comparison, the IRD-layer onsets of the last ice age are more sporadic than those of MIS 8. In the latter, they either slightly lead or lag the DP module, but most importantly, their small temporal shifts show no cohesive alignment in either direction, which would be a strong indication of a longer or shorter cycle length.

The other aspect of confirming the exact cycle length relates to a peculiar anomaly in solar activity reconstructions about 41 kyr BP (see Fig. 2.9). During this so-called Laschamp event, the Earth's magnetic field underwent a short reversal and was unusually weak, exposing the atmosphere to a heavier bombardment of cosmic particles. The Laschamp event has been used, for example, in cross-matchings of Beryllium-10 abundances to improve synchronization between interhemispheric ice-core records [Raisbeck et al., 2017; Adolphi et al., 2018]. Again, production rates of cosmogenic isotopes should be identical at both poles, and this kind of synthesis of reconstructions helped to reveal the nearby DP module profile of 43.3 kyr BP, as presented in Chapter 2. However, the precise date is disputed. A highly accurate age-dating method, based on Uranium/Thorium isotope measurements from speleothem and coral samples, suggests that the Laschamp event may be about 250 years older than previously thought [Adolphi et al., 2018]. This small shift would have a fundamental impact on the 3.75-kyr cycle and the whole rotation pattern of the MMSCs, adding +22.7 years per cycle and extending the 105-kyr full-scale loop by +636 years. Attempts to synchronize ice-core reconstructions led to this provocative shift, but is it the bottom line?

Two compelling arguments favor an even number as the correct cycle length for the DP module. The precision of dating over the last twelve thousand years is very reliable, as is the regular pacing of

IRD layers in various core sites. These two features contradict the visual-profile matching of the anomalous ^{10}Be abundance around 41 kyr BP. In order to find answers to these questions we are next looking into the proxy records of the longest continuous ice core and the total solar irradiance cycle.

4.4.2 Glacial Terminations I–V

As much as we can rely on the Antarctic EDC ice-core record and its GICCO05 timescale to picture the past climatic fluctuations of Antarctica [Bazin et al., 2013; Veres et al., 2013], there is some degree of uncertainty related to the Arctic. What could describe the importance of the TSI-cycle peaks for the past five Antarctic deglaciations better than the following dates: 11, 130, 242, 333, and 424 kyr BP? The three oldest represent climatic tipping points in Antarctica, which may be relevant to the bipolar seesaw phenomenon (Fig. 4.14). The idea would be the same as with the famous climate oscillations of MIS 3, making it even more interesting. The ramp warming of a typical southern deglaciation came to a sudden halt after advancing six to eight thousand years but likely began a more abrupt warming in the Arctic. The halt phase in Antarctica was not just a sideways movement but usually comprised a prominent decline. It is less obvious what consequences there were in Greenland, as proxies are not fully consistent. But as the latest, similar observations indicate, the accumulated heat was extracted from the Southern Hemisphere to the Northern Hemisphere by the bipolar seesaw mechanism. A peaking trajectory of summer insolation is typically a long episode, and the TSI maximum usually matches it, which unconditionally leads to a halt. This mechanism likely produces the same climatic pattern as with DO events, indicating that the vanishing heat must reappear somewhere else. While the melting of ice consumes a huge amount of heat, by the time of the polar temperature maximum, a vast portion of the waning ice sheets has already been lost, implying that the heat is redistributed through the Atlantic MOC.

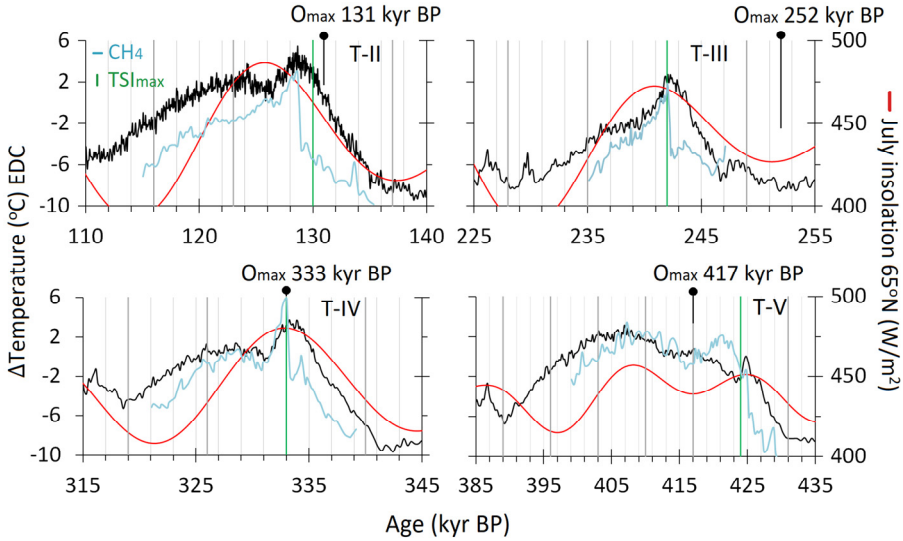

Figure 4.14. Antarctic interglacials (II–V) from the Eemian to the Hoxnian [Jouzel et al. 2007]. The July insolation at 65° N latitude (red) and obliquity maximum (O_{max}) [Berger, 1992]. The green lines indicate the maxima of the 7-kyr TSI cycle at 130, 242, 333, and 424 kyr BP, which correspond to glacial terminations (T) and often coincide with a cooling period in Antarctica that is likely associated with a rapid warming event in Greenland. The atmospheric methane proxy (blue; CH_4) is derived from the EDC ice-core record [Loulergue et al., 2008]. The sharp, early interglacial peaks observed near the TSI maxima serve as indicators of Arctic warming events [see Petrenko et al., 2017; Buizert et al., 2015].

The five latest interglacials from the Holocene to the Hoxnian have a precise pinnacle moment near their 7-kyr TSI maxima. However, relatively little is known about whether these moments led to a significant temperature difference between the polar regions. In the case of Aveley, there is some evidence of this disparity, relying on a synthesized reconstruction [Barker et al., 2011; Obrochta et al., 2014]. The resourceful Antarctic ice-core record serves scientific purposes by helping to adjust climatic correspondence with Greenland. Globally well-mixed trace gases like methane (CH_4) get trapped in annual ice layers, and their chemical composition and concentrations are analyzed to synchronize the otherwise difficult phasing of the bipolar seesaw with sub-centennial precision [Buizert et al., 2015]. A sharp methane peak at the end of each deglaciation essentially reveals the northern breakthrough point, indicating the

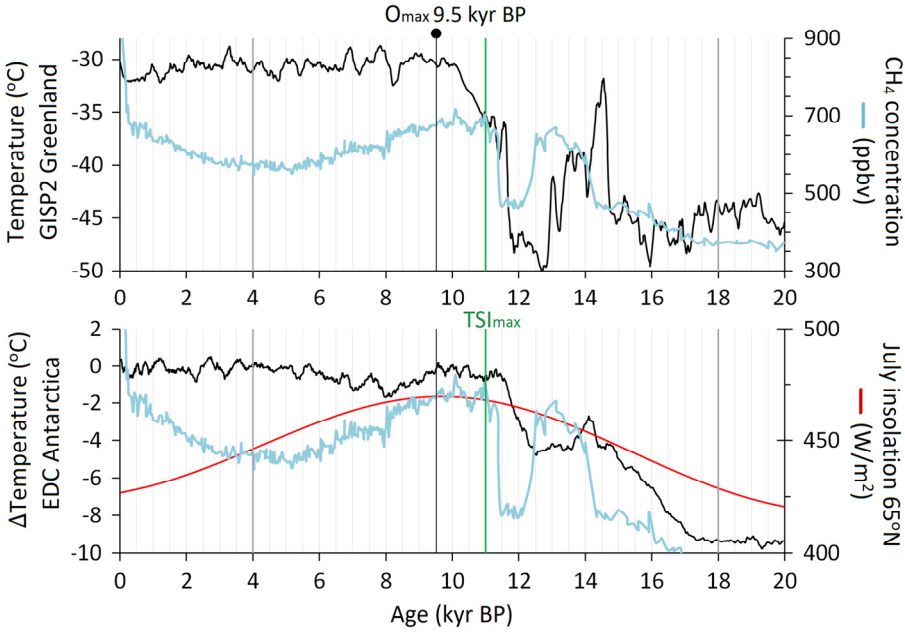

Figure 4.15. Upper panel: Comparison of Greenland temperature and global methane (CH_4) concentration as recorded in Antarctica [Loulergue et al., 2008]. Lower panel: Temperature change in Antarctica's EDC ice core (black) [Jouzel et al., 2007], and July insolation at 65° N latitude (red) and obliquity maximum (O_{max}) [Berger, 1992]. A summer insolation level of c. 450 W/m² was sufficient to trigger DO 1 and the Hoxnian, but not the Holocene.

accelerated melting of northern ice sheets every 100 kyr or so [Loulergue et al., 2008; Christensen et al., 2000].

Large-scale shifts in polar climates rarely occur without implications elsewhere. However, the limited span of Greenland ice-core records prevents us from drawing direct conclusions about the drastic changes in Greenland that followed when Antarctica suddenly became colder after deglaciations. A sufficient resolution of pre-Holocene documentation provides an essential reference to previous glacial terminations.

The first halt in Antarctica after the TSI maximum led to a notably long downward trend, proceeding from 9.5 to 8 kyr BP. Unlike previous interglacials, this one was delayed by over a millennium, similar to the Eemian. In this respect, Greenland's 8.2 kyr BP cold event was only a sudden cold snap associated with the c. 1.5 °C

depression in Antarctic temperatures, indicating the bipolar seesaw phenomenon during the early Holocene. The interval from 12 to 8.5 kyr BP bears a startling resemblance to the famous, long interstadials 8 and 12 (Fig. 4.12). Moreover, their subsequent, frequently oscillating DO phases (5–7 and 9–11) broadly approximate the climatic fluctuation of the Boreal–Atlantic Holocene (9–5 kyr BP), although the former suffered from harsh ice-age conditions, which hindered and modified northward heat supply at rates and rhythms unseen in the Holocene. The subsequent period from 8.5 to 6.5 kyr BP in Greenland and the past few millennia BP underwent volatile climatic responses around their TSI minima. The highest and lowest temperature values around 8 kyr BP highlight this volatility (Fig. 4.15). In the last ice age, the frequently oscillated short-term DOs were extended over the entire length of one quasi-cycle, commencing from an s3.5-kyr-like module. One interpretation is that the interhemispheric heat imbalances of the last ice age became much more prominent than those of the Holocene, as the corresponding 'Great Warm Plateaus' of nowadays are mostly stable phases.

The tipping point in the Northern Hemisphere that is associated with the bipolar seesaw seems to be, by and large, inherently dynamic and bound to existing forcing conditions. There does not seem to be any established threshold level to initiate an abrupt onset. However, no single temperature proxy from the Antarctic ice sheet is a proper measure for these thresholds. Equally, it is hard to imagine that the climate over Antarctica could be isolated from the adjacent oceanic influences, which propagate energy to the coldest continent. The AMOC shutdown and recovery have been proposed as a two-step process with two stable modes [Ng et al., 2018; Renold et al., 2009], where the shift between modes is very rapid. It suggests that thresholds are building up the potential that is unleashed at a considerable rate but is also swiftly disbursed. Altogether, the influence of the variable AMOC strength on the northern Atlantic climate is under frequent study [Buckley et al., 2016; Johnson et al., 2019; Weijer et al., 2019]. The dynamic state of the thermohaline circulation in the Southern Hemisphere could be equally important. Some studies suggest that what is happening in the joint region of

the western Indian and Atlantic Oceans off the South African coast is an important factor for the salinity balance and the deep-water formation in the northern North Atlantic. The net inflow of salt and heat through the Mozambique and Agulhas Currents to the Atlantic Ocean may help to re-establish and maintain full interglacial conditions [Peeters et al., 2004; Weijer et al., 2019].

4.4.2.1 The Last Interglacial (MIS 5e)

The Eemian deglaciation in central Greenland may not have been as turbulent as the GRIP record suggests, but evidence differs [Bauch et al., 2012; Irvali et al., 2016; Zhuravleva et al., 2017]. The global trace gases methane and carbon dioxide marked neither significant Bølling–Allerød-type warming nor a Younger Dryas-like cooling before the AMOC reinvigorated and deepened, while Antarctic bottom waters retreated southwards for some time after the first TSI maximum around 130 kyr BP (see Fig. 4.16). In either case, the climate finally stabilized c. 128–129 kyr BP, presumably after the nearly concurrent Solar Surge and DP module events (129.5 kyr BP). After this thermal breakthrough point in the Northern Hemisphere, coral reefs grew several meters above present-day sea level, which rose even further, exceeding +6 m towards the interglacial end [Stirling et al., 1998; Hearty et al., 2007]. Fossil coral reefs, bioerosional notches, and benches are visible landmarks of the past global mean sea-level stillstands.

Suggestions that ice rafting persevered in the northern North Atlantic until approximately 124 kyr BP, while ceasing much earlier in the mid-latitudes [Govin et al., 2012], present a nuanced perspective of the last interglacial period. This indicates the presence of both regional disparities and pronounced shifts in latitude and longitude, along with the potential for weakened or shallow deep-water circulation in the Labrador and Nordic Seas (refer to Fig. 4.17) [Hillaire-Marcel et al., 2001; Van Nieuwenhove et al., 2011]. Emerging IRD events well over a thousand years after the early climatic optimum of Antarctica, partly describe how unpredictable the interhemispheric interplay of polar climates may have been. The timing of the TSI maximum around 130 kyr BP was slightly premature for the onset of

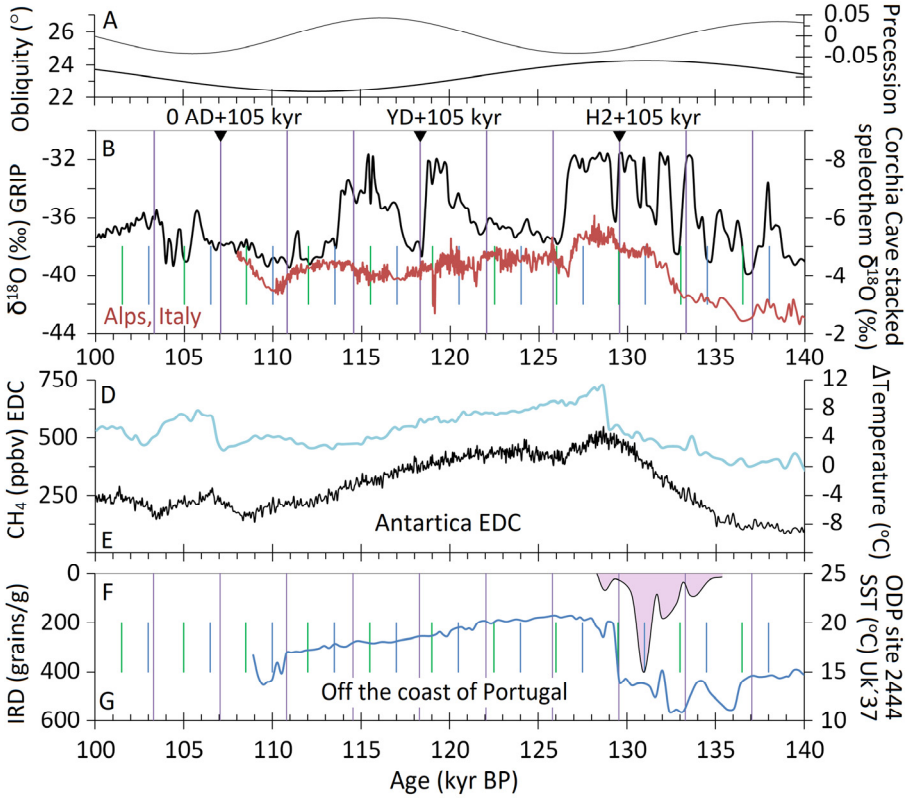

Figure 4.16. The interpretation of the northern deglaciation and the early Eemian period is challenging and relies on a commonly used age model [Shackleton et al., 2000; Govin et al., 2012, 2014; Lisiecki et al., 2021]. (A) The transition from MIS 6 to MIS 5 is influenced by a 4.5-kyr gap between the 65° N insolation maximum of c. 125.5 kyr BP [Berger, 1992] and the TSI_{max} at c.130 kyr BP. (B–C) Climate proxies from central Greenland and Corchia Cave (Italy, Alps) indicate a cold event related to TSI_{min} at around 126.5 kyr BP [Johnsen et al., 1997; Tzedakis et al., 2018]. Following the TSI_{max}, a Solar Surge equivalent (the green line) may have triggered a rapid Arctic warming. (E) A sharp rise in atmospheric methane concentration at c. 129 kyr BP followed the warming and correlated with (G) an increase in sea-surface temperature (SST) off the coast of Portugal, as observed at site MD01-2444 [Martrat et al., 2007]. (F) The intensity of ice-rafted debris (IRD) events off the Portuguese coast increased toward TSI_{max} [Skinner et al., 2006].

the Arctic's thermal breakaway. Notably, a sharp increase in the atmospheric methane concentration (EDC, 128.9–128.5 kyr BP) and a strengthening of the Asian monsoon (c. 129 kyr BP) are both associ-

ated with an AMOC recovery, a concurrent northward shift of the ITCZ, and a potentially warmer Arctic Ocean.

The abnormally high temperatures and sea levels throughout the early Eemian exceeded those of the Holocene. Nevertheless, the story of the Eemian comprises spatial and temporal contradictions. A full interstadial condition may not have been achieved until ice rafting diminished around 124–123 kyr BP [Hodell et al., 2009; Galaasen et al., 2014; Zhuravleva et al., 2017]. The prolonged Arctic deglaciation hindered a large-scale intrusion of warm and salty Atlantic water, and consequently, the deep-water cells could not establish their full interstadial mode until the second TSI maximum emerged, marking the halfway point of MIS 5e. By this time, the 65° N summer insolation had already passed its peak several thousand years earlier. The onset of glacial conditions can be traced back to around 116 kyr BP, coinciding with the third TSI maximum [NGRIP members, 2004; Galaasen et al., 2014]. However, the timing remains somewhat ambiguous due to its dependence on proxies and location, spanning from approximately 113 to 118 kyr BP [Siegenthaler et al., 2005; Rohling et al., 2019].

Intriguingly, ominous cold events within the Eemian period occurred around the North Atlantic at approximately 117–118, 122, 124–126, and 129 kyr BP, as evidenced by various proxies [Hearty et al., 2007; Irvali et al., 2012, 2016; Tzedakis et al., 2018; 125.7 and 129.5 kyr BP]. Subtracting the 105-kyr solar loop from these dates reveals their close ties to the YD, H1, and H2 events, which resonate with the chilly times of the Last Glacial Maximum in the northern Atlantic region. The involvement of the DP module in each cold event seems plausible, but other solar events and neighboring modules could also have disrupted climatic stability. These grand-minima gaps are undoubtedly small, as their onsets are separated by only a few centuries when we examine them over a 100-kyr time span. Certain combinations of inactivity series could enhance and prolong their overall impact on paleoclimatic proxies. To draw direct conclusions about the climate during the last interglacial period, accurately dated high-resolution proxies are needed. However, they never quite attain the same level of trust as Holocene proxies do.

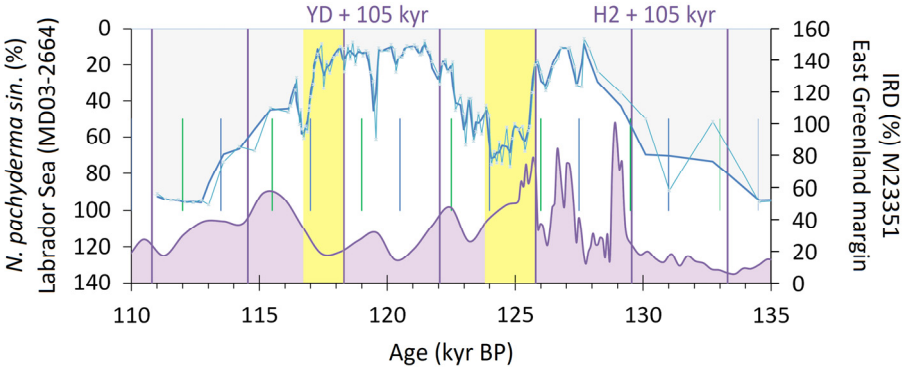

Figure 4.17. The record of the polar planktonic foraminifer N. pachyderma (sin.) [Irvali et al., 2016] from the Labrador Sea site MD03-2664 reveals two dramatic hydrographic shifts (depicted by yellow bands) occurring about 7.5 kyr apart, leading to colder conditions. Additionally, an ice-rafted debris (IRD) record from the East Greenland margin (M23351) [Zhuravleva et al., 2017] indicates a prolonged deglaciation.

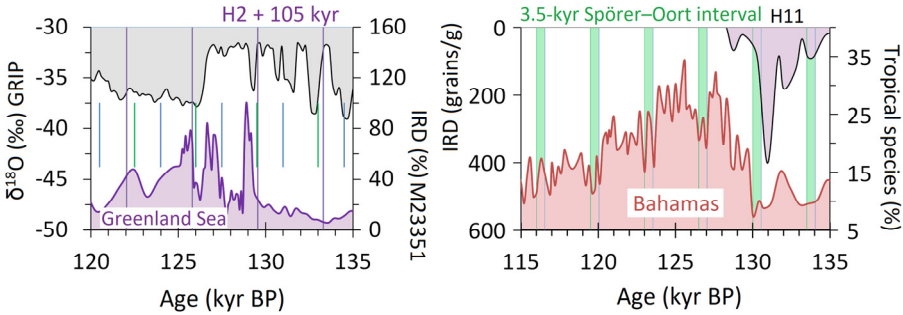

Figure 4.18. The Little Bahama Bank (MD99-2022) reveals a biological production pattern of tropical, single-cell species that repeatedly decreased in 3.5-kyr cycles (green) [Zhuravleva et al., 2018]. The ceasing of the H11 event off the Portuguese coast (MD01-2444) coincided with an abrupt warming of the subtropical waters of the Bahamas [Skinner et al., 2006]. Additionally, an ice-rafted debris (IRD) record from the East Greenland margin site M23351 indicates a prolonged deglaciation [Zhuravleva et al., 2017]. The GRIP record is referenced from Johnsen et al. [1997].

The most severe early Eemian cooling recorded in central Greenland (GRIP) and the Alps, Italy, dates back to c. 126–127 kyr BP (Fig. 4.16). It coincided with an extended, LIA-like grand-minima series from Oort to Sprörer (1–0.5 kyr PB) as well as the first TSI minimum. It temporarily ended the early Eemian (128.5–126.5 kyr BP) progres-

sion in the northern Atlantic [Irvali et al., 2016; Tzedakis et al., 2018]. In Antarctica, temperatures had already begun a gradual decline since the AMOC partly recovered. These are both typical characteristics of the bipolar seesaw mechanism, and their climatic progression is familiar from the MIS-3 stadial–interstadial fluctuations as well as the early Holocene. The cold reversals in the polar regions culminated around 126.5 kyr BP, when temperatures finally dropped in the northern Atlantic after a milder period lasting a few thousand years (Fig. 4.17). Whether triggered by an accelerated freshwater input during the preceding high-activity epoch, resembling the medieval-like conditions, or other factors, the northern cold response appears to be associated with the extended grand minima series reminiscent of the Little Ice Age

Another cold reversal appeared exactly seven thousand years later, suggesting that this particular grand-minima series (Oort, Wolf, and Spörer) was consistently associated with a significant decrease in tropical sea-water species around the Bahamas [Zhuravleva et al., 2017]. The biological production of single-cell foraminera is sensitive to sea-surface temperature and salinity changes. Their Eemian-time evolution (Fig. 4.18) conveniently shows that both warm tropical waters and the mean annual shift of the Atlantic ITCZ are inherently altered by solar variability in 3.5-kyr cycles. Interestingly, the DP module did not seem to influence Bahama's sea-surface temperature, although it is otherwise strongly coupled to the cold Heinrich stadials and southward migration of the ITCZ. Again, highly contradictory climate issues characterize the Eemian era.

The dramatic freshening of the Labrador Sea surface c. 126 kyr BP, as indicated by low planctic $\delta^{18}O$ values (see Fig. 4.17) [Irvali et al., 2016], could be associated with the late phase of a Solar Surge warming and ice-sheet melting. The subsequent cooling period continued regionally from c. 125 to 123 kyr BP until ice rafting diminished.

Notably, the shift from a grand solar maximum to the following minimum, c. 126 kyr BP, started a rather exceptional solar-activity millennium, as its analog is from the Last Glacial Maximum (21 kyr

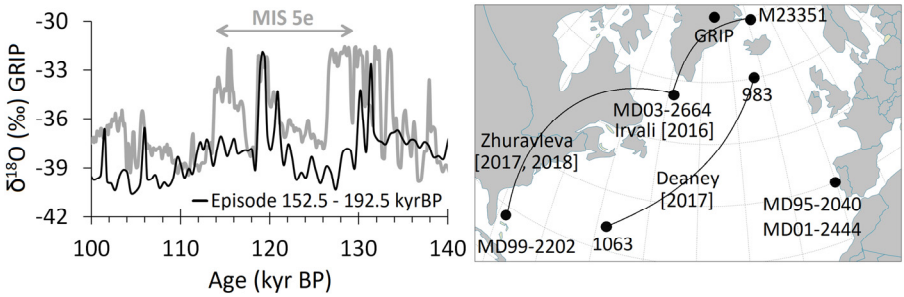

Figure 4.19. The Eemian interglacial (MIS 5e) is characterized by a distinct interstadial counterpart that occurred 52.5 thousand years earlier, as indicated by the GRIP record [Johnsen et al., 1997].

BP). In the center was a clustered DP module, in which the Maunder and Homeric modules presumably overlapped (see Fig. 2.12).

The early-to-mid-Eemian climate fluctuation appears to have been repeated once before, with a strikingly similar pattern of highs and lows occurring precisely 52.5 kyr earlier in central Greenland. The coherence of these events is most evident in the GRIP record (Fig. 4.19). This episode happened between 170 and 183 kyr BP, in the middle of the MIS-6 glacial period, and is likely the best interstadial counterpart for the Eemian (MIS 5e). High summer insolation values during this period make it loosely comparable to the three famous interstadials of the last ice age. Temperature levels, nearly as high as those during the late MIS 5e, were briefly attained before a major collapse. Additionally, a strangely cold intermediate phase was a reality and equally persistent.

The high correlation between episodes indisputably implies strong solar involvement. It was partly behind their climatic similarity, but the most central factor is the orbital configuration. Their exerted forces were more similar than what followed. These two external forcing factors appear to be the most important for millennial-scale climate variability in the Northern Hemisphere.

The book suggests that the extreme events of YD and DO 1 are inherently associated with the 17.5-kyr solar-activity loop. These climatic disturbances were unlikely to have occurred without the preceding heat accumulation in the Southern Hemisphere and the suitable arrangement of solar cycles. Pre-Eemian conditions

substantially differed from those in the pre-Holocene era in this respect. Firstly, a similar solar-activity phase responsible for an H3/DO 5-type oscillation coincided with the early Eemian deglaciation (134–137 kyr BP) instead of a YD/DO 1-type oscillation. These oscillations do not commonly coincide with glacial terminations, as the MIS 1←2 and MIS 5e←6 transitions imply despite convenient matches. However, bipolar seesaw fluctuations of similar magnitude can occur at both ends of an interglacial. Secondly, the pacing of the TSI cycle reverses for the Quasi cycle every 17.5 kyr, meaning that the TSI-based heat accumulation had barely commenced at around 137 kyr BP when a DO-5-type abrupt warming should have emerged. It provides a logical explanation for the failed start of the Arctic glacial termination (II). However, the realization of such oscillations, as revealed in the GRIP record, remains uncertain in many ways.

The elongated H11 event of the pre-Eemian appears to have had two beginnings, reflecting the progression of H3 and the potentially identical solar variability behind it. Depending on the core site location, various H11 events progressed from approximately 137 to 129 kyr BP. Nevertheless, Eemian's IRD activities did not end there. At higher latitudes, ice rafting continued until 126–124 kyr BP, depending on the core site location [Deaney et al., 2017; Irvali et al., 2012, 2016; Govin et al., 2012; Zhuravleva et al., 2017]. This continuation requires open sea access from the shore, at least seasonally, to propagate vast quantities of iceberg-carried lithic grains over the North Atlantic. During the frigid stadials of the Last Glacial Maximum the winter sea-ice edges stretched to around 40° N, blocking potential shore-ice locations such as the Hudson Strait. However, during the summer, the margins retreated to higher latitudes, even above the central Greenland level [Li, 2010].

Numerous proxy-evidence sources paint a versatile and contradictory picture of the last interglacial. They indicate that the last interglacial in the northern Atlantic progressed unusually compared to the Holocene: strong climate and sea-level fluctuations in the whole interglacial period were recorded in the ice sheets and fossil coral reefs. Moreover, seafloor sediments revealed tenacious

IRD events continuing to the halfway point of the Eemian, and finally, uncertainty related to the start as well as termination dates of them. Those are controversial pieces of the puzzle and produce an increasingly incoherent picture of the last interglacial, undermining the view that its proxies and their reasoning could provide relatively good insight into the Holocene.

CHAPTER V

5 MULTI-MILLENNIAL SOLAR CYCLES IN EXPLAINING THE CHAOTIC GLACIAL CLIMATE

Ice-core records are invaluable tools in scientific research due to their consistent nature and relatively high resolution. However, even ice-core records located in close proximity can contain contradictions. The Greenland Ice Sheet Project 2 (GISP2) is an example of this, as it does not offer an entirely unambiguous view of the central Greenland climate [Svensson et al., 2008]. Therefore, any interpretations presented in this book, no matter how evident and exciting they may seem (Fig. 5.1), should be approached with a degree of caution.

In central Greenland, heavy snowfall produces thick annual layers with noticeable interannual changes, providing a reliable basis for accurate core dating when layer-by-layer counting is used. The dating error of this method is cumulative, and while the GISP2 record's error is estimated to be only a few years at around 15 kyr BP [Rahmstorf, 2003], it increases to 1–2 kyr near 50 kyr BP. It is worth noting that the otherwise excellent correlation between the neighboring GISP2 and GRIP cores suddenly ceases at 2750 m depth, which corresponds to c. 100 kyr BP. Below this level, the reliability of the GISP2 record becomes questioned. According to Meese et al. [1997], the GISP2 core ice at a depth of 2800 m is 110,000 years old, with an estimated error of 1–10%.

5.1 Solar-Induced Climate Loops in Central Greenland

Looking ahead to millennial-scale climate scenarios in the distant future, two factors are likely to have a significant impact. The first is the 17.5-kyr climate loop, which suggests that a turbulent Younger Dryas/Boreal Atlantic-type fluctuation is likely to re-emerge in three

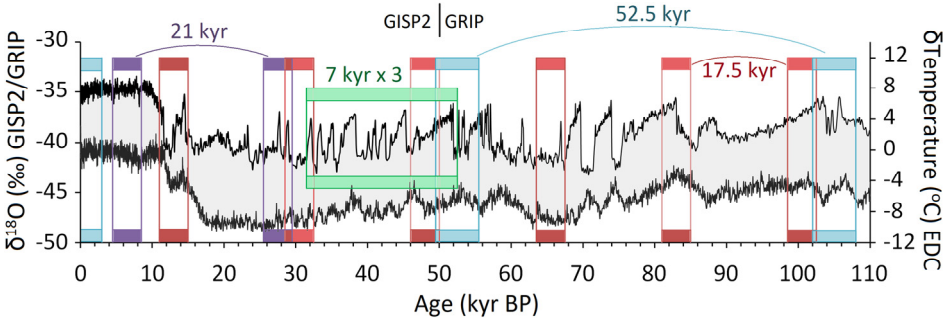

Figure 5.1. A representation of the climatic cycles in central Greenland and the Antarctic EDC record spans the past 110,000 years. In the midst of the last ice age, the 7-kyr climate cycle (green) clearly dominated. Surrounding it were longer climate cycles: 17,500 years (red), 21,000 years (violet), and 52,500 years (blue). The quasi-cycle has become more distinctly evident since the H3 event, while the late Holocene climate has finally unveiled its true periodic features. The data sources are Grootes et al. [1999], Johnsen et al. [1997], and Jouzel et al. [2007].

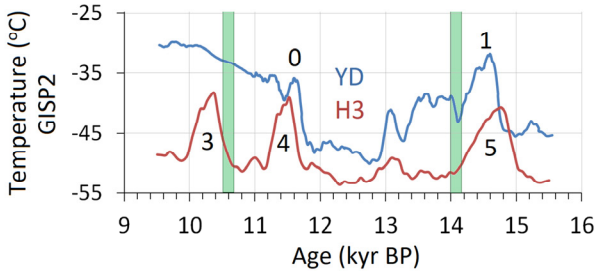

Figure 5.2. A comparison between the last glacial termination and the third Heinrich event, using the 17.5-kyr loop, reveals remarkable climatic similarities in terms of amplitude, duration, and timing. However, there is a notable difference observed in Dansgaard–Oeschger events (DOs). A slower response to rising solar activity led to greater warmth, and possibly as a consequence, the subsequent warmings induced by Solar Surges (green fields) did not occur (c. 14 kyr BP) following the initial DOs.

thousand years. However, defining the quantitative variables that determine its severity remains a far-off goal. The second factor is that in about five thousand years, the tilt angle of the Earth's axis will be much closer to its full minimum, potentially exposing the northern Atlantic climate to a considerable threat from an exceptional cold spell.

To advance quantitative paleoclimatology, it is essential to separate the solar variability effect from the orbital forcing effect. This

step is natural, as long-term solar cycles have been resolved to a large extent and can be extrapolated. Lockwood et al. [2006] proposed preliminary guidelines for this purpose. While the reactions and traveling pathways of cosmogenic isotopes are well known [Beer, 2000; Abreu et al., 2012a], the varying range of relative intensities of different reconstructions poses a challenge. The following sections provide a closer look at the 17.5- and 21-kyr loops. It is worth noting how profoundly the Quasi- and 2.5-kyr cycles are intertwined, and that the latter is mostly created by the former.

5.1.1 Was the Third Heinrich Event a Younger Dryas Equivalent?

An impressive climatic coupling can be identified for intermittently occurring periods of 33–29 and 15.5–11.5 kyr BP. These intervals encompass the surroundings of the Younger Dryas and the third Heinrich event and associate with the 17.5-kyr solar loop, as illustrated in Figure 5.2. Despite the evolving deglaciation, their climatic profiles exhibit an unprecedented similarity, with minimal climatic controversy after the Older Dryas cooling (c. 13.9–14.1 kyr BP). The cold Heinrich event 3 separates the abrupt DO 4 and 5 events in the middle, which clearly follow a 3.3-kyr cyclicity. On the other hand, the abrupt Holocene (DO 0) and Bølling (DO 1) warmings follow a 3-kyr cyclicity. A medieval-like, high-activity epoch appears to be present when all four abrupt warmings occur, despite the incomplete cycle length, mainly due to the delayed responses of the two leading DOs (1 and 5).

However, a few differences highlight the existence and intermittency of the 17.5-kyr loop. Firstly, there is a notable inconsistency among the four medieval-like warmings. The two leading DOs (1 and 5) started unusually late but lasted a couple of centuries longer than the subsequent DOs (0 and 4), which responded more rapidly. Secondly, the leading DOs are not genuinely followed by prominent solar surge-induced warmings, suggesting unusual solar activity or a changing sensitivity of oceanic circulations.

Uncertainty surrounds the sluggish response of the Bølling warming, as it coincides with the turning point of solar activity. It is

paradoxically plausible that the steepest part of the warming arrived during a Wolf-like minimum. The most convincing aspect of high-activity relations is the almost parallel H3/DO 5 sequence, which suggests that DO 5 started around 300 years earlier than the Bølling warming, clearly occurring during a medieval-like high-activity phase. When considering this outcome in the broader context of rapid climate responses, we can identify a distinct category associated with the northern Atlantic. The delayed onset of the Bølling warming is surprising, given the vivid responses observed in most cases. Interestingly, the Bølling is distinctively late despite the immense interhemispheric temperature gradient, but it also accompanies the TSI minimum, creating a gap with DO 5. The precise answer may be elusive today, as sub-harmonics of the MMSCs are non-figurative and can only be seen as reflections through paleoclimatic records. Nonetheless, the visible Quasi-cycle in the Greenland Holocene record suggests that the internal dynamics of the ocean–atmosphere system were involved.

As previously mentioned, sequences of Wolf- and Spörer-like minima have consistently followed these abrupt warmings. Even so, these examples cannot confirm a general rule, and the subsequent DO declines responded to solar inactivity at varying rates. Therefore, individualizing the solar variability effects from each other while taking both the geographical and complex AMOC variations into account is an arduous task. Not least because all of the forcing factors are acting together.

The colder intermediate phases between short-term DOs could be seen as consequences of the alternating AMOC strengths. Still, the phrase 'return-to-normal' better characterizes these intermediate phases. Temperature-scale issues may not fully capture the nuances of these milder episodes, given the prominence of abrupt temperature increases. The difference between a cold normal and the bottommost is not so easily discerned from paleotemperature figures, but it occasionally exceeds 4 °C.

Magnificent Spörer-like minima coincide with the top formation of the foremost DOs (1 and 5) and practically end before the steepest temperature declines begin. The bipolar thermal seesaw across the

Equator plays a major part, and the South Atlantic is directly connected to the global oceanic district, circulating around Antarctica. Possible perturbations caused by solar forcing are inevitably reflected in the Arctic, but the exact location of the switch and the size of the area from which the northern Atlantic convection anomalies gather their strength remain inexact. What is certain though is that Heinrich- and DO-related perturbations have been identified in Indian Ocean sediments [Schulz et al., 1998; Marzin et al., 2013].

The 17.5-kyr loop brings together the YD, H3, and H5 events, although the resulting climatic outcomes differ slightly in each case. These events occurred approximately 13, 30.5, and 48 kyr BP, coinciding with the onsets of the IRD events in the eastern Atlantic margins [Peck et al., 2006; de Abreu et al., 2003]. The fact that these three Heinrich events follow the 17.5-kyr periodicity more closely than the 3.75-kyr periodicity suggests that their origins may not be entirely controlled by the DP module alone. Their responses may be more complex than those explored in Chapter 2. Taking a more comprehensive view, the relative placement of the DP module on the TSI cycle becomes an important factor, which undermines the role of singular DP modules compared to clustered ones. Indeed, the H0 and 36 kyr BP events deviate from the usual coupling pattern. As revealed by paleotemperature proxies, these two events were as profoundly chilly in Greenland as the genuine Heinrich events. Therefore, it is a bit of a mystery how the climatic conditions truly differed, prompting us to consider whether massive ice rafting is the sole prerequisite for shutting down the overturning circulation.

The most frigid episodes in Greenland were thin in ice as a consequence of the thick and extensive sea-ice cover. Arctic conditions must have been both cold and dry, with vast sea ice effectively blocking oceanic heat and moisture during the chilliest events, which were not always Heinrich events. The sun's remarkable ability to influence regional climate anomalies is unparalleled. It is especially true for the Atlantic Ocean, which resembles a vast 'cul-de-sac' nearly reaching from pole to pole, wherein the sun has concealed its slowly unfolding mechanisms of abrupt climate change.

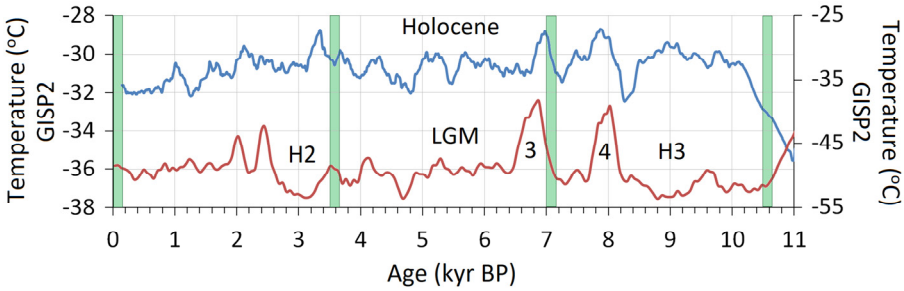

Figure 5.3. A climatic comparison between the Holocene and the Last Glacial Maximum (LGM) was conducted using a 21-kyr pacing. This comparison magnificently demonstrates the impact of the MMSCs on Greenland climate profiles (GISP2), despite the differences in their orbital forcings. Notably, the third Heinrich event (H3) occurs prior to this highly correlated period, suggesting a missing period of c. 3.5 kyr between 8.5 and 12 kyr BP.

5.1.2 The Holocene and The Last Glacial Maximum Correlate Via 21 kyr

Upon closer examination of the multi-millennial period following the third Heinrich event, one can observe a remarkable resemblance to the climatic fluctuations of the mid-Holocene and beyond (Fig. 5.3). It is unclear why the 21-kyr pacing produced such an accurate climatic correlation and features, given that there are numerous arbitrary multiples (such as 14, 28 kyr, etc.) that originate from the 3.5- and 7-kyr cycles. However, this climatic correlation followed the 21-kyr pacing despite the largest conceivable disparity in the Earth's axial tilt angles. The reason for this is not simply because the difference is 21 kyr, but specifically because the local maximum and minimum of obliquity were passed around 9 and 30 kyr BP, resulting in a completely opposite effect.

Variations in orbital obliquity affect the amount of insolation that the polar regions receive during the summer season. The length of the summer season determines the amount of snow accumulation and the rate of sea ice expansion, providing important substructures for the substance with the highest albedo effect, i.e., freshly fallen snow. The oceanic albedo (0.08) and the fresh snow (0.95) represent extreme values of reflectance compared to the mean Earth albedo (0.3). The absorption rates of solar energy depend on the incident

angle of incoming radiation, and features such as the calmness of the ocean can also affect the rate. Thus, these are guiding values, and other factors such as terrestrial formations and coverage ratio, which are almost complete opposites between hemispheres, particularly above mid-latitudes, further increase the polarization effect in terms of the different properties of the ocean and land.

The climatic profiles in Greenland from the mid-Holocene to the Last Glacial Maximum exhibit surprising similarities over a 4,000-year period, despite the fact that their general climatic conditions were substantially different. These highly synchronous climate profiles begin with the 8.2k cold event and the late Heinrich 3 event, respectively, and are both terminated by short-lived, abrupt warmings. The periodic warm–cool–warm sequences are so prominent that they cannot be ignored. The abrupt warmings around 7 and 8 kyr BP are almost identical to the DO 3 and 4 events, respectively. The two twin peaks match elegantly via the 21-kyr pacing, making them typical climatic outcomes of Solar Surges and their medieval-like high-activity counterparts. They are separated by a cooler inactivity period that has been well-described on many occasions. The DO pair exhibits a temperature rise of 12 °C or so, which is more than three times that measured throughout the Holocene.

A comparison of the profiles also suggests that a YD/BA equivalent (in this case, the H3/DO 5) would be directly attached to the 8.2k cold event, indicating that the early Holocene cycle (12–8.5 kyr BP) was neatly removed, despite the stark glacial–interglacial contrast. The ability of the 17.5-kyr intermittent cycle to periodically alter the typical climate-cycle profiles raises several questions, but it likely holds some answers to the puzzling solar–climate interactions.

A broader survey of the two episodes reveals a few more interesting similarities. The cold and persistent H2 event shares parallels with both the eastern Mediterranean crisis and the Greek Dark Ages, which occurred roughly between 3.2–2.75 kyr BP. The descent into environmental difficulties closely followed the end of Solar Surge warmings in both episodes. Notably, the DP module was absent in the more recent epoch and may have disrupted the late part of a Solar Surge equivalent around 24.5 kyr BP (Fig. 4.10). The chilly and vi-

cious epoch of crisis is surrounded by the more favorable conditions of the Roman and Late Bronze Ages, which also have glacial-time counterparts.

5.2 Semi- and Full-Scale Loops

It is natural to be tempted to look beyond the Last Glacial Maximum in the climate record to identify familiar features that resemble recent developments or the entire Holocene period. While examining the past, present, and future using these records, it is essential to keep in mind that even relatively high synchrony over the last five thousand years may be due to limitations in measurement methods.

The climatic variability over the 52.5-kyr loop, as depicted in Figure 5.4, offers valuable insights. It clearly illustrates two significant warming spikes, one narrow and the other broad, which can be traced back to the Solar Surge and its high-activity counterpart resembling the medieval period. In fact, the resemblance is striking between the late Holocene, Marine Isotope Stage 3, and the post-Eemian. This close correlation is intriguing, considering the varying orbital forcings. Notably, this comparison reveals the absence of a scheduled YD/BA equivalent around 47.5–50 kyr BP and again between 100 and 102.5 kyr BP. Their absence suggests that the severity we attribute to the YD/BA series might not always be as pronounced as previously thought. Even though 47.5–50 kyr BP coincides with an obliquity maximum, it did not prevent the YD from occurring at the start of the Holocene, indicating that obliquity alone is not a decisive factor. What further complicates matters is the NGRIP record, which introduces a cold stadial initiation around 49 kyr BP. If accurate, this would provide convincing evidence of the inevitable continuity of the 17.5-kyr series. Unfortunately, NGRIP seems to displace the two warming spikes, shifting them even deeper in time compared to GRIP and GISP2, where their positions are presumably accurate. The inconsistency is substantial, with NGRIP placing the distinctive pair nearly one Quasi-cycle ahead.

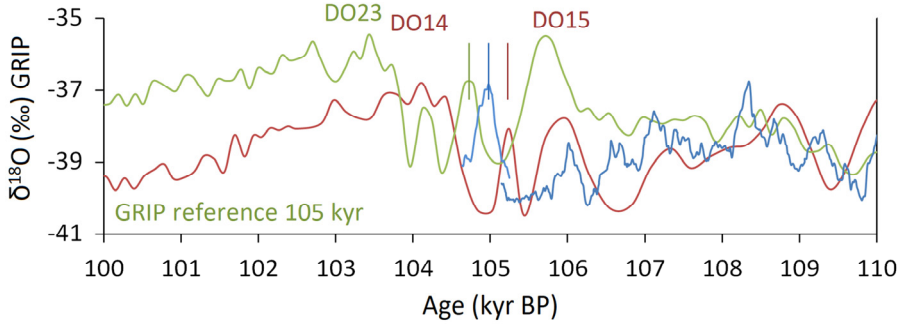

Figure 5.4. A late Holocene climate curve (blue) was established in relation to the 52.5-kyr loop (red) [GISP2 data from Blunier and Brooks, 2001], and with the 105-kyr loop (green) [GRIP data from Johnsen et al., 1997]. This viewpoint predicts no catastrophic BA/YD-type climatic turbulence in four thousand years, but rather a very steady decline. The 52.5-kyr loop supports the idea that the current warmth is likely a temporary spike; however, there is a fundamental contradiction concerning the famous 7-kyr climate cycle and the trigger agent for the warmth spike. It is improbable that a Solar Surge equivalent could have caused both phenomena, although it could have triggered either one. The GISP2 and GRIP records show good correlation during this period, but do not provide additional insight into this controversy. It is worth noting that the Holocene temperature curve (blue) has been amplified, extended, and fitted using GISP2 data from Alley, [2004].

A novel approach provides a different perspective on the central Greenland climate. However, the periodic variations in orbital parameters, particularly those associated with the 405-kyr eccentricity cycle, should make this comparison somewhat trivial, but they fail to do so. As a result, the balance is tilting towards the Blue trendline solution, which allows even the strongest climatic upheavals to occur without being perturbed by it, as illustrated in Chapter 1.

While researching climate data using the longest solar activity loops, there is evidence to support the perception that recent climate changes, since at least AD 500, have been occurring time after time. Specifically, an anomalous medieval-like warming is starkly visible in the 52.5- and 105-kyr loops, both of which appear to have been much broader and more intense local upheavals than the original. Similar to what is represented in Figure 5.2, where the parallel BA and DO 5 events emerged almost time-coevally when observed through the 17.5-kyr loop. Although the GRIP record is known to

suffer from more accuracy issues than the GISP2 and NGRIP records, this is only because its age profile is determined using a flow model instead of layer-by-layer counting. These minor inconsistencies may be reflected in the 105-kyr loop.

The comparison around present-day warming shows much greater variability in timing, leaving behind some uncertainty regarding how the climatic response to activity has evolved over time. It is unclear whether the Solar Surge event is the only solution to provide a sufficient activity contrast or a specific accumulation stage in the 7-kyr TSI cycle. The abrupt Late Bronze Age warming was delayed over a hundred years relative to the Solar Surge event, implying that these temporal shifts are not extraordinary.

5.2.1 Comparing the NGRIP Record to the Holocene via the 52.5-kyr Loop

Some readers may have noticed a contradiction within the 52.5-kyr loop (red) centered around 105 kyr BP (Fig. 5.4). Specifically, there is an ambiguous role of a Solar Surge equivalent as the trigger for both an abrupt modern-like warming and the subsequent DO-14 interstadial, as it is located between them. The DO-14 event started the famous trio of 7-kyr climate oscillations about 52 kyr ago. The following long-term interstadials, the 12th and 8th, are clearly in line with the abrupt Late Bronze Age warming, as shown earlier (see Fig. 3.3). However, the first warm episode, DO 14, matches less precisely. An apparent solution to this paradox could be deduced from the GRIP record, as it shows similar behavior and is associated with a prominent elevation in base temperatures up to around 104 kyr BP. However, a 500-year gap in their inceptions hides the possible cause, suggesting that general conditions or sub-harmonics played a greater role than a single solar-activity anomaly. The 52.5-kyr loop, in its elusive way, could hold the answer, but the periods are too wide for Greenland ice cores. The NGRIP record implies that DO 12 and 14 would have respectively emerged about 1.5 kyr and one Quasi-cycle earlier than what is seen in GISP2, which is a viable option from the perspective of solar activity (Fig. 5.5). However, these crucial chang-

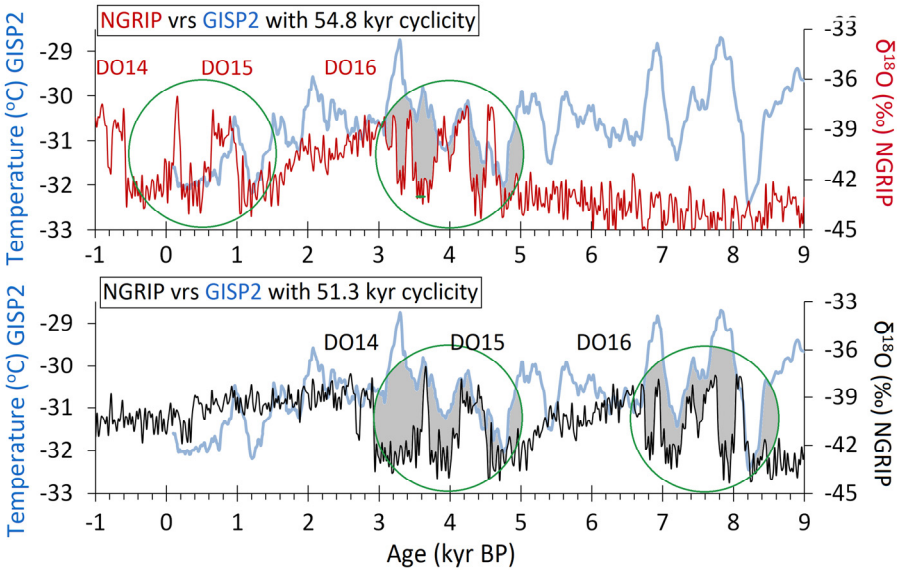

Figure 5.5. In the NGRIP record, early MIS 3 does not show a strong comparison to the climate variability of the Holocene, unless we consider either the 51.8-kyr or 54.8-kyr period instead of the 52.5 kyr. Phases of strong climatic variability (indicated by green circles) could be equivalent to the Little Ice Age (LIA) or Medieval Warm Period (MWP). These phases are separated by c. 3.5 kyr, as anticipated.

es in NGRIP ages versus GISP2 ages date prior to 40 kyr BP and contradict the Heinrich layers, compromising the evident IRD linkage to cold stadial phases. The conventional explanation for these sudden coolings is freshwater runoff, but their causal relationship would be difficult to justify if they were not properly sequenced. Therefore, the paleoclimatic records lead to wider branching. Overall, the 52.5-kyr loop reinforces the view of the past few thousand years as an expected manifestation of intrinsic climate cycles and highlights its greater climatic significance compared to other cycles.

The connection and proper sequencing of DO-12 and H5 events may contain essential information about causality and therefore become critical in understanding the differences between Heinrich and non-Heinrich stadials. However, the starting point of DO-12 is uncertain, as the NGRIP record sets it to around 47 kyr BP, which is a crossing point of a DP module and a medieval-like, high-activity epoch in terms of solar activity. While these factors can explain odd

climatic behaviors, there is a huge contradiction in that an abrupt warming coinciding with massive ice rafting goes against the basic theory of freshwater perturbation. It is difficult to accept that these two events could still coincide, especially since there are virtually no traces of the Heinrich layer in the next cycle. However, an assumption of perturbed North Atlantic overturning circulation would be required to explain the missing medieval-like warm anomaly. These contradictory features do not seem to fit together well and stretch the limits of imagination. The general conclusion is that, in most cases, excessive heat in the Southern Hemisphere is undoubtedly a prerequisite condition for initiating abrupt warming in the northern Atlantic.

5.3 The Tajo Interglacial (MIS 19)

5.3.1 Background Conditions of the Best Orbital Analogue

Interpreting the future of climate becomes increasingly challenging beyond 300 to 500 years from now, particularly in terms of solar-activity-based climate loops. Although both the semi- and full-scale loops suggest that a long-lasting increase in temperature levels will occur after the next abrupt warming, scheduled to begin in 500–1000 years, this is in sharp contrast to earlier conclusions about the Blue trendline serving as a definitive climatic guide. Furthermore, the echoes of the last TSI minimum still persist despite the historically high solar activity of the 20th century. The Tajo is expected to have a trendline, but does it follow the same well-defined path as the Holocene? Before addressing this, a brief examination of orbital symmetry and concurrent solar activity is necessary. The Tajo is considered one of the best analogs for the Holocene in terms of orbital geometry, but can it reconcile the near-future warming contradiction in Greenland? Subtracting their deglacial TSI maxima of 788 and 11 kyr BP yields 777 kyr. A derived comparison reveals nearly coherent July 65° N insolation patterns for the next 50 kyr (Fig. 5.6), but somewhat incoherent insolation patterns before the deglacial inceptions. The prob-

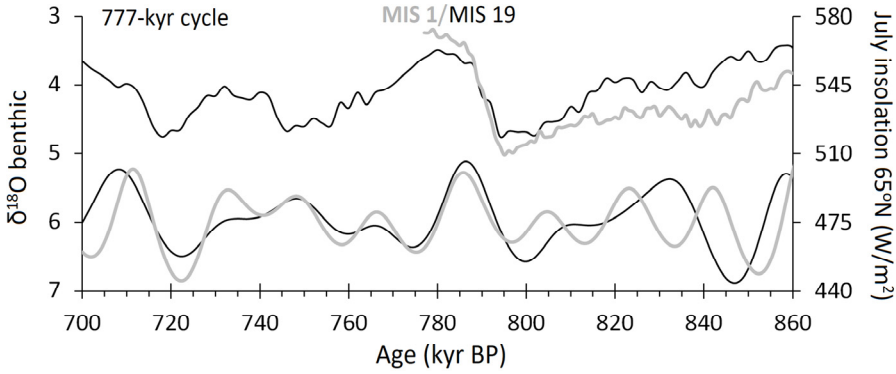

Figure 5.6. The Tajo (MIS 19) and the Holocene (MIS 1) exhibit relatively good symmetry in terms of orbital cycles, particularly from 18 kyr BP onwards (795 kyr BP). The climate proxy records, specifically the July 65°N insolation (W/m²) patterns, and TSI maxima, are consistent over a span of 777 kyr. However, there is a divergence of c. 1 kyr between the obliquity maxima at the end of the deglaciations. The sources of data: LR04 benthic $\delta^{18}O$ stack [Lisiecki and Raymo, 2005] and the orbital solution [Laskar et al., 2004].

lem is that their climate patterns correlated before the deglaciations, but their insolation patterns did not, questioning the predictive power of insolation in this context. However, their obliquity phases differ by only 1 kyr, and the precessional effects are mostly muted by the 405-kyr eccentricity cycle. Simultaneous step changes in millennial-scale climate variability suggest similar forcing conditions. Yet, it is unclear whether the role of orbital configuration or prevailing background conditions is more significant in generating solar-activity-modulated, regional, or global climatic coherency. If the Sun has already set its course, can a 1-kyr obliquity gap or diverging background conditions affect the climate such that their climatic progressions differ substantially? As seen in Chapter 1, the insolation patterns and climate proxies of MIS 15 and MIS 19 were largely coherent but only c. 210 kyr apart (Fig. 1.4). Hence, the 105-kyr solar-activity loop (x2) closely followed a similar rhythm and seemingly produced highly alike climatic fluctuations. These offer an intriguing test bench for further investigations.

The TSI-coordinated deglaciations became less evident after the Tajo interglacial (MIS 19) until the emergence of the Hoxnian (MIS 11), which changed the course again. The discordant interval had

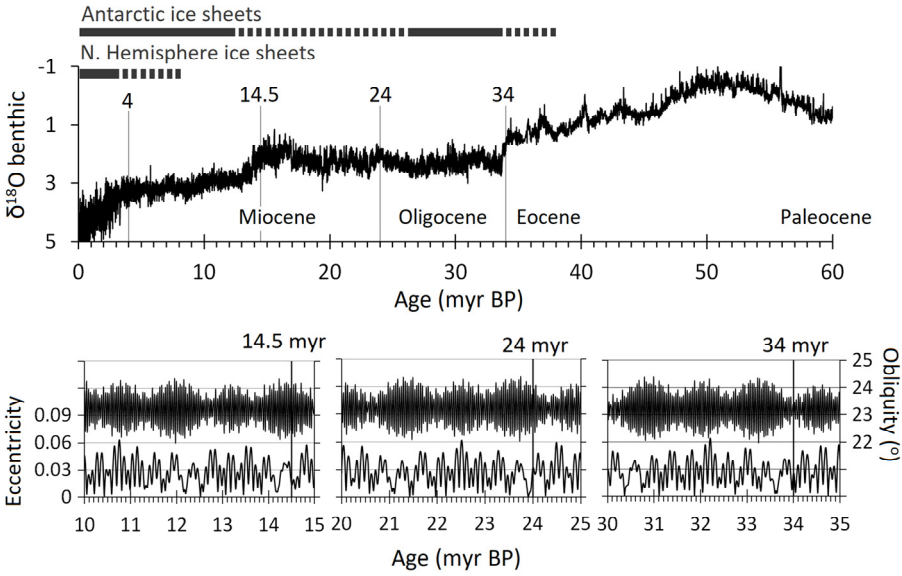

Figure 5.7. A 60-million-year record of global climate history. Approximately 34 million years ago, Antarctica experienced a complete glaciation, which was subsequently followed by periodic climate reversals. The sources of data: the $\delta^{18}O$ benthic foraminifera dataset [Westerhold et al., 2020] and the orbital solution [Laskar et al., 2004].

lower climatic amplitudes and characteristically corresponded to lower obliquity amplitudes, which are part of the 1.2 million-year obliquity cycle [Hinnov and Ogg, 2007]. Although there is no conclusive evidence that they are strongly coupled, the highest amplitudes of obliquity seem to roughly favor the coldest glacial intervals in cycles of about 10 million years. A larger inclination of the Earth's axis further intensifies seasonality at higher latitudes. Over half-degree smaller tilt angles are also in phase with periodic multi-million-year eccentricity variations. The 2.4-myr eccentricity cycle is composed of two alternating phases of 2.8 myr and 2.0 myr. They have a complex symmetry with the periodic 1.2-myr obliquity variations, but the coupling is not absolute over geological time epochs that endure tens of millions of years. For example, the Earth–Mars orbital resonance is thought to have undergone transitions between 50 and 100 million years ago, which led to the current variability in resonance. Also, 14.5 myr BP or so is a clear mirror point in eccentricity periodicity.

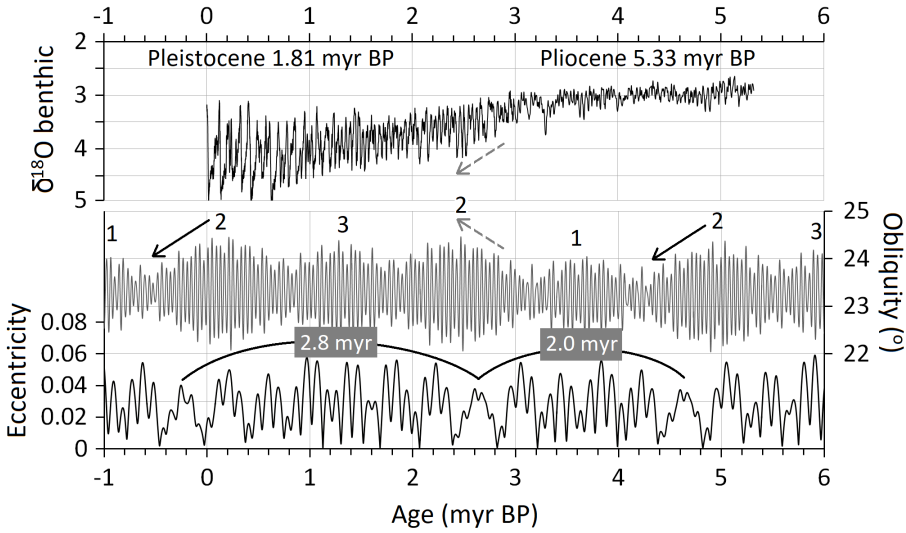

Figure 5.8. Long-term orbital cycles of obliquity and eccentricity exhibit quasi-phase dependence and form complex periodic patterns. Orbital symmetry can be observed over a span of about 4.8 million years. This symmetry primarily results from the fusion of alternating periodicities of around 2 and 2.8 million years for eccentricity. Occasionally, the phase dependence of orbital cycles may change. The data sources are the LR04 benthic $\delta^{18}O$ stack dataset [Lisiecki and Raymo, 2005] and the orbital solution [Laskar et al., 2004].

Instead of the usual alternations, two successive 2.0-myr phases emerged and permanently reversed the sequence. This rearrangement postponed an ominous phase of oscillations by 2 myr or so.

Over the last 40 million years, a 10-myr cycle appears to have modulated global paleotemperature, which is evident in various temperature proxies [Billups et al., 2002; Pälike et al., 2006; Zachos et al., 2008; Westerhold et al., 2020]. It is quite interesting that the second multiple of the 4.8-myr cycle contributes so prominently to a series of relatively rapid coolings approximately 34, 24, 14.5, and 3 myr BP (Fig. 5.7), despite being consistent with a similar Jurassic cycle [Martinez et al. 2015]. The two oldest dates are near successive epoch boundaries from the Eocene-to-Oligocene and Oligocene-to-Miocene [Hinnov and Ogg, 2007]. However, the latest part of the series is not as well-described in terms of epoch transitions from the Miocene-to-Pliocene (5.33 myr BP) and Pliocene-to-Pleistocene (1.81 myr BP).

It is challenging to ascertain whether the internal changes in the cycles or their relative movements to each other caused the most recent cooling event to be delayed by c. 2 million years due to the latest step-change in 2.8- and 2.0-myr cyclicity. However, the crucial point to note is that the obliquity amplitude was on a downward trend between 4.8 and 4 myr BP (refer to Fig. 5.8). This trend is contrary to what is needed to induce a cooling event once the 100-kyr eccentricity amplitudes, as well as precessional amplitudes, are essentially subdued. This represents a potential deviation from previous periodic cooling events, and thus the iconic phrase 'the exception proves the rule' seems to aptly describe the phenomenon.

The amplitude variation of the c. 100-kyr eccentricity cycle is at its most subdued in the 405-kyr round (occurring primarily every 2.0 or 2.8 myr), and the obliquity amplitude is on its highest increasing trend (2), as it was again approximately 2.5–3 myr BP. This combination generates a forcing effect that appears to contribute to a major cooling and is characteristically associated with the establishment of full-scale ice sheets in the Northern Hemisphere. Since then, glacial cycles have become cooler and longer, while interglacials have remained nearly as warm.

5.3.2 Similarities between the Tajo and the Holocene

The expansion of the ice sheets during MIS 19, also known as glacial inception, was region-dependent and began between 777 and 774 thousand years BP [Head, 2021]. Despite the temporal proximity of this period to the present day (see Fig. 5.9), there is currently little evidence of cooling in either hemisphere without the anomaly of the Little Ice Age. However, the Antarctic EDC record [Jouzel et al., 2007] identifies a turning point at around 776 kyr BP, when a relatively steep, multi-millennial cooling period began, despite the increasing Total Solar Irradiance, which peaked a few thousand years later. It is worth noting that the Tajo's obliquity maximum advances that of the Holocene by a thousand years. Nevertheless, their angle trajectories intersect again around the glacial inception of 774 kyr BP, which occurs roughly 3 kyr after the present.

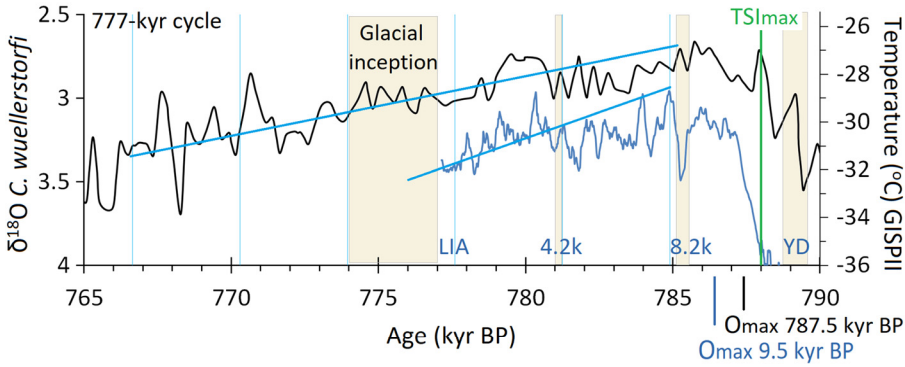

Figure 5.9. The Holocene climate is compared to that of the Tajo interglacial by using the 777-kyr TSI and orbital matches. However, the 3.75-kyr modules do not align in this comparison, and hence the last massive IRD event preceding the Tajo likely began c. 789.4 kyr BP [Barker et al., 2019]. Comparatively, this occurred around 700 years after the onset of the Younger Dryas IRD event (13.2 kyr BP). The megadrought at 4.2 kyr BP and the cold event at 8.2 kyr BP had at least regional significance during the Tajo interglacial [Giaccio et al., 2015], displaying a 3.5-kyr cycle dependency. The data sources for this analysis include the benthic foraminifera ($\delta^{18}O$) from the Iberian margin site U1385 [Sánchez Goñi et al., 2018], and the GISP2 record from Alley [2004].

The higher obliquity values from the early to mid-Holocene increase the likelihood that the Holocene is going to be warmer for a longer time. On the other hand, the obliquity trajectories will cross at some point, leading to a more rapid deterioration of the climate afterward [Tzedakis, 2010]. This phenomenon is region-dependent and is influenced by the interplay between total solar irradiance and orbital changes. Although a TSI maximum is expected to determine the final turning point in Antarctica, the latest age chronology (AICC2012) of the Antarctic EDC record (since GICCO05) suggests that a cooling phase started 3 kyr earlier, around 779 kyr BP [PAGES, 2016]. In this light, it could be argued that the recent climatic descent from ancient Roman times to the Little Ice Age was a precursor to glacial inception in Greenland but not in the Southern Hemisphere. From this perspective, a small climatic controversy could currently exist between the polar regions, despite their common trend; but was it the Sun, the climate system, or man behind this warming? By comparing the temperatures over one TSI-minima cycle, we may

gain insights into the interglacial progression at the poles. In a rough comparison, the Antarctic record indicates that the Little Ice Age was 0.5–1 °C warmer than its equivalent in the 8th millennium BP, while the Greenland record shows a net cooling of about -0.5 °C.

Comparing the Little Ice Age with the climatic conditions seven thousand years ago is challenging due to high climatic volatility. Therefore, only the lowest temperatures were considered for comparison. The Holocene's abrupt climatic fluctuations reveal a partially visible parabolic shape in the proxies. Currently, the wide parabolic temperature curve of Antarctica's EPICA Dome C (EDC) shows greater warmth than most interglacials at this point in the cycle. However, the question remains: will the paradigm of a warmer Antarctica and a cooler Greenland persist? For instance, Tajo's Antarctica moved in the opposite direction, cooling by approximately 1.5 °C between similar TSI minima, while the Eemian was just beginning to turn colder (EDC Antarctica). Only the Hoxnian interglacial compares to the Holocene in this respect, but it is unique in many ways. Its deglacial threshold level of insolation (65° N) was particularly low, making it distinct from recent interglacials. None of the others initiated an interglacial era under such modest solar radiation values. Moreover, it is essential to consider that the bipolar seesaw mechanism plays a central role in glacial terminations and inceptions, preserving hemispheric climate anomalies for millennia and promoting unpredictability with devastatingly drastic consequences.

5.3.3 Younger Dryas and Cold Event Equivalents of the Tajo

According to research by Jouzel et al. [2007] and PAGES [2016], temperatures in Antarctica began gradually increasing around 795.5 kyr BP and peaked about 8,000 years later at 787.5 kyr BP. In contrast, the Northern Hemisphere's glacial termination did not witness such a dramatic climate reversal as the Younger Dryas, although it did experience a cold spell with substantial ice-rafting, as seen in many glacial terminations following the Mid-Pleistocene Transition. The record from Icelandic ocean drilling (ODP 983) shows a massive ice-rafting event beginning around 789.4 kyr BP [Tzedakis et al., 2012b;

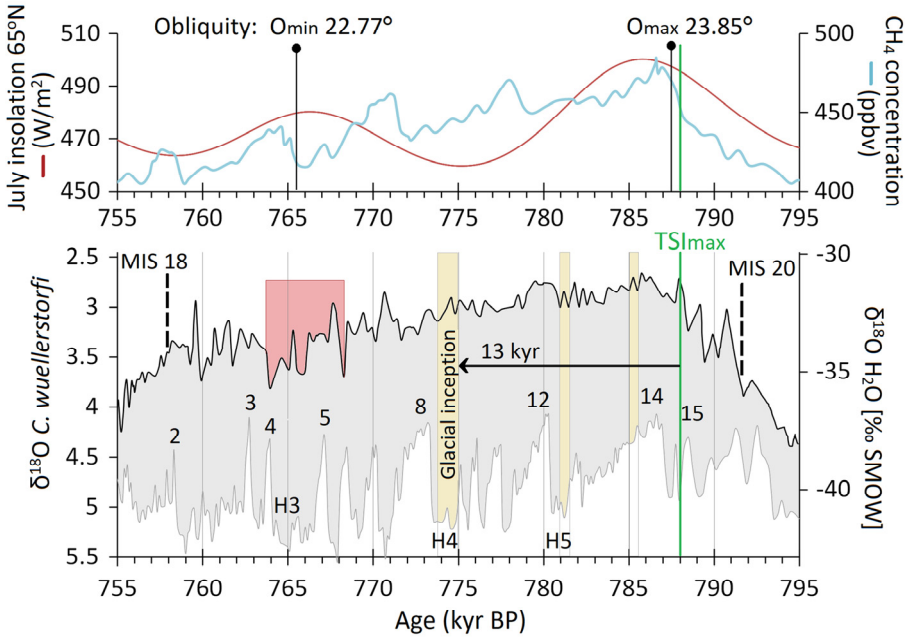

Figure 5.10. A Tajo proxy, based on the abundance of $\delta^{18}O$ benthic foraminifera (Cibicidoides wuellerstorfi), was recovered from the Atlantic coast of Portugal (U1385) [Sánchez Goñi et al., 2018]. It is compared to MIS 3 (based on GISP2) using the 105-kyr multiples [Grootes et al., 1999]. The H3/DO5 sequence exhibits a turbulent counterpart (highlighted in red). The obliquity maximum (O_{max}) at c. 787.5 kyr BP and minimum (O_{min}) at around 765.5 kyr BP show some similarity to those of MIS 3. The insolation data is sourced from Laskar et al. [2004], and the methane (CH_4) data is sourced from the EDC ice-core record [Loulergue et al., 2008].

Barker et al., 2019], which is almost a millennium-scale IRD event and matches the DP module series prior to c. AD 0 (2 kyr BP + 52.5 kyr + 7 x 105 kyr = 789.5 kyr BP).

A multi-clustered DP module is expected to emerge c. 1.75 kyr from the present, and it should be identical to the 785.6 kyr BP activity phase that apparently induced the cold event. Both the s3.5- and 3.75-kyr modules could act as triggers, and their prehistoric progressions with climate change are undeniable. However, instead of viewing future modules and grand minima as potentially hazardous, it is more likely that the next TSI maximum will mark the start of a global glacial period. The advancement of this period will be modulated by both obliquity and insolation, in concert with the bipolar seesaw

mechanism. Nonetheless, it is essential to recall that model experiments indicate that the Holocene will continue as long as the atmospheric CO_2 concentration remains at its present level [Loutre et al., 2000; Tzedakis et al., 2012b]. Therefore, a new glacial inception cannot occur until the preindustrial CO_2 level of 230 ppmv is again reached.

The early cold event of the Tajo c. 785.6 kyr BP can be detected in central Italy records, and it may reflect ocean-circulation perturbations [Regattieri et al., 2019]. Also, the U1385 sediment record off southern Portugal shows abrupt changes [Sánchez Goñi et al., 2018]. A comparison to the 8.2k cold event makes it interesting because both emerged c. 2,500 years after their TSI maxima. An educated guess would place them in the s3.5-kyr module family, but in the cluster formation of early MIS-19 grand minima, they are hardly separable within error margins. The 52.5-kyr solar loop indicates that the Sun produced a typical, clustered DP module during the 785.8–785.0 cold event, with an additional s3.5-kyr module fittingly located in the middle.

Where the first TSI maximum of 788 kyr BP and the concurrent steep methane rise characterize the emerging Tajo in the Northern Hemisphere, the two subsequent TSI maxima reflect its climatic progression until ice sheets started to expand again after c. 774 kyr BP. It took possibly about 14 thousand years from the interglacial starting boundary of MIS 19c/20 to the glacial inception (MIS 19b/c). It could be the destiny of the Holocene as well. However, a straight comparison to the Holocene is not viable in terms of the 105-kyr solar loop. Instead, the Tajo straightly parallels the Marine Isotope Stage 3 (Fig. 5.10). Nonetheless, we can see a splendid similarity in their proceedings, including the Heinrich 4 event and the following TSI maximum, as they deftly parallel the glacial inception of the Tajo. From Figure 5.10, one can draw even further conclusions: the 52.5-kyr loop conveniently links the present day to the onset of MIS 19 (788 kyr BP), with the exception that the TSI cycles are in antiphase. As a result, the Tajo starts where we are now in terms of solar activity (excluding TSI), which simplifies comprehension of its grand-minima evolution.

The periodic YD-like event emerges in 17.5-kyr cycles and skips the MIS 19c/20 deglaciation, but seems to have induced a distinctive climatic upheaval c. 20 thousand years after the interglacial onset. By then, the glacial inception has already advanced by about 7 thousand years, and obliquity has reached its minimum. In this respect, it is an unlikely scenario for the Holocene to experience such drastic climate swings prior to the next TSI maximum. The fact that this is not a Greenland record but an ocean-drilling record off southern Portugal is an unfavorable aspect with speculative elements. Yet, its climatic ups and downs suddenly seem so familiar when visually examined with the well-studied stages of MIS 3 and the Holocene. The comparison strengthens the view of similar fundamentals causing the three cold Heinrich stadials (H3, H4, and H5) and climate changes of the Tajo, independent on their evident orbital mismatch. The problem is that the global, hemispheric, and regional scales of these events may still be partially unresolved.

5.3.4 Climate Models and the Future

To simulate the climate system and its complex ocean–atmosphere circulations, one has to make simplifications to the model. Otherwise, modelling work of long-term scenarios becomes time-consuming and requires a tremendous amount of calculation capacity. Global climate models are used, for example, to simulate the influence of sea-surface temperature variations on the thermohaline circulation. These models have demonstrated that increasing concentrations of CO_2 in the atmosphere are associated with higher sea-surface temperatures and can significantly reduce sinking near current deep-water cells by leveling out regional sea-water density differences.

Surprisingly, a computer model was able to achieve a climate fluctuation over the next half-millennium that is stunningly similar to the 52.5-kyr loop revealed in Figure 5.4. Approximately 50 kyr ago, more clement conditions prevailed in Greenland than during the ice age on average, making it a suitable basis for this kind of assessment despite the evident contrast in amplitudes. Interstadial 14

rather rapidly restored warmth after a cold stadial condition, driven by astronomical forcing and a plentiful supply of southern-sourced heat. Its climatic profile resembles those of simulations carried out with elevated concentrations of atmospheric carbon dioxide.

A simulation on a doubled carbon dioxide level predicts a 50% reduction in AMOC flux (Sv) within 150 years and a gradual yet complete recovery at the end of the experiment. It is, however, uncertain what the full recovery means for Arctic temperatures. Will a Great Warm Plateau-like epoch prevail as predicted, or will modern-day warming return? At a higher, quadrupled CO_2 concentration, the Atlantic overturning circulation completely halts in 250 years and produces an adverse LIA-like or worse condition for the next 1,500 years or so. [Manabe et al., 1994; Stouffer et al., 2003]. These simulated scenarios are pretty much in line with the outcomes that the semi- and full-scale solar loops produced c. 52.5 and 105 kyr BP, although their basic ideas for climate change are very different. The climatic loops rely on the bipolar seesaw mechanism, which is conducted to some extent by solar variability. Nothing in the recent past suggests that the fading Arctic warmth will return in the coming Holocene. However, the multi-millennial climate cycle does not directly tell much about the changing rate of AMOC flux; it only shows temperature changes. The interhemispheric energy budget across the entire Atlantic basin has been relatively well balanced over the Holocene. Its climatic changes have thus far been negligible compared to glacial fluctuations. From AD 2300 onward, the climate over Greenland is hardly as susceptible to flamboyant shifts as the previous millennium was.

What about the advancing twenty-first century? Should we not be exposed to a most vigorous danger because of the recent melting in Greenland that could lead to freshwater pooling in the northern Atlantic? It all points to the same question: what are the physical mechanisms [Stanford et al., 2006; 2011] and sequence of events that eventually increase the Atlantic overturning circulation, leading to abrupt warming and immediately after that an abrupt cooling, as seen so frequently throughout the ice age in the form of short-term DO events?

5.4 A 1.3-million-Year Bond to the Early Pleistocene

In the absence of millions of years of reliable cosmogenic isotope data, it is possible to rely on appropriate climatic comparisons to trace possible similarities over time. The Tajo interglacial, for example, clearly indicates the presence of a progenitor of the H3 event, suggesting that a sediment core on the Iberian margin recorded such climatic turmoil in the North Atlantic. Building upon this finding and Shackelton et al.'s [2000] insightful research, we are now expanding our exploration even further by studying biological productivity over time on the southwest Iberian margin off southern Portugal at ODP Site U1385, also known as the 'Shackleton Site.'

This location is ideal for studying millennial-scale climate variability because isotope records ($\delta^{18}O$ and $\delta^{13}C$) of planktonic and benthic foraminifera from this region have documented rapid climatic changes in both Greenland and Antarctica during the last ice age. Furthermore, an analysis of these records has revealed that periodicities of 2.6, 3.5, and 6/6.5 kyr over a million years ago were among those that governed millennial-scale climate variability in glacial, deglacial, and interglacial fluctuations [Birner et al., 2015].

Randomly selected climate periods such as MIS 2–3 and MIS 39–40 can correlate via the MMSCs, even if the insolation patterns are largely divergent (Fig. 5.11). The millennial-scale climatic variability of this early Pleistocene stage was first researched by Raymo et al. [1998] and later in more detail by Birner et al. [2015]. These considerable research efforts have enabled us to discern some key differences across the Middle Pleistocene Transition (MPT).

Even though a YD-type sequence is enigmatically absent in a rough screening, its traces capture the observer's full attention in a more detailed inspection. This dramatic sequence was not only a cornerstone of the rapid onset of the MIS-39 interglacial, but the next event in the sequence also terminated it. Therefore, one might expect to see some typical features of YD equivalents in at least one of the ends, but instead, their voids were filled with interglacial warmth. As we concluded earlier, there must be other factors at play that are affecting these mega-scale upheavals. A high-activity epoch, similar

to the medieval period, convincingly coupled the abrupt DO-1 and 5 warmings, and at the time of glacial MIS 40, a DO-5 equivalent served as a stepping stone into the sustained warmth of MIS 39.

IRD events are predominantly triggered by the 3.75-kyr cycle, with a few notable exceptions. The Homeric-Maunder modules, whether fully or partly joined, appear to have relevance to a few beginnings (1287 and 1305 kyr BP) and simultaneously address the fact that they are unlikely to be mere coincidences. The solar module-related anomaly is now taking a new twist, potentially different from earlier observations (see Chapter 4). The reasons why the DP module was solely capable of initiating IRD events can finally be questioned. Over the course of more than a million years, conditions have changed enough to provide evidence of the 3.5-kyr Homeric module, which consistently aligns with IRD events. Unless the massive iceberg discharges of the last ice age had not responded so systematically to this singular solar event, it would have been much more difficult to confirm such a module structure in the first place.

The progenitors of the H4 and H5 events at the time of glacial MIS 40 evidently characterized similar 7-kyr climate oscillations as they did 50 thousand years ago. The 7-kyr climate oscillations are not a hallmark of any ice age; instead, they seem to have emerged at a specific locus. The full-scale solar loop suggests that the sequence of famous interstadials (8, 12, and 14) emerges possibly independently of an existing orbital configuration yet requires glacial conditions. Impressive similarities between glacial climate patterns again put the TSI maximum and its high-activity solar events in the spotlight. The pace of these long interstadials in both ages notably clarifies the importance of solar variability.

The spectrum analysis of isotope records reveals essentially the same variability pacing as the MMSCs for the Holocene. However, the significance of a 2.6-kyr cycle and the subharmonics of 1.3 kyr and 1.7 kyr pose challenges due to their invisibility, for example, in GISP2. Nevertheless, a periodicity of about 1.5 kyr has been associated, with varying success and agreement, with the Bond cycle of the last ice age. It could be a fusion of these two subharmonics.

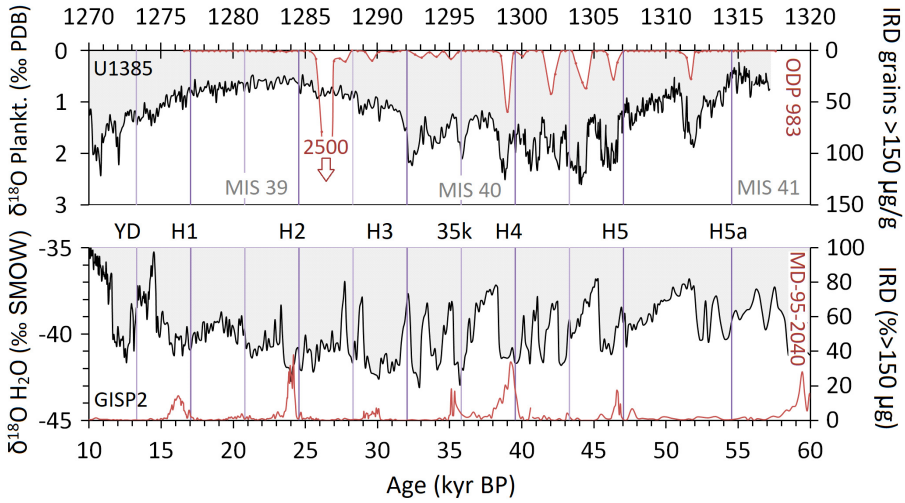

Figure 5.11. The early and late Pleistocene intervals of MIS 39–40 and MIS 2–3 display parallelism over a period of 1260 kyr, which is a multiple of the 105-kyr solar cycle. Counterparts can be identified for interstadials 8, 12, and 14. The two youngest interstadials precisely match those of MIS 40. For early Pleistocene data, references include Birner et al. [2015] and Raymo et al. [1998]. For late Pleistocene data, references include Grootes et al. [1999] and de Abreu et al. [2003].

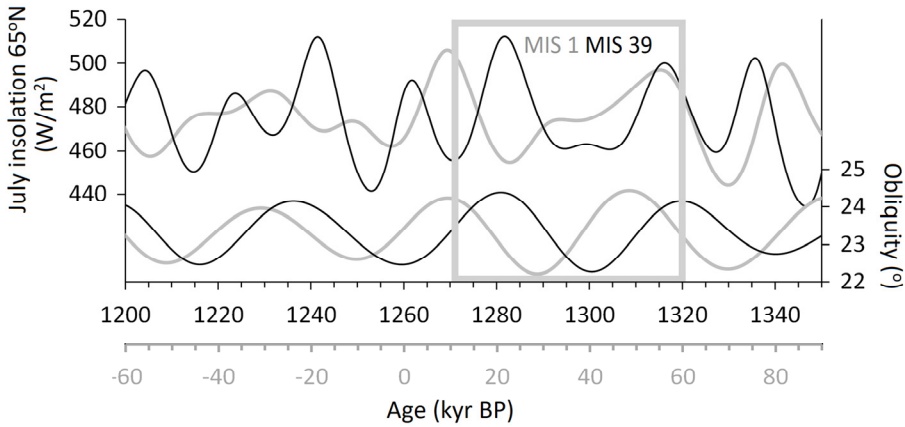

Figure 5.12. Neither insolation at 65°N nor obliquity fluctuations are coherent over a 1260 kyr period. A divergence in obliquity of c. 10 kyr opens a narrow time-window when obliquity is low in both stages (MIS 1 and 39). However, there is a high similarity in millennial climatic variability between the stages over a much longer time span. The data for orbital obliquity (°) and July insolation at 65°N (W/m²) are sourced from Laskar et al. [2004].

The Beyond EPICA Project in Antarctica aims to extract a continuous ice-layer record spanning over 1.5 million years by drilling a core. The record will hopefully uncover TSI-cycle-oriented top formations for glacial MIS 39 that coincided with the onset of Greenland interstadials similar to the last ice age. It is not unusual for an abrupt interglacial or interstadial warming in the northern Atlantic to begin at the TSI cycle's peak. The tendency is visible in the Holocene, MIS 39/40, and the famous interstadials of MIS 3. One could speculate that this is the reason why the Bølling warming did not start the Holocene, while its MIS-40 counterpart (DO 3) succeeded.

The glacial periods of MIS 40 and 3, randomly selected from both sides of the Middle Pleistocene Transition (c. 800–1200 kyr BP), provide strong evidence that ice sheets in the northern Atlantic region extensively amplified millennial-scale climatic variability across various ages. However, there is a catch. Even though the interstadials of MIS 3 (50 kyr ago) did not result in an interglacial, their equivalent counterpart succeeded in the 41-kyr 'world'. The key is to recognize what could have been but was not. A new way to compare and represent the Last Glacial Maximum and the MIS-39 interglacial periods reveals their potential for climatic variability. The two periods' synchronized, and thus nearly identical, solar activity phases should reflect highly similar climatic variability. During the obliquity maximum, the interstadial–interglacial warmth was fueled, while during the obliquity minimum, their stability and length were disturbed. Despite the separating effects of obliquity extremes, the prevailing glacial conditions harmonized their progressions in both periods, as shown in Fig. 5.12.

The most prominent aspect of millennial climate variability is the period spanning the last 1,500 years. Its solar variability has been shown to have modulated the northern Atlantic climate as early as 1.3 million years before the present, on the brink of the Middle Pleistocene Transition. In these unique conditions, a DO-5 equivalent was the igniter of the MIS-39 interglacial. It led straight up to a warmer era mimicking the Greenland Holocene, although an ominous YD equivalent with disruptive potential could have definitively caused the opposite outcome. Much later, the Middle Pleistocene Transition

caused a major change in the world's climatic fundamentals. The obliquity-controlled, 41-kyr climatic alterations were replaced by the eccentricity-governed, 100-kyr alterations for good.

Is it possible that the current upward trend in temperature could lead to sustained multi-millennial warmth? Clues from past glaciations, specifically Marine Isotope Stages 3, 4, and 38, suggest that this is an alternative scenario. Familiar, long-term interstadials emerged around 1260 and 1312 kyr BP about 52.5 kyr apart, following their respective peaks in insolation. They clearly inform the viewer of the stupendous continuity in this particular locus characterized with increasing northern warmth. However, the question remains as to whether it is possible to sustain such an abruptly elevated temperature during an interglacial. Historically, any significant upheaval has ultimately led to stabilization within centuries rather than millennia. Only time will tell if the present situation is different. Unfortunately, the available time resolution does not provide insight into the prospects of the current Holocene interglacial.

The comparison to the 41-kyr 'world' consolidates the earlier view of the coming millennia, as shown in Figure 5.4. Instead of a Younger Dryas equivalent, the mid-phases of a staggering 7-kyr-long interstadial are characterized by a smooth and gradual decline. The interstadial began abruptly around 1260 kyr BP and gradually declined, eventually leading to the subsequent cold stadial. Its shape, timing, and amplitude give the impression that they are consistent with the interstadial profiles produced by the semi- and full-scale loops after the Eemian, but most essentially, they are products of glacial times. Conveniently, the 1260-kyr period is divisible by the longer 405-kyr eccentricity cycle, and in this respect, glacial MIS 40 parallels relatively well with MIS 3.

The more we study past variability, the more it expands our range of options for interpreting the future. However, the broad picture is definitively crystallizing. To what extent solar variability is modifying climatic variability remains to be seen, but the first steps are being taken to link them and profoundly clarify their complex relationship.

Appendix

REFERENCES

Abram, N.J., Gagan, M.K., Liu, Z., Hantoro, W.S., McCulloch, M.T., Suwargadi, B.W., (2007), Seasonal characteristics of the Indian Ocean dipole during the Holocene epoch. Nature, 445, 299-302.

Abreu, J. A., J. Beer, and A. Ferriz-Mas (2010), Past and future solar activity from cosmogenic radionuclides, in Astronomical Society of the Pacific Conference Series: Soho-23: Understanding a Peculiar Solar Minimum, vol. 428, edited by S. R. Cranmer, J. T. Hoeksema, and J. L. Kohl, pp. 287–295, Astronomical Society of the Pacific Conference Series, Utah.

Abreu, J. A., J. Beer, F. Steinhilber, F. Christl, and P. W. Kubik (2012a), ^{10}Be in Ice Cores and ^{14}C in Tree Rings: Separation of Production and Climate Effects, Space Sci. Rev., 1–7.

Abreu, J. A., Is there a planetary influence on solar activity? Astronomy & Astrophysics, A&A 548, A88 (2012).

Adolphi, F., Ramsey, C. B., Erhardt, T., Edwards, R. L., Cheng, H., Turney, C. S. M., Cooper, A., Svensson, A., Rasmussen, S. O., Fischer, H., and Muscheler, R., (2018), Connecting the Greenland ice-core and U/Th timescales via cosmogenic radionuclides: testing the synchroneity of Dansgaard-Oeschger events, Climate of the Past, 14, 1755–1781.

Ágústsdottir, M. A., Alley, R. B., (2005), The 8k event: cause and consequences of a major Holocene abrupt climate change, Quaternary Science Reviews 24 1123–1149.

Alley, R. B., and Clark, P. U., (1999), The deglaciation of the northern hemisphere: A global perspective, Annu. Rev. Earth Planet. Sci. 27:149–182.

Alley, R. B., (2000), The Younger Dryas cold interval as viewed from central Greenland, Quaternary Science Reviews 19 213-226.

Alley, R. B., (2004), GISP2 Ice Core Temperature and Accumulation Data, IGBP PAGES/World Data Center for Paleoclimatology Data Contribution Series 2004-013, NOAA/NGDC Paleoclimatology Program, Boulder CO, USA.

Alley, R. B., (2007), Wally Was Right: Predictive Ability of the North Atlantic 'Conveyor Belt' Hypothesis for Abrupt Climate Change, Annu. Rev. Earth Planet. Sci. 35:241–72.

Altabet, M. A., Higginson, M. J., and Murray, D. W., (2002), The effect of millennial-scale changes in Arabian Sea denitrification on atmospheric CO_2, Nature, 415, 159–162.

Amesbury, M. J., Charman, D. J., Fyfe, R. M., Langdon, P. G. & West, S., (2008), Bronze Age upland settlement decline in south-west England: testing the climate change hypothesis, Journal of Archaeological Science 35: 87–98.

Anderson, R. Y., (1982), A long geoclimatic record from the Permian, Journal of geophysical research 87 (C9): 7285-7294.

Anderson, R. F., Ali, S., Bradtmiller, L. I., et al., (2009), Wind-driven upwelling in the Southern Ocean and the deglacial rise in atmospheric CO_2, Science, 323, 1443–1448.

Andrews, J.T., Jennings, A.E., Kerwin, M., et al., (1995), A Heinrich-like event, H-0 (Dc-0) – source(s) for detrital carbonate in the North Atlantic during the Younger Dryas chronozone. Paleoceanography 10, 943–952.

Andrews, J.T., (1998), Abrupt changes (Heinrich events) in late Quaternary North Atlantic marine environments: a history and review of data and concepts, JOURNAL OF QUATERNARY SCIENCE 13 (1) 3–16.

Anet J. G., Rozanov, E. V., Muthers, S., et al., (2013), Impact of a potential 21st century "grand solar minimum" on surface temperatures and stratospheric ozone, Geophysical Research Letters Vol 40, 16, 4420-4425.

Baek, S. H., Smerdon, J. E., Dobrin, G. C. et al., (2020), A quantitative hydroclimatic context for the European Great Famine of 1315–1317, Communications Earth & Environmental, 1, 19.

Bamber, J. L, et al., (2018), The land ice contribution to sea level during the satellite era, Environmental Research Letters, 13, 063008.

Bard, E., Rostek, F., Turon, J.-L., Gendreau, S., (2000). Hydrological impact of Heinrich events in the subtropical northeast Atlantic, Science, 289, 1321-1324.

Barker, S., Knorr, G., Edwards, R.L., et al., (2011), 800,000 years of abrupt climate variability, Science, 334 (6054), 347–351.

Barker, S., Chen, J., Gong, X., et al., (2015), Icebergs not the trigger for North Atlantic cold events, Nature letter, Vol 520, April.

Barker, S., Knorr, G., Conn, S., et al., (2019), Foraminifer and IRD counts from ODP Site 162-983. PANGAEA, https://doi.org/10.1594/PANGAEA.904398.

Bauch, H. A., Kandiano, E. S., and Helmke, J. P., (2012), Contrasting ocean changes between the subpolar and polar North Atlantic during the past 135 ka, Geophysical Research Letters, 39, L11604.

Bauch, M., Labbe, T. et al., (2020), A prequel to the Dantean Anomaly: the precipitation seesaw and droughts of 1302 to 1307 in Europe, Climate of the Past.

Bazin, L., Landais, A., Lemieux-Dudon, et al., (2013), An optimized multi-proxy, multi-site Antarctic ice and gas orbital chronology (AICC2012): 120-800 ka. Clim. Past. 9, 1715-1731.

Beer, J., (2000), Long-term indirect indices of solar variability, Space Science Reviews, 94, 53–66.

Berdyugina, S.V., Pelt, J., Tuominen, I., (2002), Magnetic activity in the young solar analog LQ Hydrae, I. Active longitudes and cycles, Astronomy and Astrophysics 394, 505.

Berger, A., (1992), Orbital Variations and Insolation Database. IGBP PAGES/World Data Center for Paleoclimatology Data Contribution Series # 92-007. NOAA/NGDC Paleoclimatology Program, Boulder CO, USA.

Bigg, G. R., The Oceans and Climate, (2003), 2nd Edition, Cambridge University Press (New York).

Billups, K., Channell, J. E. T. & Zachos, J., (2002), Late Oligocene to early Miocene geochronology and paleoceanography from the subantarctic South Atlantic. Paleoceanography 17, U39–U49.

Birner, B., Hodell, D. A., Tzedakis, P. C., and Skinner, L. C., (2016), Similar millennial climate variability on the Iberian margin during two early Pleistocene glacials and MIS 3, Paleoceanography, 31, 203–217.

Blunier, T., and Brook, E. J., (2001), Timing of millennial-scale climate change in Antarctica and Greenland during the last glacial period, Science, 291, 109-112.

Bond, G. C., Showers, W., Elliot, M., Evans, M., Lotti, R., Hajdas, I., Bonani, G., Johnson, S., (1999), The North Atlantic's 1-2 Kyr Climate Rhythm: Relation to Heinrich Events, Dansgaard/Oeschger Cycles and the Little Ice Age, Mechanisms of Global Climate Change at Millennial Time Scales. (1999), Geophys. Monogr. Ser., vol. 112, edited by U. Clark, S. Webb, and D. Keigwin, pp. 35-58, AGU, Washington, D. C.

Bond, G., Kromer, B., Beer, J., Muscheler, R., Evans, M.N., Showers, W., Hoffmann,S., Lotti-Bond, R., Hajdas, I., and Bonani, G., (2001), Persistent solar influence on North Atlantic climate during the Holocene, Science 294, 2130–2136.

Booth, R. K., et al., (2005), A severe centennial-scale drought in mid-continental North America 4200 years ago and apparent global linkages. The Holocene, 15, 321–328.

Box, J. E, (2009), Greenland Ice Sheet Surface Air Temperature Variability: 1840–2007, Amer. Meteorological Soc., p. 4029-4049.

Braithwaite, J., (2009), Axisymmetric magnetic fields in stars: relative strengths of poloidal and toroidal components, Monthly Notices of the Royal Astronomical Society, Vol 397, 2, 763–774.

Bray, J. R., (1968) Glaciation and Solar Activity since the Fifth Century BC and the Solar Cycle, Nature 220 672–674 Nov.

Brink, H.-J., (2015), Periodic Signals of the Milky Way Concealed in Terrestrial Sedimentary Basin Fills and in Planetary Magmatism?, International Journal of Geosciences, 06, 831-845.

Broecker, W. S., Denton, G. H., (1990), What Drives Glacial Cycles?, Scientific American Vol. 26, No. 1, Jan.

Broecker, W.S., (1998), Paleocean circulation during the last deglaciation: a bipolar seesaw?, Paleoceanography, 13, 119–21.

Broecker, W. S., Denton, G. H., Edwards, R. W., Cheng. H., Alley, R. B., Putnam, A. E., (2010), Putting the Younger Dryas cold event into context, Quaternary Science Reviews 29, 1078-1081.

Brown, T. M., Christensen-Dalsgaard, J., Dziembowski, W. A., Goode, P., Gough, D. O. & Morrow, C. A., (1989), Inferring the Sun's internal angular velocity from observed p-mode frequency splittings, Astrophysical Journal, 343, 526.

Brun, A. S. and Browning, M. K., (2017), Magnetism, dynamo action and the solar-stellar connection, Living Review Solar Physics, 14:4.

Buckley, M. W. and Marshall, J., (2016), Observations, inferences, and mechanisms of Atlantic Meridional Overturning Circulation variability: A review, Rev. Geophys., 54.

Buizert, C., Adrian, B., Ahn, J., Albert, M., Alley, R. B., Baggenstos, D., Woodruff, T. E., (2015), Precise interpolar phasing of abrupt climate change during the last ice age, Nature, 520 (7549), 661-665.

Burroughs W. J., (2005), Climate change in prehistory – The End of the Reign of Chaos, Cambridge University Press (New York).

Callebaut, D. K., de Jager, C., Duhau, S., (2012), The influence of planetary attractions on the solar tachocline, Journal of Atmospheric and Solar–Terrestrial Physics, 80 (2012), pp. 73-78.

Candy, I., (2014) Marine Isotope Stage 11: Palaeoclimates, palaeoenvironments and its role as an analogue for the current interglacial, Earth-Science Reviews Volume 128, 18-51.

Channell, J.E.T et al., (2012), A 750-kyr detrital-layer stratigraphy for the North Atlantic (IODP Sites U1302–U1303, Orphan Knoll, Labrador Sea). Earth and Planetary Science Letters, 317-318, 218-230.

Chaplin, W. J., (2006), Music of the Sun – the Story of Helioseismology, Oneworld Publication Oxford England, ISBN-13: 978–1–85168–451–9.

Chappell, J. (2002), Sea level changes forced ice breakouts in the last glacial cycle: New results from coral terraces, Quat. Sci. Rev., 21, 1229–1240.

Charbonneau, P., Christensen-Dalsgaard, J. Henning., R, et al., (1999), Helioseismic Constraints on the Structure of the Solar Tachocline, The Astrophysical Journal, 527:445-460.

Charbonneau, P., (2010), Dynamo Models of the Solar Cycle, Living Review Solar Physics, 7, 3.

Charbonneau, P., (2014), Solar Dynamo Theory, The Annual Review of Astronomy and Astrophysics, 2014. 52:251–90.

Charbonneau, P., (2020), Dynamo Models of the Solar Cycle, Living Review Solar Physics, 17, 4.

Charvatova, I., (2000), Can origin of the 2400-year cycle of solar activity be caused by solar inertial motion? Annales Geophysicae 18, 399 - 405.

Cheng, W., J. C. H. Chiang, and D. Zhang, (2013), Atlantic meridional overturning circulation (AMOC) in CMIP5 models: RCP and historical simulations, Journal of Climate, 26, 7187–7197.

Christensen, T. R., Ekberg, A., and Strom, L., (2003), Factors controlling large scale variations in methane emissions from wetlands. Geophysical Research Letters, 30.

Christensen-Dalsgaard, J. (2002), Helioseismology, Review of Modern Physics 74, 1073

Clark, P. U., et al., (2002), The role of the thermohaline circulation in abrupt climate change, Nature, 415, 863-869.

Clark, P. U., McCabe, A. M., Mix, A. C. and Weaver, A. J., (2004), Rapid Rise of Sea Level 19,000 Years Ago and Its Global Implications, Science, Vol 304, May.

Clark, P. U., Hostetler, S. W. Pisias, N. G. Schmittner, A. and Meissner, K. J. (2007), Mechanisms for an ~7-kyr climate and sea-level oscillation during marine isotope stage 3, in *Ocean Circulation: Mechanisms and Impacts – Past and Future Changes of Meridional Overturning*, edited by A. Schmittner, J. C. H. Chiang, and S. R. Hemming, pp. 209–246, AGU, Washington, D. C.

Cline, E. H., (2014), 1177 B.C.: the year civilization collapsed. Princeton: Princeton University Press; 2014.

Cliver, E.W. & Svalgaard, L., (2004), Solar Phys. 224, 407, doi:10.1007/s11207-005-4980-z.

Crawford, D., (2007), Deadly Companions How Microbes Shaped Our History Dec.2007, Oxford University Press USA.

Cutler, K.B., et al., 2003: Rapid sea-level fall and deep-ocean temperature change since the last interglacial period, Earth Planet. Sci. Lett., 206, 253–271.

Dahl-Jensen, D., (2018), Drilling for the oldest ice, Nature Geoscience 11, 703–704.

Dansgaard W, Johnsen SJ, Clausen HB, Dahl-Jensen D, Gundestrup NS, et al. 1993. Evidence for general instability of past climate from a 250-kyr ice-core record. Nature 364:218–20.

de Abreu, Lucia; Shackleton, Nicholas J; Schönfeld, Joachim; Hall, Michael A; Chapman, Mark R (2003): Planktonic foraminifera, stable isotope record and temperature reconstruction of sediment core MD95-2040. PANGAEA, https://doi.org/10.1594/ PANGAEA.66811.

Deaney, E. L. Barker, S., van de Flierd, T., (2017), Timing and nature of AMOC recovery across Termination 2 and magnitude of deglacial CO_2 change, Nature Communication, 8, 14595.

deMenocal, P., Ortiz, J., Guilderson T., Adkins, J., Sarnthein, M., Baker, L., Yarusinsky, M., (2000) Abrupt onset and termination of the African Humid Period: rapid climate responses to gradual insolation forcing, Quaternary Science Reviews 19 347-361.

deMenocal, P. B., (2004), African climate change and faunal evolution during the Pliocene-Pleistocene, Earth and Planetary Science Letters, 220, 3-24.

Denton, G.H., Broecker, W.S., Alley, R.B., (2006), The mystery interval 17.5 to 14.5 kyrs ago. PAGES News 14, 14-16.

Deplazes, G, Lückge, A., Peterson, L. C., et al., (2013), Links between tropical rainfall and North Atlantic climate during the last glacial period, Nature Geoscience, 6(3), 213-217.

Deplazes, G., Lückge, A., Stuut, J.-B. W. et al., (2014), Weakening and strengthening of the Indian monsoon during Heinrich events and Dansgaard-Oeschger oscillations, Paleoceanography, 29, 99–114.

de Winter N. J. Goderis, S., Van Malderen, S. J. M., Sinnesael, M., et al., (2020), Subdaily-Scale Chemical Variability in a Torreites Sanchezi Rudist Shell: Implications for Rudist Paleobiology and the Cretaceous Day-Night Cycle, Paleoceanography and Paleoclimatology, 35, 2.

Dijkstra, H. A., & Weijer, W., (2005), Stability of the global ocean circulation: Basic bifurcation diagrams, Journal of Physical Oceanography, 35, 933–948.

Donati J.-F., Landstreet J. D., (2009), Magnetic Fields of Nondegenerate Stars Annual Review of Astronomy and Astrophysics Vol. 47:333-370.

Dowdeswell, J. A., Maslin, M. A., Andrews, J. T., and McCave, I. N., (1995), Iceberg production, debris rafting, and the extent and thickness of Heinrich layers (H1,H2) in North Atlantic sediments: Geology, v. 23, p. 301–304.

EASAC policy report, A sea of change: Europe's future in the Atlantic realm, Eldevik, T., Beckers, J-M., Hansen, B., Uotila, P., Duplessy, J-C., et al., (2021), EASAC Secretariat, Deutsche Akademie der Naturforscher Leopoldina, 45 p. (EASAC policy report; nro 42).

Eddy, J. A., (1976), The Maunder Minimum, Science Vol. 192, 1189.

Edvardsson, J., (2013) Holocene climate change and peatland dynamics in southern Sweden based on tree-ring analysis of subfossil wood from peat deposits Department of Geology, Lund Univ.. p 19.

Elliott & Gough 1999, Calibration of the Thickness of the Solar Tachocline, The Astrophysical Journal. 516, 475.

Feng, F., Bailer-Jones, C. A. L., (2015), Obliquity and precession as pacemakers of Pleistocene deglaciations, Quaternary Science Reviews, May 2015, p. 1-20.

Feulner, G., and S. Rahmstorf (2010), On the effect of a new grand minimum of solar activity on the future climate on Earth, Geophysical Research Letters, 37, L05707.

Finne, Â. M., Holmgren, K., Shen, C.-C., Hu, H.-M., Boyd, M., Stocker, S., (2017), Late Bronze Age climate change and the destruction of the Mycenaean Palace of Nestor at Pylos, PLoS ONE 12(12):e0189447.

Fleitmann, D., Burns, S. J., Mangini, A., Mudelsee, M.. et al., (2007), Holocene ITCZ and Indian monsoon dynamics recorded in stalagmites from Oman and Yemen (Socotra), Quaternary Science Reviews, 26, 170–188.

Flückiger, J., R. Knutti, and J. W. C. White (2006), Oceanic processes as potential trigger and amplifying mechanisms for Heinrich events, Paleoceanography, 21, PA2014.

Frajka-Williams, E., Beaulieu, C. & Duchez, A., (2017), Emerging negative Atlantic Multidecadal Oscillation index in spite of warm subtropics. Nature, Scientific Reports, 7, 11224.

Galaasen, E. V., Ninnemann, U. S., Irvalı N. et al., (2014), Rapid reductions in North Atlantic Deep Water during the peak of the last interglacial period. Science 343, 1129–1132.

Gebregiorgis, D., Clemens, S.C., Hathorne, E. C., Giosan, L., et al., (2020), A Brief Commentary on the Interpretation of Chinese Speleothem $\delta^{18}O$ Records as Summer Monsoon Intensity Tracers, Quaternary, 3, 7.

Giaccio, B., Regattieri, E., Zanchetta, G. et al., (2015), Duration and dynamics of the best orbital analogue to the present interglacial, Geology, 43 (7): 603–606.

Gordon, A. L., Visbeck, M., Comiso, J. C., (2007), A Possible Link between the Weddell Polynya and the Southern Annular Mode, Journal of Climate, 20, 2558–2571.

Govin, A., Braconnot, P., Capron, E. et al., (2012), Persistent influence of ice sheet melting on high northern latitude, climate during the early Last Interglacial, Climate of the Past, 8, 483–507.

Grant, K. M.,Rohling, E. J., Westerhold, T., Zabel, M., et al., (2017), A 3 million year index for North African humidity/aridity and the implication of potential pan-African Humid periods, Quaternary Science Reviews, Vol. 171, 100-118.

Gray, L. J., et al. (2010), Solar influences on climate, Rev. Geophys., 48, RG4001.

Green, J. L., Boardsen, S., Odenwald, S., Humble, J. and Pazamickas, K A., (2006), Eyewitness reports of the great auroral storm of 1859, Advances in Space Research, 38, 145–154.

Grootes, P. M., Stuiver, M., (1999), GISP2 Oxygen Isotope Data. PANGAEA, https://doi.org/10.1594/PANGAEA.56094.

Grousset, F., Labeyrie, L., Sinko, J. et al., (1993), Patterns of Ice-Rafted Detritus in the Glacial North Atlantic (40-55°N), Paleoceanography, American Geophysical Union, 8 (2), pp.175-192.

Gunnarson, B. E., (2008), Temporal distribution pattern of subfossil pines in central Sweden: perspective on Holocene humidity fluctuations, The Holocene 18, 69-77.

Haigh, J. D., (2007), The Sun and the Earth's Climate, Living Reviews, Solar Physics, 4, 2.

Hanslmeier, A. and Brajša, R., (2010), The chaotic solar cycle I. Analysis of cosmogenic ^{14}C-data, Astronomy & Astrophysics, 509, A5.

Haug, G. H., Hughen, K. A., Peterson, L. C. et al. (2001). Southward migration of the Intertropical Convergence Zone through the Holocene. Science, 293, 1304–1308.

Hayes, C. T., Martínez-García, A., Hasenfratz, A. P., et al., (2014), A stagnation event in the deep South Atlantic during the last interglacial period, Science, 346, 1514–1517.

Head, M. J., (2021), Review of the Early–Middle Pleistocene boundary and Marine Isotope Stage 19, Progress in Earth and Planetary Science, 8:50.

Hearty, P. J., Hollin, J. T., Neumann, A. C., et al., (2007), Global sea-level fluctuations during the Last Interglaciation (MIS 5e), Quaternary Science Review, 26, 2090–2112.

Heinrich, H., (1988), Origin and consequences of cyclic ice rafting in the Northeast Atlantic Ocean during the past 130,000 years, Quaternary Research, 29 (2):142-152 March.

Hemming, S. R., (2004), Heinrich events: Massive late Pleistocene detritus layers of the North Atlantic and their global climate imprint, Rev. Geophys., 42, RG1005.

Henry, L. G., McManus, J. F., Curry, W. B., Roberts, N. L, Piotrowski, A. M. and Keigwin. L. D., (2016), North Atlantic ocean circulation and abrupt climate change during the last glaciation. Science.

Hillaire-Marcel, C., de Vernal, A., Bilodeau, G. and Weaver, A. J., (2001), Absence of deep-water formation in the Labrador Sea during the last interglacial period. Nature, 410, 1073-1077.

Hinnov, L. and Ogg, J. G., (2007). Cyclostratigraphy and the Astronomical Time Scale, Beyond the GSSP: New Developments in Chronostratigraphy, Stratigraphy 4 (2-3): 239-251.

Hodell, D. A., Channell, J. E. T., Curtis, J. H., et al., (2008), Onset of ''Hudson Strait'' Heinrich events in the eastern North Atlantic at the end of the middle Pleistocene transition (~640 ka)?, Paleoceanography, 23, PA4218.

Hodell, D. A., Minth, E. K., Curtis, J. H., et al. (2009), Surface and deep-water hydrography on Gardar Drift (Iceland Basin) during the last interglacial period, Earth Planetary Science Letters, 288, 10–19.

Hoffman, P. F., Kaufman, A. J., Halverson, G. P., & Schrag, D. P., (1998), A Neoproterozoic Snowball Earth, Science, 281(5381), 1342-1346.

Hoffman, P. F., & Schrag, D. P., (2002), The snowball Earth hypothesis: testing the limits of global change, Terra Nova, 14(3), 129-155.

Howe, R., (2009), Solar Interior Rotation and its Variation, Living Review Solar Physics, 6, 1.

Hoyt, D.V, Schatten, (1997), Role of the Sun in Climate Change, Oxford Univ. Press, (1997).

Hu, A., Meehl, G. A., Han, W., and Yin, J., (2011), Effect of the potential melting of the Greenland ice sheet on the meridional overturning circulation and global climate in the future, Deep-Sea Research II, 58, 1914–1926.

Imbrie, J., et al., (1993), On the structure and origin of major glaciation cycles ii. the 100,000–year cycle, Paleoceanography, 8, 699–735.

Irvali, N., et al., (2012), Rapid switches in subpolar North Atlantic hydrography and climate during the Last Interglacial (MIS 5e), Paleoceanography, Vol. 27, PA2207.

Irvalı N., Ninnemann, U. S., Kleiven, H. F. et al., (2016), Evidence for regional cooling, frontal advances, and East Greenland Ice Sheet changes during the demise of the last interglacial, Quaternary Science Reviews, 150, 184-199.

Jansen, E. J., et al., (2007), The Fourth Assessment Report of the IPCC, Cambridge University Press, Cambridge, United Kingdom and New York, NY, USA. *In 6.5.1.6 Are There Long-Term Modes of Climate Variability Identified During the Holocene that Could Be Involved in the Observed Current Warming? p. 463*.

Johnsen, S.J., Clausen, H.B., Dansgaard, W., Gundestrup, N.S., Hammer, C.U, Andersen, U., Andersen, K.K., Hvidberg, C.S., Dahl-Jensen, D., Steffensen, J.P., Shoji, H., Sveinbjrnsd'uttir, A.E., White, J.W.C., Jouzel, J., Fisher, D., (1997). The d18O record along the Greenland Ice Core Project deep ice core and the problem of possible Eemian climatic instability. Journal of Geophysical Research 102 (C12), 26397–26410.

Johnsen, S. J., (1999), GRIP Oxygen Isotopes. PANGAEA, doi.org/10.1594/PANGAEA.55091.

Johnson H.L. et al., (2019), Recent contributions of theory to our understanding of the Atlantic Meridional Overturning Circulation. Journal of Geophysical Research: Oceans 12 (8), 5376–5399.

Jouzel, J., Masson-Delmotte, V., (2007): EPICA Dome C Ice Core 800KYr deuterium data and temperature estimates, PANGAEA, https://doi,org/10,1594/PANGAEA,683655.

Jullien, E, Grousset, F., E., Hemming, S. R., Peck, V. L., Hall, I. R., Jeantet, C., Billy, I., (2006), Contrasting conditions preceding MIS3 and MIS2 Heinrich events, Global and Planetary Change 54 225–238.

Kaniewski D, Paulissen E, Van Campo E, Weiss H, et al., (2010), Late second-early first millennium BC abrupt climate changes in coastal Syria and their possible significance for the history of the Eastern Mediterranean. Quaternary Research, 74, 207-215.

Kaniewski, D., Van Campo, E., Weiss, H., (2012), Drought is a recurring challenge in the Middle East, Proceedings of the National Academy of Sciences, 109 (10), 3862-3867.

Kaniewski D, Van Campo E, Guiot J, Le Burel S, Otto T, Baeteman C., (2013), Environmental Roots of the Late Bronze Age Crisis, PLoS ONE 8(8): e71004.

Kataoka, R., Ebisuzaki, T., Miyahara, H.,, Maruyama, S., (2013), Snowball Earth events driven by starbursts of the Milky Way Galaxy, New Astronomy, 21 50–62.

Kathayat, G., Cheng, H., Sinha, A. et al., (2016), Indian monsoon variability on millennial-orbital timescales. Sci Rep 6, 24374.

Kilian, M.R., Van Der Plicht, J., Van Geel, B., & Geel, B. V., (1995), Dating raised bogs: New aspects of AMS C-14 wiggle matching, a reservoir effect and climatic change. Quaternary Science Reviews, 14(10), 959-966.

Knapp, A. B., Manning, S. W., (2016), Crisis in Context: The End of the Late Bronze Age in the Eastern Mediterranean, American Journal of Archaeology, 120, 1, 99–149.

Kosovichev A.G., (1996), Astrophysical Journal. 469, L61.

Koutavas, A., and Joanides, S., (2012), El Niño–Southern Oscillation extrema in the Holocene and Last Glacial Maximum, ,Paleoceanography, Vol 27, 4, PA4208.

Kuhlbrodt, T., A. Griesel, M. Montoya, A. Levermann, M. Hofmann, and S. Rahmstorf (2007), On the driving processes of the Atlantic meridional overturning circulation, Rev. Geophys., 45, RG2001.

Käpylä, P. J., Mantere, M. J., Cole, E., Warnecke, J., and Brandenburg, A., (2013), Effects of enhanced stratification on Equatorward Dynamo Wave Propagations, Astrophysical Journal, 778:41 (18pp), 2013 November 20.

Käpylä, M. J., Käpylä, P. J., Olspert, N., Brandenburg, A., Warnecke, J., Karak ,B. B. and Pelt, J., (2016), Multiple dynamo modes as a mechanism for long-term solar activity variations, Astronomy and Astrophysics, Vol 589 A56.

Larrasoaña J, C., Roberts, A. P., Rohling, E. J., (2013), Dynamics of Green Sahara Periods and Their Role in Hominin Evolution, PLoS ONE, 8(10): e76514.

Laskar J., Robutel, P., Joutel, F., et al., (2004), A long-term numerical solution for the insolation quantities of the Earth. Astronomy and Astrophysics, 428: 261-285.

Laskar, J., Fienga, A., Gastineau, M., and Manch, H., (2011), La2010: a new orbital solution for the long-term motion of the Earth, Astronomy and Astrophysics 532, A89.

Lauterbach, S., Andersen, N., Wang, Y. V., et al., (2020), An ~130 kyr record of surface water temperature and $\delta^{18}O$ from the northern Bay of Bengal: Investigating the linkage between Heinrich events and Weak Monsoon Intervals in Asia, Paleoceanography and Paleoclimatology, 35, e2019PA003646.

Levermann, A., Griesel, A., Hofmann, M., Montoya, M., & Rahmstorf, S. (2005). Dynamic sea level changes following changes in the thermohaline circulation. Climate Dynamics, 24(4), 347–354.

Li, C., (2010), Can North Atlantic Sea Ice Anomalies Account for Dansgaard–Oeschger Climate Signals?, American Meteorological Society, https://doi.org/ 10.1175/ 2010JCLI3409.1.

Lima, M. Climate change and the population collapse during the 'Great Famine' in preindustrial Europe. Ecol. Evol. 4, 284–291 (2014).

Little, C. M., Hu, A., Hughes, C. W., McCarthy, G. D., Piecuch, C. G., Ponte,R. M., & Thomas, M. D., (2019), The Relationship between U.S. East Coast sea level and the Atlantic Meridional Overturning Circulation: A review. Journal of Geophysical Research: Oceans, 124, 6435–6458.

Lisiecki, L. E., and M. E. Raymo, (2005), A Pliocene-Pleistocene stack of 57 globally distributed benthic delta O-18 records, Paleoceanography, 20.

Lisiecki, L. E., et al., (2021), Age models for ten Iberian Margin sediment cores during the last glacial cycle (0-150 ka BP). PANGAEA.

LISIRD (LASP Interactive Solar Irradiance Datacenter) data/image, Colorado, USA.

Lockwood, M. (2001a), Long-term variations in the magnetic fields of the Sun and the heliosphere: Their origin, effects and implications, Journal of Geophysical Research 106, 16,021–16,038

Lockwood, M., Foster, S.S., and Stamper, R. (2006), The Use of Cosmogenic Isotopes as an Indicator of Total Solar Irradiance in Paleoclimate Research, Annales Geophys.

Lockwood, M., (2010), Solar change and climate: an update in the light of the current exceptional solar minimum, Proceedings of the Royal Society (A), 466, 303-329.

Loulergue, L., A. Schilt, R. Spahni, V. Masson-Delmotte, T. Blunier, B. et al., (2008), Orbital and millennial-scale features of atmospheric CH_4 over the past 800,000 years. Nature, Vol. 453, pp. 383-386.

Loutre, M. F. & Berger, A. Future climatic changes: are we entering an exceptionally long interglacial? Climatic Change 46, 61–90 (2000).

Lucas, H. S., (1930), 'The Great European Famine of 1315-7', Speculum 5:4, 343-377.

Lüdecke, H.-J., Weiss, C. O. and Hempelmann, A., (2015), Paleoclimate forcing by the solar De Vries/Suess cycle, Climate of the Past Discussion, 11, 279–305.

MacDonald, G., (2011), Potential influence of the Pacific Ocean on the Indian summer monsoon and Harappan decline, Quaternary International, 229: 140-148.

Manabe, S., and R. J. Stouffer, (1994), Multiple-century response of a coupled ocean-atmosphere model to an increase of atmospheric carbon dioxide, J. Clim., 7, 5–23.

Manley, G. (1974). Central England temperatures: monthly means 1659 to 1973. Quarterly Journal of the Royal Meteorological Society 100: 389–405.

Marcott, S. A., Peter, U. C., Padman, L et al., (2011), Ice-shelf collapse from subsurface warming as a trigger for Heinrich events, PNAS, vol. 108, 33, 13415–13419.

Martin-Puertas, C. K., (2012), Regional atmospheric circulation shifts induced by a grand solar minimum, Nature Geosci., 5, 397–401.

Martinez, M., and Dera, G., (2015), Orbital pacing of carbon fluxes by a ∼9-My eccentricity cycle during the Mesozoic, PNAS, 112, 41.

Martrat, B. et al., (2007), Four climatic cycles of recurring deep and surface waterdestabilizations on the Iberian Margin. Science 317, 502–507.

Marzin, C, Kallel, N, Kageyama, M, Duplessy, J.-C. and Braconnot, P., (2013), Glacial fluctuations of the Indian monsoon and their relationship with North Atlantic climate: new data and modelling experiments, Climate of the Past, 9, 2135–2151.

Masarik, J. and Beer, J., (1999), Simulation of particle fluxes and cosmogenic nuclide production in the Earth's atmosphere, Journal of Geophysical Research -Atmosphere, 104, 12099–12111.

Masarik, J. and Beer, J., (2009), An updated simulation of particle fluxes and cosmogenic nuclide production in the Earth's atmosphere, Journal of Geophysical Research, 114, D11103.

Maslin, M. A., (1995), Changes in North Atlantic Deep-Water Formation Associated with the Heinrich Events, Naturwissenschaften 82, 330-333, Springer-Verlag.

Mauquoy., D., van Geel, B., Blaauw, M., Speranza, A., and van der Plicht, J., (2004), Changes in solar activity and Holocene climatic shifts derived from ^{14}C wiggle-match dated peat deposits, The Holocene 14,1, pp. 45–52.

McGee, D., deMenocal, P.B, Winckler, G.,.Stuut, J.B.W, Bradtmiller, L.I., (2013), The magnitude, timing and abruptness of changes in North African dust deposition over the last 20,000 yr, Earth and Planetary Science Letters 371–372, 163–176.

McCracken, K. G. (2004a), Geomagnetic and atmospheric effects upon the cosmogenic ^{10}Be observed in polar ice, J. Geophysical Research., 109, A04101.

McCracken, K. G., and Beer, J., (2007), Long-term changes in the cosmic ray intensity at Earth, 1428–2005, Journal of Geophysical Research: Space Physics, Vol 112, A10.

McPhaden, M. J., S. Zebiak, and N. H. Glantz, (2006), ENSO as an integrating concept in Earth Science, Science, 314, 1740–1745.

Meehl, G: A., Arblaster, J. M., and Marsh, D. R., (2013), Could a future 'Grand Solar Minimum' like the Maunder Minimum stop global warming?, Geophysical Research Letters, Vol. 40, 1789–1793.

Meese, D. A., Gow, A. J. Alley, R. B. Zielinski G. A., Grootes, P. M. Ram, M. Taylor,K. C. Mayewski, P. A. and Bolzan, J. F., (1997), The Greenland Ice Sheet Project 2 depth-age scale: Methods and results, Journal of Geophysical Research, 102(C12), 26, 411–26,423.

Mekhaldi, F., Czymzik, M., Adolphi, F., Sjolte J., Björck, S., et al., (2020), Radionuclide wiggle matching reveals a nonsynchronous early Holocene climate oscillation in Greenland and western Europe around a grand solar minimum, Climate of the Past, 16, 1145–1157.

Miesch, M. S., (2012) Solar dynamo, Philosophical Transactions of Royal Society A, 370, 3049–3069.

Milankovitch, M., (1941), Canon of insolation and the ice-age problem, R. Serb. Acad. Spec. Publ., 132.

Moat, B. I., Smeed, D. A., Frajka-Williams, E., Desbruyères, D. G., etal., (2020), Pending recovery in the strength of the meridional overturning circulation at 26° N, Ocean Science, 16, 863–874.

Moros, M., Andrews, J. T., Eberl, D. D. and Jansen, E., (2006), Holocene history of drift ice in the northern North Atlantic: Evidence for different spatial and temporal modes, Paleoceanography, 21, PA2017.

Moy, C. M., et al., (2002), Laguna Pallcacocha Sediment Color Intensity Data, IGBP PAGES/World Data Center for Paleoclimatology Data Contribution Series #2002-76. NOAA/NCDC Paleoclimatology Program, Boulder CO, USA.

Msadek, R., Johns, W. E., et al., (2013), The Atlantic Meridional Heat Transport at 26.5°N and Its Relationship with the MOC in the RAPID Array and the GFDL and NCAR Coupled Models, Journal of Climate, Vol 12, 26. 4335–4356.

Muscheler, R., Joos, F., Beer, J., Müller, S.A., Vonmoos, M., et al., (2007), Solar activity during the last 1000 yr inferred from radionuclide records. Quat. Sci. Rev., 26, 82–97.

Muscheler, R., Kromer, B., Björck, S., Svensson, A., Friedrich, M., Kaiser, K. F. & Southon, J., (2008), Tree rings and ice cores reveal ^{14}C calibration uncertainties during the Younger Dryas, Nature Geoscience 1, 263–267.

Muscheler, R., Mekhaldi, F., Adolphi, F., Aldahan, A., Beer, J., McConnell, J. R, Possnert, G., Sigl M., Svensson, A., Synal, H.-A., Welten, K.C. & Woodruff, T. E., (2015), Multiradionuclide evidence for the solar origin of the cosmic-ray events of AD 774/5 and 993/4, Nature Communications.

Muscheler, R., Adolphi, F., Herbst, K. and Nilsson, A., (2016), The Revised Sunspot Record in Comparison to Cosmogenic Radionuclide-Based Solar, Solar Physics, 291:3025–3043.

Nerem, R. S, Chambers D. P, Choe C., Mitchum G. T., (2010), Estimating mean sea level change from the TOPEX and Jason altimeter missions. Mar Geod 33(Suppl 1):435–446.

Nerem, R. S. et al., (2018), Climate-change–driven accelerated sea-level rise detected in the altimeter era. Proc. Natl. Acad. Sci. U.S.A. 115, 2022–2025.

Ng, H. C., Robinson, L. F., McManus, J. F., Mohamed, K. J., et al. (2018). Coherent deglacial changes in western Atlantic Ocean circulation. Nature Communications, 9, 2947.

NGRIP members, (2004), High-resolution record of Northern Hemisphere climate extending into the last interglacial period, Nature, 2805 -10/8/2004.

Niebler, H.-S., Arz, H. W., Donner, B., et al., (2003), Sea surface temperatures in the equatorial and South Atlantic Ocean during the Last Glacial Maximum (23–19 ka), PALEOCEANOGRAPHY, VOL. 18, 3, 1069.

North Greenland Ice Core Project, (2004), Oxygen Isotope Data. IGBP PAGES/World Data Center for Paleoclimatology, Data Contribution Series #2004-059. NOAA/NGDC Paleoclimatology Program, Boulder CO, USA.

Obrochta, S. P., Miyahara H., Yokoyama Y., Crowley T., (2012), A re-examination of evidence for the North Atlantic "1500-year cycle" at Site 609, Quaternary Science Reviews, Vol. 55, Pages 23-33.

Obrochta, S. P., Crowley, T. J., Channell, J. E.T., Hodell, D. A., et al., (2014), Climate variability and ice-sheet dynamics during the last three glaciations, Earth and Planetary Science Letters 406 198–212.

Oppo, D. W., McManus, J. F., Cullen, J. L., (2006), Planktonic foraminifera and stable isotope record of ODP Site 162-980, PANGAEA.

Ossendrijver, M., (2003), The Solar Dynamo, The Astronomy and Astrophysics Review, 11: 287–367.

PAGES, Past Interglacials Working Group of, (2016), Interglacials of the last 800,000 years, Rev. Geophys., 54, 162–219.

Parker, E. N., (1958), Dynamics of the Interplanetary Gas and Magnetic Fields, Astrophysical Journal, vol. 128, p.664.

Paterne, M., Kalle, N., Labeyrie, L., et al., (1999), Hydrological relationship between the North Atlantic Ocean and the Mediterranean Sea during the past 15-75 kyr, Paleoceanography, 14(5), 626-638.

Pausata, F. S. R., Gaetani, M., Messori, G. et al., (2020), The Greening of the Sahara: Past Changes and Future Implications, One Earth, 2.

Peck, V. L., Hall I.R., Zahn, R., Grousset F., Hemming, S.R., Scourse, J.D., (2007) The relationship of Heinrich events and their European precursors over the past 60 ka BP: a multi proxy ice-rafted debris provenance study in the North East Atlantic, Quaternary Science Reviews. 26 862–875.

Pedro, J. B., van Ommen, T. D., Rasmussen, S. O., Morgan, V. I., Chappellaz, J. Moy, A. D., Masson-Delmotte, V. and Delmotte, M., (2011), The last deglaciation: timing the bipolar seesaw, Climate of the Past, 7, 671–683.

Pedro, J. B., Jochum, M., Buizert, C., He, F., Barker S., Rasmussen, S. O., (2018), Beyond the bipolar seesaw: Toward a process understanding of interhemispheric coupling, Quaternary Science Reviews, 192, 27–46.

Peeters, F. J. C., Acheson, R., Brummer, G. J. A., et al., (2004), Vigorous exchange between the Indian and Atlantic ocean at the end of the past five glacial periods, Nature, 430(7000), 661–665.

Pena, L. D., Goldstein, S. L., (2014), Thermohaline circulation crisis and impacts during the mid-Pleistocene transition, Paleoceanography, Vol. 345, 6194.

Penn, M. J. and Livingston, W., (2010), Long-term Evolution of Sunspot Magnetic Fields, IAU Symposium No. 273.

Peristykh, A. N., Damon, P. E., (2003), Persistence of the Gleissberg 88-year solar cycle over the last ~12,000 years: Evidence from cosmogenic isotopes, Journal of Geophysical Research, VOL. 108, NO. A1, 1003.

Petrenko, V. V., Smith A. M., Schaefer, H. et al., (2017), Minimal geological methane emissions during the Younger Dryas–Preboreal abrupt warming event, Nature, 548, pages 443–446.

Pälike, H., Norris, R. D., Herrle, J. O., et al., (2006), The heartbeat of the Oligocene climate system. Science 314, 1894–1898.

Rahmstorf, S. (1996), On the freshwater forcing and transport of the Atlantic thermohaline circulation, Climate Dynamics, 12, 799–811.

Rahmstorf, S., (2002), Ocean circulation and climate during the past 120,000 years, Nature, 419, 207–214.

Rahmstorf, S., (2003), Timing of abrupt climate change: a precise clock, Geophysical Research Letters, Vol. 30, No. 10, 1510.

Rahmstorf, S., (2006), Thermohaline Ocean Circulation. In: Encyclopedia of Quaternary Sciences, Edited by S. A. Elias. Elsevier, Amsterdam 2006.

Rahmstorf, S., Hoffman, M., (2009), On the stability of the Atlantic meridionaloverturning circulation, PNAS, doi 10.1073 pnas.0909146106.

Raisbeck, G. M., Cauquoin, A., Jouzel, J., et al., (2017), An improved north-south synchronization of ice core records around the 41 kyr ^{10}Be peak, Climate of the Past, 13, 217–229.

Rasmussen, T. L., D. W. Oppo, E. Thomsen, and S. J. Lehman, (2003), Deep sea records from the southeast Labrador Sea: Ocean circulation changes and ice-rafting events during the last 160,000 years, Paleoceanography, 18(1), 1018.

Rasmussen, S. O., Seierstad, 1, I. K., Andersen, K. K., Bigler, M., Dahl-Jensen, D., Johnsen, S. J., (2007), Synchronization of the NGRIP, GRIP, and GISP2 ice cores across MIS 2 and palaeoclimatic implications, Quaternary Science Reviews.

Regattieri, E., Giaccio, B., et al., (2019), Frequency and dynamics of millennial-scale variability during Marine Isotope Stage 19: Insights from the Sulmona Basin (central Italy), Quaternary Science Reviews, Vol 214, 28-43.

Rein, B., A. Lückge, L. Reinhardt, F. et al., (2005), El Niño variability off Peru during the last 20,000 years, Paleoceanography, 20, PA4003.

Reiners, A., (2012), Observations of Cool-Star Magnetic Fields, Living Reviews in Solar Physics, 9, 1.

Renold, M., C. C. Raible, M. Yoshimori, and T. F. Stocker, (2009), Simulated resumption of the North Atlantic meridional overturning circulation –Slow basin-wide advection and abrupt local convection, Quaternary Science Reviews ,29(1), 101–112.

Ribes, J.C., Nesme-Ribes, E., (1993), The solar sunspot cycle in the Maunder minimum AD1645 to AD1715, Astronumy and Astrophysics, 276, 549–563.

Rohling, E.J., Hibbert, F.D., Grant, K.M. et al., (2019), Asynchronous Antarctic and Greenland ice-volume contributions to the last interglacial sea-level highstand, Nature Communicationa, 10:5040

Ruddiman, W.F., (1977), Late Quaternary deposition of ice-rafted sand in the sub-polar North Atlantic (40–65N). Geological Society of America Bulletin 88, 1821–1831.

Sarnthein, M., Jansen, E., Weinelt, M., Arnold, M., Duplessy, J. C., et al., (1995), Variations in Atlantic surface ocean paleoceanography, 50°–80°N—A time-slice record of the last 30,000 years. Paleoceanography 10:1063–94.

Sánchez Goñi, M. F., Desprat, E., Fletcher, W. J., Morales-Molino, C., Naughton, F., Dulce Oliveira, D., Urrego, D. H. and Zorzi, C., (2018), Pollen from the Deep-Sea: A Breakthrough in the Mystery of the Ice Ages, Frontiers in Planet Science, 9:38.

Scafletta, N., (2014), The complex planetary synchronization structure of the solar system, Pattern Recogn. Phys., 2, 1–19.

Schou, J., Bogart, R.S., (1998), Astrophysical Journal, 504, L131.

Schrijver C. J. and Siscoe G. L., (2010), Heliophysics – Evolving Solar Activity and the Climates of Space and Earth, Cambridge University Press (New York).

Schulz, H., von Rad, U. & Erlenkeuser, H., (1998), Correlation between Arabian Sea and Greenland climate oscillations in past 110,000 years. Nature, 393, 54–57.

Schwabe, A. N., (1844), Sonnen-Beobachtungen im Jahre 1843, Astronomische Nachrichten, 21, 233.

Seidov, D., Sarnthein, M., Stattegger, K., Prien, R., and Weinelt, M., (1996), North Atlantic ocean circulation during the last glacial maximum and subsequent meltwater event: A numerical model: Journal of Geophysical Research, v. 101, p. 16,305–16,332.

Severinghaus, J.P., Sowers, T., Brook, E.J., Alley, R.B., Bender, M.L., (1998), Timing of abrupt climate change at the end of the Younger Dryas interval from thermally fractionated gases in polar ice. Nature 391, 141–146.

Shackleton, N. J., (2000), The 100,000 yr ice-age cycle identified and found to lag temperature, carbon dioxide and orbital eccentricity, Science, 289, 1897–902.

Shackleton, N. J., Hall, M. A. & Vincent, E., (2000), Phase relationships between millennial-scale events 64,000–24,000 years ago. Paleoceanography 15, 565–569.

Shanahan, T. M., McKay, N. P., Hughen, K. A., Overpeck, J. T., Otto-Bliesner, B., Heil, C. W., King, J., Scholz, C. A. and Peck J., (2015), The time-transgressive termination of the African Humid Period, Nature geoscience, Vol 8, Feb.

Shea, M. A., Smart, D. F. (2006), Advanced Space Research. 38(2).

Siddall, M., Rohling, E. J., Thompson, W. G., and Waelbroeck, C., (2008), Marine isotope stage 3 sea level fluctuations: Data synthesis and new outlook, Rev. Geophys., 46, RG4003.

Siegenthaler, U., Stocker, T. F., Monnin, E., et al., (2005), Stable carbon cycle-climate relationship during the late Pleistocene, Science, 310, 1313–1317.

SILSO (Sunspot Index and Long-term Solar Observations) data/image, Royal Observatory of Belgium, Brussels.

Skinner, L. C. & Shackleton, N. J., (2006), Deconstructing terminations I and II: revisiting the glacioeustatic paradigm based on deep-water temperature estimates. Quaternary Science Reviews 25, 3312–3321.

Skonieczny, C., McGee, D., Winckler, G., Bory, A., Bradtmiller, L. I., Kinsley, C. W., Polissar, P. J., De Pol-Holz, R., Rossignol, L., and Malaizé, B., (2019), Monsoon-driven Saharan dust variability over the past 240,000 years, Science Advances, Vol. 5, no. 1.

Solanki, S. K., I. G. Usoskin, B. Kromer, M. Schüssler, and J. Beer (2004), Unusual activity of the Sun during recent decades compared to the previous 11,000 years, Nature, 431, 1084– 1087.

Stanford, J. D., Rohling, E. J., Hunter, S. E., Roberts, A. P., Rasmussen, S. O., Bard, E., McManus, J., and Fairbanks, R. G., (2006), Timing of meltwater pulse 1a and climate responses to meltwater injections, Paleoceanography, Vol. 21, PA4103.

Stanford, J. D, Hemingway, R., Rohling, E.J., Challenor, P.G., Medina-Elizalde, M., and Lester, A.J., (2011), Sea-level probability for the last deglaciation: A statistical analysis of far-field records, Global and Planetary Change, 79, 193-203.

Stanley, S. ,(2017), Ocean dynamics may drive North Atlantic temperature anomalies, Eos, 98, https://doi.org/10.1029/2017EO083253.

Steinhilber, F., Beer, J., Fröhlich, C., (2009), Total solar irradiance during the Holocene, Geophysical Research Letters, 36, L19704.

Steinhilber, F., (2013), Prediction of solar activity for the next 500 years, Journal of geophysical research physics, 118 1861-1867.

Stirling, C.H., Esat, T.M., Lambeck, K., and McCulloch, M.T., (1998), Timing and duration of the last interglacial: evidence for a restricted interval of widespread coral reef growth. Earth Planetary Science Letters, 160, 745–762.

Stouffer, R. J., and S. Manabe, (2003), Equilibrium response of thermohaline circulation to large changes in atmospheric CO_2, Clim. Dyn., 20, 759–773.

Svensmark, J., (2016), The response of clouds and aerosols to cosmic ray decreases, Journal of Geophysical Research: Space Physics, 121(9), 8152–8181.

Svensson, A. Andersen, K K. and Bigler, M. et al., (2008), A 60 000 year Greenland stratigraphic ice core chronology, Climate of the Past, 4, 47–57.

Talley, L. D., (2013). Closure of the global overturning circulation through the Indian, Pacific, and Southern Oceans: Schematics and transports, Oceanography 26(1):80–97.

Thiagarajan, N., Subhas, A. V., Southon, J. R., Eiler, J. M. & Adkins, J. F., (2014), Abrupt pre-Bølling–Allerød warming and circulation changes in the deep ocean, Nature Letter, Vol 511, Jul.

Thomas, M. D., & Fedorov, A. V. (2019). Mechanisms and impacts of a partial AMOC recovery under enhanced freshwater forcing. Geophysical Research Letters, 46.

Thompson, L. G., Davis, M. E., Mosley–Thompson, E. et al., (1998), A 25,000 year tropical climate history from Bolivian ice cores, Science, 282, 1858–1864.

Threnberth K. E., (2005), The Impact of Climate Change and Variability on Heavy Precipitation, Floods, and Droughts, Encyclopedia of Hydrological Sciences. Edited by M. G. Anderson, 2005 John Wiley & Sons, Ltd.

Tierney, J. E., Pausata, F. S. R., deMenocal, P. B., (2017), Rainfall regimes of the Green Sahara, Science Advances, 3, e1601503.

Timmerman, A, Okumura, Y, et al., (2007), The influence of a weakening of the Atlantic meridional overturning circulation on ENSO. Jouranl of Climate, 20:4899–4919.

Toggweiler J. R., Samuels, B., (1993), Is the Magnitude of the Deep Outflow from the Atlantic Ocean Actually Governed by Southern Hemisphere Winds? NATO ASI Series, ed Heimann M (Springer, Berlin), pp 333–366.

Toggweiler J.R., Samuels, B., (1993), New Radiocarbon Constraints on the Upwelling of Abyssal Water to the Ocean's Surface. NATO ASI Series, ed Heimann M (Springer, Berlin), pp 303–331.

Trenberth, K. E., Fasullo, J. & Smith, L., (2005), Trends and variability in column-integrated atmospheric water vapor, Climate Dynamics, 24, 741–758.

Tu, X., Zheng, F., Wang, J., Cai, H., Wang, P., Buhring, C., Sarnthein, M., (2001), An abrupt cooling event early in the Last Interglacial in the northern South China Sea. Science in China, 44 (10), 865–870.

Turney, C. S. M., Jones, R. T., Thomas, Z. A., et al., (2016), Extreme wet conditions coincident with Bronze Age abandonment of upland areas in Britain, Anthropocene, 13, 69-79.

Tzedakis, P. C, (2010), The MIS 11 – MIS 1 analogy, southern European vegetation, atmospheric methane and the 'early anthropogenic hypothesis', Climate of the Past, 6, 131–144.

Tzedakis, P. C., Wolff, E.W., Skinner, L. C., Brovkin, V., Hodell, D. A., McManus, J. F. and Raynaud, D., (2012), Can we predict the duration of an interglacial?, Climate of the Past, 8, 1473–1485

Tzedakis, P. C., Channell, J. E. T., Hodell D. A., et al., (2012b), Determining the natural length of the current interglacial, National Geoscience, 5:138–141.

Tzedakis, P. C., Drysdale, R. N., Margari, V. et al., (2018), Enhanced climate instability in the North Atlantic and southern Europe during the Last Interglacial, Nature Communications, 9, 4235.

Usoskin, I. G., S. K. Solanki, M. Schu¨ssler, K. Mursula, and K. Alanko, (2003), A millennium scale sunspot number reconstruction: Evidence for an unusually active Sun since the 1940's, Phys. Rev. Lett., 92, 211101.

Usoskin, I. G., Solanki , S. K., and Kovaltsov, G. A., (2007), Grand minima and maxima of solar activity: new observational constraints, Astronomy & Astrophysics 471, 301–309.

Usoskin, I. G., (2008), A History of Solar Activity over Millennia, Living Review Solar Physics, 5, 3.

Usoskin, I. G., Kovaltsov, G. A., (2012), Occurrence of extreme solar particle events: Assessment from historical proxy data, The Astrophysical Journal, Volume 757, Number 1.

Usoskin, I. G., Gallet, Y., Lopes F., Kovaltsov, G. A. and Hulot, G., (2016), Solar activity during the Holocene: the Hallstatt cycle and its consequence for grand minima and maxima, Astronomy & Astrophysics, 587, A150.

Van der Plicht, J., van Geel, B., Bohncke, S. J. P., et al., (2004), The Preboreal climate reversal and a subsequent solar-forced climate shift. Journal of Quaternary Science, Vol. 19 pp. 263–269.

Van Nieuwenhove, N., Bauch, H. A., Eynaud, F. et al., (2011), Evidence for delayed poleward expansion of North Atlantic surface waters during the last interglacial (MIS 5e). Quaternary Science Review, 30, 934-946.

Vavrus, S. J., He, F., Kutzbach, J. E., (2018), Glacial Inception in Marine Isotope Stage 19: An Orbital Analog for a Natural Holocene Climate, Scientific Reports, Nature, 8:10213.

Veres, D., Bazin, L., Landais, et al., (2013), The Antarctic ice core chronology (AICC2012): an optimized multi-parameter and multi-site dating approach for the last 120 thousand years. Clim. Past. 9, 1733-1748.

Vieira, L. E., Solanki, S. K., Krivova, N., Usoskin, I., (2011), Evolution of the solar irradiance during the Holocene, Astron. & Astrophys., http://www2,mps,mpg,de/projects/sun-climate/data,html.

Vonmoos, M., Beer, J., Muscheler, R., (2006), Large variations in Holocene solar activity: Constraints from ^{10}Be in the Greenland Ice Core Project ice core, Journal of Geophysical Research, VOL. 111.

Wang, C., and Fiedler, P. C., (2006), ENSO variability and the eastern tropical Pacific: A review, Progress in Oceanography, 69, 239–266.

Wanner H., Solomina, O., Grosjean, M., Ritz, S. P, Jetel, M., (2011), Structure and origin of Holocene cold events, Quaternary Science Reviews xxx 1-15.

Weijer, W., Cheng, W., Drijfhout, S. S., Federov, A.V., Hu, A., Jackson, L. C., et al. (2019). Stability of the Atlantic Meridional Overturning Circulation: A review and synthesis. Journal of Geophysical Research: Oceans, 124.

Weijer, W. Cheng, W., Garuba, O. A., Hu, A., Nadiga, B. T., (2020), CMIP6 Models Predict Significant 21st Century Decline of the Atlantic Meridional Overturning Circulation, Geophysical Research Letters, Vol 47, 12.

Weiss, H. & Bradley, R. S., (2001), What drives societal collapse?, Science, 291, 609–610.

Weiss, H., (2016), Global megadrought, societal collapse and resilience 4.2–3.9 ka BP across the Mediterranean and West Asia. PAGES (Past Global Changes) 24/2:62–63.

Westerhold et al., (2020), An astronomically dated record of Earth's climate and its predictability over the last 66 million years, Science, 369, 1383–1387.

White, B., Curran, H.L., Wilson, M.A., (1998), Bahamian coral reefs yield evidence of a brief sea-level lowstand during the Last Interglacial, Carbonates and Evaporites, 13 (1), 10–22.

Widlansky, M. J., Long, X. & Schloesser, F., (2020), Increase in sea level variability with ocean warming associated with the nonlinear thermal expansion of seawater, Communications Earth & Environment, 1:9.

Wilcox, P. S., Honiat, C., Trüssel, M., (2020), Exceptional warmth and climate instability occurred in the European Alps during the Last Interglacial period, Communications Earth & Environment, 1: 57.

Williamson, M., Collins, M., Drijfhout, S., et al., (2017), Effect of AMOC collapse on ENSO in a high resolution general circulation model, Climate Dynamics, 50, 1–16.

Wunsch, C., (2002), What is the thermohaline circulation?, *Science,* 298, 1179.

Yang, X., Scuderi, L. A., Wang, X., et al., (2015), Groundwater sapping as the cause of irreversible desertification of Hunshandake Sandy Lands, Inner Mongolia, northern China, PNAS, 112 (3) 702-706.

Zachos, J. C., Dickens, G. R., & Zeebe, R. E. (2008), An early Cenozoic perspective on greenhouse warming and carbon-cycle dynamics, Nature, Vol 451, 17, Jan 2008.

Zhang, R. & Delworth, T. L., (2005), Simulated Tropical Response to a Substantial Weakening of the Atlantic, Journal of Climate, Letters, Vol 18, 1853-1860.

Zhang, R. & Delworth, T. L., (2006), Impact of Atlantic Multidecadal Oscillations on India/Sahel rainfall and Atlantic hurricanes. Geophysical Research Letters 33, L17712.

Zhang H., Ait Brahim Y., Li, H., et al., (2019), The Asian Summer Monsoon: Teleconnections and Forcing Mechanisms – A Review from Chinese Speleothem ^{18}O Records, Quaternary, 2, 26.

Zhuravleva, A et al. (2017), Last Interglacial (MIS5e) hydrographic shifts linked to meltwater discharges from the East Greenland margin, Quaternary Science Reviews, 164, 95-109.

Zhuravleva, A, Bauch, H. A., (2018), Last interglacial ocean changes in the Bahamas: climate teleconnections between low and high latitudes, Climate of the Past, 14, 1361–1375.

BIBLIOGRAPHY

Beerling, D, (2007), The Emerald Planet How Plants Changed Earths History, Oxford University Press (New York).

Bigg, G. R., (2003), The Oceans and Climate, 2nd Edition, Cambridge University Press (New York).

Burroughs W. J., (2005), Climate change in prehistory – The End of the Reign of Chaos, Cambridge University Press (New York).

Chaplin, W. J., (2006), Music of the Sun – the Story of Helioseismology, Oneworld Publication Oxford England.

Eldevik, T., Beckers, J-M., Hansen, B., Uotila, P., et al., (eds.) (2021), A sea of change: Europe's future in the Atlantic realm, EASAC Secretariat, Deutsche Akademie der Naturforscher Leopoldina, 45 p. (EASAC policy report; nro 42).

Hoyt, D.V. Schatten, K. H., (1997), Role of the Sun in Climate Change, Oxford University Press (New York).

IPCC, 2007, Climate Change 2007: The Physical Science Basis. Contribution of Working Group I to the Fourth Assessment Report of the Intergovernmental Panel on Climate Change, Cambridge University Press, Cambridge, U.K.; New York, U.S.A.

Schrijver C. J. and Siscoe G. L., (eds.) (2010), Heliophysics – Evolving Solar Activity and the Climates of Space and Earth, Cambridge University Press (New York).

Thompson M. J., Christensen-Dalsgaard J., (2003), Stellar Astrophysical Fluid Dynamics, Cambridge University Press 2003, (New York).

Yokoyama, Y. and Esat, T.M., (2011), Global climate and sea level: Enduring variability and rapid fluctuations over the past 150,000 years. Oceanography 24(2):54–69, doi:10.5670/oceanog.2011.27.

INDEX

100-kyr ‘world’; 7
17.5-kyr loop; 36, 48, 52, 74, 115, 136
17.5-kyr loop, climate; 139–43, 145–48, 159

3.65-kyr cycle; 7–10, 13, 21, 22, 61, 67

41-kyr ‘world’; 17, 164, 165

500-year gap; 38, 148
52.5-kyr loop
  Heinrich events; 126
  Holocene; 146–49
  Tajo; 157–60

7-kyr climate oscillation; 68, 122, 140, 148, 162
7-kyr TSI cycle; 33

8.2 kyr BP cold event; 9, 10, 9–10, 24, 66, 67, 73, 82, 90, 145, 158

African Humid Period; 12, 30, 75, 87, 110, 111
Agulhas; 103, 131
Akkadian Empire; 87
albedo; 106, 144
Allerød; 10, 40, 66, 131
Alps, Italy; 134
AMOC shutdown and recovery; 100, 103, 130, 131, 160
AMOC, three-mode model; 100
Antarctic Bottom Waters; 98
Antarctic Circumpolar Current; 100
Antarctic interglacials (II–V); 128
Arabian Sea; 8, 102
Arctic Circle; 5
Arctic Ocean; 5, 101, 133
astronomical forcing; 16, 21, 160
Atlantic meridional overturning circulation; 96

Aveley; 17, 63, 121, 124

Bahamas; 135
beryllium-10; 23, 28, 29, 30, 43, 44, 82, 124, 126, 127
Beyond EPICA; 13
bipolar seesaw; 67, 103, 117, 120, 127–30, 135, 137, 156, 157, 160
Blue Columns; 11, 12, 15, 19, 63
Blue trendline; 21, 70, 147, 150
Bond cycle; 162
Bray–Hallstatt cycle; 30, 69, 74
bubonic plague; 88
Byrd core; 122
Bølling; 10, 12, 64, 66, 131, 141, 164

carbon dioxide
  AMOC halt; 160
  doubling; 160
  Eemian; 131
  manmade; 115
  partial pressure; 115
carbon-14; 28, 30, 40, 53, 59, 82, 124
Carrington event AD 1859; 43, 68
CET series; 81
Conveyor Belt; 89, 97
cosmogenic isotopes; 28, 30, 82, 126, 141
crop failures; 81, 88

Dalton minimum; 29, 70, 74, 90, 91
Dansgaard–Oeschger events; 66
deep-water cell; 100
DO (8, 12, and 14); 64, 122, 123, 162, 163
DO 0; 141
DO 1; 66, 129, 136, 141
DO 12; 148, 149
DO 14; 148
DO 16; 123
DO 18; 123

DO 3; 86, 145, 164
DO 4; 86, 141, 145
DO 5; 141, 142
Drake Passage; 3
drought; 85–89, 104, 155
dwarf star; 49

early pleistocene
  3.75-kyr cycle; 162
  41-kyr 'world'; 165
  H4 and H5 progenitors; 162
  insolation; 163
  Shackleton site; 161
East Greenland margin; 134
eccentricity; 4–6, 13–15, 48, 77, 110, 121, 165
Eddy's 1-ka cycle; 30
Eemian; 20–22, 121, 123, 124, 131–37
El Niño–Southern Oscillation; 102, 103, 112
EPICA; 2, 13, 156, 164
Eurasian continent; 102
evolution of modules; 37, 38, 40, 46, 51

famine; 81, 88
famous interstadials; 64, 120, 162
Fast Fourier Transformation; 59
foraminifera; 134, 152, 155, 157, 161
  marine organisms; 107
fossil fuels; 115
freezing point; 98
freshwater; 98, 100, 119, 135, 149, 150, 160
functional overlapping; 52

galactic cosmic-ray particles; 28
Galilei, Galileo; 78, 80
GICCO05 timescale; 127
GISP2; 7
glacial termination; 8, 128, 137, 156
Glacial Terminations; 127
Gleissberg 88-yr cycle; 30
grand minimum
  average length; 74
  definition; 74
  hemispheric asymmetry; 81
Great Famine; 88
Greek Dark Ages; 145
Green Sahara Periods; 110
green-house Earth; 1
greenhouse gases; 3, 116, 118
GRIP; 8, 20, 21, 63, 121, 123, 131, 137, 146–48
Gulf Stream; 82, 98

H3/DO 5; 63, 137, 142, 145
Hadley cell; 101
half-lives; 28
heat capacity; 96
Heinrich events
  classification; 41
  Iberian margin; 107
  layer thickness; 105
  layers; 30, 41, 42, 44, 87, 97, 113, 124–27, 149
  Orphan Knoll site; 107
helioseismology; 26
Heliosphere; 28, 82
Holocene
  analogy; 7, 14, 15, 63, 150
  Boreal–Atlantic; 130
  decline rate; 17
  obliquity minimum; 19
  warmest point; 12
  zigzag pattern; 15
Homeric minimum; 23, 24, 52, 82
Homeric module; 31, 32, 35, 40, 44, 45, 58, 162
Hoxnian; 13–17, 63, 151, 156
Hudson Strait; 97, 124, 137

ice-rafting events; 40, 109
Indian Ocean; 101, 103, 143
Indian subcontinent; 102, 104
Intertropical Convergence Zone; 86, 101, 102, 112, 133, 135
IRD comparison; 125
  coral samples; 126

Jupiter; 49, 76, 77, 124

Labrador Sea; 67, 98, 107, 109, 134, 135
Lake Bosumtwi; 110, 111
Laschamp event; 126
Last Glacial Maximum; 10, 66, 112, 118, 122, 135, 137, 144, 145, 146, 164
Late Bronze Age; 24, 25, 61, 67, 83, 84, 85, 87, 89, 91, 92, 148
Late Bronze Age crisis; 85
Laurentide ice sheet; 30, 41, 105
Little Ice Age; 19, 21, 34, 46, 55, 63, 66, 81, 86–91, 93–95, 154, 156

magnetic field
  active region; 27
  fossil; 26
  global; 49
  poloidal; 26
  relic; 77
  toroidal; 26
Marine Isotope Stages; 62
  MIS 1/19; 151
  MIS 11; 7, 13, 151
  MIS 15/19; 151
  MIS 19; 7
  MIS 2; 86, 87
  MIS 3; 64, 84, 120, 146, 158, 165
  MIS 3/19; 157
  MIS 3/40; 164
  MIS 38; 165
  MIS 39; 161
  MIS 4; 165
  MIS 40; 162
  MIS 5; 20, 131
  MIS 6; 124
  MIS 7; 17
  MIS 8; 123, 124–26
Mars; 124
mass balance; 14
Maunder minimum; 38, 59, 71, 77, 79, 81
Medieval Warm Period; 29, 32, 33, 45, 46, 55, 71, 88, 89, 93, 149
megadrought (BC 2200–1900); 87, 89, 155
Mesopotamia; 87
methane; 63, 128, 129, 131, 132, 157, 158
Middle Pleistocene Transition; 4, 7, 13, 15, 156, 164
Milankovitch cycles; 1, 13
Milky Way galaxy; 1
MIS 6; 132
MIS 8
  IRD events; 124
monsoon; 102–4, 111–12, 132
multi-millennial solar cycles
  21st millennium BP; 52
  auto-correcting; 50
  common multiple; 49, 124
  cycle–group systems; 51
  dynamo model; 50
  Heinrich layers; 41
  perturbation waves; 50, 53
  systemic problem; 45
Mystery Interval (17.5 kyr BP); 65, 113, 114

Neo-glacial transition; 37
Neptune; 50, 76
NGRIP; 8, 20, 62, 63, 102, 120, 123, 146–49
Nordic Sea; 67, 98, 100
North Atlantic Deep-Water; 67, 98
North Atlantic Drift; 98

obliquity; 4, 13, 15–19, 64, 67, 123, 144, 146, 150–58, 159, 164, 165
Older Dryas; 10, 53, 141
Oort minimum; 33, 36, 56, 73, 90
orbital cycles; 4
  Milankovitch; 1
  myr cycles; 110
  parameters; 2
  past 800 kyr; 2

orbital period; 49, 50, 124

Pacific Ocean; 98, 101
paleoclimatology, quantitative; 140
parameters for an active star; 49
partial overlapping; 45
planetary interactions; 75
plateau series; 10
Pliocene–Pleistocene stack; 6
Pluto; 49, 76
Portugal; 122, 132, 134, 157, 158, 159, 161
post-Homeric minimum; 23, 24, 75, 77
post-Maunder minimum; 78, 91
power spectrum, carbon-14; 59
Preboreal Oscillation; 13, 93
precession; 3–6, 15, 111, 121, 151
Puerto Rico; 68

radionuclides; 28
Ramses III; 85
Roman times, ancient; 146, 155
Ross Sea; 98, 99, 103
rotation mechanism; 45

s3.5 minimum; 31, 33, 37–38, 61, 62, 64, 73, 112, 130, 157, 158
Schwabe; 1, 30, 177
sea level
  2100; 119
  ice age; 13
  Last Glacial Maximum; 118
  satellite data; 118
Sea Peoples; 85
sea surface temperature, LGM; 113
snowball Earth; 5
solar dynamo; iv, 22, 95
solar particle events; 69
Solar Surge event; 32, 57, 61, 64–67, 75
  28 kyr BP; 86
  52.5-kyr loop; 148
  8th millennium BP; 91
  bipolar seesaw; 118
  bipolar seesaw, MIS 3; 122
  ENSO; 112
  H6 event; 125
  Late Bronze Age; 83
  MIS 8; 123
solar system; 28, 49, 76, 124
solar wind; 27, 30, 81
Southern Ocean; 5, 100–103, 122
Spörer minimum; 29, 58, 88
subfossil tree-ring; 84, 85
Suess–De Vries 208-yr cycle; 30
Sun
  convection zone; iv, 25, 26, 49, 50, 77
  radius; 24
  rotation period; 26
  tachocline; 26, 51, 95
sunspot cycle; 25, 26, 27, 30, 49, 50, 124
sunspot record; 27, 78
Sweden; 84

Tajo; 6, 63, 150–61
thermal equator; 86
thermohaline circulation; 96–100, 124, 130, 159
Total Solar Irradiance; 27, 34
trace gases, global; 131
Trade Winds; 98, 101, 103
triple cluster; 52
TSI-coordinated deglaciations; 151

Weddell Sea; 99, 103
Venezuela; 8, 102
Venus; 124
westerly winds; 3, 99, 100
Wolf minimum; 29, 88

Younger Dryas; 8–12, 16, 39–42, 52–54, 82, 93, 106, 131, 139, 141, 156, 165

LIST OF ABBREVIATIONS

Φ	Solar Modulation function (see Vonmoos et al., 2006)
8.2k	8.2 kyr BP (refers to cold event that began c. 8,400 years ago)
a	year
ACC	Antarctic Circumpolar Current
AD	Anno Domini
AHP	African Humid Period
AMOC	Atlantic meridional overturning circulation
AP	After Present (present = AD 2000)
Arb.	Arbitrary
BC	Before Christ
BA	Bølling–Allerød warming
^{10}Be	Beryllium-10 isotope
BP	Before the Present (present = AD 2000)
^{14}C	Carbon-14 isotope
CH_4	Methane
CET	Central England Temperature
CO_2	Carbon dioxide
d	Day
D	Deuterium, hydrogen isotope
DO	Dansgaard–Oeschger warming
DP	Double Peak module or 3.75-kyr module
EBA	Early Bronze Age
EDC	EPICA Dome C
EPICA	European Project for Ice Coring in Antarctica
FFT	Fast Fourier Transformation
GISP	Greenland Ice Sheet Project
GCR	Galactic Cosmic Rays
GM	Grand minimum
GRIP	Greenland Ice-Core Project
H_2CO_3	Carbonic acid
H	Heinrich Event
HM	Homeric minimum
HTM	Holocene temperature maximum
$I_{min/max}$	Insolation minimum/maximum
Insolation	Incoming Solar Irradiation (W/m²)
IRD	Ice-rafted debris
ITCZ	Intertropical Convergence Zone
LBA	Late Bronze Age
LGM	Last Glacial Maximum, (c. 18–23 kyr BP)
k	kilo; thousand
LIA	Little Ice Age (by solar activity AD 1250–1700)
m	million
MM	Maunder minimum
MeV	Mega electron Volt
MIS	Marine Isotope Stage
MMSC	Multi-Millennial Solar Cycles

MPT	Middle Pleistocene transition (c. 800–1200 kyr BP)
MHA	Medieval High Acticity
MWP	Medieval Warm Period
NA	North Atlantic
NADW	North Atlantic Deep-Water formation
$O_{min/max}$	Obliquity minimum/maximum
OD	Older Dryas (c. 13.9–14.1 kyr BP)
^{18}O	Oxygen isotope
PBO	Preboreal Oscillation
PH	Post-Homeric Minimum
PM	Post-Maunder Minimum
s3.5 ka	A grand-minimum module of the 3.5-ka Quasi-cycle
SS	Solar Surge event c. AD 2000–1850
SSN	Sunspot Number
SST	Sea surface temperature
Sv	Sverdrup (a flow of 1 million cubic meters per second)
THC	Thermohaline Circulation
TRW	Tree Ring-Width
TSI	Total Solar Irradiance (W/m^2)
YD	Younger Dryas, (c. 11.8–12.8 kyr BP)
yr	year